SCALED BOUNDARY FINITE ELEMENT METHOD FOR FLUID-STRUCTURE INTERACTION

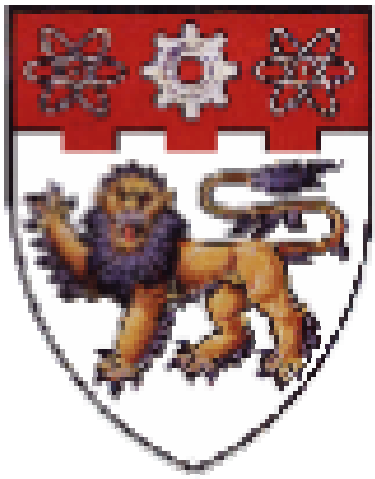

LI SHANGMING

School of Civil and Environmental Engineering

Nanyang Technological University

2006

SCALED BOUNDARY FINITE ELEMENT METHOD FOR FLUID-STRUCTURE INTERACTION

LI SHANGMING

B. Eng.

School of Civil and Environmental Engineering

A Thesis submitted to the Nanyang Technological University in fulfillment of the requirement for the Degree of Doctor of Philosophy

2006

ACKNOWLEDGEMENTS

The author would like to express his sincere appreciation to his supervisor, professor Fan Sau Cheong, for his invaluable advice and encouragement throughout the course of this research project. His constructive advice and care give the author a great help when the author is in a difficult situation.

The author also thanks Dr. Yu Guoyou for his generous and patient help and some constructive discussions.

Finally, the author would like to thank Nanyang Technological University for supporting him financially over the period of this research project.

TABLE OF CONTENTS

SUMMARY

Fluid-structure-interaction (FSI) occurs whenever relative motion between a structure and a fluid medium occurs. Over the last three decades or four, a wealth of numerical computational methods have been developed to address the FSI problems, including both bounded and unbounded fluid domains. Amongst those available numerical computational methods, the most popular ones are the traditional finite element method (FEM) and the boundary element method (BEM). This study presents the first attempt to extend the scaled boundary finite element method (SBFEM) for FSI problems.

In this study, the SBFEM is enhanced and extended for modeling the bounded/unbounded acoustic fluid medium, while the FEM is employed to model the structure. To enable the SBFEM to be employed in FSI problems, a relationship between fluid velocity and fluid pressure corresponding to scattered waves needs to be developed. The author developed that new relationship based on the SBFEM and acoustic approximations. By combining the fluid velocity-to-pressure relationship, a FEM/SBFEM coupling procedure is developed. Its performances are investigated through 2-dimensional FSI problems. Satisfactory results are obtained. The results demonstrate that the SBFEM is very efficient in modeling both unbounded and bounded acoustic fluid. However, the solution of the SBFEM for bounded acoustic fluid was found to be sensitive to the dissipation coefficient when applying the numerical Newmark time-integration scheme.

In addition, two modified SBFEM formulations are developed for solving problems related to infinite beams on visco-elastic-typed fluid foundations and a dam-reservoir system with an absorptive reservoir's bottom. The formulations are validated by checking against benchmark results.

LIST OF TABLES

LIST OF FIGURES

NOTATIONS

a	=	acceleration amplitude
$\mathbf{a}$	=	structural accelerations velocity vector
a_0	=	dimensionless frequency variable
$\mathbf{a}_{ff}$	=	acceleration vector for incident wave
$\mathbf{a}_{inf}$	=	total accelerations vector on wet surface
a_{n1}	=	normal acceleration at dam-reservoir Interface 1
A	=	cross-section area of beam
$\mathbf{A}$	=	converting matrix
$\hat{A}$	=	modified cross-section area of beam
$\mathbf{B}$	=	stain-displacement relationship of a fluid medium
$\mathbf{B}^1$	=	sub-matrix of $\mathbf{B}$
$\mathbf{B}^2$	=	sub-matrix of $\mathbf{B}$
$\mathbf{B}_c$	=	curvature-displacement matrix
$\mathbf{B}_s$	=	shear strain-displacement matrix
c	=	wave speed in fluid
$\mathbf{c}^0$	=	the equivalent $\mathbf{C}^0$ in time domain
c_l	=	wave speed in an elastic rod
c_p	=	wave speed in an elastic rod
c_s	=	wave speed in fluid or beam
$\mathbf{C}$	=	structural damping matrix
$\mathbf{C}^0$	=	coefficient matrix of the SBFEM corresponding to a

		foundation
$\mathbf{C}^b$	=	damping matrix of a bounded fluid medium
$\mathbf{C}^d$	=	damping matrix of dam
$\mathbf{C}_f$	=	the damping properties of a visco-elastic foundation
$\mathbf{C}_{f\,jl}$	=	sub-matrices of $\mathbf{C}_f$ (j,l=2,3)
$\mathbf{d}$	=	structural displacement vector
d, d_l	=	translational and rotational viscous-damping coefficients, respectively
d_r, d_{rl}	=	critical translational and rotational viscous-damping coefficients, respectively
d_s	=	structural displacement at mean radius
$\mathbf{e}^1, \mathbf{e}^2$	=	the equivalent forms of $\mathbf{E}^1$, $\mathbf{E}^2$ in time domain, respectively
E	=	Young's modulus of beam
$\mathbf{E}^0, \mathbf{E}^1, \mathbf{E}^2$	=	coefficient matrices of the SBFEM
$\mathbf{E}'^2$	=	coefficient matrix of the SBFEM for a beam
$\mathbf{E}_e^0, \mathbf{E}_e^1, \mathbf{E}_e^2$	=	elements' coefficient matrices of the SBFEM
$\mathbf{E}_f^2$	=	coefficient matrix of the SBFEM corresponding to a foundation
E_s	=	Young's modulus of shell
$\mathbf{F}$	=	force vector of a beam at a spatial position
$\mathbf{F}^n$	=	value of force vector of $\mathbf{F}$ at time $t = n\Delta t$
$\mathbf{F}_e$	=	external force vector
$\mathbf{F}_{ext}$	=	external force of a beam; body or traction force vector

$\mathbf{F}_f$	=	force acting underneath a semi-infinite beam; hydrodynamic force vector
$\mathbf{F}_{ff}$	=	force vector for incident wave
$\mathbf{F}_j$	=	force vector of a beam at spatial position x_j (j=2,3)
$\mathbf{F}_{inf}$	=	force vector for unbounded fluid medium
$\mathbf{F}_{sc}$	=	force vector for scattered wave
g	=	gravity acceleration
G	=	shear modulus of beam
h	=	height of a beam; thickness of a cylindrical shell
H	=	height of a layered infinite fluid medium
H(t-0)	=	Heaviside function
i	=	nodal number; imaginary index
I	=	unit matrix
$\mathbf{I}_n$	=	integral term for $\mathbf{m}^{\infty}$
j	=	nodal number; j^{th} time step; j^{th} iteration
j_{mn}	=	component of **J** (m,n=1,2)
J	=	second moment of a beam's cross-sectional area
J	=	component of $\bar{\mathbf{J}}$
$\mathbf{J}_n$	=	integral term for $\mathbf{m}^{\infty}$
$\bar{\mathbf{J}}$	=	Jacobian matrix
k, k_1	=	translational and rotational spring constants, respectively
k_0, k_{10}	=	critical translational and rotational spring constants, respectively
K	=	global stiffness matrix of structure or fluid

$\mathbf{K}^{b}$	=	static-stiffness matrix of a bounded fluid medium
$\mathbf{K}^{d}$	=	stiffness matrix of dam
$\mathbf{K}^{e}$	=	element stiffness matrix of fluid
$\mathbf{K}^{f}$	=	stiffness matrix of a near-field fluid domain
$\mathbf{K}_{c}$	=	the stiffness matrix corresponding to $\mathbf{B}_c$
$\mathbf{K}_{f}$	=	the stiffness of a visco-elastic foundation
$\mathbf{K}_{f\,jl}$	=	sub-matrices of $\mathbf{K}_f$ (j,l=2,3)
k_{g}	=	stiffness of an elastic foundation
$\mathbf{k}_{ij}$	=	sub-matrix of $\mathbf{K}^e$ (i,j=1,2)
$\mathbf{K}_{ij}^{0}$, $\mathbf{K}_{ij}^{1}$, $\mathbf{K}_{ij}^{2}$	=	components of $\mathbf{k}_{ij}$ (i,j=1,2); components $\mathbf{K}_{jl}$ (j,l=1,2, or j,l=2,3)
$\mathbf{K}_{jl}$	=	sub-matrices of $\mathbf{K}$ (j,l=1,2, or j,l=2,3)
$\mathbf{K}'_{jl}$	=	sub-matrices of $\mathbf{K}+\mathbf{K}_f$ (j,l=2,3)
$\mathbf{K}'^{2}_{jl}$	=	component of $\mathbf{K}'_{jl}$
$\mathbf{K}_{s}$	=	the stiffness matrix corresponding to $\mathbf{B}_s$
l	=	the height of a element in a SFE cell
M	=	a dimensionless quantity; bending moment
$\mathbf{M}$	=	global mass matrix of structure or fluid
$\mathbf{M}^{-1}$	=	inverse of fluid-added mass matrix
$\mathbf{M}^{0}$	=	coefficient matrix of the SBFEM
$\mathbf{m}^{0}$	=	the equivalent form of $\mathbf{M}^0$ in time domain
$\mathbf{M}^{b}$	=	static-mass matrix of a bounded fluid medium
$\mathbf{M}^{d}$	=	mass matrix of dam
$\mathbf{M}^{e}$	=	element mass matrix of fluid
$\mathbf{M}^{f}$	=	mass matrix of a near-field fluid domain

$\mathbf{M}^{\infty}$	=	dynamic mass matrix of an infinite fluid medium
$\mathbf{m}^{\infty}$	=	an equivalent form of $\mathbf{M}^{\infty}$ in time domain
$\mathbf{m}_j^{\infty}, \mathbf{M}_j^{\infty}$	=	values of $\mathbf{m}^{\infty}$ and $\mathbf{M}^{\infty}$ at $t = j\Delta t$, respectively (j=1,2,…,n)
m_b	=	bending moment acting on a beam from a foundation
$\mathbf{M}_e^0$	=	element's coefficient matrix of the SBFEM
$\mathbf{m}_{ij}$	=	sub-matrix of $\mathbf{M}^e$ (i,j=1,2)
$\mathbf{M}_{ij}^2$	=	component of $\mathbf{m}_{ij}$ (i,j=1,2) or $\mathbf{M}_{jl}$ (j,l=1,2)
M_j	=	bending moment of a beam at spatial position x_j (j=2,3)
$\mathbf{M}_{jl}$	=	sub-matrices of $\mathbf{M}$ (j,l=1,2 or j,l=2,3)
n	=	n^{th} time step
$\mathbf{n}$	=	unit normal vector
$\mathbf{N}$	=	shape function for fluid, structure and beam
$\mathbf{N}(\eta)$	=	shape function of a surface corresponding to an interior/exterior boundary surface
N_1, N_2	=	shape functions at spatial positions x_2, x_3 for a beam, respectively
$\mathbf{N}_1, \mathbf{N}_2$	=	shape functions on faces 1 and 2 for a layered medium, respectively
$\mathbf{N}_f$	=	shape function for fluid element
$\mathbf{N}_i$, $\mathbf{N}_e$	=	shape functions on interior and exterior surfaces, respectively
$\mathbf{N}_p$	=	interpolation function for scattered wave pressure
O	=	scalar center
p	=	pressure acting on a beam from a foundation; fluid

		pressure
p^s	=	prescribed pressure on S_f
$\mathbf{p}_1$	=	nodal pressure column vector at Interface 1
p_{ff}	=	fluid pressure on wet surface caused by free-field incident wave
$\mathbf{p}_{ff}$	=	fluid pressure vector caused by free-field incident wave
p_{inc}	=	fluid pressure on wet surface caused by incident wave
$\mathbf{p}_{inc}$	=	fluid pressure vector caused by incident wave
p_{inf}	=	total fluid pressure on wet surface
$\mathbf{p}_{inf}$	=	total fluid pressure vector
p_{sc}	=	fluid pressure on wet surface caused by scattered wave
$\mathbf{p}_{sc}$	=	fluid pressure vector caused by scattered wave
$\mathbf{p}_{sc}^j$	=	value of $\mathbf{p}_{sc}$ at time $j\Delta t$, j=1,2,3,…,n
Q	=	shear force
Q_j	=	shear force at spatial position x_j (j=2,3)
r	=	radial coordinate; characteristic length
R	=	mean radius of cylindrical shell
R	=	global vector of an integral of normal velocity along fluid boundary; acceleration transformation matrix
$\mathbf{R}^e$	=	vector of an integral of normal velocity along the fluid boundary of an element
R_e	=	radius of outer surface of cylindrical shell
$\mathbf{R}_e, \mathbf{R}'_e$	=	global vector of an integral of normal velocity along the

		exterior surface
r_i, r_e	=	characteristic lengths of the interior and exterior surface, respectively
R_i	=	radius of inner surface of cylindrical shell
$\mathbf{R}_i, \mathbf{R}_i'$	=	global vector of an integral of normal velocity along the interior surface
$\mathbf{R}_{n+1}$	=	value of $\mathbf{R}$ at time step n+1
s	=	spatial dimension of an acoustic fluid
$\mathbf{S}$	=	dynamic stiffness of a SFE cell
$\mathbf{S}^b$	=	dynamic stiffness matrix of a bounded fluid medium
$\mathbf{S}_i^b, \mathbf{S}_e^b$	=	$\mathbf{S}^b$ at interior and exterior surface, respectively
$\mathbf{S}^\infty$	=	dynamic stiffness matrix of an infinite fluid medium
$\mathbf{S}_1^\infty, \mathbf{S}_2^\infty$	=	$\mathbf{S}^\infty$ at interior (face1) and exterior (face2) surface, respectively
$\mathbf{S}_2^\infty, \mathbf{S}_3^\infty$	=	dynamic-stiffness matrices of an infinite beam at spatial positions x_2 and x_3, respectively
$\mathbf{S}_i^\infty, \mathbf{S}_e^\infty$	=	$\mathbf{S}^\infty$ at interior and exterior surface, respectively
$\overline{\mathbf{S}}^\infty$	=	a function matrix of the dimensionless frequency variable a_0
S_f	=	prescribed pressure boundary
$\mathbf{S}_{ii}, \mathbf{S}_{ie}, \mathbf{S}_{ei}, \mathbf{S}_{ee}$ $\mathbf{S}_{11}, \mathbf{S}_{12}, \mathbf{S}_{21}, \mathbf{S}_{22}$ $\mathbf{S}_{22}, \mathbf{S}_{23}, \mathbf{S}_{32}, \mathbf{S}_{33}$	=	sub-matrices of $\mathbf{S}$
S_v	=	prescribed velocity boundary
t	=	time variable

T	=	dimensionless time
$\mathbf{U}$	=	a decomposed matrix of $\mathbf{E}^0$; displacement vector of dam
$\ddot{\mathbf{U}}_g$	=	ground acceleration vector
u	=	displacement of a rod
$\mathbf{u}$	=	deformations vector of a beam element
$\mathbf{u}_j$	=	deformations of a beam element at spatial positions x_j (j=2,3)
$\dot{\mathbf{u}}_j$	=	the first derivative of $\mathbf{u}_2$ with respect to time at time $t = j\Delta t$
v	=	beam deflection
$\mathbf{v}$	=	velocity vector of a fluid particle or structures
V	=	fluid volume
v^e	=	fluid element volume
v_{ff}	=	normal velocity on wet surface caused by free-field incident wave
$\mathbf{v}_{ff}$	=	normal velocity vector on wet surface caused by free-field incident wave
$\mathbf{v}_{inc}$	=	normal velocity vector on wet surface caused by incident wave
v_{inf}	=	total normal velocity at one point on wet surface
$\mathbf{v}_{inf}$	=	total normal velocity vector on wet surface
v_j	=	beam deflection at spatial position x_j (j=2,3)
v_n	=	normal velocity on fluid boundary or of structure
$\mathbf{V}_n$	=	integral vector of normal velocity along the boundary of

		fluid medium
v_n^s	=	prescribed velocity normal to S_v
v_{n2}	=	normal velocity along the Interface 2
$\mathbf{V}_{n2}$	=	normal velocity integral vector along the Interface 2
$\mathbf{V}_{n1}, \mathbf{V}'_{n2}, \mathbf{V}_{n3}$	=	sub-matrices of $\mathbf{V}_n$
v_r	=	normal velocity on wet surface caused by incident wave
v_{sc}	=	normal velocity on wet surface caused by scattered wave
$\mathbf{v}_{sc}$	=	normal velocity vector on wet surface caused by scattered wave
$\mathbf{V}_{sc}$	=	efficient normal velocity vector for scattered wave
$\mathbf{V}_{sc}^n$	=	value of $\mathbf{V}_{sc}$ at time $n\Delta t$
w	=	characteristic width of scalar finite element cell
x	=	x coordinate of a node
$\mathbf{x}$	=	x coordinate vector of nodes
$\mathbf{x}_1, \mathbf{x}_2$	=	x coordinates of nodes lying on faces 1 and 2, respectively
$\mathbf{x}_i, \mathbf{x}_e$	=	x coordinates of nodes lying on interior and exterior boundary, respectively
x_j	=	spatial position (j=2,3)
y	=	y coordinate of a node
$\mathbf{y}$	=	y coordinate vector of nodes
$\mathbf{y}_1, \mathbf{y}_2$	=	y coordinates of nodes lying on faces 1 and 2, respectively

$\mathbf{y}_i, \mathbf{y}_e$	=	y coordinates of nodes lying on interior and exterior boundary, respectively
α	=	dissipation coefficient of Newmark scheme; coefficient in Newmark scheme; stiffness ratio
β	=	parameter of Newmark scheme; an exponential efficient; bulk modulus of an acoustic fluid; shear angle
δ	=	variational symbol; coefficient in Newmark scheme
ε	=	a very small dimensionless quantity
ϕ	=	fluid velocity potential
$\mathbf{\Phi}$	=	nodal velocity potential vector
$\mathbf{\Phi}_2$	=	vector of nodal velocity potentials along the Interface 2
$\mathbf{\Phi}_i, \mathbf{\Phi}_e$	=	velocity potential vector at interior and exterior surfaces, respectively
$\mathbf{\Phi}_{n+1}$	=	nodal velocity potential vector at time step n+1
$\boldsymbol{\varphi}$	=	nodal velocity potential vector
$\boldsymbol{\varphi}_j$	=	value of φ at the $j\Delta t$, j=0,1,2,…,n
γ	=	parameter of Newmark scheme; measure of angle
Γ	=	boundary of a fluid volume; wet surface
Γ_1	=	Interface 1
Γ^e	=	fluid element boundary
Γ_w	=	Interface 2
η	=	axis along circumferential direction
μ	=	shear factor
θ	=	bending rotation; measure of angle

θ_j	=	bending rotation at spatial position x_j (j=2,3)
ρ	=	beam density; fluid density
ρ_s	=	density of shell
$\sum_e$	=	assemblage of finite elements
σ	=	stress in a rod
ν	=	Poisson's ratio
ω	=	frequency variable
ω_c	=	cut-off frequency
Ω	=	a dimensionless frequency
Ω_a	=	analytical solution for Ω
ξ	=	damping ratio; radial axis
∞	=	infinite
$O(w)$	=	the order of error (w)
$O(w^2)$	=	the order of error (w^2)
$O(\omega)$	=	the order of error (ω)
∇	=	gradient operator
Δt	=	time increment
[L], [M], [T]	=	the dimensions of length, mass and time, respectively

OBJECTIVE AND LAYOUT OF THE THESIS

OBJECTIVE OF THE THESIS

The primary objective of this study is to develop a new approach for solving fluid structure interaction (FSI) problems. In this approach, the scaled boundary finite element method (SBFEM) concept is employed to model the fluid, while the finite element method (FEM) is used to model the structure. Particularly, the focus is on the dynamic responses of FSI problems in the time domain. This current study is the first attempt at extending the SBFEM to solve FSI problems. To ensure that the SBFEM could be successfully extended to solve FSI problems, the following two tasks must be done.

The first task is to establish a relationship between the normal velocity and pressure at the fluid-structure interface or the bounded/unbounded (truncated) boundary surfaces. Based on this relationship, an appropriate FEM-SBFEM coupling procedure is then developed.

The second task is to verify and validate the procedure developed. The computer code is checked against two benchmark problems. The first is the application to the dynamic responses of submerged structures subjected to shock waves. The other is the dam-reservoir interaction problem subjected to horizontal ground motions.

LAYOUT OF THE THESIS

In Chapter One, introduction of FSI problems are presented and includes backgrounds and reviews of FSI problems.

Chapter Two contains detailed SBFEM formulation for a 2-dimensional homogeneous infinite acoustic fluid medium. The infinite acoustic fluid medium has been discretized into sectors.

Chapter Three presents detailed SBFEM formulation for a 2-dimensional infinite acoustic fluid medium. The infinite acoustic fluid medium has been discretized into layers.

Chapter Four extends the layered SBFEM formulation to beams resting on foundation, and an analytical formulation based on the SBFEM concept is derived.

Chapter Five describes a SBFEM formulation for a 2-dimensional bounded acoustic fluid medium, and its accuracy and efficiency are evaluated. A Newmark scheme with a numerical dissipation coefficient is recommended for obtaining better results.

Chapter Six presents the acoustic formulation for FSI problems with non-layered infinite acoustic fluid medium. It includes the implementation of the FEM/SBFEM coupling procedure. Applications to responses of submerged structures to shock waves are demonstrated.

Chapters Seven and Eight present the FEM/SBFEM coupling procedure for a dam-reservoir system with a layered infinite acoustic fluid medium in the frequency and time domains respectively, and a new SBFEM formulation for a dam-reservoir system with an absorptive reservoir's bottom.

Finally in Chapter Nine, general conclusions are drawn based on the finding of this study. Future works of the SBFEM for FSI problems are recommended.

CHAPTER ONE

INTRODUCTION

1.1 BACKGROUND

Current technologies evolved and new techniques are being developed. More complex structures have been constructed, and even more complicated structures will be designed in future. Sophisticated and traditional structures can be seen on land, in the air, floating on or submerged in the sea in increasing numbers. Nevertheless, the needs and desires for new structures and function do not stop, and this development demands more versatile and efficient tools for structural analyses. These tools are required to deal with various kinds of loadings (e.g. fluid pressure, shocking waves, seismic and impact) acting on a variety of structures (e.g. submerged or floating structures, dam-reservoir system and aerospace structures). Many of these problems fall under the category of fluid-structure interaction (FSI) problems. For most FSI problems, the associated analytical solutions are scarce, and even if they exist, they are difficult to use because of the complexity of the structural geometry or loading. Hence, numerical methods turn out to be the only viable solution as no easier alternatives are available.

In the past three or four decades, a number of numerical methods had been developed to address the FSI problems; examples include the Finite Element Method (FEM), the Finite Difference Method (FDM) and the Boundary Element Method (BEM). Mechanical models and accurate solutions based on FEM or FDM for bounded domain problems are readily available. However, for unbounded (infinite) fluid domain problems, adopt the FEM and FDM approaches would encounter difficulties. To obtain a satisfactory solution for an infinite fluid domain, the FEM and FDM approaches need further developments in the techniques. Boundary element method (BEM) was found to be a good candidate for modeling an infinite fluid domain, but very often more difficulties occur when coupling with

the finite-element model of a structure. Recently, more efficient methods have been developed, especially for coupling problems involving unbounded (infinite) medium, such as the Scaled Boundary Finite Element Method (SBFEM) and the Reflected-afterflow-virtural-source (RAVS) model. The SBFEM is chosen for the current study as it combines the advantages of the FEM and the BEM. The FEM requires no fundamental solutions and thus has a wide scope of applications, whereas the BEM reduces the spatial dimension by one as only the boundary is discretized with surface finite elements so that the boundary condition at infinity are satisfied exactly.

1.1.1 FLUID-STRUCTURE INTERACTION PROBLEMS

FSI occurs whenever a relative motion of the two media occurs. In a broader sense, the treatment of these problems involves all aspects of solid and fluid mechanics. In practice however, it is possible to identify different behaviors and categorize them into groups so that simplifications may be made. In general, there are 3 categories of FSI problems [Zienkiewicz and Bettess (1978)]:

(i) Long-duration FSI problems. They involve long-duration fluid motion such as the response of structures to waves or earthquakes. In those cases, the fluid wave effects are important.

(ii) Short-duration FSI problems. They involve short-duration fluid motion such as explosive waves and impacts. In those cases, fluid inertia usually has much greater effect than the structure's. An example is an incident shock wave impinging on a submerged structure.

(iii) Large-relative-motion FSI problems. In those cases, the behavior is usually governed by flow characteristics. A typical example is the interaction involving fluttering of aircraft wings.

In the current study, the scope is limited to the FSI problems of the first and second categories. In the first-category problems, dam-reservoir system interactions following horizontal ground motions are considered. In the second-category problems, the interaction between submerged structures and the surrounding infinite fluid medium is considered when it is subjected to an underwater explosive shock. In these problems, evaluations of the structural responses are amongst the most important objectives of the FSI analyses. Against this background, the author was motivated to develop an accurate and efficient tool for modeling the infinite fluid domain with the objective of obtaining a good estimation of the structural responses.

1.1.2 METHODS AVAILABLE FOR FSI PROBLEMS (CATEGORIES I and II)

It has been that reported, traditional methods such as the FEM, FDM and BEM have successful solved some FSI problems. For the first-category FSI problems, those traditional methods are often employed together with some transmitting boundary conditions such as Sommerfeld radiation condition. For the second-category FSI problems, those traditional methods are usually employed together with some acoustic approximations such as Plane Wave Approximation (PWA), Doubly Asymptotic Approximation (DAA). This study presents a first attempt on the use of the SBFEM with FEM to solve these two categories of FSI problems. Advantages of the SBFEM over the FEM and BEM are shown in Table 1.1. Of note in BEM, the resulting matrix is normally asymmetric, but by using some special techniques, the asymmetrical matrix can become symmetrical (Chen et al. 2000).

In addition, for the second-category FSI problems, the SBFEM is able to yield more accurate results at late time in comparison with Plane Wave Approximation (PWA). Furthermore, it is simpler than the Doubly Asymptotic Approximations (DAA) in which the fluid mass matrix is fully populated and asymmetric. In the SBFEM, the surrounding infinite fluid is modeled by a dynamic mass matrix which is symmetric. While for the first-category FSI problems, the transmitting (truncated) boundary can

be placed very near to structures and even directly on the structure-fluid interface when the SBFEM is used. Other methods can not do so. Further elaboration is presented in Chapters 2-6.

Table 1.1 Advantages of SBFEM over FEM and BEM

	BEM	FEM	SBFEM
No fundamental solution required	×	√	√
Able to reduce spatial dimension by one	√	×	√
Satisfy radiation condition exactly for unbounded medium	√	×	√
Suitable for anisotropic material	×	√	√
Formulation leads to symmetric stiffness and mass matrices	×	√	√
Formulation leads to a dynamic-stiffness matrix	×	√	√
No singular integrals to be evaluated	×	√	√
Boundary conditions on free, fixed and inter-material surfaces are satisfied without discretization	×	×	√
Closed-form solution in domain permitting efficient calculation of displacements, stresses and stress-intensity factors	×	×	√
Yields no fictitious eigenfrequencies in unbounded medium	×	√	√

1.2 REVIEWS ON MODELING OF INFINITE FLUID MEDIUM

In FSI problems where the fluid medium is infinite, it is crucial to model accurately and efficiently the infinite fluid medium in order to obtain an accurate solution. In

traditional numerical methods, an infinite fluid domain is generally truncated into two parts (near- and far-field fluid domains) so that the infinite fluid domain can be modeled by the finite near-field domain and a transmitting boundary on the truncated surface (the near-far domains interface). This treatment shrinks an infinite domain to a bounded (finite) domain. It reduces the calculation cost. However, if the transmitting boundary cannot correctly model the effect of far-field fluid domain, the truncated (artificial) surface may produce spurious reflections which contaminate the solutions. Therefore, the transmitting boundary needs some special treatments to eliminate those reflections. A simple way to get rid of the unwanted effect of reflections is to extend the near-field fluid domain to a sufficient distance so that the crucial response is obtained before the reflections return. However, in most practical cases, the near-field domain could become so huge that computational cost becomes very expensive when the response at late-time is required.

An alternative approach to the above is to put in place a non-radiating boundary which is "transparent" to the scattered waves. Available methods which satisfy the non-radiating boundary condition are mainly based on one of the following approaches:

(i) Infinite element method
(ii) Boundary element method
(iii) Reflected-afterflow-virtual-source model
(iv) Methods based on acoustic approximations
(v) Boundary finite element method

In the following, brief discussions of the above are presented. A more detailed elaboration is given to the methods based on acoustic approximations and the scaled boundary finite element method (SBFEM).

1.2.1 INFINITE ELEMENT METHOD

This method was originally based on using shape functions analogous to Lagrangian polynomials but having an extra exponentially decaying term, which diminishes at infinity (Bettess 1977). There is an approach which maps the exterior domain onto the interior one through local mapping functions defined for each element (Zienkiewicz et al. 1981). In the latter approach, little modification of the coding (i.e. the derivation of the appropriate shape functions and the corresponding Jacobian matrix) is required.

Saini et al. (1978) employed the infinite element method based on the first approach to couple FEM to analyze the frequency response of dam-reservoir systems. Nicolas-Vullierme and Blumstein (1984) applied the Bettess-Zienkiewicz approach to construct a family of axisymmetric infinite elements. Then they used these elements to study the harmonic vibrations of an axisymmetric elastic structure submerged in an unbounded incompressible fluid. Buragohain and Agrawal (1981) proposed an infinite element with three nodes on a circular arc and two nodeless radial rays. In it, the shape functions are periodic in the circumferential direction, and depend on a "delay parameter" which is determined by a trial-and-error procedure. Simpson's rule is used for the numerical integration in the infinite direction. Nachbin and Wrobel (1984) combined the ideas of Bettess and Zienkiewicz (1977) and Buragohain and Agrawal (1981) to devise an infinite element with six nodes. The shape functions are periodic in the circumferential direction, and depend on a "decay parameter". They used that element to solve fluid-structure interaction problems and reasonable results were obtained. Recently, the idea of infinite elements was carried over to the boundary element method.

1.2.2 BOUNDARY ELEMENT METHOD

In BEM formulations, the weighted residual techniques are used to reduce the dimension of the problem by one, and thus may lead to reduction on computational

cost and the hardware storage requirements. However, it has the following disadvantages.

(i) Although the dimension of the problem is reduced, the resulting matrix equations are full, and the advantages of banded matrices are lost. Eventually, the overall computational cost may not be lower but higher.

(ii) In the case of geometric and material non-linearity problems, it becomes necessary to discretize the domain as well as the boundary. As a result, the advantages achieved in reduction of dimensionality are partially offset.

Nevertheless, the BEM is frequently used for modeling infinite medium in the frequency and time domain analyses.

Recently, Rajakumar and Ali (1996) used BEM to model the fluid medium and used FEM to model the structure, and then coupled them to perform the eigen analysis for a fluid-structure interaction system. Berot and Peseux (1998) coupled FEM with BEM to study the hydroelastic or vibro acoustic behavior of cylindrical thin shells immersed in an unbounded, inviscid and heavy fluid. In it, plane boundary element and ring boundary element were employed. Theirs results in the frequency domain were found in good agreement with analytical solutions. Chen et al. (2000) presented a symmetric formulation for the coupling of BEM with FEM to compute responses of submerged elastic structures in a heavy acoustic medium. In it, the acoustic loading derived from BEM was formulated in a symmetric complex matrix. The symmetry of the acoustic loading matrix had been proven by an acoustic reciprocal principle. The computational efficiency of theirs FEM/BEM formulations was verified by an example - a constant thickness spherical shell subjected to a point alternating force. Chen's numerical results in the frequency domain were also found to be in good agreement with the analytical solutions. Czygan and Estorff (2002) used coupled BEM/FEM to analyze the dynamic response of fluid-structure interaction systems in the time domain, where the unbounded fluid was modeled by BEM and the structure was modeled by nonlinear FEM. Their formulation for the transient analysis of fluid-structure systems encountered instability problems.

Mansur et al. (2000) employed a linear θ method to improve the numerical stability, and BEM was employed to model the infinite fluid domain while FEM was employed to model the solid structure. The linear θ method was also employed in fluid-structure interaction procedure by Yu et al. (2002), who used two classical examples to demonstrate the validity of the coupling procedure and stable schemes for fluid-structure interaction problems.

1.2.3 REFLECTED-AFTER-FLOW-VIRTUAL-SOURCE (RAVS)

RAVS is a recently developed theoretical approximation for fluid-structure interactions used by Lam et al. (1998). Pressures due to scattered and radiated waves produced by underwater explosions at the point of interest on the structural surface are determined by modeling the waves as if they are emanating from a virtual source. The position of the virtual source is determined by the explosion position and the geometrical shape of the structure's surface. The fluid velocity and scattered wave velocity at each point have an analytical relationship with fluid pressure and scattered wave pressure, respectively. RAVS has been employed in transient response of a two-layered elastic cylindrical shell impacted by an underwater shock wave. According to published reports, the results are in good agreement with those using FDM available in the software USA (Underwater Shock Analysis) /LS-DYNA3D. It is also noted that this method does not need truncation of the surrounding fluid domain, and the non-radiating boundary based on RAVS is placed on the fluid-structure interface.

1.2.4 ACOUSTIC APPROXIMATIONS

In acoustic approximations, the infinite fluid surrounding structures is considered as an acoustic medium and modeled as a membrane covering the wet surface of structures (fluid-structure interface). The acoustic approximations on the membrane are presented in the form of differential equations which are obtained by Kirchhoff's retarded potential formulation. The acoustic approximations can be classified into a number of types. Three common types are shown below.

(i) Early-time approximations. The response obtained by this method approaches the exact one at early time in transient interactions (Felippa 1977), i.e. this response characterizes the high-frequency behavior of fluid-structure systems. Due to the local nature of this formulation, this formulation has a simple form. Its implementation in FEM codes is easy and does not affect the bandedness of the resulting set of equations.

(ii) Late-time approximations. The response predicted using this method approaches the exact one at late time in the transient response. In this approach, the infinite fluid medium is represented by an added mass matrix produced by using boundary elements (Felippa 1977), but the resulting added mass matrix is asymmetric and fully populated, which increases the calculation cost.

(iii) Doubly asymptotic approximations. The response calculated from this method exhibits the correct asymptotic behavior in both the high-frequency (early-time) and low-frequency (late-time) limits. It has two one-sided asymptotic expressions: one for early-time approximation and another for late-time approximation. They are added together to form a corresponding Doubly Asymptotic Approximation (DeRuntz and Geers 1978, Geers 1978). Through using a wet-surface fluid frequency matrix, the responses at a particular intermediate-frequency or time can be obtained. However, this method inherits the same disadvantage as that of the late-time approximations, i.e. the resulting matrices are asymmetric and fully populated.

In what follows, these 3 approximations are discussed in details.

1.2.4.1 Early-time approximations

The early-time approximations, (i.e. Plane-Wave-Approximation (PWA) methods) which have a simple mathematical expression and can obtain accurate early-time solutions, were developed by Mindlin and Bleich (1953), Bedrosian and Dimaggio (1972a,1972b), Felippa (1980) and others. Mindlin and Bleich (1953) were amongst the first researchers to develop the PWA for a submerged cylindrical shell. In it, an analytical method was employed. Bedrosian and DiMaggio (1972a, 1972b) introduced an analogous approximation for submerged spherical and spheroidal shells. Their formulation was implemented in a FDM code and validated by testing the response of submerged spherical and spheroidal steel shells. Felippa (1980) derived a hierarchical family of early- time surface interaction approximations for a structure submerged in an infinite acoustic fluid through using Kirchhoff's retarded-potential method.

Wright et al. (1981) implemented the PWA in a FDM code and applied it to analyze the response of a submerged fluid-filled cylindrical shell subjected to a step pressure wave. DiMaggio et al. (1981) implemented and applied the PWA to determine the response characteristics of submerged structures surrounded by a cavitating fluid. The structure and the cavitating fluid were modeled by finite elements. In all cases, good agreements with analytical results were reported. Rehak et al. (1985) employed the PWA to study the response of a floating structure subjected to an exponentially decaying plane wave. Numerical tests showed that their formulation was sufficiently accurate in determining the structural response.

More recently, Hamdan and Dowling (1995) developed two-dimensional and axi-symmetric elements based on the PWA, which were implemented into the general-purpose package ASAS-NL-FSI. These elements were applied to study the transient response of several spherical and cylindrical shells submerged in water and subjected to various loadings (internal pressures, stepped and exponential plane shock waves), respectively. McCoy and Sun (1997) applied the PWA to fluid-structure interaction analyses of a thick-section composite cylindrical shell

subjected to an underwater blast loading using a commercial finite-element code, ABAQUS. A solution approaching exact solution was obtained. Fan et al. (2001) used spline shell elements to model structures and used the PWA to model unbounded fluid medium for the dynamic analysis of a submerged shell subjected to an underwater explosion at far distance. Their solutions are in good agreement with analytical solutions at early time.

1.2.4.2 Late-time approximations

Geers (1969) developed an analytical method based on a Virtual Mass Approximation of an infinite acoustic medium. The method was validated by studying the elastic response of a cylindrical shell excited by a transient acoustic wave. Geers (1970) employed the method to study the response of an elastic cylindrical shell to a transverse acoustic shock wave submerged in a light fluid medium. Compared to the PWA, Geers' results demonstrate the superior performance of his formulation particularly for late-time behaviors and low frequencies. However, substantial discrepancies were observed during the early times. Chertok (1970) applied the same method to determine the transient flexural vibrations of ship-like structures exposed to underwater explosions. Only low-frequency motions of the structure were considered. Results were found comparative to experimental data in low frequency modes; however, discrepancies were observed in high frequency modes. Felippa (1977) presented a top-down derivation of late-time approximations based on an exact Retarded Potential Formulation. Deruntz and Geers (1978) presented a method to calculate the virtual mass by the boundary integral method. However, the resulting mass matrix is asymmetric and fully banded.

1.2.4.3 Doubly asymptotic approximations (DAA)

In many instances, when a submerged structure is excited by a shock wave, its response peaks at early time. Therefore, it is crucial to have an accurate prediction for the early-time behaviour. On the other hand, it has also been recognised that

types of loadings and geometries of structures, amongst other factors, also influence the peak position, magnitude and general shape of the response. This leads to some cases where the peak response occurs at intermediumte or late time. In such cases, early-time approximations cannot predict the accurate peak response of structures. Against this background, the DAA was developed. It was expected to be able to predict the responses both at early time and late time.

The DAA formulation is a superimposition of two one-sided asymptotic expressions. One is the early-time approximation and another is the late-time approximation. As a result, the resulting solutions would approach the exact ones towards the limit of high or low frequency motions.

Everstine (1976) developed a DAA formulation and implemented it into the general-purpose finite element code, NASTRAN. The resulting FSI system was symmetric and banded through treating the non-symmetric fluid-structure coupling terms in an explicit manner. However, the accuracy implications of treating the low frequency matrix explicitly were not assessed.

By superimposing the PWA and the Virtual Mass Approximation, Ranlet et al. (1977) used the DAA to analyze the elastic response of submerged shells with internally attached structures subjected to shock loadings. Modal analysis method was employed for the dynamic response and a good agreement with analytical results was obtained.

Although the DAA was proved to be accurate for both early and late time behaviors, discrepancies with analytical solutions have often been observed at intermediate times or frequencies. Geers (1978) proposed an enhanced DAA for the intermediate transient range. The enhanced DAA was validated by studying the transient response of a submerged spherical shell excited by a step plane wave. Numerical results showed that the enhanced DAA is more accurate than other numerical methods for intermediate times. However, it demands much higher computational cost.

Zilliacus et al. (1979) developed a DAA code and implemented it in the general-purpose finite element code ADINA. Infinite fluid medium were modeled by an added mass matrix which was calculated by a boundary integral approach, while axisymmetric finite elements were used to model structures. The response of a submerged spherical shell subjected to a step incident plane wave was investigated and results showed good agreements with theoretical results. Zilliacus (1983) employed the same approach to study the response of a submerged fluid-filled cylinder subjected to an incident plane step wave. Results also showed good agreements with other numerical results based on finite elements/DAA.

Atkatsh et al. (1983) developed a nonlinear, large deflection, elasto-plastic code (EPSA) for the analyses of shells in an acoustic medium subjected to a dynamic loading through discretizing the shell using FDM and employing the DAA based on orthogonal fluid expansion functions to model infinite fluid medium. They verified the EPSA code by studying the transient nonlinear response of stiffened cylindrical panels. Results showed good agreements with experimental data. However, the effect of the material non-linearity to the solution was not discussed.

Felippa and DeRuntz (1984) developed a DAA formulation based on a boundary integral approach and implemented it in an Underwater Shock Analysis (USA) code. The responses of FSI problems were resolved by coupling the structural code STAGS-C1 and the fluid code CFA. The DAA formulation was validated by studying the response of one- and two-dimensional submerged structures excited by stepped and exponential plane waves.

Rehak et al. (1985) studied the response of floating structures subjected to shock waves using the PWA and DAA. The PWA and DAA were applied on the wet surface of the structure and on a fluid boundary surrounding the structure, respectively. Numerical results showed that the PWA is sufficient to determine the response characteristics for this class of problems. It was also found that the DAA offered no additional accuracy in this case.

Huang (1986) used the DAA to study the response of a submerged spherical shell excited by plane step waves. Numerical results showed good agreements with those of analytical methods. However, the comparison revealed that Huang's method overestimates the fluid damping force such that the responsive oscillations damped out prematurely. It was concluded that by augmenting this method with an intermediate frequency matrix, DAA method might be able to alleviate the deficiency.

O'Reagan and DiMaggio (1990) compared the performance of the DAA with the PWA by studying the dynamic response of an infinite circular cylindrical shell with plate appendages excited by plane waves. Numerical results showed that both methods yielded good results only if the waves were applied on the convex surface of a structure. It attributed to the occurrence of multiple reflections between the structure and the external appendages.

Recently, various formulations had been reported for the first and second order DAA non-reflecting boundaries (Nicolas 1991, Geers and Zhang 1994a, Geers and Zhang 1994b, Geers and Lewis 1997). The second-order approximations were derived from the corresponding first-order by employing the method of operator matching.

Ergin (1996) used the DAA non-reflecting boundary to study the response of a flexible steel cylindrical shell subjected to an impulsive excitation. Two cases for the unbounded medium were considered, i.e. air and water. Good agreements of theoretical and experimental results were observed.

More recently, Gong and Lam (1998, 1999) employed FEM and BEM based on the DAA to resolve the transient responses of a stiffened composite submersible hull and a floating composite ship section subjected to underwater explosion shocks, respectively. Gong et al. (2000) used FEM to couple the DAA to execute structural analyses of a submarine pipeline subjected to underwater shocks. In these works,

the shock pressure generated by underwater explosions was determined by an empirical equation, and the fluid-structure interaction was solved by USA/LS-DYNA3D, in which USA (Underwater Shock Analysis) was based on a DAA while LS-DYNA3D was based on the FDM. Shin and Hooker (1996) and Shin (2004) employed the USA/LS-DYNA3D to analyze the responses of submerged imperfect cylindrical structures and floating ships subjected to underwater explosions again, respectively. The LS-DYNA simulation results were close to the ship shock test data.

1.2.5 SCALED BOUNDARY FINITE ELEMENT METHOD

Wolf and Song (1996a) developed a so-called "consistent infinitesimal boundary finite element method". They applied it to solve soil-structure interaction problems. The characteristics of unbounded soil medium were described by scalar or vector wave equations (Wolf and Song (1996b), Song and Wolf (1996)). They derived a series of displacement dynamic-stiffness matrix in frequency domain and a displacement unit-impulse response matrix in time domain for unbounded medium. The displacement dynamic-stiffness matrix and unit-impulse response matrix were expressed in terms of some coefficient matrices, which depended only on the geometry of the infinitesimal finite element in unbounded medium in contact with the structure surface. They derived these coefficient matrices for 2D/3D scalar/vector wave equations. Making use of those coefficient matrices and a dimensional analysis led to a differential equation at a fixed characteristic length surface in frequency domain. Furthermore, applying the inverse Fourier transformation to the differential equation yielded an integral equation at a fixed characteristic length surface in the time domain. The above derivation is referred to as the "mechanically-based" derivation. Deeks and Wolf (2002a) proposed a virtual work derivation of the SBFEM for elastostatics. Subsequently, coupling the differential equation or the integral equation with the conventional FE model for the structure yields solutions for the dynamic response of soil-structure interaction problems.

Wolf and Song (1996a) verified the accuracy of their solutions in the frequency domain and in the time domain through an example, in which spherical cavity is embedded in a full-space medium with a uniform normal displacement prescribed on the structure-medium interface. They showed that the dynamic-stiffness coefficient for the spherical cavity and the acceleration unit-impulse response coefficient were in good agreement with the exact solutions. In addition, they demonstrated the robustness of the method with applications in other cases (e.g. spherical cavity embedded in full-space medium with varying material properties in radial direction; out-of-plane motion of circular cavity embedded in full-plane medium with varying shear modulus in radius direction; circular cavity embedded in full-plane medium etc.). The results were found in good agreement with exact solution or BEM solutions.

Wolf and Song (1996a) further extended the application of the consistent infinitesimal finite-element cell method to solve incompressible elasticity problems, statics problems, diffusion problems and bounded medium problems. The basic procedures are the same as those for soil-structure interaction problems. The results were also found in good agreement with analytical solutions. Later, Wolf and Song renamed it as the "scaled boundary element method", or SBFEM.

Song and Wolf (1997) proposed the SBFEM formulation for elasto-dynamics. The formulation was validated by some benchmarks in which a stress singularity with crack problems was considered. Song and Wolf (1998) presented the analytical solution of the SBFEM in the frequency domain through applying a series expansion. An eigenvalue problem of a Hamiltonian matrix was solved. Applications to bounded and unbounded domains validated the accuracy of the formulation. Song and Wolf (1999) enhanced the performance of the SBFEM. The solution of the SBFEM equations in displacement with body loads was derived. Wolf and Song (2000) presented two derivations of the SBFEM. The first was named after the "scaled boundary transformation based derivation", the other was named after the "mechanically based derivation". Song and Wolf (2000) presented a solution procedure of the SBFEM based on a single line finite element with two

nodes. Deeks and Wolf (2002b) presented an h-hierarchical adaptive procedure for the SBFEM. Deeks and Wolf (2002c) proposed a stress recovery and error estimation procedure for the SBFEM.

By far, the SBFEM have been applied in many research fields widely. Song and Wolf (2002) applied the SBFEM to solve stress singularities problems. Genes and Kocak (2002) used a combination of FEM and the SBFEM to model large-scale soil-structure interaction systems. Ekevid and Wiberg (2002) coupled the FEM and the SBFEM to analyze a wave propagation problem related to a high-speed train. Deeks and Wolf (2003) employed the SBFEM to present a semi-analytical solution of a Laplace's equation in non-equilibrating unbounded problems. Doherty and Deeks (2003a-c) used the SBFEM to solve the non-homogeneous half-space problems. However, few investigations have been reported on using the SBFEM concept together with the finite element method to solve FSI problems.

1.3 Review of FSI coupling numerical techniques

1.3.1 Coupling numerical techniques for short-duration FSI problems

Since analytical solutions are difficult to obtain for a general FSI problem, numerical techniques for FSI problem are developed. Normally, the numerical techniques for FSI problem are obtained through coupling two or more numerical methods.

Amongst the prevailing numerical techniques, the finite element method (FEM) and boundary element method (BEM) are commonly used. Very often, the FEM is employed to model the structure, while either FEM or BEM is used to model the fluid domain. In those numerical simulations, FEM-to-FEM domain coupling procedures or FEM-to-BEM domain coupling procedures are necessary. Nevertheless, both FEM-FEM and FEM-BEM simulations exhibit some pitfalls.

When both the structure and fluid domain are bounded, FEM-FEM simulations

have been shown to be efficient and able to yield reasonably accurate dynamic responses for FSI problems as reported in some literatures (Hamdan (1999), Belytschko (1980), Bathe et al. (1995), Morand and Ohayon (1979), Mellado and Rodriguez (2001), Biswal et al. (2003), Olson and Bathe (1985), Pal et al. (2003), Nitikitpaiboon and Bathe (1993) and others). In those FEM-FEM analyses, various formulations were presented with regard to the acoustic fluid domain: Lagrangian fluid finite elements formulation in Hamdan (1999); a generic displacement formulation in Belytschko (1980); a mixed displacement-based finite element formulation in Bathe et al. (1995); displacement and pressure mixed formulation in Morand and Ohayon (1979), Mellado and Rodriguez (2001) and Biswal et al. (2003); and the velocity potential formulation in Olson and Bathe (1985), Pal et al. (2003), and Nitikitpaiboon and Bathe (1993). All these formulations demonstrated their robustness in coupling with the conventional solid structural elements. According to their characteristics, those formulations can be classified into two major categories, namely: the displacement-based formulations and the potential-based formulations. In the displacement-based formulations, the fluid motion is described by the nodal displacements. The coupling responses between fluid and structures are ensured by equating the normal displacement components along the fluid-structure interface. This type of formulation is identical with the displacement formulation for continuum mechanics but with zero shear modulus at the interface. However, this pure displacement formulation for an inviscid fluid will exhibit spurious circulation modes. On the other hand, the potential-based formulations can avoid these spurious circulation modes because the fluid motion is represented by some form of scalar potential functions. In it, both the compatibility and the equilibrium conditions along the interface are explicitly enforced.

When the FEM is employed to model an unbounded fluid domain, the size of the numerical model is limited and thereby the unbounded fluid domain has to be truncated but at a sufficiently far distance such that all major responses are not distorted. It requires the domain to be stretched beyond where the scattered waves can reach. By doing so, the effects of the scattered waves will be implicitly taken into account and no further complications will arise. However, in most practical

cases, the FE mesh discretization for such a huge fluid domain will become prohibitively expensive in terms of computational cost. Practically, a compromised solution is to truncate the unbounded fluid domain at a reasonable not-too-far distance away from the structure. Consequently, some scattered waves will reach the truncated (artificial) boundary before the termination of the analysis. It results in artificial waves reflecting back into the fluid mesh and contaminating the responses. To overcome or minimize these undesired wave reflections from the artificial boundary, an alternative is to put in place a kind of non-radiating boundary which is 'transparent' to the scattered waves.

In modeling a fluid domain with a non-radiating boundary, many researchers have been heralding the approach described without using FEM. Mindlin and Bleich (1953) are among the pioneers. They developed an early-time approximation technique, namely plane wave approximation (PWA). Successful applications of the PWA technique for the analyses of submerged spherical and spheroidal shells were reported by DiMaggio et al. (1981), Hamdan and Dowling (1995) and Fan et al. (2001). Very often, the early-time responses obtained from the PWA method agree well with the exact solution, but it is not so for the late-time responses. Geers (1969) developed an analytical method based on the virtual mass approximation (VMA) of the infinite acoustic medium. The validity of the VMA was illustrated through a study of the elastic response of a cylindrical shell excited by a transient acoustic wave. Compared to the results obtained from PWA, the VMA results demonstrated its superior performance, in particular the late-time behaviors and the low frequency response. By superimposing the PWA and the VMA, Ranlet et al. (1977) developed the doubly asymptotic approximation (DAA), which was used to model the infinite fluid medium, while modal analysis was employed for the structure. The DAA method had been proven to be accurate to model both early- and late- time behavior. Zilliacus (1983) used the DAA method to analyze the response of a submerged fluid-filled cylinder subjected to an incident plane step wave. It is worth noting that, in the DAA formulation, the mass matrix for the fluid medium is fully populated. More comprehensive reviews of the non-radiation boundary can be found in Givoli

(1991). Normally, the PWA and DAA are called acoustic approximations together. The detail reviews about the acoustic approximations are described in section 1.2.4.

In solving the general FSI problems, the exact or analytical non-radiating boundary is difficult to implement. With the emergence of the BEM which has been gradually recognized to have advantages in modeling infinite domain, FEM-BEM coupling procedures had been developed. Estorff and Antes (1991), Czygan and Estorff (2002) and Yu et al. (2002) demonstrated the advantages of using FEM-BEM procedures for FSI problems. In their numerical simulations, no artificial boundaries or wave reflections were present. Moreover, the FEM-BEM procedures are able to gain computational advantages derived from its BEM formulation, which reduces the spatial dimension by one. However, it inherits the disadvantages of the BEM which demands for pre-requisite fundamental solutions, which can be very complicated or may not be available. Furthermore, it leads to asymmetric coefficient matrices in its formulation. Not only it increases the requirement for memory storage, but also compromises (if not nullifies) its other computational efficiency.

1.3.2 Coupling numerical techniques for long-duration FSI problems

To build a structurally sound dam-reservoir system which belongs to long-duration FSI problem, the hydrodynamic forces acting on the upstream side of the dam is of the major concern, particularly due to earthquake ground motions. The interactive hydrodynamic forces can be obtained using analytical methods or numerical solutions. For the simplistic rigid dam with one vertical or sloping upstream face, a number of analytical solutions are available. Westergaard (1933) first presented rigorous analytical solutions of hydrodynamic pressures acting on vertical rigid dams; Chopra (1967) obtained solutions for hydrodynamic pressures on vertical rigid dams under horizontal and vertical ground motions analytically; and Chwang (1978), Chwang and Housner (1978) reported analytical solutions of the hydrodynamic pressures for sloping dams. Nevertheless, these solutions are not suitable to analyse dam structures with even slightly more complex upstream face, such as dams with multi-sloping upstream faces or arch dams. For dams with

complex geometries, Tsai (1992) presented a semi-analytical solution based on the least square method or the Galerkin method, but reportedly, inferior solutions were obtained near the base of a dam which has a large sloping angle. On the other hand, the advent of computer technology enables numerical solutions to be an alternative if not a better choice. Amongst the numerical solutions, Finite-Element-Method (FEM) solutions, Boundary-Element-Method (BEM) solutions or their combination solutions are the popular ones.

In most of the numerical models, the semi-infinite fluid domain is often divided into two sub-domains: a near-field and a far-field domain. This is to ensure the analysis to be valid over a manageable computational domain. Usually, the near-field domain is modeled by FEM or BEM, while the far-field domain is modeled by imposing a kind of transmitting boundary conditions (TBC), or using BEM or some kinds of tailor-made infinite elements. Regarding the TBC, a variety of techniques are available. Sommerfeld (1949) derived a technique called "Sommerfeld radiation condition". Sharan (1985) presented another called "Sharan's boundary condition". Tsai and Lee (1989) presented an analytical frequency solution. Maity and Bhattacharyya (1999) proposed a novel far-boundary condition. Solutions for the whole dam-reservoir system were subsequently obtained by coupling either FEM or BEM with their TBC. In their solutions, some pitfalls were identified. To obtain good results, Sommerfeld radiation condition and Sharan's condition demanded a large extent of the near-field domain; the analytical frequency solution of Tsai and Lee (1989) needed full eigen-values and eigen-modes of the interface between the near- and far-field. The novel far-boundary condition by Maity and Bhattacharyya (1999) was only suitable for curtain low frequencies cases. Another approach was adopted by Saini et al. (1978), who tailor made a kind of specialized infinite elements to model the far-field domain, but it still required a large near-field domain. Other researches such as Felippa (1981), Hanna and Humar (1982) and Tsai and Lee (1987) used BEM to model the far-field domain. Although the BEM allows one to deploy a smaller near-field domain, the BEM's unfavourable characteristics of singular integral and asymmetrical matrices remains.

The above reviews are about the steady analysis for a dam-reservoir system. The following is about the time-domain analysis for a dam-reservoir system.

In time-domain analysis, the analytic or semi-analytic solutions of hydrodynamic pressures on dams are much more difficult to obtain than those in frequency-domain analysis. To alleviate the difficulties, the semi-infinite fluid in a reservoir is usually modeled by dividing the domain into two parts: a near-field and a far-field domain. The effect of the far-field domain can be represented by some kind of transmitting boundary conditions (TBC) at the interface between the near-field and the far-field domain. The most commonly-used TBC is Sommerfeld (1949) radiation condition, which was used by Zienkiewicz and Bettess (1978) but precautions have to be taken as the approach may introduce significant errors when the near-field domain is small. Another TBC was developed by Sharan (1985). Although Sharan's TBC produced better results than Sommerfeld's, it does not represent the behaviour of the far-field domain well when the near-to-far-field interface is too near to the dam-reservoir interface. Tsai et al. (1990) developed an efficient semi-analytical TBC and later, its application by Tsai and Lee (1991) exhibited good results, but it required the full eigen-modes of the near-to-far-field interface. In order to get rid of this requirement, Yang et al. (1993) developed an explicit time-domain TBC which only needs curtain eigen-modes. However, these two types of TBC have complex forms, which further increase the complexities of the problem. Recently, Maity and Bhattacharyya (1999), Cetin and Mengi (2003) and Kucukarslan (2005) developed a novel far-boundary condition, a TBC based on spectral properties of radiating waves and an exact truncation boundary condition at the near-to-far-field interface, respectively. Although these TBC's have simple forms, they are only fit for 2-dimensional problems. On the other hand, instead of using a TBC to represent the far-field domain, Lotfi et al. (1987) developed the fluid hyper-element and Valliapan and Zhao (1992) tailor-made an infinite element to model the far-field domain, respectively, but the shape function of the fluid hyper-element or infinite element will effect results when they cannot represent efficiently far-field domain.

Against all of the above reviews, it can be easy to find that the SBFEM is very necessary to extend or develop further to solve FSI problem. One reason is that the SBFEM is a semi-analytic method in radial direction and very efficient to model an infinite domain. Another reason is that no investigations have been reported on using the SBFEM concept together with the finite element method to solve FSI problem so far.

CHAPTER TWO

SBFEM FORMULATION FOR INFINITE ACOUSTIC FLUID MEDIUM

Originally developed by Wolf and Song (1996a) for soil-structure interaction problems, the SBFEM formulas are only suitable for soil-structure interaction systems, and not applicable to the fluid-structure interaction (FSI) problems. Moreover, when dealing FSI problems involving infinite fluid medium, most traditional numerical methods encounter difficulties. Against this background, the writer recognizes the possibility and necessity to extend the SBFEM to model an infinite fluid field. It was inspired by the SBFEM's accuracy and efficiency when modeling an infinite soil domain reported by Wolf and Song (1996a). In this chapter, the SBFEM formulation for infinite acoustic fluid medium will be presented and described, while its accuracy and efficiency will be validated in chapter 6.

2.1 FEM FORMULATION FOR ACOUSTIC FLUID MEDIUM

Essentially, SBFEM and FEM share the same idea of discretization of a continuum but differ entirely in their approaches. Prior to the presentation of the SBFEM formulation, it is necessary to describe the FEM discretization of acoustic fluid medium. The detailed derivation has been described in the literature (Bathe (1996)). The basic derivation is shown in section below.

The acoustic fluid medium is treated as an inviscid isentropic fluid with the fluid particles undergoing only small displacements. Not including body force effects, the

equation governing the response of the fluid is an acoustic equation as follows:

$$\nabla^2\phi = \frac{1}{c^2}\ddot{\phi} \tag{2.1}$$

where ϕ and c denotes a fluid velocity potential and the wave speed in fluid, respectively. The velocity of a fluid particle satisfies

$$\mathbf{v} = \nabla\phi \tag{2.2}$$

where $\mathbf{v}$ is the velocity vector of fluid particles, while the fluid pressure p satisfies

$$p = -\rho\dot{\phi} \tag{2.3}$$

where ρ denotes the fluid density. The boundary conditions for acoustic fluid problems include two types. One is a prescribed velocity boundary S_v, and the other is a prescribed pressure boundary S_f.

On the boundary S_v, a prescribed velocity v_n^s in the direction of the unit normal vector $\mathbf{n}$ (pointing outward) to the fluid boundary satisfies

$$\mathbf{v} \bullet \mathbf{n} = v_n^s = \left.\frac{\partial\phi}{\partial n}\right|_{s_v} \tag{2.4}$$

On the boundary S_f, a prescribed pressure p^s satisfies

$$p|_{S_f} = p^s = -\rho\dot{\phi}|_{S_f} \tag{2.5}$$

Eqs.(2.1) (2.4) and (2.5) together describe a boundary-value problem. The corresponding variational form of Eq.(2.1) is expressed as

$$\int_V \left(\nabla^2\phi - \frac{1}{c^2}\ddot{\phi}\right)\delta\phi dV = 0 \tag{2.6a}$$

Eq.(2.6a) is re-written as

$$\int_V (\nabla \bullet \nabla\phi)\delta\phi dV - \int_V \frac{1}{c^2}\ddot{\phi}\delta\phi dV = 0 \tag{2.6b}$$

where $\delta\phi$ is a scalar quantity and V denotes the fluid volume. Appling the divergence theorem to Eq.(2.6b) leads to the following equation:

$$\delta\int\left((\nabla\phi)^2+\frac{1}{c^2}\ddot{\phi}\phi\right)dV=\delta\int_\Gamma\phi\nabla\phi\bullet\mathbf{n}d\Gamma=\delta\int_\Gamma\phi v_n d\Gamma \tag{2.6c}$$

where Γ denotes the boundary of the fluid volume and v_n is normal velocity on the boundary Γ. The finite element equation of Eq.(2.6c) is expressed as

$$\mathbf{M}\ddot{\Phi}+\mathbf{K}\Phi=\mathbf{R} \tag{2.7}$$

where Φ denotes the nodal velocity potential vector; $\mathbf{M}$, $\mathbf{K}$ and $\mathbf{R}$ denote the global mass matrix, stiffness matrix and the vector of an integral of the normal velocity along the boundary Γ, respectively. The corresponding element mass and stiffness matrices $\mathbf{M}^e$, $\mathbf{K}^e$ and the element's vector $\mathbf{R}^e$ are as follows.

$$\mathbf{M}^e=\int_{v^e}\frac{1}{c^2}\mathbf{N}^T\mathbf{N}dv^e \tag{2.8a}$$

$$\mathbf{K}^e=\int_{v^e}\mathbf{B}^T\mathbf{B}dv^e \tag{2.8b}$$

$$\mathbf{R}^e=\int_{\Gamma^e}\mathbf{N}^T v_n d\Gamma^e \tag{2.8c}$$

where v^e, Γ^e denotes the element volume and boundary, respectively; $\mathbf{N}$ and $\mathbf{B}$ are the shape function and the derivative of $\mathbf{N}$ with respect to spatial dimensions, respectively. $\mathbf{M}$, $\mathbf{K}$ and $\mathbf{R}$ can be obtained by assembling all $\mathbf{M}^e$, $\mathbf{K}^e$ and $\mathbf{R}^e$, respectively. Note that Eq.(2.8c) appears on the right hand side of the SBFEM equation in Section 2.2.

2.2 SBFEM MODELING FOR INFINITE FLUID MEDIUM

When the SBFEM is employed to model infinite fluid medium as shown in Fig.2.1a, the infinite fluid medium is discretized into sectors. In this sense, it is similar to the concept of BEM, in which the infinite fluid medium is discretized only along the fluid-structure interface. Each element *ij* on the fluid-structure interface denotes its

associated sector as shown in Fig.2.1b. Along the fluid-structure interface, the relationship between a normal velocity v_n and the associated velocity potential ϕ in frequency domain can be expressed as

$$\mathbf{R}(\omega) = \mathbf{S}^{\infty}(\omega)\Phi(\omega) \tag{2.9a}$$

$$\mathbf{R}(\omega) = \mathbf{M}^{\infty}(\omega)\ddot{\Phi}(\omega) \tag{2.9b}$$

where $\mathbf{R}(\omega)$ is expressed in the form of Eq.(2.8c); $\Phi(\omega)$ denotes the nodal velocity potential vector; $\mathbf{S}^{\infty}(\omega)$ and $\mathbf{M}^{\infty}(\omega)$ are called the "dynamic stiffness" and "dynamic mass" of the infinite fluid medium, respectively, and satisfy the relationship:

$$\mathbf{S}^{\infty}(\omega) = (i\omega)^2\mathbf{M}^{\infty}(\omega) \tag{2.10}$$

Applying inverse Fourier transformation to Eqs.(2.9a) and (2.9b) and using the zero initial conditions below

$$\Phi(t=0) = \mathbf{0} \tag{2.11a}$$

$$\dot{\Phi}(t=0) = \mathbf{0} \tag{2.11b}$$

yields

$$\mathbf{R}(t) = \int_0^t \mathbf{S}^{\infty}(t-\tau)\Phi(\tau)d\tau \tag{2.12a}$$

$$\mathbf{R}(t) = \int_0^t \mathbf{M}^{\infty}(t-\tau)\ddot{\Phi}(\tau)d\tau \tag{2.12b}$$

where $\mathbf{S}^{\infty}(\omega)$ and $\mathbf{S}^{\infty}(t)$, $\mathbf{M}^{\infty}(\omega)$ and $\mathbf{M}^{\infty}(t)$, $\mathbf{R}(\omega)$ and $\mathbf{R}(t)$ are Fourier transform pairs, respectively. The superscript ∞ denotes an infinite medium. Both the "dynamic stiffness" $\mathbf{S}^{\infty}(\omega)$ and the "dynamic mass" $\mathbf{M}^{\infty}(\omega)$ are dependant on the geometry of the fluid-structure interface, so that $\mathbf{S}^{\infty}(\omega)$ and $\mathbf{M}^{\infty}(\omega)$ are normally written as $\mathbf{S}^{\infty}(r,\omega)$ and $\mathbf{M}^{\infty}(r,\omega)$, respectively, with a characteristic length r. The expression for $\mathbf{S}^{\infty}(\omega)$ can be derived from a scalar-finite-element

(SFE) cell.

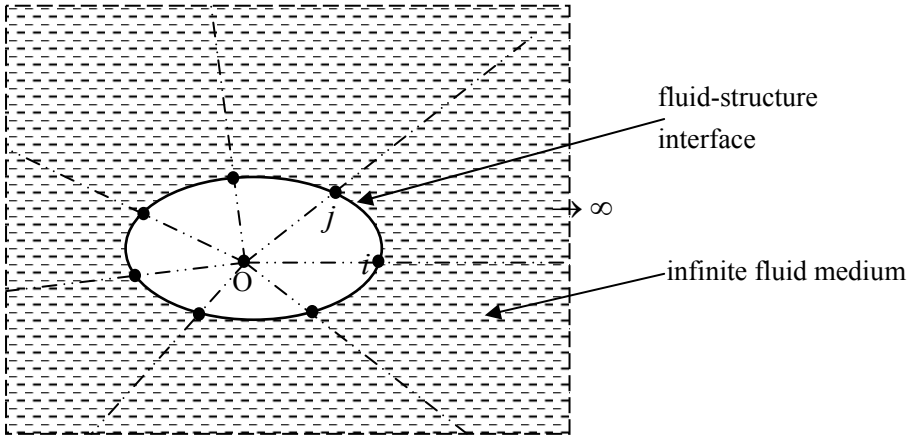

Fig.2.1a Sectorial discretization of an infinite fluid domain

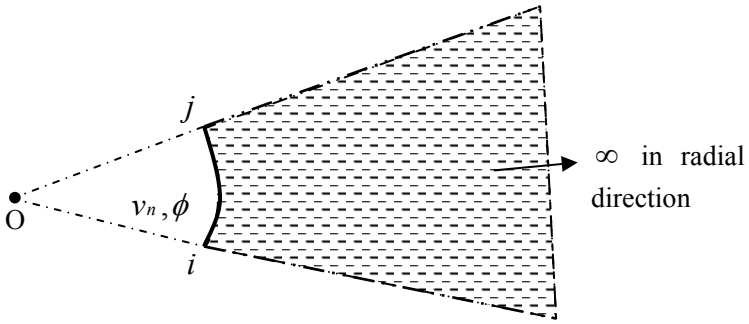

Fig.2.1b A typical SBFEM element of an infinite domain

2.3 SCALAR-FINITE-ELEMENT CELL

Consider a fluid-structure interaction system as shown in Fig.2.2a. The inside part indicates a submerged structure. An infinite fluid medium surrounds the structure. The outside fluid medium is discretized into finite sectors with a characteristic length r_i as shown in Fig.2.2b, and it can be also discretized into some sectors with another characteristic length r_e as shown in Fig.2.2c, and a section between r_i and r_e. This section is called a scalar-finite-element (SFE) cell as shown in

Fig.2.2a, which is bounded by two similar surfaces, each characterized by a nominal distance r (namely r_i and r_e), radiating from an origin O (scalar center) as shown in Figs.2.2a-d. The finite-element discretization of the SFE cell is shown in Fig.2.2d. The outward unit normal vectors **n** of the corresponding boundaries are shown in Figs.2.2b-d, as well.

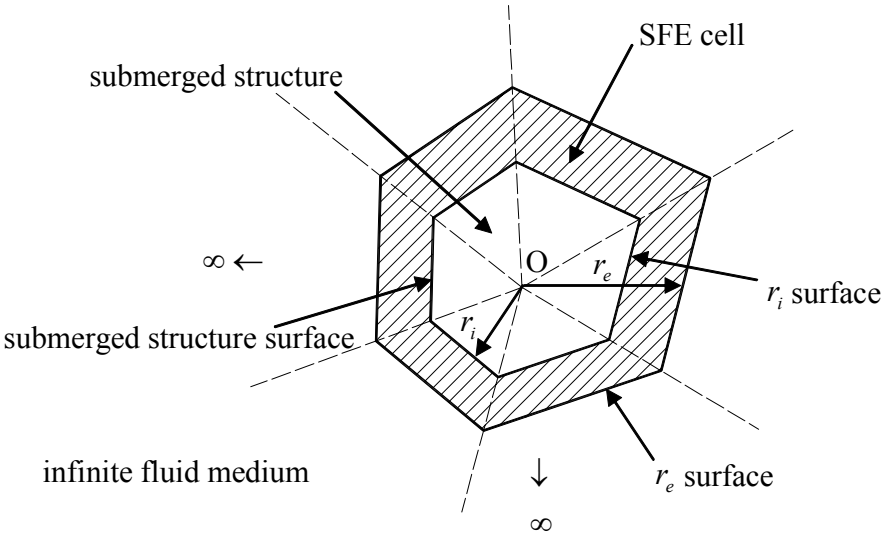

Fig.2.2a A fluid-structure interaction system

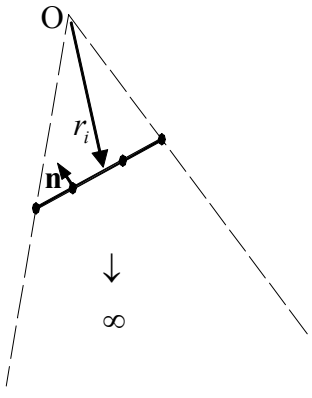

Fig.2.2b A sector of the infinite bounded domain defined by characteristic length r_i

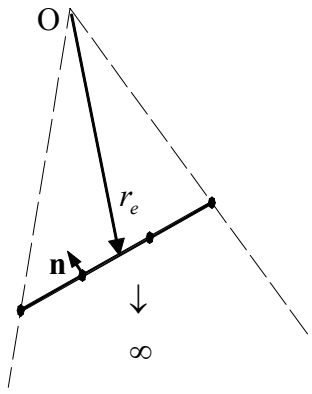

Fig.2.2c A sector of the infinite bounded domain defined by characteristic length r_e

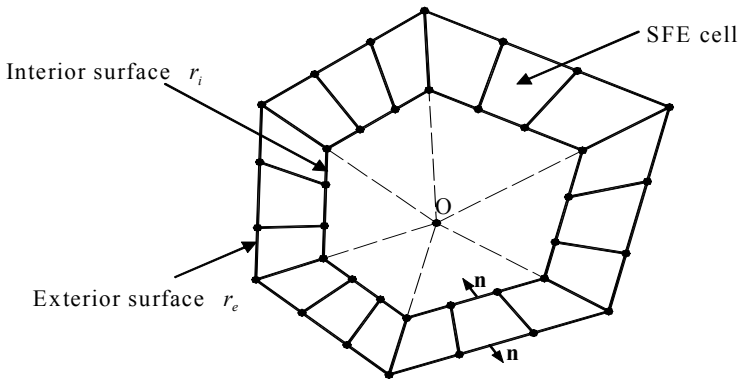

Fig.2.2d FE discretization of SFE cell bounded by surfaces r_i ***and*** r_e

2.3.1 RELATIONSHIP BETWEEN THE INTERIOR AND EXTERIOR BOUNDED SURFACES

On the interior surface r_i and exterior surface r_e shown in Fig.2.2a, Eq.(2.9a) is re-written as

$$\mathbf{R}(r_i,\omega)=\mathbf{S}^{\infty}(r_i,\omega)\Phi(r_i,\omega) \tag{2.13a}$$

$$\mathbf{R}(r_e,\omega)=\mathbf{S}^{\infty}(r_e,\omega)\Phi(r_e,\omega) \tag{2.13b}$$

For simplicity, Eqs.(2.13a) and (2.13b) are re-written as

$$\mathbf{R}_i(\omega)=\mathbf{S}_i^{\infty}(\omega)\Phi_i(\omega) \tag{2.14a}$$

$$\mathbf{R}_e(\omega)=\mathbf{S}_e^{\infty}(\omega)\Phi_e(\omega) \tag{2.14b}$$

The finite element equation (2.7) of the SFE cell for a harmonic type response is re-written as

$$\mathbf{R}(\omega)=\left(\mathbf{K}-\omega^2\mathbf{M}\right)\Phi(\omega)=\mathbf{S}(\omega)\Phi(\omega) \tag{2.15}$$

where

$$\mathbf{S}(\omega)=\mathbf{K}-\omega^2\mathbf{M} \tag{2.16}$$

Through partitioning $\mathbf{R}(\omega)$, $\Phi(\omega)$ and $\mathbf{S}(\omega)$ with respect to the interior and exterior surfaces, Eq.(2.15) becomes

$$\begin{bmatrix} \mathbf{S}_{ii}(\omega) & \mathbf{S}_{ie}(\omega) \\ \mathbf{S}_{ei}(\omega) & \mathbf{S}_{ee}(\omega) \end{bmatrix} \begin{Bmatrix} \Phi_i(\omega) \\ \Phi_e(\omega) \end{Bmatrix} = \begin{Bmatrix} \mathbf{R}'_i(\omega) \\ \mathbf{R}'_e(\omega) \end{Bmatrix} \tag{2.17}$$

On the interior surface r_i, the unit normal vectors $\mathbf{n}$ shown in Figs.2.2b and 2.2d are identical, while those on the exterior surface r_e shown in Figs.2.2c and 2.2d are in the opposite direction. Using Eq.(2.8c) and Eqs.(2.14a,b) yields

$$\begin{Bmatrix} \mathbf{R}'_i(\omega) \\ \mathbf{R}'_e(\omega) \end{Bmatrix} = \begin{Bmatrix} \mathbf{R}_i(\omega) \\ -\mathbf{R}_e(\omega) \end{Bmatrix} = \begin{bmatrix} \mathbf{S}_i^{\infty}(\omega) & \mathbf{0} \\ \mathbf{0} & -\mathbf{S}_e^{\infty}(\omega) \end{bmatrix} \begin{Bmatrix} \Phi_i(\omega) \\ \Phi_e(\omega) \end{Bmatrix} \tag{2.18}$$

Substituting Eq.(2.18) into Eq.(2.17) leads to

$$\begin{bmatrix} \mathbf{S}_{ii}(\omega) & \mathbf{S}_{ie}(\omega) \\ \mathbf{S}_{ei}(\omega) & \mathbf{S}_{ee}(\omega) \end{bmatrix} \begin{Bmatrix} \Phi_i(\omega) \\ \Phi_e(\omega) \end{Bmatrix} = \begin{bmatrix} \mathbf{S}_i^{\infty}(\omega) & \mathbf{0} \\ \mathbf{0} & -\mathbf{S}_e^{\infty}(\omega) \end{bmatrix} \begin{Bmatrix} \Phi_i(\omega) \\ \Phi_e(\omega) \end{Bmatrix} \tag{2.19}$$

By eliminating $\Phi_e(\omega)$ from Eq.(2.19), the relationship between $\mathbf{S}_i^{\infty}(\omega)$ and $\mathbf{S}_e^{\infty}(\omega)$ can be obtained as follows

$$\left(\mathbf{S}_i^{\infty}(\omega) - \mathbf{S}_{ii}(\omega) + \mathbf{S}_{ie}(\omega)\left(\mathbf{S}_e^{\infty}(\omega) + \mathbf{S}_{ee}(\omega)\right)^{-1}\mathbf{S}_{ei}(\omega)\right)\Phi_i(\omega) = \mathbf{0} \tag{2.20}$$

where $\Phi_i(\omega)$ becomes arbitrary, and thus the associated coefficient matrix must vanish, i.e.

$$\mathbf{S}_i^{\infty}(\omega) = \mathbf{S}_{ii}(\omega) - \mathbf{S}_{ie}(\omega)\left(\mathbf{S}_e^{\infty}(\omega) + \mathbf{S}_{ee}(\omega)\right)^{-1}\mathbf{S}_{ei}(\omega) \tag{2.21}$$

which describes the relationship of the dynamic stiffness $\mathbf{S}^{\infty}(\omega)$ between the interior surface r_i and the exterior surface r_e. In order to determine the relationship, the coefficient matrices $\mathbf{S}_{ii}(\omega)$, $\mathbf{S}_{ie}(\omega)$, $\mathbf{S}_{ei}(\omega)$ and $\mathbf{S}_{ee}(\omega)$ must be solved. These coefficients can be obtained through using Eqs.(2.8a) and (2.8b). In what follows, derivations for these coefficient matrices are given in details with respect to an element of the 2-dimensional SFE cell shown in Fig.2.2d.

2.3.2 FINITE-ELEMENT FORMULATION FOR AN ELEMENT IN A SFE CELL

An element in the SFE cell is shown in Fig.2.3, which is assumed 6 nodes, of which 3 nodes lie on the interior surface and 3 nodes on exterior surface.

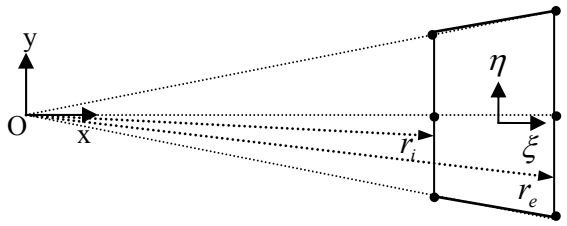

Fig.2.3 An element of the SFE cell

The shape function **N** for the element is chosen as

$$\mathbf{N} = \begin{bmatrix} \mathbf{N}_i & \mathbf{N}_e \end{bmatrix} = \begin{bmatrix} \frac{1}{2}(1-\xi)\mathbf{N}(\eta) & \frac{1}{2}(1+\xi)\mathbf{N}(\eta) \end{bmatrix} \tag{2.22}$$

where $\mathbf{N}(\eta)$ denotes the shape function of a surface corresponding to the interior/exterior bounding surface; the ξ axis corresponds to the radial direction which points from the fluid-structure interface towards infinity and the η axis corresponds to the circumferential direction. For a 3-node element,

$$\mathbf{N}(\eta) = \begin{bmatrix} \frac{1}{2}(\eta^2 - \eta) & 1-\eta^2 & \frac{1}{2}(\eta^2 + \eta) \end{bmatrix} \tag{2.23}$$

Due to radial similarity, the coordinates $\mathbf{x}_e$, $\mathbf{y}_e$ of a node lying on the exterior boundary r_e can be expressed in terms of nodal coordinates $\mathbf{x}_i$, $\mathbf{y}_i$ of its associated node lying on the interior boundary r_i and the characteristic width of the SFE w as follows.

$$\mathbf{x}_e = (1+w)\mathbf{x}_i \tag{2.24a}$$

$$\mathbf{y}_e = (1+w)\mathbf{y}_i \tag{2.24b}$$

where

$$w = \frac{r_e}{r_i} - 1 \tag{2.24c}$$

By using an isoparametric mapping technique, the geometrical interpolation for the position of an arbitrary point (x, y) inside the element can be expressed as follows.

$$\begin{Bmatrix} x \\ y \end{Bmatrix}^T = \begin{bmatrix} \mathbf{N}_i & \mathbf{N}_e \end{bmatrix} \begin{bmatrix} \mathbf{x}_i & \mathbf{y}_i \\ \mathbf{x}_e & \mathbf{y}_e \end{bmatrix} \tag{2.25a}$$

Substituting Eq.(2.22) and Eqs.(2.24a) and (2.24b) into Eq.(2.25a) leads to

$$\begin{Bmatrix} x \\ y \end{Bmatrix}^T = \left(1 + \frac{w}{2}(1+\xi)\right) \mathbf{N}(\eta) \begin{bmatrix} \mathbf{x}_i & \mathbf{y}_i \end{bmatrix} \tag{2.25b}$$

The relation between the differentials of the two mapped coordinate systems is the called "Jacobian" matrix $\bar{\mathbf{J}}$, i.e.

$$\bar{\mathbf{J}} = \begin{bmatrix} \frac{\partial x}{\partial \xi} & \frac{\partial y}{\partial \xi} \\ \frac{\partial x}{\partial \eta} & \frac{\partial y}{\partial \eta} \end{bmatrix} \tag{2.26a}$$

Substituting Eq.(2.25b) into Eq.(2.26a) yields

$$\bar{\mathbf{J}} = \begin{bmatrix} \frac{w}{2} & 0 \\ 0 & 1 + \frac{w}{2}(1+\xi) \end{bmatrix} \mathbf{J} \tag{2.26b}$$

where

$$\mathbf{J} = \begin{bmatrix} \mathbf{N}(\eta)\mathbf{x}_i & \mathbf{N}(\eta)\mathbf{y}_i \\ \frac{d\mathbf{N}(\eta)}{d\eta}\mathbf{x}_i & \frac{d\mathbf{N}(\eta)}{d\eta}\mathbf{y}_i \end{bmatrix} \tag{2.26c}$$

The determinant of the "Jacobian" matrix $\bar{\mathbf{J}}$ is

$$\left|\bar{\mathbf{J}}\right| = \frac{w}{2}\left(1 + \frac{w}{2}(1+\xi)\right)\left|\mathbf{J}\right| \tag{2.27}$$

The inverse of the "Jacobian" matrix $\bar{\mathbf{J}}$ is

$$\bar{\mathbf{J}}^{-1} = \mathbf{J}^{-1}\begin{bmatrix} \frac{2}{w} & 0 \\ 0 & \frac{1}{1+\frac{w}{2}(1+\xi)} \end{bmatrix} \tag{2.28}$$

Denoting the components of $\mathbf{J}^{-1}$ as j_{mn}, i.e.

$$\mathbf{J}^{-1} = \begin{bmatrix} j_{11} & j_{12} \\ j_{21} & j_{22} \end{bmatrix} \tag{2.29}$$

we have the derivatives of the shape functions as follows.

$$\begin{Bmatrix} \frac{\partial \mathbf{N}}{\partial x} \\ \frac{\partial \mathbf{N}}{\partial y} \end{Bmatrix} = \bar{\mathbf{J}}^{-1}\begin{Bmatrix} \frac{\partial \mathbf{N}}{\partial \xi} \\ \frac{\partial \mathbf{N}}{\partial \eta} \end{Bmatrix} = \frac{1}{w}\begin{Bmatrix} j_{11} \\ j_{21} \end{Bmatrix}\begin{bmatrix} -\mathbf{N}(\eta) & \mathbf{N}(\eta) \end{bmatrix} + \frac{1}{1+\frac{w}{2}(1+\xi)}\begin{Bmatrix} j_{12} \\ j_{22} \end{Bmatrix}\begin{bmatrix} \frac{1}{2}(1-\xi)\frac{d\mathbf{N}(\eta)}{d\eta} & \frac{1}{2}(1+\xi)\frac{d\mathbf{N}(\eta)}{d\eta} \end{bmatrix} \tag{2.30a}$$

Eq.(2.30a) is the strain-displacement relationship matrix $\mathbf{B}$ of a fluid medium, which is re-written as

$$\mathbf{B} = \frac{1}{w}\begin{bmatrix} -\mathbf{B}^1 & \mathbf{B}^1 \end{bmatrix} + \frac{1}{1+\frac{w}{2}(1+\xi)}\begin{bmatrix} \frac{1}{2}(1-\xi)\mathbf{B}^2 & \frac{1}{2}(1+\xi)\mathbf{B}^2 \end{bmatrix} \tag{2.30b}$$

where

$$\mathbf{B}^1 = \begin{Bmatrix} j_{11} \\ j_{21} \end{Bmatrix}\mathbf{N}(\eta) \tag{2.31a}$$

$$\mathbf{B}^2 = \begin{Bmatrix} j_{12} \\ j_{22} \end{Bmatrix}\frac{d\mathbf{N}(\eta)}{d\eta} \tag{2.31b}$$

Note that $\mathbf{B}^1$ and $\mathbf{B}^2$ are functions of η only.

Now, rewrite Eq.(2.8b) for an element stiffness matrix in terms of ξ and η as

$$\mathbf{K}^e = \int_{v^e} \mathbf{B}^T\mathbf{B}dv^e = \int_{-1}^{1}\int_{-1}^{1} \mathbf{B}^T\mathbf{B}|\bar{\mathbf{J}}|d\xi d\eta \tag{2.32}$$

Note that $\mathbf{K}^e$ can be integrated analytically. Partitioning $\mathbf{K}^e$ into sub-matrices

with respect to the interior and exterior surfaces leads to

$$\mathbf{K}^{e}=\begin{bmatrix}\mathbf{k}_{11} & \mathbf{k}_{12}\\ \mathbf{k}_{21} & \mathbf{k}_{22}\end{bmatrix} \tag{2.33}$$

of which, each sub-matrix $\mathbf{k}_{ij}$ $(i,j=1,2)$ can be written as

$$\mathbf{k}_{ij}=\frac{1}{w}\mathbf{K}_{ij}^{0}+\mathbf{K}_{ij}^{1}+w\mathbf{K}_{ij}^{2}+O(w^{2}) \tag{2.34}$$

where

$$\mathbf{K}_{ij}^{0}=\xi_i\xi_j\mathbf{E}^{0} \tag{2.35a}$$

$$\mathbf{K}_{ij}^{1}=\frac{\xi_i\xi_j}{2}\mathbf{E}^{0}+\frac{\xi_j}{2}\mathbf{E}^{1}+\frac{\xi_i}{2}\mathbf{E}^{1^{T}} \tag{2.35b}$$

$$\mathbf{K}_{ij}^{2}=\frac{1}{4}\left(1+\frac{\xi_i\xi_j}{3}\right)\mathbf{E}^{2} \tag{2.35c}$$

in which

$$\mathbf{E}^{0}=\int_{-1}^{1}\mathbf{B}^{1^{T}}\mathbf{B}^{1}|\mathbf{J}|d\eta \tag{2.36a}$$

$$\mathbf{E}^{1}=\int_{-1}^{1}\mathbf{B}^{2^{T}}\mathbf{B}^{1}|\mathbf{J}|d\eta \tag{2.36b}$$

$$\mathbf{E}^{2}=\int_{-1}^{1}\mathbf{B}^{2^{T}}\mathbf{B}^{2}|\mathbf{J}|d\eta \tag{2.36c}$$

and $\xi_1=-1$, $\xi_2=1$. $\mathbf{E}^{0}$, $\mathbf{E}^{1}$ and $\mathbf{E}^{2}$ can be conveniently determined by an approximate numerical integration scheme. Note that $\mathbf{E}^{0}$, $\mathbf{E}^{1}$ and $\mathbf{E}^{2}$ are functions of η only and thus associated with the discretization of the interior surface of the SFE cell. In addition, $\mathbf{E}^{0}$ is positive definite and symmetric; $\mathbf{E}^{2}$ is semi-infinite definite and symmetric. The last tem on the right hand side of Eq.(2.34) represents the order of error (w^{2}).

Similar to the element stiffness matrix, the element mass matrix $\mathbf{M}^{e}$ (Eq.(2.8a)) can be partitioned into sub-matrices accordingly, i.e.

$$\mathbf{M}^{e} = \begin{bmatrix} \mathbf{m}_{11} & \mathbf{m}_{12} \\ \mathbf{m}_{21} & \mathbf{m}_{22} \end{bmatrix} \tag{2.37}$$

in which

$$\mathbf{m}_{ij} = w\mathbf{M}_{ij}^{2} + O(w^{2}) = \frac{w}{4}\left(1 + \frac{\xi_i \xi_j}{3}\right)\mathbf{M}^{0} + O(w^{2}) \tag{2.38}$$

where

$$\mathbf{M}^{0} = \int_{-1}^{1} \frac{1}{c^{2}} \mathbf{N}(\eta)^{T} \mathbf{N}(\eta) |\mathbf{J}| d\eta \tag{2.39}$$

which is positive definite and symmetric. Note that the last term on the right hand side of Eq.(2.38) stands for the order of error (w^{2}). When w tends to zero, the error term $O(w^{2})$ on the right hand side of Eqs.(2.34) and (2.38) vanish.

2.4 SBFEM FORMULATION IN FREQUENCY DOMAIN

Assembling all elements in the SFE cell, i.e. assembling all of coefficients matrices $\mathbf{E}^{0}$, $\mathbf{E}^{1}$, $\mathbf{E}^{2}$ and $\mathbf{M}^{0}$ yields the global stiffness matrix $\mathbf{K}$ and mass matrix $\mathbf{M}$ in Eqs.(2.7) and (2.16). For the sake of simplicity, the coefficient matrices for the $\mathbf{K}$ and $\mathbf{M}$ will adopt the same symbols as those for individual elements.

2.4.1 DERIVATION OF SBFEM FORMULATION

Firstly, in order to be consistent with the matrix nomination, the subscripts i and e for the interior and exterior surface are renamed as 1 and 2, respectively. Re-write Eq.(2.21) as follows

$$\mathbf{S}_{1}^{\infty}(\omega) = \mathbf{S}_{11}(\omega) - \mathbf{S}_{12}(\omega)\left(\mathbf{S}_{2}^{\infty}(\omega) + \mathbf{S}_{22}(\omega)\right)^{-1}\mathbf{S}_{21}(\omega) \tag{2.40a}$$

Re-arranging leads to

$$\left(\mathbf{S}_{2}^{\infty}(\omega) + \mathbf{S}_{22}(\omega)\right)\mathbf{S}_{12}(\omega)^{-1}\left(\mathbf{S}_{1}^{\infty}(\omega) - \mathbf{S}_{11}(\omega)\right) + \mathbf{S}_{21}(\omega) = 0 \tag{2.40b}$$

Secondly, partitioning the global matrices $\mathbf{S}$, $\mathbf{M}$ and $\mathbf{K}$ in Eq.(2.16) with respect to the interior and exterior surfaces leads to

$$\mathbf{S}=\begin{bmatrix}\mathbf{S}_{11} & \mathbf{S}_{12}\\ \mathbf{S}_{21} & \mathbf{S}_{22}\end{bmatrix}=\begin{bmatrix}\mathbf{K}_{11} & \mathbf{K}_{12}\\ \mathbf{K}_{21} & \mathbf{K}_{22}\end{bmatrix}-\omega^2\begin{bmatrix}\mathbf{M}_{11} & \mathbf{M}_{12}\\ \mathbf{M}_{21} & \mathbf{M}_{22}\end{bmatrix} \tag{2.41}$$

Now consider $\mathbf{S}_{11}$, i.e.

$$\mathbf{S}_{11}=\mathbf{K}_{11}-\omega^2\mathbf{M}_{11} \tag{2.42}$$

Substituting Eqs.(2.34) and (2.38) into Eq.(2.42) yields

$$\mathbf{S}_{11}=\frac{1}{\mathrm{w}}\mathbf{K}_{11}^0+\mathbf{K}_{11}^1+\mathrm{w}\mathbf{K}_{11}^2-\mathrm{w}\omega^2\mathbf{M}_{11}^2+\mathrm{O}\left(\mathrm{w}^2\right) \tag{2.43}$$

Substituting Eq.(2.35a) into Eq.(2.43) and re-arranging lead to

$$\mathbf{S}_{11}=\frac{1}{\mathrm{w}}\mathbf{E}^0+\mathbf{K}_{11}^1+\mathrm{w}\left(\mathbf{K}_{11}^2-\omega^2\mathbf{M}_{11}^2\right)+\mathrm{O}\left(\mathrm{w}^2\right) \tag{2.44a}$$

Analogously, we can have

$$\mathbf{S}_{12}=-\frac{1}{\mathrm{w}}\mathbf{E}^0+\mathbf{K}_{12}^1+\mathrm{w}\left(\mathbf{K}_{12}^2-\omega^2\mathbf{M}_{12}^2\right)+\mathrm{O}\left(\mathrm{w}^2\right) \tag{2.44b}$$

$$\mathbf{S}_{21}=-\frac{1}{\mathrm{w}}\mathbf{E}^0+\mathbf{K}_{21}^1+\mathrm{w}\left(\mathbf{K}_{21}^2-\omega^2\mathbf{M}_{21}^2\right)+\mathrm{O}\left(\mathrm{w}^2\right) \tag{2.44c}$$

$$\mathbf{S}_{22}=\frac{1}{\mathrm{w}}\mathbf{E}^0+\mathbf{K}_{22}^1+\mathrm{w}\left(\mathbf{K}_{22}^2-\omega^2\mathbf{M}_{22}^2\right)+\mathrm{O}\left(\mathrm{w}^2\right) \tag{2.44d}$$

By using Eqs.(2.35a-c), the relationships between component matrices in Eqs.(2.44a-d) can be written as follows.

$$\mathbf{K}_{11}^0=-\mathbf{K}_{12}^0=-\mathbf{K}_{21}^0=\mathbf{K}_{22}^0=\mathbf{E}^0 \tag{2.45a}$$

$$\mathbf{K}_{21}^1+\mathbf{K}_{22}^1=-\left(\mathbf{K}_{11}^1+\mathbf{K}_{12}^1\right)^{\mathrm{T}}=\mathbf{E}^1 \tag{2.45b}$$

$$\mathbf{K}_{11}^2+\mathbf{K}_{12}^2+\mathbf{K}_{21}^2+\mathbf{K}_{22}^2=\mathbf{E}^2 \tag{2.45c}$$

$$\mathbf{M}_{11}^2+\mathbf{M}_{12}^2+\mathbf{M}_{21}^2+\mathbf{M}_{22}^2=\mathbf{M}^0 \tag{2.45d}$$

Thirdly, upon inspecting Eq.(2.40b), we notice that there exists the inverse term $\mathbf{S}_{12}(\omega)^{-1}$ which is difficult to evaluate. Hence, it is approximated as a polynomial in term of w with the unknown coefficient matrices $\mathbf{A}$ and $\mathbf{B}$ as follows.

$$\mathbf{S}_{12}(\omega)^{-1} = -\mathrm{w}\mathbf{E}^{0^{-1}} + \mathrm{w}^2\mathbf{A} + \mathrm{w}^3\mathbf{B} + \mathrm{O}(\mathrm{w}^4) \tag{2.46}$$

Note that $\mathbf{E}^{0^{-1}}$ can be evaluated via Eq.(2.36a). $\mathbf{A}$ and $\mathbf{B}$ can be obtained as follows. Consider the identity,

$$\begin{aligned}\mathbf{I} = \mathbf{S}_{12}(\omega)\mathbf{S}_{12}(\omega)^{-1} = \mathbf{I} - \mathrm{w}\left(\mathbf{K}_{12}^1\mathbf{E}^{0^{-1}} + \mathbf{E}^0\mathbf{A}\right) \\ - \mathrm{w}^2\left(\left(\mathbf{K}_{12}^2 - \omega^2\mathbf{M}_{12}^2\right)\mathbf{E}^{0^{-1}} - \mathbf{K}_{12}^1\mathbf{A} + \mathbf{E}^0\mathbf{B}\right) + \mathrm{O}(\mathrm{w}^3)\end{aligned} \tag{2.47}$$

The coefficient matrices of w and w^2 must vanish, such that

$$\mathbf{A} = -\mathbf{E}^{0^{-1}}\mathbf{K}_{12}^1\mathbf{E}^{0^{-1}} \tag{2.48a}$$

$$\mathbf{B} = -\mathbf{E}^{0^{-1}}\left(\mathbf{K}_{12}^1\mathbf{E}^{0^{-1}}\mathbf{K}_{12}^1 + \left(\mathbf{K}_{12}^2 - \omega^2\mathbf{M}_{12}^2\right)\right)\mathbf{E}^{0^{-1}} \tag{2.48b}$$

Substituting Eqs.(2.48a) and (2.48b) into Eq.(2.46) and then the result with Eqs.(2.44a-d) into Eq.(2.40b) lead to

$$\begin{aligned}&\mathbf{K}_{11}^1 + \mathbf{K}_{12}^1 + \mathbf{K}_{21}^1 + \mathbf{K}_{22}^1 \\ &- \mathrm{w}\left(\mathbf{S}_2^\infty(\omega) + \mathbf{K}_{21}^1 + \mathbf{K}_{22}^1\right)\mathbf{E}^{0^{-1}}\left(\mathbf{S}_1^\infty(\omega) - \mathbf{K}_{12}^1 - \mathbf{K}_{11}^1\right) + \mathbf{S}_2^\infty(\omega) - \mathbf{S}_1^\infty(\omega) \\ &+ \mathrm{w}\left(\left(\mathbf{K}_{11}^2 + \mathbf{K}_{12}^2 + \mathbf{K}_{21}^2 + \mathbf{K}_{22}^2\right) - \omega^2\left(\mathbf{M}_{11}^2 + \mathbf{M}_{12}^2 + \mathbf{M}_{21}^2 + \mathbf{M}_{22}^2\right)\right) = \mathrm{O}(\mathrm{w}^2)\end{aligned} \tag{2.49}$$

Substituting Eqs.(2.45a-d) into Eq.(2.49) and then dividing the whole resulting equation by w leads to

$$\left(\mathbf{S}_2^\infty(\omega) + \mathbf{E}^1\right)\mathbf{E}^{0^{-1}}\left(\mathbf{S}_1^\infty(\omega) + \mathbf{E}^{1\mathrm{T}}\right) - \frac{\mathbf{S}_2^\infty(\omega) - \mathbf{S}_1^\infty(\omega)}{\mathrm{w}} - \mathbf{E}^2 + \omega^2\mathbf{M}^0 = \mathrm{O}(\mathrm{w}) \tag{2.50}$$

Fourthly, to obtain the frequency equation for the discretized surface at $\mathrm{r_i}$, we have to condense the SFE cell by taking limit $\mathrm{w} \to 0$. Taking limit $\mathrm{w} \to 0$ for the second term in Eq.(2.50), i.e.

$$\lim_{\mathrm{w}\to 0}\frac{\mathbf{S}_2^\infty(\omega) - \mathbf{S}_1^\infty(\omega)}{\mathrm{w}} = \lim_{\mathrm{r_e}\to\mathrm{r_i}}\mathrm{r_i}\,\frac{\mathbf{S}_2^\infty(\omega) - \mathbf{S}_1^\infty(\omega)}{\mathrm{r_e} - \mathrm{r_i}} \tag{2.51a}$$

By writing $\mathbf{S}^\infty(\omega) = \mathbf{S}_1^\infty(\omega)$ and $\mathrm{r} = \mathrm{r_i}$, Eq.(2.51a) is re-formulated as

$$\lim_{\mathrm{r_e}\to\mathrm{r_i}}\mathrm{r_i}\,\frac{\mathbf{S}_2^\infty(\omega) - \mathbf{S}_1^\infty(\omega)}{\mathrm{r_e} - \mathrm{r_i}} = \mathrm{r}\frac{\partial\mathbf{S}^\infty(\omega)}{\partial\mathrm{r}} \tag{2.51b}$$

Note that when $w \to 0$, the exterior surface and interior surface will fully overlap with each other. Therefore, we have

$$\mathbf{S}_2^{\infty}(\omega) = \mathbf{S}_1^{\infty}(\omega) + O(\omega) = \mathbf{S}^{\infty}(\omega) + O(\omega) \tag{2.52}$$

where $O(\omega)$ stands for the order of error (ω). Taking limit $w \to 0$ for the whole Eq.(2.50) and substituting Eq.(2.52) into Eq.(2.50) yield

$$\left(\mathbf{S}^{\infty}(\omega) + \mathbf{E}^{1}\right)\mathbf{E}^{0^{-1}}\left(\mathbf{S}^{\infty}(\omega) + \mathbf{E}^{1^{\mathrm{T}}}\right) - r\frac{\partial \mathbf{S}^{\infty}(\omega)}{\partial r} - \mathbf{E}^{2} + \omega^{2}\mathbf{M}^{0} = O(w) \tag{2.53}$$

Note that in Eq.(2.53), there is still a term containing the derivative of the "dynamic stiffness" $\mathbf{S}^{\infty}(\omega)$ with respect to r. In next section, a dimensional analysis is employed to derive its equivalent in term of ω.

2.4.2 DERIVATIVE OF "DYNAMIC STIFFNESS"

As mentioned above in section 2.2, $\mathbf{S}^{\infty}(\omega)$ is dependant of the geometry of the fluid-structure interface, so that $\mathbf{S}^{\infty}(\omega)$ can be also written as $\mathbf{S}^{\infty}(r,\omega)$ with a characteristic length r. In what follows, a dimensional analysis is employed to obtain the relationship between the derivative $\dfrac{\partial \mathbf{S}^{\infty}(r,\omega)}{\partial r}$ and the derivative $\dfrac{\partial \mathbf{S}^{\infty}(r,\omega)}{\partial \omega}$.

Re-write Eq.(2.13a) as follows

$$\mathbf{R}(r,\omega) = \mathbf{S}^{\infty}(r,\omega)\Phi(r,\omega) \tag{2.54}$$

The dimension of the right-hand-side term $\mathbf{R}(r,\omega)$, which is evaluated from Eq.(2.8c), is $[L]^{s}[T]^{-1}$, where s (=2 for 2-D problems or =3 for 3-D problems) is the spatial dimension of an acoustic fluid. The dimension of $\Phi(r,\omega)$, which

satisfies Eq.(2.2), is $[L]^2[T]^{-1}$, and thus the dimension of $\mathbf{S}^{\infty}(r,\omega)$ should be $[L]^{s-2}$ $(=[L]^s[T]^{-1}/[L]^2[T]^{-1})$. In addition, the dynamic stiffness $\mathbf{S}^{\infty}(r,\omega)$ is a function of acoustic fluid density ρ, a characteristic length r, a frequency ω and the bulk modulus of an acoustic fluid β. The dimension of ρ, r, ω and β are $[L]^{-3}[M]$, $[L]$, $[T]^{-1}$ and $[L]^{-1}[M][T]^{-2}$, respectively. $[L]$, $[M]$ and $[T]$ are the dimensions of length, mass and time, respectively.

Assume that the quantity $\left(\mathbf{S}^{\infty}(r,\omega)\right)^{n_1} r^{n_2}\beta^{n_3}\rho^{n_4}\omega^{n_5}$ is dimensionless. By substituting associated dimensions of the dimensionless quantities into it, the equations can be produced as follows.

$$(s-2)n_1 + n_2 - n_3 - 3n_4 = 0 \tag{2.55a}$$

$$n_3 + n_4 = 0 \tag{2.55b}$$

$$-2n_3 - n_5 = 0 \tag{2.55c}$$

The rank of the coefficient matrix in Eqs.(2.55a-c) having 3 equations but 5 unknown variables is 3. Thus, it permits the two unknown variables n_1, n_5 to be chosen arbitrarily. Setting $n_1 = 1$ and $n_5 = 0$ yields $n_3 = 0, n_4 = 0, n_2 = 2-s$. By substituting these coefficients into the above dimensionless quantity, the dimensionless quantity becomes $\mathbf{S}^{\infty}(r,\omega)r^{2-s}$. When setting $n_1 = 0$ and $n_5 = 1$, $n_3 = -0.5, n_4 = 0.5, n_2 = 1$ and the dimensionless quantity becomes $r\beta^{-0.5}\rho^{0.5}\omega$. If it is denoted by a_0, $a_0 = r\omega/c_s$ which stands for a dimensionless frequency with $c_s = \sqrt{\beta/\rho}$ which represents the wave velocity in fluid medium. Note that a_0 varies with r and ω. Hence, the first dimensionless expression $\mathbf{S}^{\infty}(r,\omega)r^{2-s}$ can be equated to $\overline{\mathbf{S}}^{\infty}(a_0)$ which is defined as a function of the second dimensionless

variable a_0 as follows.

$$\mathbf{S}^{\infty}(r,\omega) = r^{s-2}\bar{\mathbf{S}}^{\infty}(a_0) \tag{2.56}$$

Based on the dimensional analysis alone, the arbitrary function $\bar{\mathbf{S}}^{\infty}(a_0)$ can not be determined. Note that ω and r do not appear explicitly in $\bar{\mathbf{S}}^{\infty}(a_0)$, but always in a product of ω and r. For different characteristic lengths r and different frequencies ω, the term $\mathbf{S}^{\infty}(r,\omega)$ has different value.

Consider two interfaces at r_i (interior) and r_e (exterior) as shown in Fig.2.2a and assume that $\mathbf{S}^{\infty}(r_i,\omega)$ is known. The dynamic-stiffness matrix at r_e can be calculated using $a_0 = \omega r_i / c_s = (r_i/r_e)\omega(r_e/c_s)$. It means that the frequency at r_e is $(r_i/r_e)\omega$ while the frequency at r_i is ω corresponding to the same dimensionless frequency a_0. From Eq.(2.56), we have

$$\left(\frac{1}{r_e}\right)^{s-2}\mathbf{S}^{\infty}\left(r_e,\frac{r_i}{r_e}\omega\right) = \left(\frac{1}{r_i}\right)^{s-2}\mathbf{S}^{\infty}(r_i,\omega) = \bar{\mathbf{S}}^{\infty}(a_0) \tag{2.57}$$

Re-arranging Eq.(2.57) leads to

$$\mathbf{S}^{\infty}\left(r_e,\frac{r_i}{r_e}\omega\right) = \left(\frac{r_e}{r_i}\right)^{s-2}\mathbf{S}^{\infty}(r_i,\omega) \tag{2.58}$$

Eq.(2.58) is a form of the relationship between two dynamic-stiffness matrices of similar interfaces in an unbounded fluid medium. For the analysis in frequency domain, another form is often used. Note that the dynamic-stiffness matrix is as a function of the characteristic length r and of the excitation frequency ω. By virtue of chain rule, the derivatives of $\bar{\mathbf{S}}^{\infty}(a_0)$ with respect to r and ω can be written as:

$$\frac{\partial\bar{\mathbf{S}}^{\infty}(a_0)}{\partial\omega} = \frac{\partial\bar{\mathbf{S}}^{\infty}(a_0)}{\partial a_0}\frac{\partial a_0}{\partial\omega} = \frac{r}{c_s}\frac{\partial\bar{\mathbf{S}}^{\infty}(a_0)}{\partial a_0} \tag{2.59a}$$

$$\frac{\partial \bar{\mathbf{S}}^{\infty}(a_0)}{\partial r} = \frac{\partial \bar{\mathbf{S}}^{\infty}(a_0)}{\partial a_0}\frac{\partial a_0}{\partial r} = \frac{\omega}{c_s}\frac{\partial \bar{\mathbf{S}}^{\infty}(a_0)}{\partial a_0} \tag{2.59b}$$

Thus,

$$\omega\frac{\partial \bar{\mathbf{S}}^{\infty}(a_0)}{\partial \omega} = r\frac{\partial \bar{\mathbf{S}}^{\infty}(a_0)}{\partial r} \tag{2.59c}$$

From Eq.(2.56), we have

$$\frac{\partial \bar{\mathbf{S}}^{\infty}(a_0)}{\partial r} = \frac{1}{r^{s-2}}\left(\frac{2-s}{r}\mathbf{S}^{\infty}(r,\omega) + \frac{\partial \mathbf{S}^{\infty}(r,\omega)}{\partial r}\right) \tag{2.60a}$$

$$\frac{\partial \bar{\mathbf{S}}^{\infty}(a_0)}{\partial \omega} = \frac{1}{r^{s-2}}\frac{\partial \mathbf{S}^{\infty}(r,\omega)}{\partial \omega} \tag{2.60b}$$

Substituting Eqs.(2.60a) and (2.60b) into Eq.(2.59c) yields

$$r\frac{\partial \mathbf{S}^{\infty}(r,\omega)}{\partial r} = (s-2)\mathbf{S}^{\infty}(r,\omega) + \omega\frac{\partial \mathbf{S}^{\infty}(r,\omega)}{\partial \omega} \tag{2.61}$$

Note that the left hand side of Eq.(2.61) is the term appeared in Eq.(2.53) and the right hand side of Eq.(2.61) consists of the terms $\mathbf{S}^{\infty}(r,\omega)$ and it is derivative with respect to ω only.

2.4.3 FINAL FREQUENCY EQUATION

Substituting Eq.(2.61) into Eq.(2.53) leads to

$$\left(\mathbf{S}^{\infty}(r,\omega) + \mathbf{E}^{1}\right)\mathbf{E}^{0^{-1}}\left(\mathbf{S}^{\infty}(r,\omega) + \mathbf{E}^{1^{T}}\right) - (s-2)\mathbf{S}^{\infty}(r,\omega) - \omega\frac{\partial \mathbf{S}^{\infty}(r,\omega)}{\partial \omega} - \mathbf{E}^{2} + \omega^{2}\mathbf{M}^{0} = 0 \tag{2.62}$$

Eq.(2.62) is the SBFEM equation for the frequency-domain analysis. It is a system of non-linear ordinary differential equations of first order. Note that the coefficient matrices $\mathbf{E}^0$, $\mathbf{E}^1$, $\mathbf{E}^2$ and $\mathbf{M}^0$ which have the form of Eqs.(2.36a-c) and (2.39) are functions of the characteristic length r only. When the characteristic length r is chosen, (for example, the fluid-structure interface is chosen as the surface with

the characteristic length r), Eq.(2.62) has only one independent variable which is the frequency ω and is re-formulated as

$$\left(\mathbf{S}^{\infty}(\omega)+\mathbf{E}^{1}\right)\mathbf{E}^{0\,-1}\left(\mathbf{S}^{\infty}(\omega)+\mathbf{E}^{1\,\mathrm{T}}\right)-(s-2)\mathbf{S}^{\infty}(\omega) - \omega\frac{\partial\mathbf{S}^{\infty}(\omega)}{\partial\omega}-\mathbf{E}^{2}+\omega^{2}\mathbf{M}^{0}=0 \tag{2.63}$$

Note that the form of the SBFEM equation (2.63) is identical to that for soil infinite medium but their coefficient matrices are totally different.

2.5 SBFEM FORMULATION IN TIME DOMAIN

The SBFEM equation in time domain can be obtained easily by applying the inverse Fourier transformation to Eq.(2.63). By comparing the SBFEM equation in Eq.(2.63) with that for soil infinite medium developed by Wolf and Song (1996a), it can be found that both of them are identical. Because the inverse Fourier transformation is a pure mathematic transformation and is independent of material properties of an infinite medium, the SBFEM equations in time domain for an infinite fluid and a soil medium are the same, which are in the form of

$$\int_0^t\mathbf{m}^{\infty}(t-\tau)\mathbf{m}^{\infty}(\tau)d\tau+\mathbf{e}^{1}\int_0^t\int_0^{\tau}\mathbf{m}^{\infty}(\tau')d\tau'd\tau+\int_0^t\int_0^{\tau}\mathbf{m}^{\infty}(\tau')d\tau'd\tau\mathbf{e}^{1\,\mathrm{T}} + t\int_0^t\mathbf{m}^{\infty}(\tau)d\tau-\frac{t^{3}}{6}\mathbf{e}^{2}H(t)-t\mathbf{m}^{0}H(t)=0 \tag{2.64}$$

where

$$\mathbf{m}^{\infty}(t)=\mathbf{U}^{-1\,\mathrm{T}}\mathbf{M}^{\infty}(t)\mathbf{U}^{-1} \tag{2.65}$$

and

$$\mathbf{e}^{1}=\mathbf{U}^{-1\,\mathrm{T}}\mathbf{E}^{1}\mathbf{U}^{-1}-\frac{s+1}{2}\mathbf{I} \tag{2.66a}$$

$$\mathbf{e}^{2}=\mathbf{U}^{-1\,\mathrm{T}}\left(\mathbf{E}^{2}-\mathbf{E}^{1}\mathbf{E}^{0\,-1}\mathbf{E}^{1\,\mathrm{T}}\right)\mathbf{U}^{-1} \tag{2.66b}$$

$$\mathbf{m}^{0}=\mathbf{U}^{-1\,\mathrm{T}}\mathbf{M}^{0}\mathbf{U}^{-1} \tag{2.66c}$$

in which $\mathbf{U}$ can be obtained by decomposing $\mathbf{E}^{0}$ via a Cholesky's method such

that

$$\mathbf{E}^0 = \mathbf{U}^{\mathrm{T}}\mathbf{U} \tag{2.67}$$

and $\mathbf{M}^{\infty}(\mathrm{t})$ satisfies Eq.(2.12b). Note that $\mathbf{e}^2$ is symmetric and $\mathbf{m}^0$ is positive definite and symmetric. After determining $\mathbf{m}^{\infty}(\mathrm{t})$ from Eq.(2.64), the matrix $\mathbf{M}^{\infty}(\mathrm{t})$ can be obtained as

$$\mathbf{M}^{\infty}(\mathrm{t}) = \mathbf{U}^{\mathrm{T}}\mathbf{m}^{\infty}(\mathrm{t})\mathbf{U} \tag{2.68}$$

Hence, the velocity-to-velocity-potential relationship in Eq.(2.12b) is determined. Details of the inverse Fourier transformation can be found in the literature (Wolf and Song (1996a)). The numerical solution for Eq.(2.64) is described in next section.

2.6 NUMERICAL SOLUTION FOR $\mathbf{M}^{\infty}(\mathrm{t})$

For the discretization of Eq.(2.64) with respect to time, $\mathbf{m}^{\infty}(\mathrm{t})$ is assumed to be constant within each of the time steps. As a consequence, integral terms in Eq.(2.64) at time t $(=\mathrm{n}\Delta\mathrm{t})$ are approximated as follows.

$$\mathbf{I}_{\mathrm{n}} = \int_0^{\mathrm{n}\Delta\mathrm{t}} \mathbf{m}^{\infty}(\tau)\mathrm{d}\tau = \mathbf{I}_{\mathrm{n}-1} + \Delta\mathrm{t}\mathbf{m}_{\mathrm{n}}^{\infty} \tag{2.69a}$$

$$\mathbf{J}_{\mathrm{n}} = \int_0^{\mathrm{n}\Delta\mathrm{t}} \int_0^{\tau} \mathbf{m}^{\infty}(\tau')\mathrm{d}\tau'\mathrm{d}\tau = \mathbf{J}_{\mathrm{n}-1} + \Delta\mathrm{t}\mathbf{I}_{\mathrm{n}-1} + \frac{\Delta\mathrm{t}^2}{2}\mathbf{m}_{\mathrm{n}}^{\infty} \tag{2.69b}$$

$$\int_0^{\mathrm{t}} \mathbf{m}^{\infty}(\mathrm{t}-\tau)\mathbf{m}^{\infty}(\tau)\mathrm{d}\tau = \Delta\mathrm{t}\sum_{\mathrm{j}=1}^{\mathrm{n}} \mathbf{m}_{\mathrm{n}-\mathrm{j}+1}^{\infty}\mathbf{m}_{\mathrm{j}}^{\infty} \tag{2.69c}$$

where $\Delta\mathrm{t}$ denotes time increment and $\mathbf{m}_{\mathrm{j}}^{\infty} = \mathbf{m}^{\infty}(\mathrm{j}\Delta\mathrm{t})$.

For $\mathrm{n}=1$, i.e. the first time-step, substituting Eqs.(2.69a-c) into Eq.(2.64) yields

$$\mathbf{m}_1^{\infty 2} + \frac{\Delta t}{2}\left(\mathbf{e}^1 + \mathbf{I}\right)\mathbf{m}_1^{\infty} + \mathbf{m}_1^{\infty}\frac{\Delta t}{2}\left(\mathbf{e}^{1\mathrm{T}} + \mathbf{I}\right) - \frac{\Delta t^2}{6}\mathbf{e}^2 - \mathbf{m}^0 = 0 \tag{2.70}$$

Eq.(2.70) is the algebraic Riccati equation, which can be computed by an algorithm based on Schur factorization of an extended matrix of size twice the order $\mathbf{m}_1^{\infty}$ and has a unique symmetric semi-positive definite solution. Upon determining $\mathbf{m}_1^{\infty}$, $\mathbf{M}_1^{\infty}$ can be obtained by the transformation

$$\mathbf{M}_1^{\infty} = \mathbf{U}^{\mathrm{T}}\mathbf{m}_1^{\infty}\mathbf{U} \tag{2.71}$$

Note that by taking the limit $\Delta t \to 0$, Eq.(2.70) results in

$$\mathbf{m}_1^{\infty 2} = \mathbf{m}^0 \tag{2.72}$$

Substituting Eq.(2.72) into Eq.(2.71) yields the value of $\mathbf{M}^{\infty}(t=0)$.

For $n \geq 2$, Eq.(2.64) is discretized as follows.

$$\begin{aligned}\left(\mathbf{m}_1^{\infty} + \frac{\Delta t}{2}\mathbf{e}^1\right)\mathbf{m}_n^{\infty} + \mathbf{m}_n^{\infty}\left(\mathbf{m}_1^{\infty} + \frac{\Delta t}{2}\mathbf{e}^{1\mathrm{T}}\right) + t\mathbf{m}_n^{\infty} = -\sum_{j=2}^{n-1}\mathbf{m}_{n-j+1}^{\infty}\mathbf{m}_j^{\infty} \\ -\mathbf{e}^1\left(\frac{\mathbf{J}_{n-1}}{\Delta t} + \mathbf{I}_{n-1}\right) - \left(\frac{\mathbf{J}_{n-1}}{\Delta t} + \mathbf{I}_{n-1}\right)\mathbf{e}^{1\mathrm{T}} + \frac{n^3\Delta t^2}{6}\mathbf{e}^2 + n\left(\mathbf{m}^0 - \mathbf{I}_{n-1}\right)\end{aligned} \tag{2.73}$$

Eq.(2.73) is a Lyapunov equation in the form of

$$\mathbf{AX} + \mathbf{XA}^{\mathrm{T}} + t\mathbf{X} = \mathbf{C} \tag{2.74}$$

which can be solved. Upon determining $\mathbf{m}_n^{\infty}$, $\mathbf{M}_n^{\infty}$ can be obtained by the transformation

$$\mathbf{M}_n^{\infty} = \mathbf{U}^{\mathrm{T}}\mathbf{m}_n^{\infty}\mathbf{U} \tag{2.75}$$

Note that all matrices $\mathbf{m}_j^{\infty}$, $\mathbf{M}_j^{\infty}$ $(j = 1,2,...,n)$ are symmetric. It can be proved through Eq.(2.73) minus the transpose of Eq.(2.73).

For short-duration cases, using Eqs.(2.69)-(2.75) can work out $\mathbf{M}^{\infty}(t)$ with ease,

but using Eqs.(2.69)-(2.75) to solve $\mathbf{M}^{\infty}(t)$ becomes expensive in computational cost for long-duration cases. In next section, a new approximate numerical method for $\mathbf{M}^{\infty}(t)$ is proposed.

2.7 ANOTHER NUMERICAL SOLUTION FOR $\mathbf{M}^{\infty}(t)$

To achieve $\mathbf{M}^{\infty}(t)$, the $\mathbf{M}^{\infty}(t)$ is decomposed as

$$\mathbf{M}^{\infty}(t) = \mathbf{C}\,H(t) + \mathbf{K}^{\infty} t\,H(t) + \mathbf{M}_f^{\infty}(t) \tag{2.76}$$

with the static-stiffness matrix of an unbounded medium $\mathbf{K}^{\infty}$ and an coefficient matrix $\mathbf{C}$ chosen in such a way as to achieve $\mathbf{M}_f^{\infty}(t \to \infty) = \mathbf{0}$. For a 2D axisymmetrical problem with an unbounded fluid medium, the dimension of $\mathbf{M}^{\infty}(t)$ is 1x1, because the coefficients matrices $\mathbf{E}^0$, $\mathbf{E}^1$, and $\mathbf{E}^2$ equal to 2π, 0 and 0, respectively. The corresponding $\mathbf{M}^{\infty}(t)$ can be obtained quickly by using Eqs.(2.69)-(2.75) and the time-history profile of $\mathbf{M}^{\infty}(t)$ is shown in Fig.2.4.

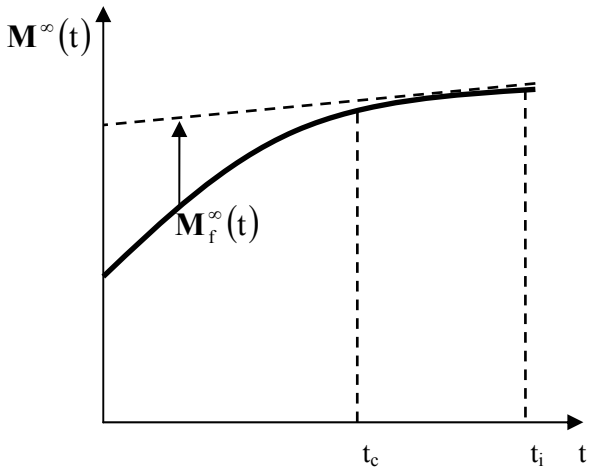

Fig.2.4 The time-history of a 1x1 $\mathbf{M}^{\infty}(t)$

From Fig.2.4, one can see that the slope of the curve becomes smaller and smaller

when time increases; the slope tends to zero when time $\to \infty$ and the slopes of the curve at time "t_c" (called cut-off time) and time infinity "t_i" are very small, so the slope of the curve (the first derivative of $\mathbf{M}^{\infty}(t)$ with respect to time) between time "t_c" and time infinity "t_i" can be assumed to compose an arithmetical progression. After discretization of the $\mathbf{M}^{\infty}(t)$ with respect to time, the $\mathbf{M}^{\infty}(t)$ is assumed to be constant within each of the time steps and assume that

$$t_i - t_c = n\Delta t \tag{2.77}$$

where n is the number of time step Δt between time t_c and time t_i. Such that, the arithmetical progression can be expressed as follows

$$\frac{d\mathbf{M}^{\infty}(t_c)}{dt} - n\Delta k = \frac{d\mathbf{M}^{\infty}(t_i)}{dt} \tag{2.78}$$

with an arithmetical mean Δk and $\frac{d\mathbf{M}^{\infty}(t_i)}{dt} = 0$ when time "t_i" tends to infinity.

When time t_c, time t_i and time step Δt are chosen, the Δk and n are easy to determine, so how to choose the "cut-off" time "t_c" and the time infinity "t_i" becomes important. A numerical method is proposed to determine the "cut-off" time "t_c" and the time infinity "t_i" in the following sections.

2.7.1 Cut-off time "t_c"

From Fig.2.4, one can find that the value of the $\frac{d\mathbf{M}^{\infty}(t)}{dt}$ is very small at late time, so the "cut-off" time "t_c" can be determined through using the following formula

$$\left(\frac{d\mathbf{M}^{\infty}(t_c)}{dt}\right) \Big/ \left(\frac{d\mathbf{M}^{\infty}(t_c + \Delta t)}{dt}\right) - 1 \le \text{tol} \tag{2.79}$$

with an error tolerance "tol". The first derivatives $\frac{d\mathbf{M}^{\infty}(t_c)}{dt}$ and $\frac{d\mathbf{M}^{\infty}(t_c + \Delta t)}{dt}$

can be solved approximately by using the following formulas, repectively.

$$\frac{d\mathbf{M}^{\infty}(t_c)}{dt} \approx \frac{\mathbf{M}^{\infty}(t_c) - \mathbf{M}^{\infty}(t_c - \Delta t)}{\Delta t} \tag{2.80a}$$

$$\frac{d\mathbf{M}^{\infty}(t_c + \Delta t)}{dt} \approx \frac{\mathbf{M}^{\infty}(t_c + \Delta t) - \mathbf{M}^{\infty}(t_c)}{\Delta t} \tag{2.80b}$$

After choosing the error tolerance "tol" and determining these $\mathbf{M}^{\infty}(t_c - \Delta t)$, $\mathbf{M}^{\infty}(t_c)$, $\mathbf{M}^{\infty}(t_c + \Delta t)$, the "cut-off" time "$t_c$" can be determined by using Eqs.(2.79-80).

2.7.2 Time infinity "t_i"

In principle, the time infinity "t_i" can be chosen as any time more than the final time "t_e" of an analysis. However, from Eq.(2.78), one can see that the arithmetical mean Δk will be too large or too small when the time infinity "t_i" is too small or too large. Obviously, these too large or too small Δk will induce an incorrect solution of $\mathbf{M}^{\infty}(t)$. So it is necessary to choose an appropriate time infinity "t_i". A process for determining the time infinity "t_i" is presented in the following.

Firstly, use the method presented in section 2.6 to determine all 1x1 $\mathbf{M}^{\infty}(t)$ from time zero to final time "t_e".

Secondly, employ the method presented in section 2.7.1 to determine the "cut-off" time "t_c".

Thirdly, choose an initial time infinity "t_i" and use the initial "t_i" to calculate the $\mathbf{M}^{\infty}(t)$ between the "cut-off" time "t_c" and final time "t_e". Re-formulate Eq.(2.77) as follows.

$$n = (t_i - t_c)/\Delta t \tag{2.81}$$

Substituting Eq.(2.81) and $\frac{d\mathbf{M}^{\infty}(t_i)}{dt} = 0$ into Eq.(2.78) yields

$$\frac{d\mathbf{M}^{\infty}(t_c)}{dt} - \frac{t_i - t_c}{\Delta t}\Delta k = 0 \tag{2. 82a}$$

Substituting Eq.(2.80a) into Eq.(2.82a) leads to

$$\frac{\mathbf{M}^{\infty}(t_c) - \mathbf{M}^{\infty}(t_c - \Delta t)}{\Delta t} - \frac{t_i - t_c}{\Delta t}\Delta k = 0 \tag{2. 82b}$$

So the Δk satisfies

$$\Delta k = \left(\mathbf{M}^{\infty}(t_c) - \mathbf{M}^{\infty}(t_c - \Delta t)\right)/(t_i - t_c) \tag{2. 82c}$$

After determining the Δk, the $\frac{d\mathbf{M}^{\infty}(t)}{dt}$ at time $t_c + j\Delta t$ can be expressed approximately as

$$\frac{d\mathbf{M}^{\infty}(t_c + j\Delta t)}{dt} = \frac{d\mathbf{M}^{\infty}(t_c + j\Delta t - \Delta t)}{dt} - \Delta k \tag{2. 83}$$

where j denotes the j^{th} time step after the "cut-off" time t_c. As the $\frac{d\mathbf{M}^{\infty}(t_c + j\Delta t)}{dt}$ can be expressed as follows,

$$\frac{d\mathbf{M}^{\infty}(t_c + j\Delta t)}{dt} \approx \frac{\mathbf{M}^{\infty}(t_c + j\Delta t) - \mathbf{M}^{\infty}(t_c + j\Delta t - \Delta t)}{\Delta t} \tag{2. 84}$$

Eq.(2.83) is re-written as

$$\mathbf{M}^{\infty}(t_c + j\Delta t) = \mathbf{M}^{\infty}(t_c + j\Delta t - \Delta t) + \left(\frac{d\mathbf{M}^{\infty}(t_c + j\Delta t - \Delta t)}{dt} - \Delta k\right)\Delta t \tag{2. 85}$$

Through substituting Eq.(2.78) into Eq.(2.85) and as Eq.(2.78) is a arithmetical progression, Eq.(2.85) can be re-formulated as

$$\mathbf{M}^{\infty}(t_c + j\Delta t) = \mathbf{M}^{\infty}(t_c + j\Delta t - \Delta t) + \left(\frac{d\mathbf{M}^{\infty}(t_c)}{dt} - j\Delta k\right)\Delta t \tag{2. 86}$$

Eq.(2.86) is a recurrence formula. Therefore, all the $\mathbf{M}^{\infty}(t_c + j\Delta t)$ can be calculated by using Eq.(2.86) when knowing the Δk, $\mathbf{M}^{\infty}(t_c)$, and $\frac{d\mathbf{M}^{\infty}(t_c)}{dt}$.

Fourthly, determine a proper time infinity "t_i". To judge whether the chosen initial time "t_i" is proper or not, a comparison between the two values of $\mathbf{M}^{\infty}(t_e)$ at final time "t_e" obtained by using the above two methods, respectively, must be made. Here use the symbol $\mathbf{M}^{\infty}(t_e)_c$ to denote the value of $\mathbf{M}^{\infty}(t_e)$ obtained by using the method presented in section 2.6, while use the symbol $\mathbf{M}^{\infty}(t_e)_r$ to denote the value of $\mathbf{M}^{\infty}(t_e)$ obtained by using the recurrence formula in Eq.(2.86). When $\mathbf{M}^{\infty}(t_e)_r - \mathbf{M}^{\infty}(t_e)_c > 0$, that means that the time "t_i" is too large so that the Δk is too small. Reversely, when $\mathbf{M}^{\infty}(t_e)_r - \mathbf{M}^{\infty}(t_e)_c < 0$, that means that the time "t_i" is too small so that the Δk is too large. When $\mathbf{M}^{\infty}(t_e)_r \approx \mathbf{M}^{\infty}(t_e)_c$, that means that the time "ti" is proper. Therefore, the time infinity "t_i" is determined. As the dimension of the $\mathbf{M}^{\infty}(t)$ is 1x1, the process of determining the proper "t_i" is fast.

Note that all characteristics and formulations of the 1x1 $\mathbf{M}^{\infty}(t)$ in the section 2.7 are corresponding to a 2D axisymmetrical problem with an unbounded fluid medium. That is to say, all characteristics and formulations of the 1x1 $\mathbf{M}^{\infty}(t)$ in the section 2.7 are corresponding to a 2D axisymmetrical surface with an unbounded fluid medium. Obviously, a 2D axisymmetrical problem can be modeled by some non-axisymmetrical elements, which induces that the dimension of the $\mathbf{M}^{\infty}(t)$ for an unbounded medium is not 1x1 any more. But the 1x1 $\mathbf{M}^{\infty}(t)$ and the non-1x1 $\mathbf{M}^{\infty}(t)$ must have same characteristics because the $\mathbf{M}^{\infty}(t)$ only

depends on the geometry of the surface with a characteristic length r_i as shown in Fig.2.2a. That means that the 1x1 $\mathbf{M}^{\infty}(t)$ and the non-1x1 $\mathbf{M}^{\infty}(t)$ have the same "cut-off" time "t_c", the time infinity "t_i" and the same recurrence formula in Eq.(2.86) . Such that, the "cut-off" time "t_c" and time infinity "t_i" of the non-1x1 $\mathbf{M}^{\infty}(t)$ for a non-axisymmetrical problem with a 2D axisymmetrical surface can be determined by those of an axisymmetrical problem with the same 2D axisymmetrical surface. The non-1x1 $\mathbf{M}^{\infty}(t)$ can be determined through using Eq.(2.86) after knowing the Δk obtained by using Eq.(2.82c). These operations will save lots of computational efforts for the $\mathbf{M}^{\infty}(t)$ and their correctness is verified in Chapter 6.

CHAPTER THREE

SBFEM FORMULATION FOR LAYERED INFINITE FLUID MEDIUM

In practice, certain fluid-structure interaction problems such as dam-reservoir interaction problems including a layered infinite fluid medium are often encountered. Although these dam-reservoir interaction problems have been solved using traditional numerical methods (FEM or BEM) in combination with a transmitting boundary, the traditional method's efficiency and universality are still dubious. In this chapter, a SBFEM formulation for a layered infinite fluid medium is presented. Its accuracy, efficiency and universality are described in chapters 7 and 8.

3.1 SBFEM MODELING FOR LAYERED SEMI-INFINITE FLUID MEDIUM

Recall Fig.2.1b, in which a semi-infinite fluid medium is bounded by two surfaces Oj and Oi. When these two surfaces are parallel to each other, the semi-infinite fluid becomes a layered semi-infinite medium as shown in Fig.3.1 and the scalar center O is located at infinity on the left-hand side. Note that in a submerged structure-fluid system, surfaces Oj and Oi do not serve as the boundaries of the semi-infinite fluid medium because the unique boundary of the infinite fluid medium is the fluid-structure interface. However, in a layered semi-infinite system, the surfaces Oj and Oi serve as the boundaries of the layered semi-infinite fluid

medium. In the following formulation, the boundary conditions on these surfaces are taken as zero-displacement or zero-pressure. The corresponding formulations for a solid medium derived by Wolf and Song (1996a) have the same assumption. For some special cases where these boundary conditions are not zero displacement, SBFEM formulations are derived in chapter 4.

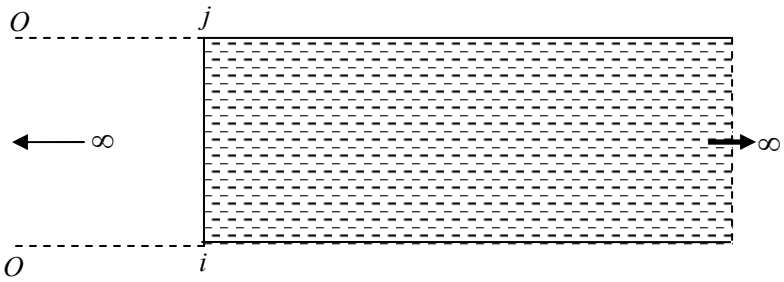

Fig.3.1 A layered semi-infinite medium

Consider a layered semi-infinite fluid medium shown in Fig.3.1 which is bounded by two surfaces Oj, Oi and the side surface ij. When using the SBFEM to model the layered semi-infinite fluid medium, only the surface ij needs to be discretized. A typical SBFEM mesh is shown in Fig.3.2. (Here, the surface ij is assumed to be perpendicular to the two surfaces Oj and Oi, in order to reduce the effect of the reflection waves.) Each element $i'\dot{j}'$ represents the region L'_{ij}, so that the whole layered semi-infinite medium is represented by an assembly of elements along the surface ij.

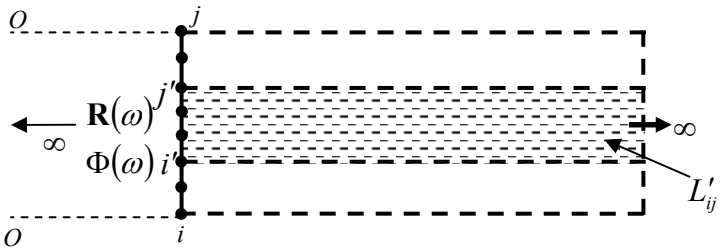

Fig.3.2 SBFEM mesh of the layered semi-infinite medium

On the surface ij, the relationship between velocity potential and normal velocity in frequency domain can be written as

$$\mathbf{R}(\omega)=\mathbf{S}^{\infty}(\omega)\Phi(\omega) \tag{3.1a}$$

$$\mathbf{R}(\omega)=\mathbf{M}^{\infty}(\omega)\ddot{\Phi}(\omega) \tag{3.1b}$$

where $\mathbf{R}(\omega)$ has the form of Eq.(2.8c); $\Phi(\omega)$ denotes the nodal velocity potential vector; $\mathbf{S}^{\infty}(\omega)$ and $\mathbf{M}^{\infty}(\omega)$ are called the "dynamic stiffness" and "dynamic mass" , respectively, of the layered semi-infinite fluid medium. They satisfy

$$\mathbf{S}^{\infty}(\omega)=(\mathrm{i}\omega)^2\mathbf{M}^{\infty}(\omega) \tag{3.2}$$

By applying inverse Fourier transformation to Eqs.(3.1a) and (3.1b) and imposing the following zero initial conditions,

$$\Phi(t=0)=\mathbf{0} \tag{3.3a}$$

$$\dot{\Phi}(t=0)=\mathbf{0} \tag{3.3b}$$

Eqs.(3.1a) and (3.1b) are re-formulated in time domain as

$$\mathbf{R}(t)=\int_0^t\mathbf{S}^{\infty}(t-\tau)\Phi(\tau)\mathrm{d}\tau \tag{3.4a}$$

$$\mathbf{R}(t)=\int_0^t\mathbf{M}^{\infty}(t-\tau)\ddot{\Phi}(\tau)\mathrm{d}\tau \tag{3.4b}$$

where $\mathbf{S}^{\infty}(t)$ and $\mathbf{S}^{\infty}(\omega)$, $\mathbf{M}^{\infty}(t)$ and $\mathbf{M}^{\infty}(\omega)$, $\mathbf{R}^{\infty}(t)$ and $\mathbf{R}^{\infty}(\omega)$ are Fourier transform pairs, respectively. The superscript ∞ denotes infinite medium. Note

that the "dynamic stiffness" $\mathbf{S}^{\infty}(\omega)$ and the "dynamic mass" $\mathbf{M}^{\infty}(\omega)$ are both dependant of the geometry of the surface ij. Therefore $\mathbf{S}^{\infty}(\omega)$ and $\mathbf{M}^{\infty}(\omega)$ can be written as $\mathbf{S}^{\infty}(\mathrm{r},\omega)$ and $\mathbf{M}^{\infty}(\mathrm{r},\omega)$ with a characteristic length r. The expression for $\mathbf{S}^{\infty}(\omega)$ can be derived from a scalar-finite-element (SFE) cell bounded by face 1 and face 2 shown in Fig.3.3.

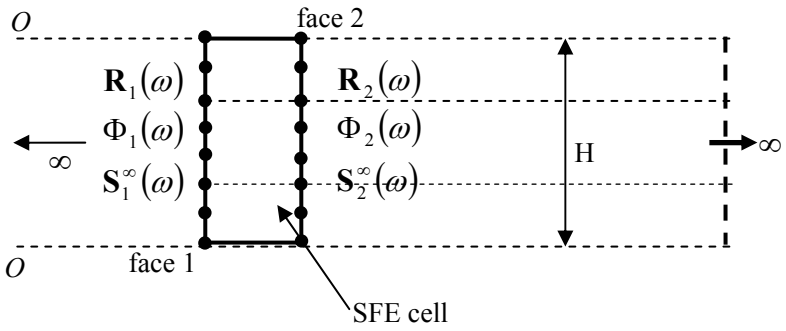

Fig.3.3 Scalar-finite-element cell

3.2 SBFEM FORMULATION FOR LAYERED INFINITE MEDIUM

The "dynamic stiffness" relationship between face 1 and face 2 has the same form of Eq.(2.21), which is rewritten as

$$\mathbf{S}_1^{\infty}(\omega)=\mathbf{S}_{11}(\omega)-\mathbf{S}_{12}(\omega)\left(\mathbf{S}_2^{\infty}(\omega)+\mathbf{S}_{22}(\omega)\right)^{-1}\mathbf{S}_{21}(\omega) \tag{3.5a}$$

According to Eq.(2.58), we have $\mathbf{S}_1^{\infty}(\omega)=\mathbf{S}_2^{\infty}(\omega)=\mathbf{S}^{\infty}(\omega)$ because the characteristic lengths $\mathrm{r}_1=\mathrm{r}_2=\infty$. Hence, Eq.(3.5a) can be rewritten as

$$\mathbf{S}^{\infty}(\omega)=\mathbf{S}_{11}(\omega)-\mathbf{S}_{12}(\omega)\left(\mathbf{S}^{\infty}(\omega)+\mathbf{S}_{22}(\omega)\right)^{-1}\mathbf{S}_{21}(\omega) \tag{3.5b}$$

The solution for $\mathbf{S}^{\infty}(\omega)$ in Eq.(3.5b) can be determined after all coefficient matrices are known. The coefficient matrices $\mathbf{S}_{11}(\omega)$, $\mathbf{S}_{12}(\omega)$, $\mathbf{S}_{21}(\omega)$ and

$\mathbf{S}_{22}(\omega)$ are the sub-matrices of the global dynamic stiffness $\mathbf{S}(\omega)$ of the SFE cell corresponding to the face 1 and the face 2, respectively. The global dynamic stiffness $\mathbf{S}(\omega)$ satisfies

$$\mathbf{S}=\begin{bmatrix}\mathbf{S}_{11} & \mathbf{S}_{12}\\ \mathbf{S}_{21} & \mathbf{S}_{22}\end{bmatrix}=\begin{bmatrix}\mathbf{K}_{11} & \mathbf{K}_{12}\\ \mathbf{K}_{21} & \mathbf{K}_{22}\end{bmatrix}-\omega^2\begin{bmatrix}\mathbf{M}_{11} & \mathbf{M}_{12}\\ \mathbf{M}_{21} & \mathbf{M}_{22}\end{bmatrix} \tag{3.6}$$

where $\mathbf{K}_{jl}$, $\mathbf{M}_{jl}$ $(j,l=1,2)$ are the sub-matrices of the global stiffness and mass matrices of the SFE cell corresponding to the face 1 and the face 2 and can be obtained by assembling all element stiffness matrices $\mathbf{K}^e$ and mass matrices $\mathbf{M}^e$ in the SFE cell. What follows will show how to determine the element stiffness matrix $\mathbf{K}^e$ and mass matrix $\mathbf{M}^e$ in the SFE cell.

3.2.1 ELEMENT STIFFNESS AND MASS MATRICES

To determine the element stiffness and mass matrices, a 2-dimensional SFE cell is considered and a 6-node element in the SFE cell is analyzed as shown in Fig.3.4. For other types of elements, the same procedure can be used to obtain the matrices.

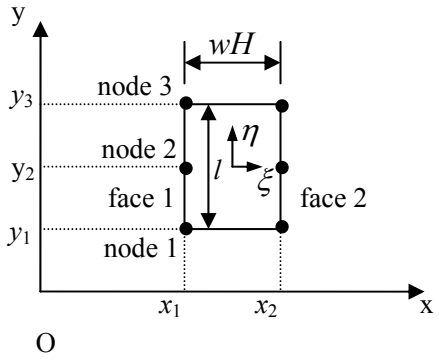

Fig.3.4 A finite element of a SFE cell

The shape function **N** of the element is chosen as

$$\mathbf{N} = \begin{bmatrix} \mathbf{N}_1 & \mathbf{N}_2 \end{bmatrix} = \begin{bmatrix} \frac{1}{2}(1-\xi)\mathbf{N}(\eta) & \frac{1}{2}(1+\xi)\mathbf{N}(\eta) \end{bmatrix} \tag{3.7}$$

where $\mathbf{N}(\eta)$ denotes the shape function in the direction η; the ξ axis corresponds to the radial direction which points from the face 1 towards the infinity on the right side and the η axis corresponds to the circumferential direction. $\xi = -1$ corresponds to the face 1, while $\xi = 1$ corresponds to the face 2. For a 3-node element in the η-direction, $\eta = -1,0,1$ corresponds to the nodes 1,2 and 3, respectively. Hence, the function $\mathbf{N}(\eta)$ is expressed as

$$\mathbf{N}(\eta) = \begin{bmatrix} \frac{1}{2}(\eta^2 - \eta) & 1-\eta^2 & \frac{1}{2}(\eta^2 + \eta) \end{bmatrix} \tag{3.8}$$

The coordinate vectors $\mathbf{x}_2$ and $\mathbf{y}_2$ of nodes lying on the face 2 can be expressed in terms of the nodal coordinate vector $\mathbf{x}_1$ and $\mathbf{y}_1$ of nodes lying on the face 1 and the characteristic width of the SFE w as follows.

$$\mathbf{x}_2 = \mathbf{x}_1 + \begin{bmatrix} wH & wH & wH \end{bmatrix}^T \tag{3.9a}$$

$$\mathbf{y}_2 = \mathbf{y}_1 \tag{3.9b}$$

where w is a very small constant; wH denotes the width of the SFE cell and H denotes the height of the whole layered infinite medium. By using isoparametric mapping technique, the geometrical interpolation for the position of an arbitrary point (x, y) inside the element can be expressed as follows.

$$\begin{Bmatrix} x \\ y \end{Bmatrix}^T = \begin{bmatrix} \mathbf{N}_1 & \mathbf{N}_2 \end{bmatrix} \begin{bmatrix} \mathbf{x}_1 & \mathbf{y}_1 \\ \mathbf{x}_2 & \mathbf{y}_2 \end{bmatrix} \tag{3.10a}$$

Substituting Eq.(3.7) and Eqs.(3.9a,b) into Eq.(3.10a) leads to

$$\begin{Bmatrix} x \\ y \end{Bmatrix}^T = \mathbf{N}(\eta)\begin{bmatrix} \mathbf{x}_1 & \mathbf{y}_1 \end{bmatrix} + \begin{bmatrix} \frac{wH}{2}(1+\xi) & 0 \end{bmatrix} \tag{3.10b}$$

The "Jacobian" matrix $\overline{\mathbf{J}}$, i.e. the differentials of the two mapped coordinate

system is

$$\bar{\mathbf{J}} = \begin{bmatrix} \frac{\partial x}{\partial \xi} & \frac{\partial y}{\partial \xi} \\ \frac{\partial x}{\partial \eta} & \frac{\partial y}{\partial \eta} \end{bmatrix} \tag{3.11a}$$

Substituting Eq.(3.10b) into Eq.(3.11a) yields

$$\bar{\mathbf{J}} = \begin{bmatrix} \frac{w}{2} & 0 \\ 0 & 1 \end{bmatrix} \mathbf{J} \tag{3.11b}$$

where

$$\mathbf{J} = \begin{bmatrix} H & 0 \\ \frac{d\mathbf{N}(\eta)}{d\partial\eta}\mathbf{x}_1 & \frac{d\mathbf{N}(\eta)}{d\eta}\mathbf{y}_1 \end{bmatrix} \tag{3.11c}$$

The determinant of "Jacobian" matrix $\bar{\mathbf{J}}$ is

$$\left|\bar{\mathbf{J}}\right| = \frac{w}{2}\left|\mathbf{J}\right| \tag{3.12}$$

The inverse of the "Jacobian" matrix $\bar{\mathbf{J}}$ is

$$\bar{\mathbf{J}}^{-1} = \mathbf{J}^{-1}\begin{bmatrix} \frac{2}{w} & 0 \\ 0 & 1 \end{bmatrix} \tag{3.13}$$

Denoting the components of $\mathbf{J}^{-1}$ as j_{mn}, i.e.

$$\mathbf{J}^{-1} = \begin{bmatrix} j_{11} & j_{12} \\ j_{21} & j_{22} \end{bmatrix} = \frac{1}{H\frac{d\mathbf{N}(\eta)}{d\eta}\mathbf{y}_1}\begin{bmatrix} \frac{d\mathbf{N}(\eta)}{d\eta}\mathbf{y}_1 & 0 \\ -\frac{d\mathbf{N}(\eta)}{d\eta}\mathbf{x}_1 & H \end{bmatrix} \tag{3.14}$$

We have the derivatives of the shape functions as follows.

$$\begin{Bmatrix} \frac{\partial \mathbf{N}}{\partial x} \\ \frac{\partial \mathbf{N}}{\partial y} \end{Bmatrix} = \bar{\mathbf{J}}^{-1}\begin{Bmatrix} \frac{\partial \mathbf{N}}{\partial \xi} \\ \frac{\partial \mathbf{N}}{\partial \eta} \end{Bmatrix} = \frac{1}{w}\begin{Bmatrix} j_{11} \\ j_{21} \end{Bmatrix}\begin{bmatrix} -\mathbf{N}(\eta) & \mathbf{N}(\eta) \end{bmatrix} + \begin{Bmatrix} j_{12} \\ j_{22} \end{Bmatrix}\begin{bmatrix} \frac{1}{2}(1-\xi)\frac{d\mathbf{N}(\eta)}{d\eta} & \frac{1}{2}(1+\xi)\frac{d\mathbf{N}(\eta)}{d\eta} \end{bmatrix} \tag{3.15a}$$

Eq.(3.15a) is the strain-displacement relationship matrix $\mathbf{B}$ of the fluid medium, which is re-written as

$$\mathbf{B} = \frac{1}{\mathrm{w}}\left[-\mathbf{B}^1 \quad \mathbf{B}^1\right] + \left[\frac{1}{2}(1-\xi)\mathbf{B}^2 \quad \frac{1}{2}(1+\xi)\mathbf{B}^2\right] \tag{3.15b}$$

where

$$\mathbf{B}^1 = \begin{Bmatrix} \mathrm{j}_{11} \\ \mathrm{j}_{21} \end{Bmatrix} \mathbf{N}(\eta) = \frac{1}{\mathrm{H}\dfrac{\mathrm{d}\mathbf{N}(\eta)}{\mathrm{d}\eta}\mathbf{y}_1} \begin{bmatrix} \dfrac{\mathrm{d}\mathbf{N}(\eta)}{\mathrm{d}\eta}\mathbf{y}_1 \\ -\dfrac{\mathrm{d}\mathbf{N}(\eta)}{\mathrm{d}\eta}\mathbf{x}_1 \end{bmatrix} \mathbf{N}(\eta) \tag{3.16a}$$

$$\mathbf{B}^2 = \begin{Bmatrix} \mathrm{j}_{12} \\ \mathrm{j}_{22} \end{Bmatrix} \frac{\mathrm{d}\mathbf{N}(\eta)}{\mathrm{d}\eta} = \frac{1}{\mathrm{H}\dfrac{\mathrm{d}\mathbf{N}(\eta)}{\mathrm{d}\eta}\mathbf{y}_1} \begin{bmatrix} 0 \\ \mathrm{H} \end{bmatrix} \frac{\mathrm{d}\mathbf{N}(\eta)}{\mathrm{d}\eta} \tag{3.16b}$$

Note that $\mathbf{B}^1$ and $\mathbf{B}^2$ are functions of η only.

The formula for an element stiffness matrix, Eq.(2.8b) is re-written as

$$\mathbf{K}^{\mathrm{e}} = \int_{\mathrm{v}^{\mathrm{e}}} \mathbf{B}^{\mathrm{T}}\mathbf{B}\mathrm{d}v^{\mathrm{e}} = \int_{-1}^{1}\int_{-1}^{1} \mathbf{B}^{\mathrm{T}}\mathbf{B}\left|\bar{\mathbf{J}}\right|\mathrm{d}\xi\mathrm{d}\eta \tag{3.17}$$

Note that $\mathbf{K}^{\mathrm{e}}$ can be integrated analytically. Partitioning $\mathbf{K}^{\mathrm{e}}$ into sub-matrices with respect to the face 1 and the face 2 leads to

$$\mathbf{K}^{\mathrm{e}} = \begin{bmatrix} \mathbf{k}_{11} & \mathbf{k}_{12} \\ \mathbf{k}_{21} & \mathbf{k}_{22} \end{bmatrix} \tag{3.18}$$

of which, each sub-matrix $\mathbf{k}_{\mathrm{ij}}$ $(\mathrm{i},\mathrm{j}=1,2)$ can be written as

$$\mathbf{k}_{\mathrm{ij}} = \frac{1}{\mathrm{w}}\mathbf{K}_{\mathrm{ij}}^0 + \mathbf{K}_{\mathrm{ij}}^1 + \mathrm{w}\mathbf{K}_{\mathrm{ij}}^2 \tag{3.19}$$

where

$$\mathbf{K}_{\mathrm{ij}}^0 = \xi_{\mathrm{i}}\xi_{\mathrm{j}}\mathbf{E}^0 \tag{3.20a}$$

$$\mathbf{K}_{\mathrm{ij}}^1 = \frac{\xi_{\mathrm{j}}}{2}\mathbf{E}^1 + \frac{\xi_{\mathrm{i}}}{2}\mathbf{E}^{1\mathrm{T}} \tag{3.20b}$$

$$\mathbf{K}_{\mathrm{ij}}^2 = \frac{1}{4}\left(1 + \frac{\xi_{\mathrm{i}}\xi_{\mathrm{j}}}{3}\right)\mathbf{E}^2 \tag{3.20c}$$

in which

$$\mathbf{E}^0 = \int_{-1}^{1} \mathbf{B}^{1\mathrm{T}} \mathbf{B}^1 |\mathbf{J}| \mathrm{d}\eta \tag{3.21a}$$

$$\mathbf{E}^1 = \int_{-1}^{1} \mathbf{B}^{2\mathrm{T}} \mathbf{B}^1 |\mathbf{J}| \mathrm{d}\eta \tag{3.21b}$$

$$\mathbf{E}^2 = \int_{-1}^{1} \mathbf{B}^{2\mathrm{T}} \mathbf{B}^2 |\mathbf{J}| \mathrm{d}\eta \tag{3.21c}$$

and $\xi_1 = -1$, $\xi_2 = 1$. $\mathbf{E}^0$, $\mathbf{E}^1$ and $\mathbf{E}^2$ can be conveniently determined by numerical integrations. Note that $\mathbf{E}^0$, $\mathbf{E}^1$ and $\mathbf{E}^2$ are functions of η only and thus associated with the discretization of the face 1 of the SFE cell. In addition, $\mathbf{E}^0$ is positive definite and symmetric. $\mathbf{E}^2$ is semi-infinite definite and symmetric.

Similar to the element stiffness matrix, the element mass matrix $\mathbf{M}^{\mathrm{e}}$ (Eq.(2.8a)) can be partitioned into sub-matrices accordingly, i.e.

$$\mathbf{M}^{\mathrm{e}} = \begin{bmatrix} \mathbf{m}_{11} & \mathbf{m}_{12} \\ \mathbf{m}_{21} & \mathbf{m}_{22} \end{bmatrix} \tag{3.22}$$

in which

$$\mathbf{m}_{\mathrm{ij}} = \mathrm{w}\mathbf{M}_{\mathrm{ij}}^2 + \mathrm{O}\left(\mathrm{w}^2\right) = \frac{\mathrm{w}}{4}\left(1 + \frac{\xi_{\mathrm{i}}\xi_{\mathrm{j}}}{3}\right)\mathbf{M}^0 + \mathrm{O}\left(\mathrm{w}^2\right) \tag{3.23}$$

where

$$\mathbf{M}^0 = \int_{-1}^{1} \frac{1}{\mathrm{c}^2} \mathbf{N}(\eta)^{\mathrm{T}} \mathbf{N}(\eta) |\mathbf{J}| \mathrm{d}\eta \tag{3.24}$$

which is positive definite and symmetric. Note that the last term on the right hand side of Eq.(3.23) stands for the order of error $\left(\mathrm{w}^2\right)$. When w tends to zero, the error $\mathrm{O}\left(\mathrm{w}^2\right)$ on the right hand side of Eq.(3.23) will vanish.

In order to have an insight into the coefficient matrices $\mathbf{E}^0$, $\mathbf{E}^1$, $\mathbf{E}^2$ in Eq.(3.21) and $\mathbf{M}^0$ in Eq.(3.24), a special 2-dimensional element shown in Fig.3.4 is considered here. In it, the face 1 is parallel with the axis x and perpendicular to the y axis and the node 2 is assumed to be located at the center of the line between the

node 1 and the node 3, i.e.

$$y_2 = \frac{1}{2}(y_1 + y_3) \tag{3.25}$$

Substituting Eq.(3.25) into the coordinate vectors $\mathbf{x}_1 = [x_1 \quad x_1 \quad x_1]^T$ and $\mathbf{y}_1 = [y_1 \quad y_2 \quad y_3]^T$ and then the results into Eq.(3.11c) and Eqs.(3.16a,b) yields

$$\mathbf{J} = \begin{bmatrix} H & 0 \\ 0 & \dfrac{l}{2} \end{bmatrix} \tag{3.26a}$$

$$\mathbf{B}^1 = \begin{Bmatrix} j_{11} \\ j_{21} \end{Bmatrix} \mathbf{N}(\eta) = \frac{1}{H \dfrac{d\mathbf{N}(\eta)}{d\eta} \mathbf{y}_1} \begin{bmatrix} \dfrac{d\mathbf{N}(\eta)}{d\eta} \mathbf{y}_1 \\ -\dfrac{d\mathbf{N}(\eta)}{d\eta} \mathbf{x}_1 \end{bmatrix} \mathbf{N}(\eta) = \frac{1}{H} \begin{bmatrix} 1 \\ 0 \end{bmatrix} \mathbf{N}(\eta) \tag{3.26b}$$

$$\mathbf{B}^2 = \begin{Bmatrix} j_{12} \\ j_{22} \end{Bmatrix} \frac{\partial \mathbf{N}(\eta)}{d\eta} = \frac{1}{H \dfrac{d\mathbf{N}(\eta)}{d\eta} \mathbf{y}_1} \begin{bmatrix} 0 \\ H \end{bmatrix} \frac{d\mathbf{N}(\eta)}{d\eta} = \frac{2}{l} \begin{bmatrix} 0 \\ 1 \end{bmatrix} \frac{d\mathbf{N}(\eta)}{d\eta} \tag{3.26c}$$

where l denotes the height of the element $(l = y_3 - y_1)$. Substituting Eqs.(3.26a-c) into Eqs.(3.21a-c) and integrating the results with respective to η from -1 to 1 yield the following coefficient matrices for the element.

$$\mathbf{E}^0 = \int_{-1}^{1} \mathbf{B}^{1T} \mathbf{B}^1 |\mathbf{J}| d\eta = \frac{l}{30H} \begin{bmatrix} 4 & 2 & -1 \\ 2 & 16 & 2 \\ -1 & 2 & 4 \end{bmatrix} \tag{3.27a}$$

$$\mathbf{E}^1 = \int_{-1}^{1} \mathbf{B}^{2T} \mathbf{B}^1 |\mathbf{J}| d\eta = \begin{bmatrix} 0 & 0 & 0 \\ 0 & 0 & 0 \\ 0 & 0 & 0 \end{bmatrix} \tag{3.27b}$$

$$\mathbf{E}^2 = \int_{-1}^{1} \mathbf{B}^{2T} \mathbf{B}^2 |\mathbf{J}| d\eta = \frac{H}{3l} \begin{bmatrix} 7 & -8 & 1 \\ -8 & 16 & -8 \\ 1 & -8 & 7 \end{bmatrix} \tag{3.27c}$$

Substituting Eq.(3.26a) into Eq.(3.24) and then integrating the result yields the following coefficient matrix for the element

$$\mathbf{M}^0 = \int_{-1}^{1} \frac{1}{c^2} \mathbf{N}(\eta)^{\mathrm{T}} \mathbf{N}(\eta) |\mathbf{J}| d\eta = \frac{lH}{30c^2} \begin{bmatrix} 4 & 2 & -1 \\ 2 & 16 & 2 \\ -1 & 2 & 4 \end{bmatrix} \tag{3.27d}$$

Note that the solutions in Eqs.(3.27a-d) are exact. Upon determining the coefficient matrices $\mathbf{E}^0$, $\mathbf{E}^1$, $\mathbf{E}^2$ and $\mathbf{M}^0$, the element stiffness matrix $\mathbf{K}^e$ and mass matrix $\mathbf{M}^e$ can be obtained by Eq.(3.18) and Eq.(3.22), respectively.

3.2.2 FINAL SBFEM FORMULATION FOR LAYERED INFINITE MEDIUM

The final SBFEM formulation for a layered infinite medium can be obtained through taking limit $w \to 0$ as described in section 2.4 and the final frequency formulation is expressed as follows.

$$\left(\mathbf{S}^{\infty}(\omega) + \mathbf{E}^1\right)\mathbf{E}^{0^{-1}}\left(\mathbf{S}^{\infty}(\omega) + \mathbf{E}^{1^{\mathrm{T}}}\right) - \mathbf{E}^2 + \omega^2 \mathbf{M}^0 = 0 \tag{3.28}$$

where the global coefficient matrices $\mathbf{E}^0$, $\mathbf{E}^1$, $\mathbf{E}^2$ and $\mathbf{M}^0$ are obtained through assembling all element $\mathbf{E}^0$, $\mathbf{E}^1$, $\mathbf{E}^2$ and $\mathbf{M}^0$ evaluated from Eqs.(3.21a-c, 3.24) for a SFE cell. Appling the inverse Fourier transformation to Eq.(3.28) yields the final time formulation as follows.

$$\begin{aligned} &\int_0^t \mathbf{m}^{\infty}(t-\tau)\mathbf{m}^{\infty}(\tau)d\tau + \mathbf{e}^1 \int_0^t \int_0^{\tau} \mathbf{m}^{\infty}(\tau')d\tau' d\tau + \int_0^t \int_0^{\tau} \mathbf{m}^{\infty}(\tau')d\tau' d\tau \mathbf{e}^{1^{\mathrm{T}}} \\ &\qquad - \frac{t^3}{6}\mathbf{e}^2 H(t) - t\mathbf{m}^0 H(t) = 0 \end{aligned} \tag{3.29}$$

where

$$\mathbf{m}^{\infty}(t) = \mathbf{U}^{-1^{\mathrm{T}}} \mathbf{M}^{\infty}(t) \mathbf{U}^{-1} \tag{3.30}$$

and

$$\mathbf{e}^1 = \mathbf{U}^{-1^{\mathrm{T}}} \mathbf{E}^1 \mathbf{U}^{-1} \tag{3.31a}$$

$$\mathbf{e}^2 = \mathbf{U}^{-1^{\mathrm{T}}} \left(\mathbf{E}^2 - \mathbf{E}^1 \mathbf{E}^{0^{-1}} \mathbf{E}^{1^{\mathrm{T}}}\right) \mathbf{U}^{-1} \tag{3.31b}$$

$$\mathbf{m}^0 = \mathbf{U}^{-1^{\mathrm{T}}} \mathbf{M}^0 \mathbf{U}^{-1} \tag{3.31c}$$

in which $\mathbf{U}$ can be obtained by decomposing $\mathbf{E}^0$ via Cholesky's method such that

$$\mathbf{E}^0 = \mathbf{U}^{\mathrm{T}}\mathbf{U} \tag{3.31d}$$

and $\mathbf{M}^{\infty}(\mathrm{t})$ satisfies Eq.(3.4b). Note that $\mathbf{e}^2$ is symmetric and $\mathbf{m}^0$ is positive definite and symmetric. Upon determining $\mathbf{m}^{\infty}(\mathrm{t})$, the matrix $\mathbf{M}^{\infty}(\mathrm{t})$ can be obtained as

$$\mathbf{M}^{\infty}(\mathrm{t}) = \mathbf{U}^{\mathrm{T}}\mathbf{m}^{\infty}(\mathrm{t})\mathbf{U} \tag{3.32}$$

Hence, the velocity-to-velocity-potential relationship in Eq.(3.4b) can be solved. Details of the inverse Fourier transformation can be found in the literature (Wolf and Song (1996a)). The numerical solution for Eq.(3.29) is similar to those in section 2.6. The accuracies and efficiencies of Eqs.(3.28) and (3.29) will be shown through checking against some dam-reservoir interaction problems in chapters 7 and 8 in both frequency domain and time domain. It is worth mentioning that Eq.(3.28) is difficult to solve when the coefficient matrix $\mathbf{E}^1$ is present, but when $\mathbf{E}^1$ vanishes, Eq.(3.28) can be easily solved.

CHAPTER FOUR

SBFEM FORMULATION EXTENSION FOR BEAM ON VISCO-ELASTIC-TYPE FLUID FOUNDATION PROBLEMS

The writer extends the SBFEM to solve semi-infinite Timoshenko beam on visco-elastic-type fluid foundation problems. The SBFEM formulations described in chapters 2-3 are only suitable for cases where the boundary conditions along the non-discretized surfaces have zero-displacement. It is similar to the formulations for a semi-infinite soil medium as derived by Wolf and Song (1996a). For the soil medium, either the displacement or the force equals to zero along the non-discretized boundary; whereas for the fluid medium, either the pressure or the normal velocity equals to zero along the non-discretized boundary. In this chapter, a beam resting on visco-elastic foundation which has non-zero boundary conditions, is considered. An analytical formulation based on the techniques of the SBFEM for a semi-infinite Timoshenko beam on visco-elastic-type fluid foundation is derived. It is an extension of those for layered semi-infinite medium. Compared to the SBFEM formulations for zero boundary condition along the non-dicretized boundary, this formulation has one coefficient matrix modified and one new coefficient matrix produced. The two new matrices describe the effect of the visco-elastic foundation and are applicable to general cases. Note that here the analytical formulation is employed for the solid beam, not the fluid foundation. By setting the damping coefficients of the visco-elastic foundation equal to zero, the formulation is applicable for cases of elastic foundations. By setting both the damping coefficients and stiffness of visco-elastic foundations equal to zero, the

formulation describes the cases of a beam not resting on a foundation. Benchmark examples are presented to verify the accuracy and efficiency of the analytical formulation. Good results are obtained.

4.1 INTRODUCTION

Relatively very long beam resting on elastic and visco-elastic foundations are often encountered. It is a classical problem, and has attracted many attentions.

For beam-on-foundation systems, either the Bernoulli-Euler or the Timoshenko beam theory is often employed to model the beam, while the underlying foundation is often modeled as the simplest Winkler foundation (Feng and Cook, 1983). As Bernoulli-Euler beam theory has a simple mathematical form, some analytical solutions are available for homogeneous infinite beam-foundation systems (Kenney, 1954; Stadler and Shreeves, 1970; McGhie, 1990; Sun, 2001), where only flexural waves are considered and shear waves have been ignored. For cases where shear waves can not be ignored, Timoshenko beam theory has been employed (Achenbach and Sun, 1965; Wang and Gagnon, 1978; Felszeghy, 1996a,b; Billger and Folkow, 1998; Folkow et al., 1998; Chen et al.2001) and closed-form solutions have been derived for ideal homogeneous beam and foundation models.

Other than those analytical solutions, a powerful alternative is to employ numerical methods. The numerical methods are suitable for beam-foundation systems with inhomogeneous and complicated character. Wang et al. (1984) reported to use the Finite element method (FEM) to model an infinite beam. The infinite beam was truncated into a finite beam with fixed boundary conditions at the truncated boundaries. However, results were contaminated by reflected waves from the truncated boundaries. In order to avoid the effect of the reflected waves, an artificial

boundary condition along the truncated boundaries was developed (Tsynkov 1998, Givoli 1999), but it was too complicated to be implemented numerically due to the involvement of special functions and convolution integrals. Recently, Liu and Xu (2002) and Liu and Li (2003) developed high-order accurate artificial boundary conditions on truncated boundaries by using the residual radiation method, which could be easily incorporated into a conventional FEM. The residual radiation method transferred a second-order partial differential equation into a linear first-order ordinary differential equation by factorizing the partial differential equation and introducing a set of residual radiation functions. In order to obtain accurate results, many residual radiation functions must be produced, which increased the complexity of the residual radiation method.

In this chapter, an analytical formulation based on the techniques of the SBFEM for a semi-infinite Timoshenko beam on visco-elastic-type fluid foundation problems is derived. It is an extension of the traditional SBFEM formulation for layered infinite medium. To keep its derivation simple and clear, the derivation is only limited to Timoshenko beams on visco-elastic-typed fluid foundation problems. Actually, the methodology covers the general cases. It is also applicable to cases of elastic foundations or no foundations by changing some of the coefficient matrices. Its accuracy and efficiency are validated by some benchmark examples. The first one is a semi-infinite rod resting on an elastic foundation or no foundation. The second one is a semi-infinite Timoshenko beam resting on visco-elastic foundations. Parametric analyses for various foundations are carried out as well.

4.2 AN ANLYTICAL FORMULATION BASED ON THE SBFEM TECHNIQUES FOR A SEMI-INFINITE TIMOSHENKO BEAM ON A VISCO-ELASTIC FOUNDATION

An infinite elastic beam on a visco-elastic foundation as shown in Fig.4.1a is considered. It is treated as a plain-strain problem. The infinite beam is taken as a Timoshenko beam, while the visco-elastic foundation is modeled by continuous springs and dashpots uniformly distributed beneath the infinite beam. In order to obtain the response of the infinite beam, the infinite beam and the foundation are divided into two fields, as shown in Figs.4.1b and 4.1c, by two artificial (truncated) boundaries at $x = x_1$ and $x = x_2$. The near field segment is a finite beam resting on a foundation, while the far field segment consists of two semi-infinite beams resting on a foundation. This formulation permits the near-field beam to be modeled by FEM and coupled with the far-field semi-infinite beam. However, in order to derive and validate the analytical formulation based on the SBFEM techniques for semi-infinite beams, the near-field is dropped. Taking advantage of the symmetry, only half of the far-field is considered. The semi-infinite beam is modeled by the SBFEM. The semi-infinite beam on the right hand side whose artificial boundary is located at $x = x_2$ is considered.

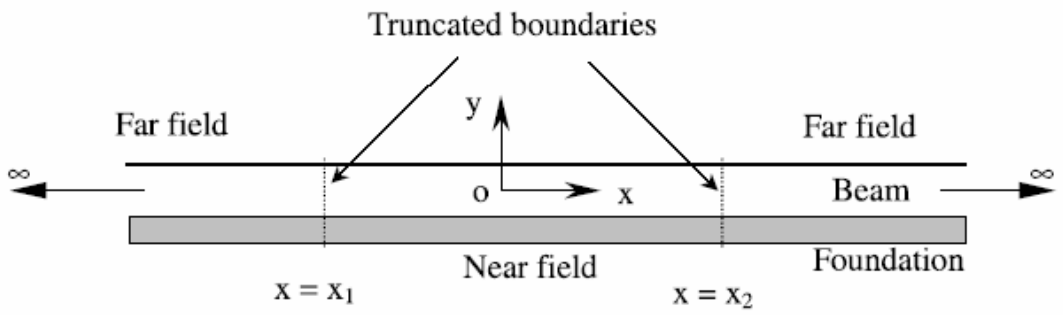

Fig.4.1a An infinite beam on a foundation

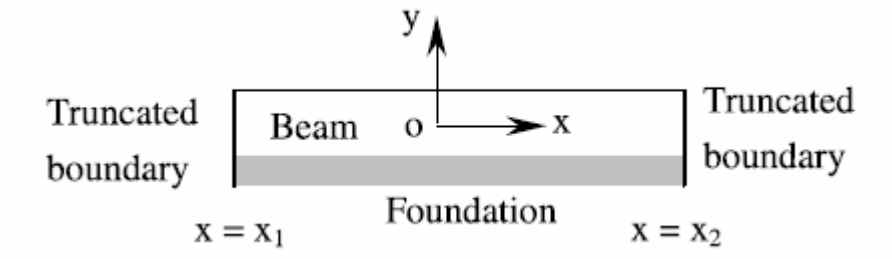

Fig.4.1b Finite beam after truncation

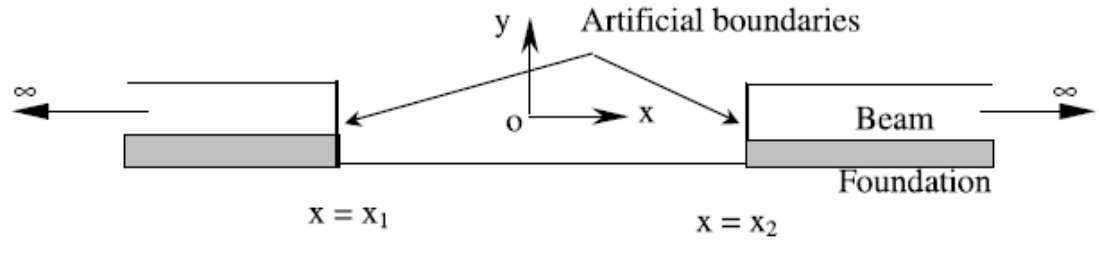

Fig.4.1c Semi-infinite beams after truncation

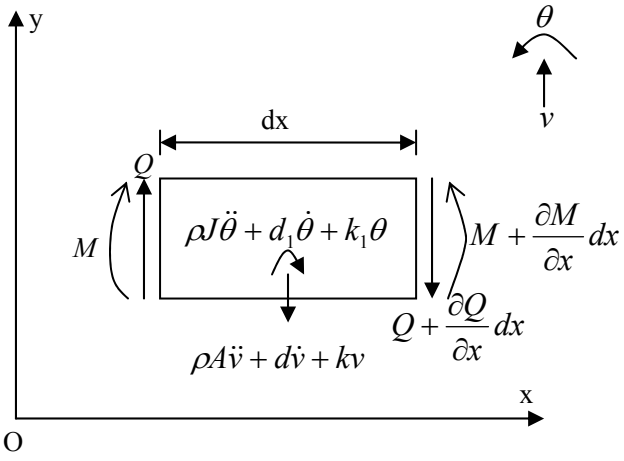

Fig.4.2 Forces of an infinitesimal beam element on foundations

The forces and the deformations of an infinitesimal beam element on a visco-elastic foundation are shown in Fig.4.2. The motion equilibrium equations of the infinitesimal beam element are expressed as (Hu, 1984)

$$\frac{\partial Q}{\partial x} = -\rho A\ddot{v} - d\dot{v} - kv \qquad (4.1a)$$

$$\frac{\partial M}{\partial x} = Q + \rho J\ddot{\theta} + d_1\dot{\theta} + k_1\theta \tag{4.1b}$$

where v and θ denote the beam deflection in the y direction and the bending rotation, respectively; ρ, A and J represent the density, the cross-section area, and the second moment of the beam's cross-sectional area, respectively; d and d_1 are the translational and rotational viscous-damping coefficients, respectively; k and k_1 are the translational and rotational spring constants, respectively; Q and M denote the shear force and the bending moment, respectively, and are related to their corresponding deformations as follows.

$$Q(x,t) = \mu AG\beta \tag{4.2a}$$

$$M(x,t) = EJ\frac{\partial \theta}{\partial x} \tag{4.2b}$$

where β and μ denote the shear angle and shear factor, respectively; and E and G are the Young's and shear moduli of the beam, respectively. The bending rotation θ and shear angle β have a relationship in the form of

$$\theta = \frac{\partial v}{\partial x} + \beta \tag{4.3}$$

Substituting Eqs.(4.2a,b,4.3) into Eqs.(4.1a,b) yields the motion equilibrium equations at any location x as follows.

$$\mu AG\frac{\partial^2 v}{\partial x^2} - \mu AG\frac{\partial \theta}{\partial x} - kv = \rho A\ddot{v} + d\dot{v} \tag{4.4a}$$

$$EJ\frac{\partial^2 \theta}{\partial x^2} + \mu AG\frac{\partial v}{\partial x} - (\mu AG + k_1)\theta = \rho J\ddot{\theta} + d_1\dot{\theta} \tag{4.4b}$$

The direction coordinates of $Q(x,t)$, $M(x,t)$, v and θ are shown in Fig.4.2.

4.2.1 FINITE-ELEMENT ANALYSIS

Consider an infinitesimal isoparametric linear element put in place between x_2 and x_3 at the end of the semi-infinite Timoshenko beam on a visco-elastic foundation as shown in Fig.4.3a, in which h denotes the height of the beam, and $w \times h$ represents the length of the linear element having a very small dimensionless quantity w times h. The equivalent finite element equation of Eqs.(4.4a,b) for the element is

$$\mathbf{M}\frac{\partial^2 \mathbf{u}}{\partial t^2} + \mathbf{K}\mathbf{u} = \mathbf{F}_{ext} + \mathbf{F}_f \tag{4.5}$$

where $\mathbf{M}$ and $\mathbf{K}$ denote the mass and stiffness matrices of the element, respectively; no damping is considered; $\mathbf{F}_{ext}$ denotes the external force which can be easily obtained and $\mathbf{F}_f$ denotes the force from foundations acting on the element; $\mathbf{u}$ denotes the deformations of the element. Of note, the external force $\mathbf{F}_{ext}$ is assumed to be applicable on the surface $x = x_2$. In other words, there is no force except the force $\mathbf{F}_f$ acting underneath the semi-infinite beam. What follows are the details of the evaluation for the terms $\mathbf{M}$, $\mathbf{K}$ and $\mathbf{F}_f$.

The deformations $\begin{Bmatrix} v(x) \\ \theta(x) \end{Bmatrix}$ at the spatial position x as shown in Fig.4.3a are linearly interpolated between the nodal values $\begin{Bmatrix} v_2 \\ \theta_2 \end{Bmatrix}$ at x_2 and $\begin{Bmatrix} v_3 \\ \theta_3 \end{Bmatrix}$ at x_3 as follows.

$$\begin{Bmatrix} v(x) \\ \theta(x) \end{Bmatrix} = \begin{bmatrix} N_1 & 0 & N_2 & 0 \\ 0 & N_1 & 0 & N_2 \end{bmatrix} \begin{Bmatrix} v_2 \\ \theta_2 \\ v_3 \\ \theta_3 \end{Bmatrix} = \mathbf{N}\mathbf{u} \tag{4.6}$$

where x denotes the distance away from the end x_2; $v(x)$ and $\theta(x)$ denote the deflection and the bending rotation of the Timoshenko beam at the spatial position x, respectively; $N_1 = \frac{1}{2}(1-\xi)$, $N_2 = \frac{1}{2}(1+\xi)$ with $\xi = \frac{2}{w \times h}\left(x - x_2 - \frac{w \times h}{2}\right)$,

$\mathbf{N} = \begin{bmatrix} N_1 & 0 & N_2 & 0 \\ 0 & N_1 & 0 & N_2 \end{bmatrix}$ and $\mathbf{u} = [v_2 \quad \theta_2 \quad v_3 \quad \theta_3]^T$. The positive directions of the deflection v and rotation θ are shown in Fig.4.3d.

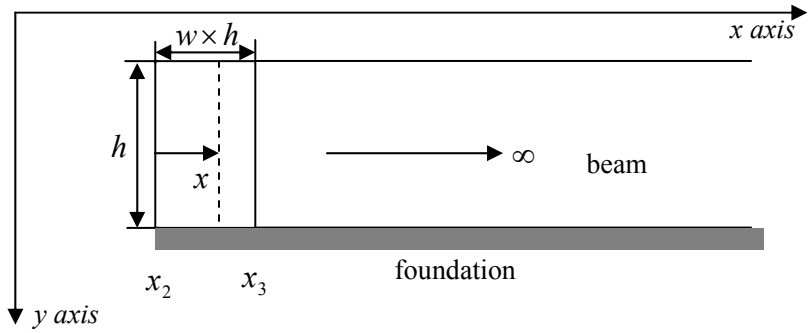

Fig.4.3a A 2-node element taken out from a Timoshenko beam

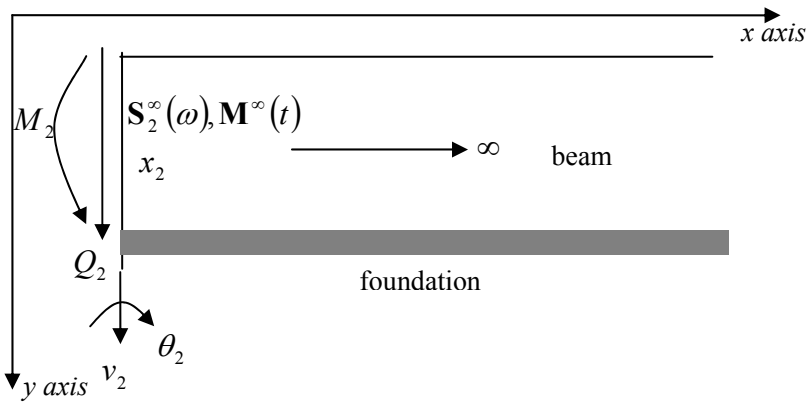

Fig.4.3b A semi-infinite Timoshenko beam from x_2 to infinity

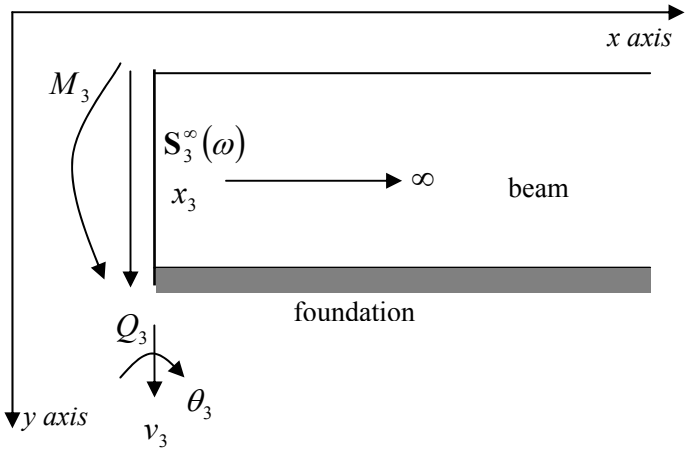

Fig.4.3c A semi-infinite Timoshenko beam from x_3 ***to infinity***

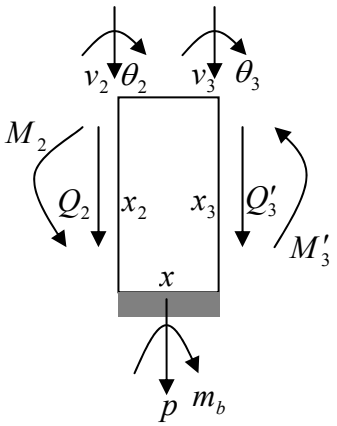

Fig.4.3d The part (a 2-node element) between x_2 ***and*** x_3

The curvature-displacement relationship is expressed as

$$-\frac{d\theta(x)}{dx} = -\begin{bmatrix} 0 & \frac{dN_1}{dx} & 0 & \frac{dN_2}{dx} \end{bmatrix} \begin{Bmatrix} v_2 \\ \theta_2 \\ v_3 \\ \theta_3 \end{Bmatrix} = \mathbf{B}_c \mathbf{u} \tag{4.7a}$$

where $\mathbf{B}_c$ denotes the curvature-displacement matrix, while the shear strain-displacement relationship is given as

$$\frac{dv(x)}{dx} - \theta(x) = \left[\frac{dN_1}{dx} \quad -N_1 \quad \frac{dN_2}{dx} \quad -N_2 \right] \begin{Bmatrix} v_2 \\ \theta_2 \\ v_3 \\ \theta_3 \end{Bmatrix} = \mathbf{B}_s \mathbf{u} \tag{4.7b}$$

where $\mathbf{B}_s$ denotes the shear strain-displacement matrix. By virtue of the principle of virtual work and the conventional finite element method, the stiffness matrix $\mathbf{K}$ of the linear Timoshenko beam element can be written as

$$\mathbf{K} = \mathbf{K}_s + \mathbf{K}_c \tag{4.8a}$$

where

$$\mathbf{K}_c = \int_{x_2}^{x_3} \mathbf{B}_c^T (EJ) \mathbf{B}_c dx \tag{4.8b}$$

$$\mathbf{K}_s = \int_{x_2}^{x_3} \mathbf{B}_s^T (G\hat{A}) \mathbf{B}_s dx \tag{4.8c}$$

in which $\hat{A} = \mu A$. The mass matrix $\mathbf{M}$ of the element can be expressed as

$$\mathbf{M} = \int_{x_2}^{x_3} \mathbf{N}^T \begin{bmatrix} \rho A & 0 \\ 0 & \rho J \end{bmatrix} \mathbf{N} dx \tag{4.8d}$$

Partitioning $\mathbf{K}$ and $\mathbf{M}$ into sub-matrices corresponding to the spatial positions x_2, x_3 leads to

$$\mathbf{K} = \begin{bmatrix} \mathbf{K}_{22} & \mathbf{K}_{23} \\ \mathbf{K}_{32} & \mathbf{K}_{33} \end{bmatrix} \tag{4.9a}$$

$$\mathbf{M} = \begin{bmatrix} \mathbf{M}_{22} & \mathbf{M}_{23} \\ \mathbf{M}_{32} & \mathbf{M}_{33} \end{bmatrix} \tag{4.9b}$$

By substituting the shape function $\mathbf{N}$ in Eq.(4.6), the curvature-displacement matrix $\mathbf{B}_c$ in Eq.(4.7a) and the shear strain-displacement matrix $\mathbf{B}_s$ in Eq.(4.7b) into Eqs.(4.8a-d), the sub-matrices $\mathbf{K}_{jl}$ and $\mathbf{M}_{jl}$ of the stiffness matrix $\mathbf{K}$ and mass matrix $\mathbf{M}$ in Eqs.(4.9a,b) can be written as

$$\mathbf{K}_{jl} = \frac{1}{w} \mathbf{K}_{jl}^0 + \mathbf{K}_{jl}^1 + w \mathbf{K}_{jl}^2 \tag{4.10a}$$

$$\mathbf{M}_{jl} = \frac{w}{4}\left(1 + \frac{\xi_j \xi_l}{3}\right)\mathbf{M}^0 \tag{4.10b}$$

where the subscripts $j,l = 2,3$, and the corresponding $\xi_2 = -1, \xi_3 = 1$; the matrix

$$\mathbf{K}_{jl}^0 = \xi_j \xi_l \mathbf{E}^0 \tag{4.11a}$$

in which

$$\mathbf{E}^0 = \begin{bmatrix} \frac{G\hat{A}}{h} & 0 \\ 0 & \frac{EJ}{h} \end{bmatrix} \tag{4.11b}$$

and

$$\mathbf{K}_{jl}^1 = \frac{1}{2}\xi_l \mathbf{E}^1 + \frac{1}{2}\xi_j \mathbf{E}^{1T} \tag{4.11c}$$

in which

$$\mathbf{E}^1 = \begin{bmatrix} 0 & 0 \\ -G\hat{A} & 0 \end{bmatrix} \tag{4.11d}$$

and

$$\mathbf{K}_{jl}^2 = \left(\frac{1}{4} + \frac{\xi_j \xi_l}{12}\right)\mathbf{E}^2 \tag{4.11e}$$

in which

$$\mathbf{E}^2 = \begin{bmatrix} 0 & 0 \\ 0 & G\hat{A}h \end{bmatrix} \tag{4.11f}$$

and

$$\mathbf{M}^0 = \begin{bmatrix} \rho Ah & 0 \\ 0 & \rho Jh \end{bmatrix} \tag{4.11g}$$

The pressure p and the bending moment m_b at the spatial position x acting on the Timoshenko beam from the visco-elastic foundation shown in Fig.4.3d can be expressed as

$$p = -kv(x) - d\frac{\partial v(x)}{\partial t} \tag{4.12a}$$

$$m_b = -k_1\theta(x) - d_1\frac{\partial \theta(x)}{\partial t} \tag{4.12b}$$

By using the conventional finite element technique, the equivalent force $\mathbf{F}_f$ in Eq.(4.5) can be expressed in terms of the pressure p and the moment m_b as follows.

$$\mathbf{F}_f = \int_{x_2}^{x_3} \mathbf{N}^T \begin{Bmatrix} p \\ m_b \end{Bmatrix} dx \tag{4.13a}$$

Substituting Eq.(4.6) into Eqs.(4.12a,b) and then re-writing the results in matrix form leads to

$$\begin{Bmatrix} p \\ m_b \end{Bmatrix} = -\begin{bmatrix} k & 0 \\ 0 & k_1 \end{bmatrix}\mathbf{N}\mathbf{u} - \begin{bmatrix} d & 0 \\ 0 & d_1 \end{bmatrix}\mathbf{N}\frac{\partial \mathbf{u}}{\partial t} \tag{4.13b}$$

Substituting Eq.(4.13b) into Eq.(4.13a) yields

$$\mathbf{F}_f = -\int_{x_2}^{x_3} \mathbf{N}^T \begin{bmatrix} k & 0 \\ 0 & k_1 \end{bmatrix}\mathbf{N}dx\mathbf{u} - \int_{x_2}^{x_3} \mathbf{N}^T \begin{bmatrix} d & 0 \\ 0 & d_1 \end{bmatrix}\mathbf{N}dx\frac{\partial \mathbf{u}}{\partial t} = -\mathbf{K}_f\mathbf{u} - \mathbf{C}_f\frac{\partial \mathbf{u}}{\partial t} \tag{4.13c}$$

where

$$\mathbf{K}_f = \int_{x_2}^{x_3} \mathbf{N}^T \begin{bmatrix} k & 0 \\ 0 & k_1 \end{bmatrix}\mathbf{N}dx \tag{4.14a}$$

$$\mathbf{C}_f = \int_{x_2}^{x_3} \mathbf{N}^T \begin{bmatrix} d & 0 \\ 0 & d_1 \end{bmatrix}\mathbf{N}dx \tag{4.14b}$$

Of note, $\mathbf{K}_f$ and $\mathbf{C}_f$ describe the stiffness and damping properties of the visco-elastic foundation. They are partitioned into sub-matrices corresponding to the spatial positions x_2 and x_3 as follows.

$$\mathbf{K}_f = \begin{bmatrix} \mathbf{K}_{f_{22}} & \mathbf{K}_{f_{23}} \\ \mathbf{K}_{f_{32}} & \mathbf{K}_{f_{33}} \end{bmatrix} \tag{4.15a}$$

$$\mathbf{C}_f = \begin{bmatrix} \mathbf{C}_{f_{22}} & \mathbf{C}_{f_{23}} \\ \mathbf{C}_{f_{32}} & \mathbf{C}_{f_{33}} \end{bmatrix} \tag{4.15b}$$

By substituting $\mathbf{N}$ in Eq.(4.6) into Eqs.(4.14a,b), the sub-matrices in Eqs.(4.15a,b) can be expressed as

$$\mathbf{K}_{\mathrm{f}\,\mathrm{jl}} = \frac{\mathrm{w}}{4}\left(1+\frac{1}{3}\xi_{\mathrm{j}}\xi_{\mathrm{l}}\right)\begin{bmatrix}\mathrm{kh} & 0\\ 0 & \mathrm{k}_1\mathrm{h}\end{bmatrix} = \frac{\mathrm{w}}{4}\left(1+\frac{1}{3}\xi_{\mathrm{j}}\xi_{\mathrm{l}}\right)\mathbf{E}_{\mathrm{f}}^{2} \tag{4.16a}$$

where

$$\mathbf{E}_{\mathrm{f}}^{2} = \begin{bmatrix}\mathrm{kh} & 0\\ 0 & \mathrm{k}_1\mathrm{h}\end{bmatrix} \tag{4.16b}$$

and

$$\mathbf{C}_{\mathrm{f}\,\mathrm{jl}} = \frac{\mathrm{w}}{4}\left(1+\frac{1}{3}\xi_{\mathrm{j}}\xi_{\mathrm{l}}\right)\mathbf{C}^{0} \tag{4.16c}$$

in which

$$\mathbf{C}^{0} = \begin{bmatrix}\mathrm{dh} & 0\\ 0 & \mathrm{d}_1\mathrm{h}\end{bmatrix} \tag{4.16d}$$

The subscripts $\mathrm{j,l} = 2,3$, and the corresponding $\xi_2 = -1, \xi_3 = 1$. Substituting Eq.(4.13c) into Eq.(4.5) and re-arranging leads to

$$\mathbf{M}\frac{\partial^2\mathbf{u}}{\partial \mathrm{t}^2} + \mathbf{C}_{\mathrm{f}}\frac{\partial\mathbf{u}}{\partial \mathrm{t}} + \left(\mathbf{K}+\mathbf{K}_{\mathrm{f}}\right)\mathbf{u} = \mathbf{F}_{\mathrm{ext}} \tag{4.17}$$

Similar to Eq.(4.9a), sub-matrices $\mathbf{K}'_{\mathrm{jl}}$ of the stiffness matrix $\mathbf{K}+\mathbf{K}_{\mathrm{f}}$ for the element shown in Fig.4.3d can be expressed as

$$\mathbf{K}'_{\mathrm{jl}} = \frac{1}{\mathrm{w}}\mathbf{K}^{0}_{\mathrm{jl}} + \mathbf{K}^{1}_{\mathrm{jl}} + \mathrm{w}\mathbf{K}'^{2}_{\mathrm{jl}} \tag{4.18a}$$

where

$$\mathbf{K}'^{2}_{\mathrm{jl}} = \left(\frac{1}{4}+\frac{\xi_{\mathrm{j}}\xi_{\mathrm{l}}}{12}\right)\left(\mathbf{E}^{2}+\mathbf{E}_{\mathrm{f}}^{2}\right) = \left(\frac{1}{4}+\frac{\xi_{\mathrm{j}}\xi_{\mathrm{l}}}{12}\right)\mathbf{E}'^{2} \tag{4.18b}$$

in which

$$\mathbf{E}'^{2} = \mathbf{E}^{2}+\mathbf{E}_{\mathrm{f}}^{2} = \begin{bmatrix}\mathrm{kh} & 0\\ 0 & \mathrm{G}\hat{\mathrm{A}}\mathrm{h}+\mathrm{k}_1\mathrm{h}\end{bmatrix} \tag{4.18c}$$

From Eq.(4.16d) and Eq.(4.18c), one can see that the coefficient matrices $\mathbf{C}^{0}$ and

$\mathbf{E}'^{2}$ depend not only on the geometry of the end of the Timoshenko beam, but also on the properties of the visco-elastic foundation.

4.2.2 THE ANLYTICAL SOLUTION BASED ON THE SBFEM TECHNIQUES

Since the semi-infinite beam on a foundation shown in Fig.4.3a is a single-layered semi-infinite medium, the SBFEM concept is employed to model the semi-infinite Timoshenko beam. The response equations at the spatial positions x_2 and x_3 in frequency domain are formulated as

$$\mathbf{F}_2(\omega) = \mathbf{S}_2^{\infty}(\omega)\mathbf{u}_2(\omega) \tag{4.19a}$$

$$\mathbf{F}_3(\omega) = \mathbf{S}_3^{\infty}(\omega)\mathbf{u}_3(\omega) \tag{4.19b}$$

where $\mathbf{F}_j(\omega) = \begin{Bmatrix} Q_j(\omega) \\ -M_j(\omega) \end{Bmatrix}$ is the force vector; $\mathbf{u}_j(\omega) = \begin{Bmatrix} v_j(\omega) \\ \theta_j(\omega) \end{Bmatrix}$ with $j = 2,3$ is the deformation vector; and $\mathbf{S}_j^{\infty}(\omega)$ denotes the dynamic stiffness matrix of the semi-infinite beam from x_j to infinity; $Q_j(\omega)$ and $M_j(\omega)$ denote the shear force and the bending moment at x_j, respectively. The positive directions of $Q_j(\omega)$ and $M_j(\omega)$ are shown in Figs.4.3b and 4.3c. Note that for a layered semi-infinite medium, the dynamic stiffness matrices $\mathbf{S}_2^{\infty}(\omega)$ and $\mathbf{S}_3^{\infty}(\omega)$ satisfy

$$\mathbf{S}^{\infty}(\omega) = \mathbf{S}_2^{\infty}(\omega) = \mathbf{S}_3^{\infty}(\omega) \tag{4.19c}$$

because of the same geometry of the end at the spatial position x_2, x_3, where $\mathbf{S}^{\infty}(\omega)$ denotes the dynamic stiffness matrix of the semi-infinite beam. In order to obtain an equation for the $\mathbf{S}^{\infty}(\omega)$, the finite element equation Eq.(4.17) for the element shown in Fig.4.3d is re-written in a frequency-analysis form as follows.

$$\mathbf{F}_{\text{ext}}(\omega)=\left(\mathbf{K}+\mathbf{K}_{\text{f}}+(\text{i}\omega)\mathbf{C}_{\text{f}}+(\text{i}\omega)^2\mathbf{M}\right)\mathbf{u}(\omega)=\mathbf{S}(\omega)\mathbf{u}(\omega) \tag{4.20a}$$

where

$$\mathbf{S}(\omega)=\mathbf{K}+\mathbf{K}_{\text{f}}+(\text{i}\omega)\mathbf{C}_{\text{f}}+(\text{i}\omega)^2\mathbf{M} \tag{4.20b}$$

Note that compatibility is enforced at x_2 and x_3. Hence, $\mathbf{F}_{\text{ext}}(\omega)$ is expressed as

$$\mathbf{F}_{\text{ext}}(\omega)=\begin{Bmatrix}\mathbf{F}_2(\omega)\\ \mathbf{F}_3'(\omega)\end{Bmatrix}=\begin{Bmatrix}[\text{Q}_2 & -\text{M}_2]^{\text{T}}\\ [\text{Q}_3' & -\text{M}_3']^{\text{T}}\end{Bmatrix}=\begin{Bmatrix}[\text{Q}_2 & -\text{M}_2]^{\text{T}}\\ [-\text{Q}_3 & \text{M}_3]^{\text{T}}\end{Bmatrix}=\begin{Bmatrix}\mathbf{F}_2(\omega)\\ -\mathbf{F}_3(\omega)\end{Bmatrix} \tag{4.21}$$

Partition Eq.(4.20a) into sub-matrices corresponding to the spatial positions x_2 and x_3. Substituting Eqs.(4.19a,b) into Eq.(4.21), and then the result into Eq.(4.20a) yields

$$\begin{bmatrix}\mathbf{S}_{22}(\omega) & \mathbf{S}_{23}(\omega)\\ \mathbf{S}_{32}(\omega) & \mathbf{S}_{33}(\omega)\end{bmatrix}\begin{Bmatrix}\mathbf{u}_2(\omega)\\ \mathbf{u}_3(\omega)\end{Bmatrix}=\begin{bmatrix}\mathbf{S}_2^{\infty}(\omega) & 0\\ 0 & -\mathbf{S}_3^{\infty}(\omega)\end{bmatrix}\begin{Bmatrix}\mathbf{u}_2(\omega)\\ \mathbf{u}_3(\omega)\end{Bmatrix} \tag{4.22}$$

Solving Eq.(4.22) and substituting Eq.(4.19c) into the result leads to

$$\mathbf{S}^{\infty}(\omega)=\mathbf{S}_{22}(\omega)-\mathbf{S}_{23}(\omega)\left(\mathbf{S}^{\infty}(\omega)+\mathbf{S}_{33}(\omega)\right)^{-1}\mathbf{S}_{32}(\omega) \tag{4.23}$$

By re-arranging Eq.(4.23) and employing the same technique presented by Song and Wolf (1996), $\mathbf{S}^{\infty}(\omega)$ satisfies

$$\left(\mathbf{S}^{\infty}(\omega)+\mathbf{E}^1\right)\mathbf{E}^{0^{-1}}\left(\mathbf{S}^{\infty}(\omega)+\mathbf{E}^{1^{\text{T}}}\right)-\mathbf{E}'^2-\text{i}\omega\mathbf{C}^0-(\text{i}\omega)^2\mathbf{M}^0=0 \tag{4.24}$$

in which the coefficient matrices $\mathbf{E}^0$, $\mathbf{E}^1$, $\mathbf{E}'^2$, $\mathbf{C}^0$ and $\mathbf{M}^0$ are as expressed in Eqs.(4.11b, 4.11d, 4.18c, 4.16d, 4.11g), respectively. Upon obtaining $\mathbf{S}^{\infty}(\omega)$, the relationship between the force and the deformation in Eq.(4.19a) can be determined. The corresponding equation of Eq.(4.19a) in the time domain with zero initial conditions (i.e. the layered semi-infinite beam is initially at rest) can be formulated as

$$\mathbf{F}(\text{t})=\int_0^{\text{t}}\mathbf{M}^{\infty}(\text{t}-\tau)\frac{\partial^2\mathbf{u}_2(\tau)}{\partial\text{t}^2}\text{d}\tau \tag{4.25}$$

where $\mathbf{F}(t)=\begin{Bmatrix} Q(t) \\ -M(t) \end{Bmatrix}$, $\mathbf{u}_2(t)=\begin{Bmatrix} v_2(t) \\ \theta_2(t) \end{Bmatrix}$ and $\mathbf{M}^{\infty}(t)$ denote the force vector, the deformation vector and the acceleration unit-impulse response matrix at x_2 of the Timoshenko beam, respectively; $Q(t)$ and $M(t)$ denote the shear force and the bending moment at x_2, respectively; $\mathbf{F}(t)$ and $\mathbf{F}_2(\omega)$, $\mathbf{u}_2(t)$ and $\mathbf{u}_2(\omega)$, and $\mathbf{M}^{\infty}(t)$ and $\mathbf{M}^{\infty}(\omega)$ form the Fourier transform pairs, respectively. The acceleration unit-impulse response matrix $\mathbf{M}^{\infty}(\omega)$ is defined as

$$\mathbf{M}^{\infty}(\omega)=\frac{\mathbf{S}^{\infty}(\omega)}{(i\omega)^2} \tag{4.26}$$

Substituting Eq.(4.26) into Eq.(4.24) and applying the inverse Fourier transformation to the results yields

$$\begin{aligned}&\int_0^t \mathbf{m}^{\infty}(t-\tau)\mathbf{m}^{\infty}(\tau)d\tau+\mathbf{e}^1\int_0^t\int_0^{\tau}\mathbf{m}^{\infty}(\tau')d\tau'd\tau \\ &+\int_0^t\int_0^{\tau}\mathbf{m}^{\infty}(\tau')d\tau'd\tau\mathbf{e}^{1\mathrm{T}}-\frac{t^3}{6}\mathbf{e}^2H(t)-\frac{t^2}{2}\mathbf{c}^0H(t)-t\mathbf{m}^0H(t)=0\end{aligned} \tag{4.27}$$

where

$$\mathbf{e}^1=\mathbf{U}^{-1\mathrm{T}}\mathbf{E}^1\mathbf{U}^{-1} \tag{4.28a}$$

$$\mathbf{e}^2=\mathbf{U}^{-1\mathrm{T}}\left(\mathbf{E}'^2-\mathbf{E}^1\mathbf{E}^{0-1}\mathbf{E}^{1\mathrm{T}}\right)\mathbf{U}^{-1} \tag{4.28b}$$

$$\mathbf{c}^0=\mathbf{U}^{-1\mathrm{T}}\mathbf{C}^0\mathbf{U}^{-1} \tag{4.28c}$$

$$\mathbf{m}^0=\mathbf{U}^{-1\mathrm{T}}\mathbf{M}^0\mathbf{U}^{-1} \tag{4.28d}$$

and $\mathbf{E}^0$ is decomposed by Cholesky's method as follows.

$$\mathbf{E}^0=\mathbf{U}^{\mathrm{T}}\mathbf{U} \tag{4.28e}$$

The $\mathbf{M}^{\infty}(t)$ in Eq.(4.25) satisfies

$$\mathbf{M}^{\infty}(t)=\mathbf{U}^{\mathrm{T}}\mathbf{m}^{\infty}(t)\mathbf{U} \tag{4.29}$$

Upon knowing $\mathbf{m}^{\infty}(t)$, the matrix $\mathbf{M}^{\infty}(t)$ is then determined and subsequently the

relationship in Eq.(4.25) can be established. Here, Eq.(4.24) and Eq.(4.27) are called the "consistent infinitesimal finite-element cell" equation in frequency and time domain, respectively. In comparison with those derived by Song and Wolf (1996), a new term ($\mathbf{C}^0$ or $\mathbf{c}^0$) accounting for the damping of a visco-elastic foundation is added. Similarly the coefficient $\mathbf{E}'^2$ is introduced to account for the stiffness of a viscoelastic foundation. Of note, $\mathbf{E}'^2$ replaces $\mathbf{E}^2$ in the derivation by Song and Wolf (1996). It is worth mentioning that the earlier formulation derived by Song and Wolf (1996) is only suitable for cases where the boundary conditions are zero along the non-discretized boundaries (i.e. the top and bottom surface of the layered medium). Therefore, their formulation is not suitable for beams on foundations. The present modified formulation works. Since all terms in Eqs.(4.24,27) are exact, Eqs.(4.24,27) are analytical, not approximate.

Although Eqs.(4.24,27) are derived for a Timoshenko beam resting on visco-elastic-type fluid foundations, the corresponding equations for any semi-infinite beam resting on an elastic foundation or without foundation has similar form of Eqs.(4.24,27) except for $\mathbf{C}^0$ and $\mathbf{E}_{\mathrm{f}}^2$. For the cases not resting on a foundation, all the visco-elastic parameters (k, k_1 and d, d_1) in Eqs.(4.12a,b) vanish, i.e.

$$\mathbf{C}^0 = \begin{bmatrix} 0 & 0 \\ 0 & 0 \end{bmatrix} \tag{4.30a}$$

$$\mathbf{E}_{\mathrm{f}}^2 = \begin{bmatrix} 0 & 0 \\ 0 & 0 \end{bmatrix} \tag{4.30b}$$

For the case of beam on an elastic foundation, the damping parameters (d, d_1) in Eqs.(4.12a,b) vanish, i.e.

$$\mathbf{C}^0 = \begin{bmatrix} 0 & 0 \\ 0 & 0 \end{bmatrix} \tag{4.31a}$$

$$\mathbf{E}_f^2 = \begin{bmatrix} kh & 0 \\ 0 & k_1 h \end{bmatrix} \tag{4.31b}$$

For the case of a 1-dimensional semi-infinite rod resting on an elastic foundation, the SBFEM formulation also has the similar forms of Eqs.(4.24,27) since the derivation process is the same as the above, but the degree of freedom corresponding to the bending rotation must be dropped. As such, the coefficient matrices are reduced to 1x1 matrices, i.e., $\mathbf{E}^0 = EA/h$, $\mathbf{E}^1 = 0$, $\mathbf{E}^2 = 0$, $\mathbf{C}^0 = 0$, $\mathbf{M}^0 = \rho Ah$ and $\mathbf{E}_f^2 = k_g h$, where k_g denotes the stiffness of the elastic foundation. When k_g equals zero, no foundation is present. Substituting these coefficient matrices for the cases of 1-dimensional semi-infinite rod without foundation into Eq.(4.24) leads to

$$\mathbf{S}^{\infty}(\omega) = \sqrt{(i\omega)^2 \mathbf{E}^0 \mathbf{M}^0} = i\omega\sqrt{\mathbf{E}^0 \mathbf{M}^0} = i\omega\sqrt{\rho EA^2} \tag{4.32}$$

The corresponding Eq.(4.25) is re-written as

$$\mathbf{F}(t) = \sqrt{\mathbf{E}^0 \mathbf{M}^0}\, H(t-0)\partial \mathbf{u}/\partial t\big|_0^t \tag{4.33}$$

where $H(t-0)$ denotes a Heaviside function. Initial conditions for the semi-infinite rod are

$$\mathbf{u}\big|_{t=0} = 0; \quad \frac{\partial \mathbf{u}}{\partial t}\bigg|_{t=0} = 0 \tag{4.34}$$

Substituting these initial conditions into Eq (4.33) and then integrating leads to

$$\mathbf{u}(t) = \int_0^t \frac{\mathbf{F}(\tau)}{\sqrt{\mathbf{E}^0 \mathbf{M}^0}\, H(t-0)} d\tau = \int_0^t \frac{\mathbf{F}(\tau)}{\sqrt{\rho EA^2}} d\tau \tag{4.35}$$

where $\mathbf{u}(t)$ and $\mathbf{F}(t)$ represent the displacement and the force at the near-end of the semi-infinite rod, respectively. Hence, Eq (4.35) actually describes the relationship between the displacement and the force at the near-end of the semi-infinite rod without foundations. Of note, it yields an exact solution. In other

words, the SBFEM techniques provide an alternate route for an analytical solution of the semi-infinite rod without foundations.

Although the analytical solution for a 1-dimensional rod can be easily obtained by the SBFEM techniques, the analytical solutions for most cases are difficult to obtain. Normally, numerical solutions are adopted. In order to obtain the numerical solution, $\mathbf{M}_j^\infty$ at time $t = j\Delta t$ (where Δt denotes an increment in time) of Eq.(4.27), Eq.(4.27) can be discretized with respect to time. The solution procedure is similar to those in section 2.6. Upon determining $\mathbf{M}_j^\infty$ and by assuming $\mathbf{u} = \mathbf{u}_2$, Eq.(4.25) is discretized with respect to time as follows.

$$\mathbf{F}^n = \sum_{j=1}^{n} \mathbf{M}_{n-j+1}^\infty \left(\dot{\mathbf{u}}_j - \dot{\mathbf{u}}_{j-1}\right) \tag{4.36a}$$

where $\mathbf{F}^n = \mathbf{F}(n\Delta t)$, and $\dot{\mathbf{u}}_j = \left.\dfrac{\partial \mathbf{u}}{\partial t}\right|_{t=j\Delta t}$. Re-arranging Eq (4.36a) to present $\mathbf{M}_1^\infty \dot{\mathbf{u}}_n$ appeared on the left hand side leads to

$$\mathbf{M}_1^\infty \dot{\mathbf{u}}_n = \mathbf{F}^n - \sum_{j=1}^{n-1} \left(\mathbf{M}_{n-j+1}^\infty - \mathbf{M}_{n-j}^\infty\right)\dot{\mathbf{u}}_j + \mathbf{M}_n^\infty \dot{\mathbf{u}}_0 \tag{4.36b}$$

where the zero initial conditions for Eq.(4.25) are expressed as

$$\mathbf{u}_0 = \mathbf{u}(t = 0) = \mathbf{0} \tag{4.37a}$$

$$\dot{\mathbf{u}}_0 = \left.\frac{\partial \mathbf{u}}{\partial t}\right|_{t=0} = \mathbf{0} \tag{4.37b}$$

Note that Eq.(4.36b) can be used to determine the deformation $\mathbf{u}$ at any time when $\mathbf{F}(t)$ is known and Eq.(4.36a) can be used to determine the force $\mathbf{F}(t)$ when the deformation $\mathbf{u}$ is known because $\mathbf{M}_j^\infty$ is independent of $\mathbf{F}(t)$ and $\mathbf{u}$.

Of note, all formulas shown in Eq.(4.5) through Eq.(4.37) are based on the coordinate system domain in Fig.4.3a which is different from the coordinate system

in Fig.4.2. In order to compare the results obtained from these two coordinate systems, a transform has to be implemented. Here, the subscript 1 denotes the quantities in Fig.4.2, while the subscript 2 is for the quantities in Fig.4.3a. The relationship between the bending and shear angle in these two coordinate systems is

$$\theta_1 = \frac{\partial v_1}{\partial x} + \beta_1 \tag{4.38a}$$

$$\theta_2 = \frac{\partial v_2}{\partial x} - \beta_2 \tag{4.38b}$$

For any cross section, the bending angle must be the same, i.e.

$$\theta = \theta_1 = \theta_2 \tag{4.39}$$

As $\frac{\partial v_1}{\partial x} = -\frac{\partial v_2}{\partial x}$, combining Eqs.(4.38a,b) and Eq.(4.39) yields

$$\beta_1 = 2\theta + \beta_2 \tag{4.40}$$

By substituting Eq.(4.40) into Eq.(4.2a), the shear force can be expressed as

$$Q_1 = \mu AG(2\theta) + \mu AG\beta_2 = \mu AG(2\theta) - Q_2 \tag{4.41a}$$

Through observing the positive direction of the bending moment, the bending moment satisfies

$$M_1 = -M_2 \tag{4.41b}$$

4.3 EXAMPLES

Two examples are used to verify the accuracy of the present SBFEM formulation shown in Eqs.(4.24,27) for a beam resting on a visco-elastic foundation..

4.3.1 A SEMI-INFINITE ROD ON ELASTIC FOUNDATIONS

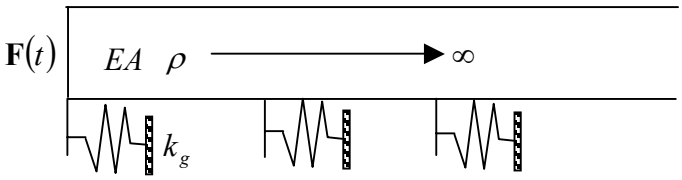

Fig.4.4 A semi-infinite rod on elastic foundations

This example is to test the accuracy of the coefficient $\mathbf{E}'^2$ which involves the effect of an elastic foundation. An axial rod on elastic foundations as shown in Fig.4.4 is considered. In it, ρ and E denote the density and Young's modulus of the rod, respectively; A and h denote the cross-section area and the height of the rod, respectively; k_g denotes the stiffness of the elastic foundation. Using the present SBFEM formulation and dropping the degree of freedom corresponding to the bending rotation yield the coefficient matrices for the rod on an elastic foundation as follows. $\mathbf{E}^0 = EA/h$, $\mathbf{E}^1 = 0$, $\mathbf{E}^2 = 0$ and $\mathbf{M}^0 = \rho Ah$; the coefficient $\mathbf{E}'^2 = k_g h$ and the damping coefficient $\mathbf{C}^0 = 0$. Substituting these coefficients into Eq.(4.24) yields $\mathbf{S}^\infty(\omega) = \sqrt{EAk_g - \omega^2 E\rho A^2}$. This result is identical to the exact solution derived by Wolf and Song (1996a). By substituting these coefficients into Eq.(4.27), $\mathbf{M}^\infty(t)$ is solved and plotted in Fig.4.5, in which $\mathbf{M}^\infty(t)$ is normalized by $\rho c_1 A$ with $c_1 = \sqrt{E/\rho}$, and the time t^* is normalized as $t^* = t c_1 / r_0$ with $r_0 = \sqrt{EA/k_g}$. The numerical results are completely identical to the exact solution of Wolf and Song (1996a). Upon determining $\mathbf{M}^\infty(t)$, the dynamic response of the rod can be obtained by Eq.(4.25). The numerical solution for the interaction force $\mathbf{F}(t)$ at the end of the rod caused by a rounded triangular displacement pulse, which is determined by

$$\mathbf{u}_2(t)=\begin{cases}\dfrac{u_0}{2}\left(1-\cos\left(2\pi\dfrac{t}{t_0}\right)\right) & 0\le t\le t_0, t_0=2\sqrt{\dfrac{\rho A}{k_g}}\\ 0 & t>t_0\end{cases} \tag{4.42}$$

is shown in Fig.4.6. The parameter is normalized by $\sqrt{EAk_g}u_0$. Of note, the exact solutions are not indicated in Figs.4.5 and 4.6, because the numerical solutions from the present method coincide with them. By comparing with the exact solution, it can be concluded that the coefficient $\mathbf{E}'^2$ in the present method is correct.

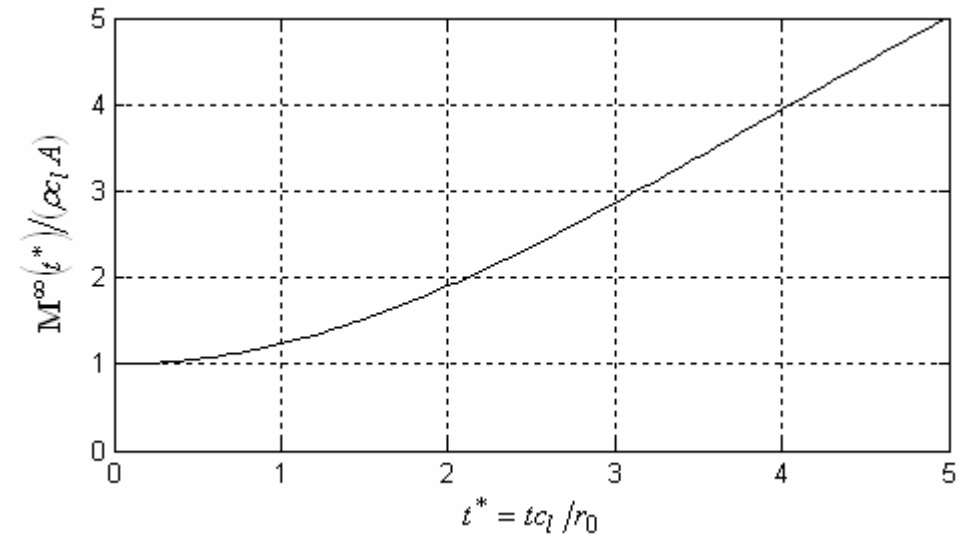

Fig.4.5 $\mathbf{M}^{\infty}(t)$ ***of the semi-infinite rod on elastic foundations***

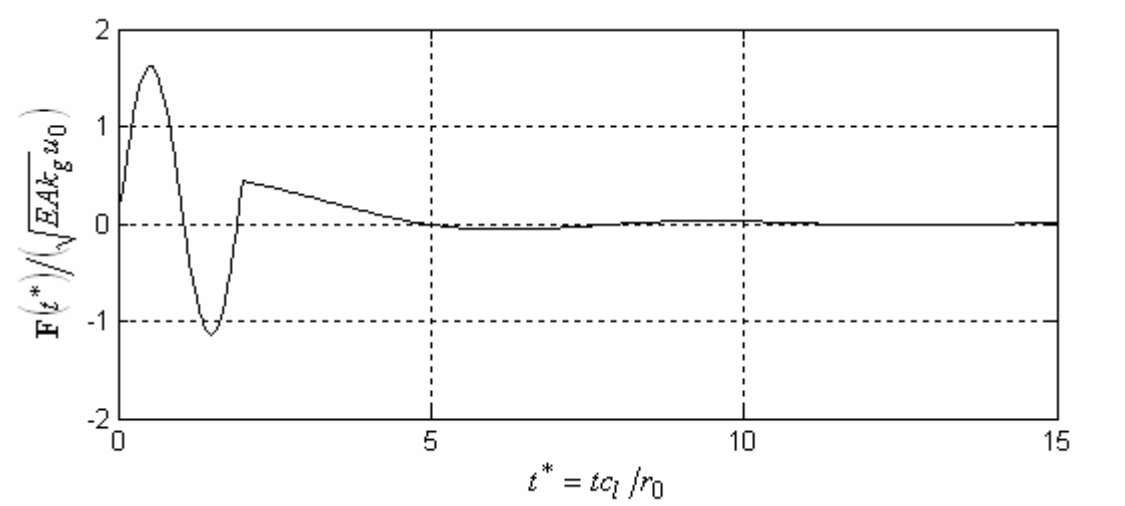

Fig.4.6 Interaction force caused by a rounded triangular displacement pulse applied to the semi-infinite rod on elastic foundations

In order to verify the efficiency of the present SBFEM, a 1-dimensional semi-infinite rod as shown in Fig.4.7 is considered. The rod is subjected to an impulse $p_0 t_0$ (pressure p_0 over a short duration t_0). The time history of the pressure p and the material properties of the rod are shown in Fig.4.7 as well.

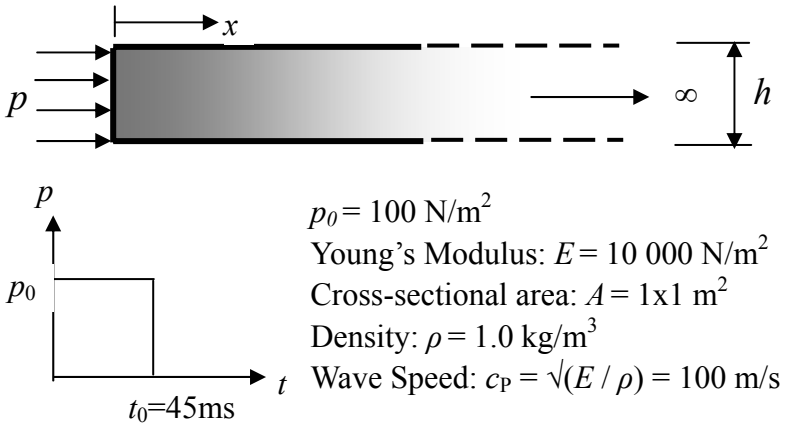

Fig.4.7 A semi-infinite rod subjected to an impulse $p_0 t_0$

Force $F(t)$ acting at the near-end boundary is

$$F(t)=\begin{cases} p_0 A, & t\in[0 \quad t_0] \\ 0, & t\in(t_0 \quad \infty) \end{cases} \tag{4.43}$$

Substituting Eq.(4.43) into Eq.(4.35) leads to

$$u(t)=\begin{cases} t\,p_0/\sqrt{\rho E}, & t\le t_0 \\ t_0\,p_0/\sqrt{\rho E}, & t>t_0 \end{cases} \tag{4.44}$$

The displacement $u(x,t)$ at a location x measured from the near-end satisfies the following 1-dimensional wave equation.

$$\partial^2 u(x,t)/\partial t^2 = c_p^2\,\partial^2 u(x,t)/\partial x^2, \quad x>0, t>0 \tag{4.45}$$

With the initial condition $u(x,t=0)=0$ and the boundary condition (at x=0) as specified in Eq (4.37a), the solution of Eq.(4.45) is

$$u(x,t)=\begin{cases} 0, & t<\dfrac{x}{c} \\ \dfrac{p_0}{\sqrt{\rho E}}\left(t-\dfrac{x}{c}\right), & \dfrac{x}{c}\le t\le t_0+\dfrac{x}{c} \\ \dfrac{p_0}{\sqrt{\rho E}}t_0, & t>t_0+\dfrac{x}{c} \end{cases} \tag{4.46}$$

Hence, the stress at location x is

$$\sigma(x,t)=E\frac{\partial u}{\partial x}=\begin{cases} 0, & t<\dfrac{x}{c} \\ -p_0, & \dfrac{x}{c}\le t\le t_0+\dfrac{x}{c} \\ 0, & t>\dfrac{x}{c}+t_0 \end{cases} \tag{4.47}$$

Note that the solution Eq.(4.47) obtained from the present SBFEM formulation is exact and is the analytical solution. For easy visualization, the solutions at time t=160ms are plotted in Fig.4.8. The same problem was previously discussed by Ponthot and Belytschko (1998). There authors used both EFG (Element-free Galerkin approximation) method and FEM to model the elastic rod with certain vibration conditions. From Fig.4.8, one can see that the results are very neat without

any vibration, so it can be concluded that the present SBFEM formulation for a semi-rod is very efficient.

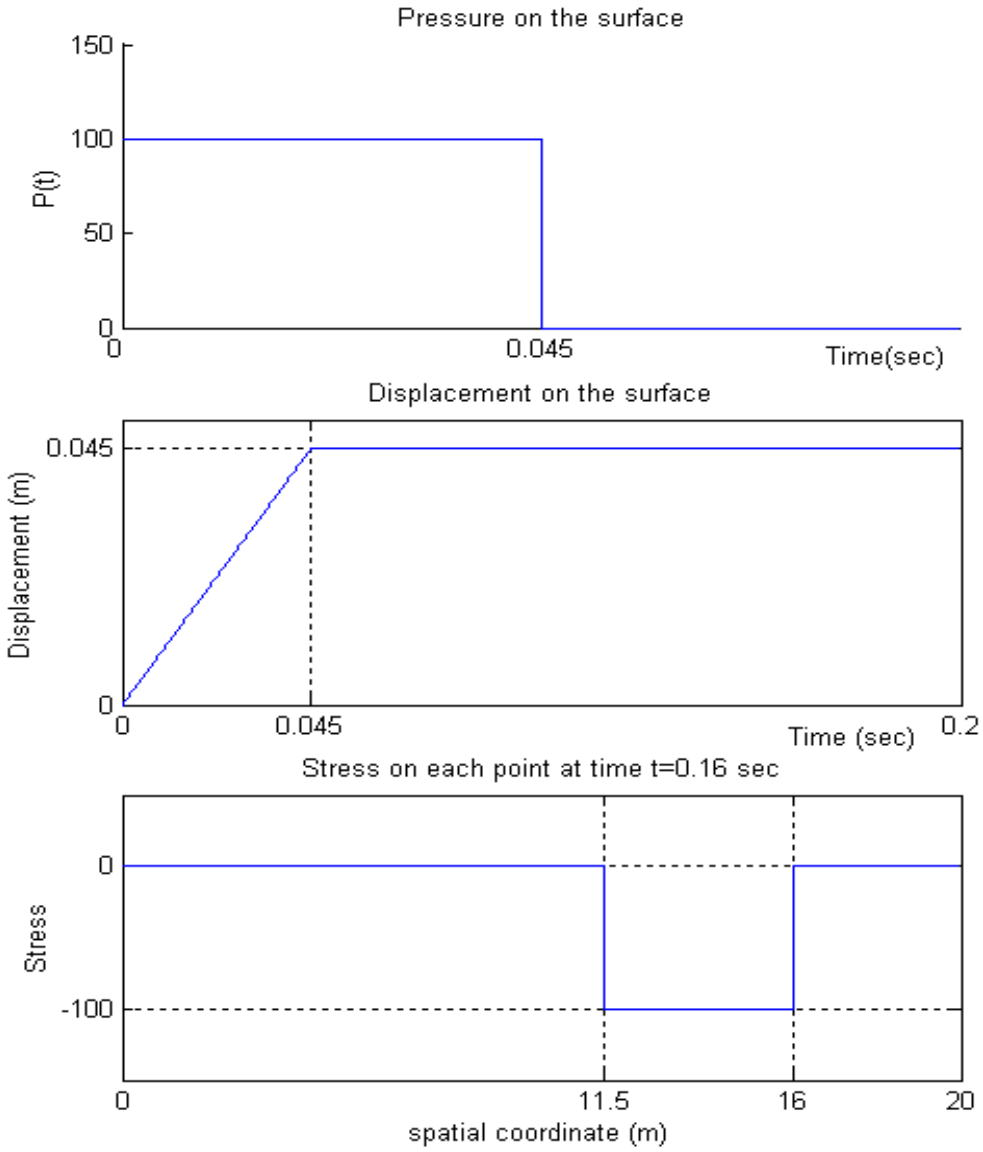

Fig.4.8 Displacements and stresses in the semi-infinite rod subjected to an impulse

4.3.2 A SEMI-INFINITE TIMOSHENKO BEAM ON VISCO-ELASTIC FOUNDATIONS

This example is used to establish the accuracy of the added term $\mathbf{C}^0$ in Eq.(4.24), i.e. $\mathbf{c}^0$ in Eq.(4.27). These coefficients describe the damping properties of visco-elastic foundations. The transient response of a semi-infinite Timoshenko beam on viscoelastic foundations as shown in Fig.4.9 is considered. The geometrical and material parameters are: area $A = 0.25 \times 1.0 \mathrm{m}^2$, shear factor $\mu = \frac{5}{6}$, second moment of area $J = 0.02083 \mathrm{m}^4$, bending stiffness $EJ = 4.29 \times 10^8 \mathrm{N/m}^2$, Poisson's ratio $\nu = 0.2$, density $\rho = 2.35 \times 10^3 \mathrm{kg/m}^3$, critical translational spring stiffness $k_0 = 3.388 \times 10^7 \mathrm{N/m}^2$, critical rotational spring stiffness $k_{10} = 4.423 \times 10^7 \mathrm{N}$, critical translational viscous damping $d_r = 2.82 \times 10^5 \mathrm{N sec/m}^2$, critical rotational viscous damping $d_{r1} = 9.3 \times 10^4 \mathrm{N sec}$, stiffness ratio $\alpha = 1.0$ and damping ratio $\xi = 0.1$. Of note, k_0 and k_{10} are the critical stiffness parameters of the foundation, so that the real stiffness parameters are defined by the stiff ratio, i.e., $\alpha = k/k_0 = k_1/k_{10}$. Likewise, the d_r and d_{r1} are the critical damping parameters of the foundation, so that the real damping parameters are defined by the damping ratio, i.e., $\xi = d/d_r = d_1/d_{r1}$. The corresponding shear wave velocity is $c_s = 1745 \mathrm{m/sec}$.

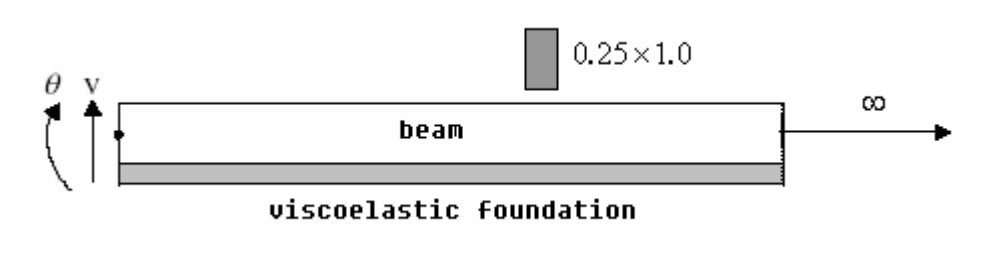

Fig.4.9 A semi-infinite Timoshenko beam on viscoelastic foundations

In order to demonstrate the accuracy of the added coefficients $\mathbf{C}^0$, $\mathbf{c}^0$, the dynamic response of the system is considered and it is subjected to an in-plane sine-square impulse deflection $v(T)\,(\theta = 0)$ as follows.

$$v(T) = \begin{cases} \sin^2(T\pi/2), & 0 \le T \le 2.0 \\ 0.0, & T > 2.0 \end{cases} \tag{4.48a}$$

where $T = c_s t / h$ denotes the dimensionless time, and h denotes the height of the beam. Upon determining $\mathbf{M}^{\infty}(t)$ by solving Eq.(4.27), substituting $\mathbf{M}^{\infty}(t)$ and $v(T)$ into Eq.(4.25) yield the forces at the boundary of the semi-infinite beam. Then, modifying the solutions using Eqs.(4.41a,b) leads to the solutions for the coordinate system shown in Fig.4.2. The solutions are shown in Figs.4.10 and 4.11. The same problem was previously considered by Kausel et al.(1975) using the consistency boundary method and Liu and Li, (2003) using the residual radiation method. These authors' results were also shown in Figs.4.10 and 4.11. In the figures, the exact solution was from Kausel et al. (1975), while those solutions with various legends associated with n were from Liu and Li (2003). Of note, n is the number of the auxiliary residual functions used in Liu and Li's solution. From Figs.4.10 and 4.11, one can see that the results from the present method are identical to the exact solution. Also, Liu and Li's solution only approaches the exact solution with n=20.

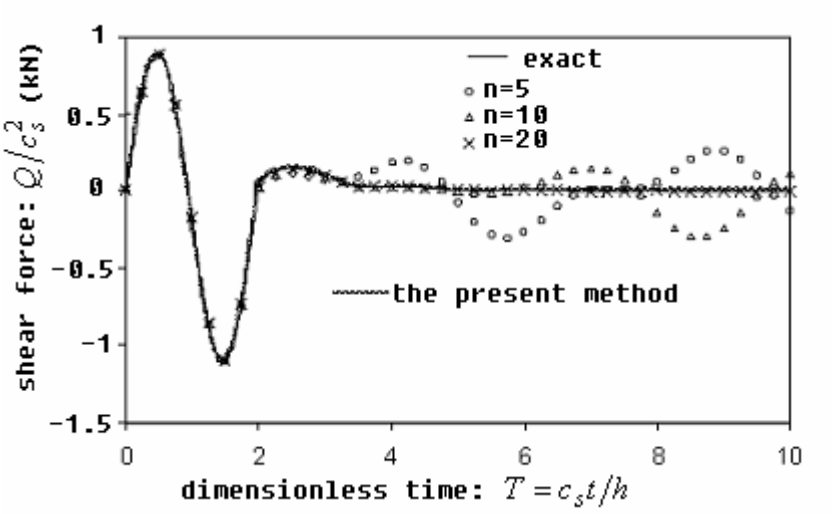

Fig.4.10 Shear force at boundary due to lateral deflection v ***at boundary***

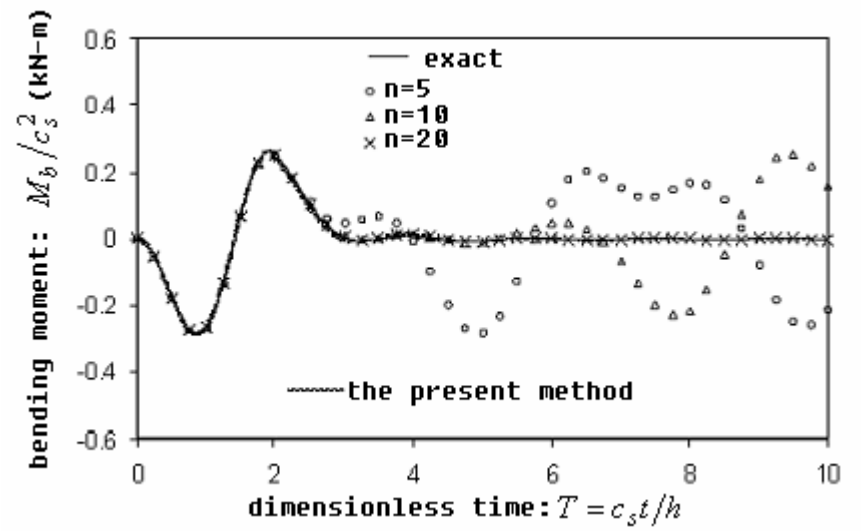

Fig.4.11 Bending moment at boundary due to lateral deflection v ***at boundary***

Next, the validity of Eq.4.41 is to be scrutinized. Consider the same case but now the beam is subjected to an in-plane sine-square impulse rotation $\theta(\mathrm{T})\,(\mathrm{v}=0)$ as follows.

$$\theta(\mathrm{T}) = \begin{cases} \sin^2(\mathrm{T}\pi/2), & 0 \le \mathrm{T} \le 2.0 \\ 0.0, & \mathrm{T} > 2.0 \end{cases} \tag{4.48b}$$

Results are shown in Figs.4.12 and 4.13, and compared with those of Kausel et al. (1975) and Liu and Li (2003). From Figs.4.12 and 4.13, one can see that the results

from the present method are identical to the exact solution again. From the results of the two cases above, it can be concluded that the added term $\mathbf{C}^0$, i.e. $\mathbf{c}^0$ is correct. In addition, the present SBFEM formulation is correct and is very efficient for a semi-infinite Timoshenko beam on a visco-elastic foundation.

Various stiffness and damping parameters are introduced to demonstrate the effect of visco-elastic foundations on the response of a Timoshenko beam. The same beam as above is subjected to an in-plane sine-square impulse deflection as defined in Eq.(4.48a). The extreme case without visco-elastic foundations ($\alpha = \xi = 0$) is investigated. The results are plotted in Figs.4.14 and 4.15. Surprisingly, it is difficult to observe the effect of the foundation on the Timoshenko beam. It is because the stiffness parameters (k and k_1) and the damping parameters (d and d_1) are too small in comparison with the stiffness of the Timoshenko beam. The effect of the foundation can only be seen with higher values of stiffness and damping parameters of the foundation. The results corresponding to higher stiffness and viscous damping ($\alpha = \xi = 10,100,1000$) are shown in Figs.4.16 and 4.17. All other parameters are unchanged. From Figs.4.16 and 4.17, one can see that the effects of the visco-elastic foundation on the Timoshenko beam are apparent when α and ξ (i.e. k, k_1, d and d_1) are relatively large, but the effect of foundations can be ignored for relatively small k, k_1, d and d_1.

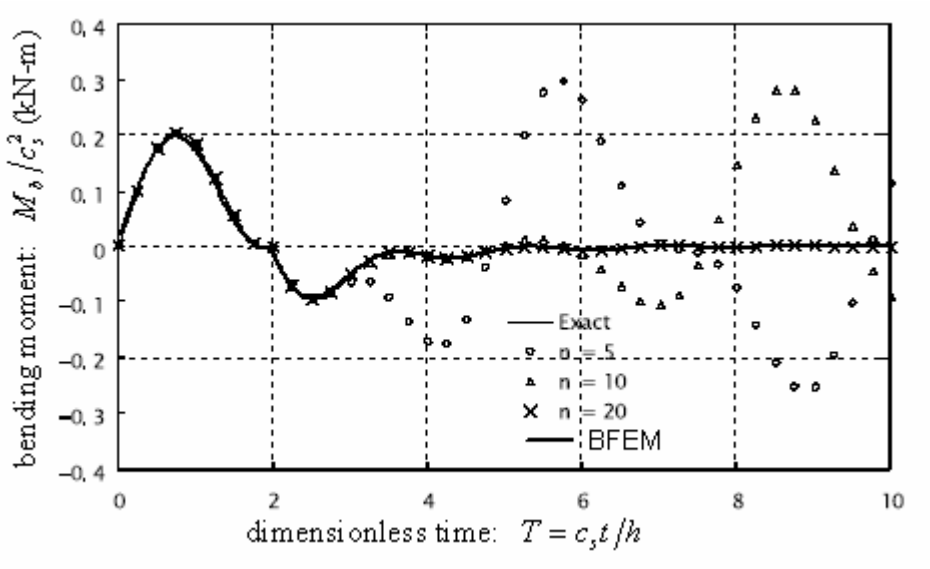

Fig.4.12 Bending moment at boundary due to lateral rotation θ at boundary

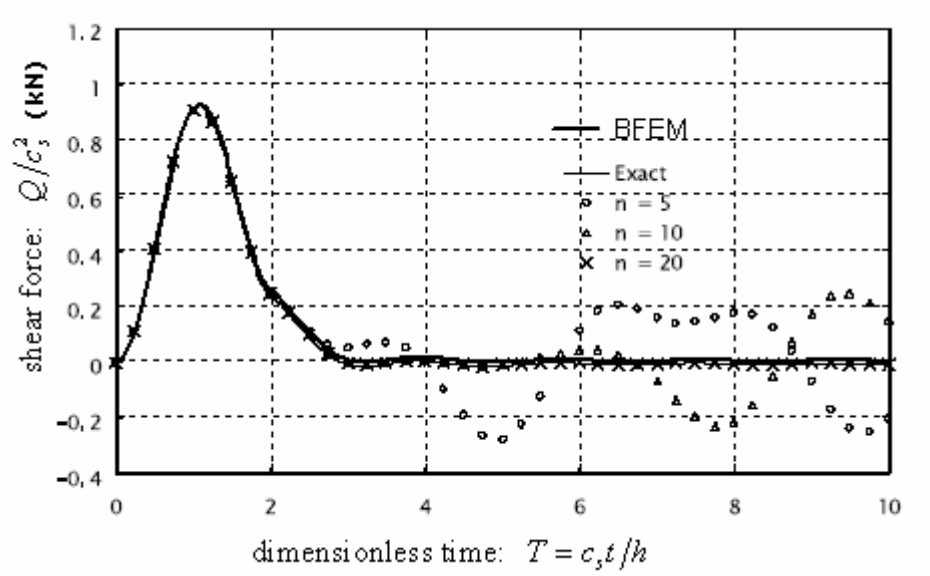

Fig.4.13 Real shear force at boundary due to lateral rotation θ at boundary

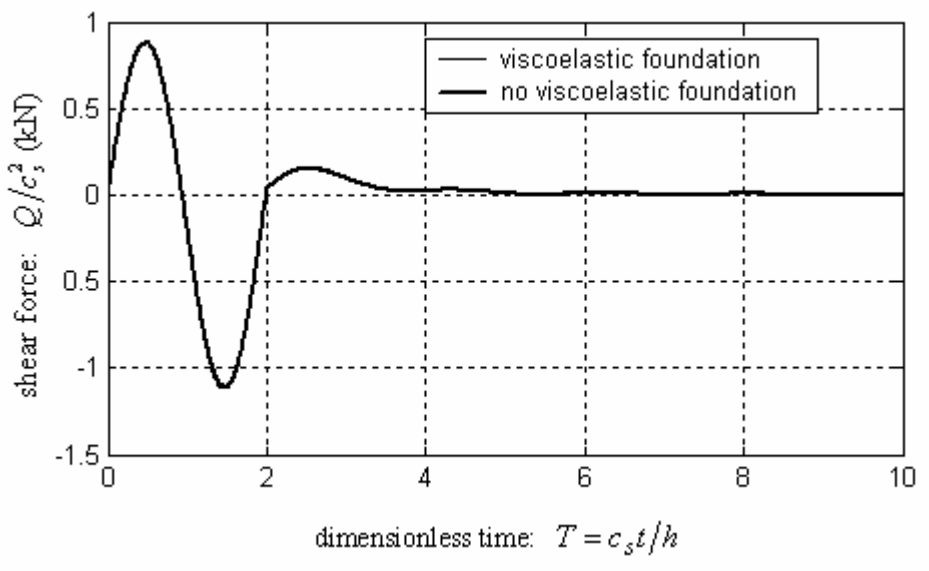

Fig.4.14 Comparison of shear force between cases with and without foundations due to lateral deflection v

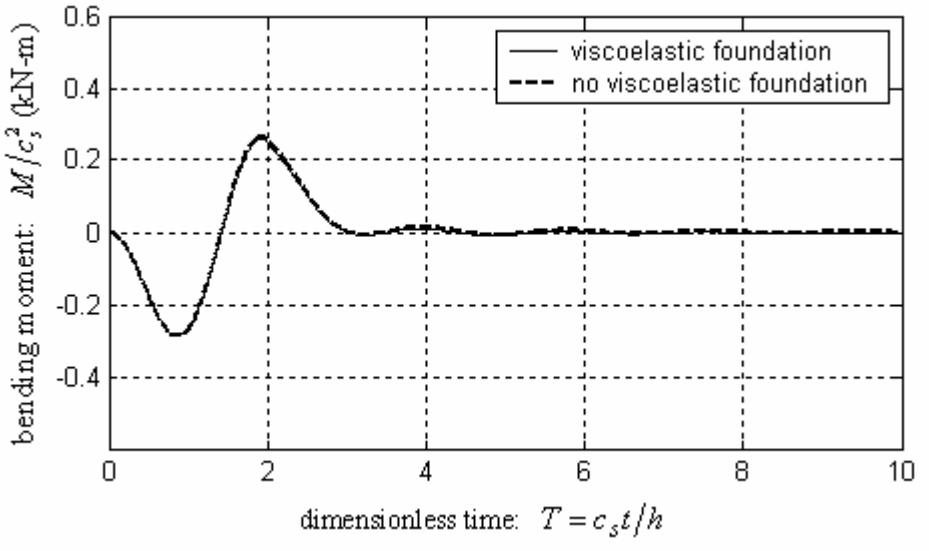

Fig.4.15 Comparison of bending moment between cases with and without foundations due to lateral deflection v

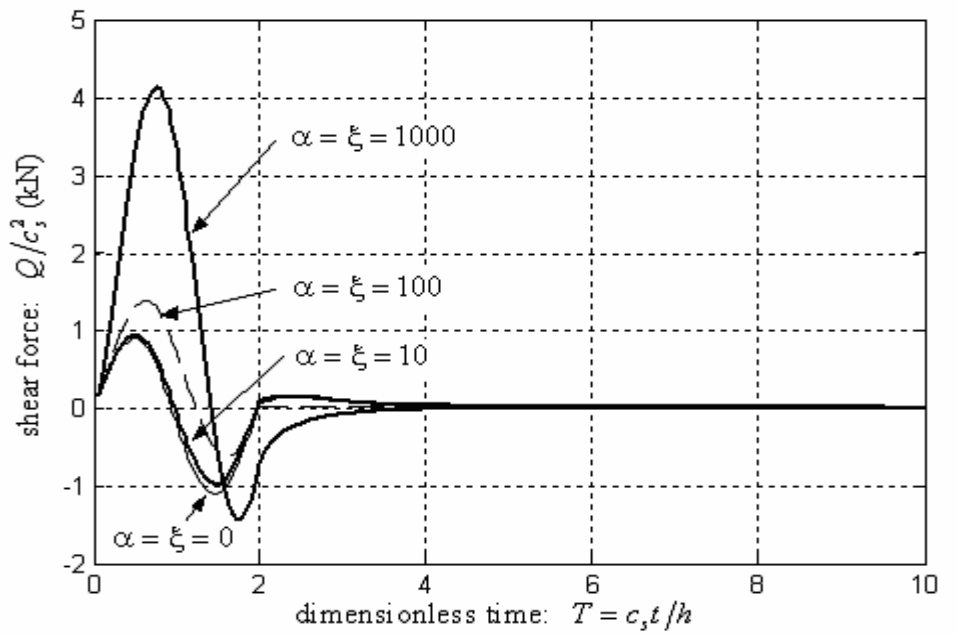

Fig.4.16 Comparison of shear force between different α ***and*** ξ ***due to lateral deflection*** v

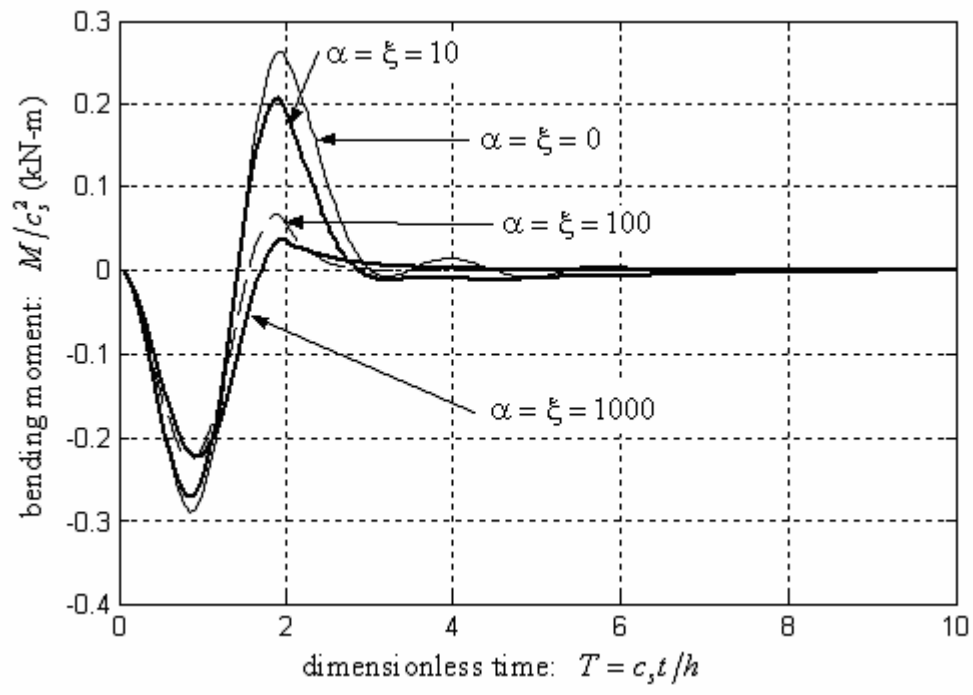

Fig.4.17 Comparison of bending moment between different α ***and*** ξ ***due to lateral deflection*** v

CHAPTER FIVE

SBFEM FORMULATION FOR BOUNDED ACOUSTIC FLUID MEDIUM

Except for infinite medium problems, more bounded medium problems are often encountered in practice. Although the traditional methods such as FEM, BEM are readily available for solving the bounded medium problems, it is still necessary to investigate the SBFEM formulation for the bounded medium problems to show the integrality of the SBFEM for the bounded or unbounded medium. In this chapter, the SBFEM formulation for a bounded medium will be presented and its accuracy and efficiency will be checked against a benchmark example.

5.1 SBFEM FORMULATION FOR A BOUNDED MEDIUM

When the SBFEM is employed to model a bounded inviscid isentropic acoustic fluid medium, the bounded isentropic fluid medium is divided into an assembly of sectors as shown in Fig.5.1a. Each sector S_{ij} is represented by the corresponding boundary ij with a characteristic length r_e. The bounded medium can be also considered as being composed of a scalar-finite-element cell as shown in Fig.5.1b. The cell is bounded by an interior boundary r_i (similar fictitious boundary), an exterior boundary r_e and another bounded medium with a characteristic length r_i as shown in Fig.5.1c. This representation is similar to the SBFEM model of an infinite medium shown in Fig.2.2.

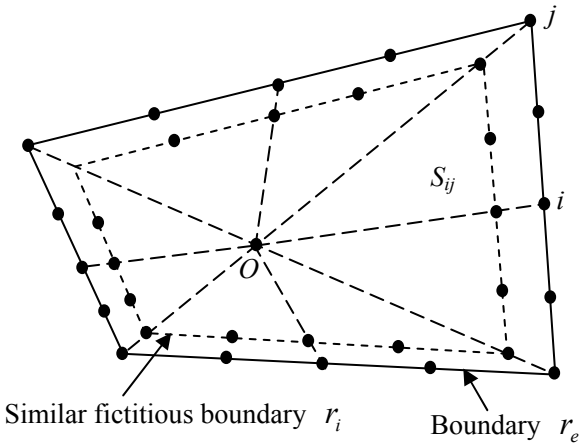

Fig.5.1a Discretization of a bounded fluid medium

On the exterior and interior boundaries, the relationship between a normal velocity v_n and its appropriate velocity potential ϕ in frequency domain is expressed as

$$\mathbf{R}(r_e,\omega)=\mathbf{S}_e^b(\omega)\Phi_e(\omega) \tag{5.1a}$$

$$\mathbf{R}(r_i,\omega)=\mathbf{S}_i^b(\omega)\Phi_i(\omega) \tag{5.1b}$$

where $\mathbf{R}(r,\omega)$ has the form of Eq.(2.8c), $\Phi(\omega)$ denotes the nodal velocity potential vector on boundaries with a characteristic length r and $\mathbf{S}^b(\omega)$ is called the "dynamic stiffness" of the bounded fluid medium with a characteristic length r. Through taking the finite-element analysis as presented in section 2.3 for a scalar finite-element cell as shown in Fig.5.1b, it can be found that the relationship between the interior and exterior boundaries of the scalar finite element cell has the similar form of Eq.(2.21). Through comparing Eq.(5.1) with Eq.(2.14) and then using the pair, $-\mathbf{S}_i^b(\omega)$ and $\mathbf{S}_e^b(\omega)$, which stand for the pair, $\mathbf{S}_i^\infty(\omega)$ and $-\mathbf{S}_e^\infty(\omega)$ in Eq.(2.21), the corresponding form of Eq.(2.21) for a bounded medium is expressed as

$$-\mathbf{S}_i^b(\omega)=\mathbf{S}_{ii}(\omega)-\mathbf{S}_{ie}(\omega)\left(-\mathbf{S}_e^b(\omega)+\mathbf{S}_{ee}(\omega)\right)^{-1}\mathbf{S}_{ei}(\omega) \tag{5.2}$$

The corresponding frequency equation for a bounded medium is

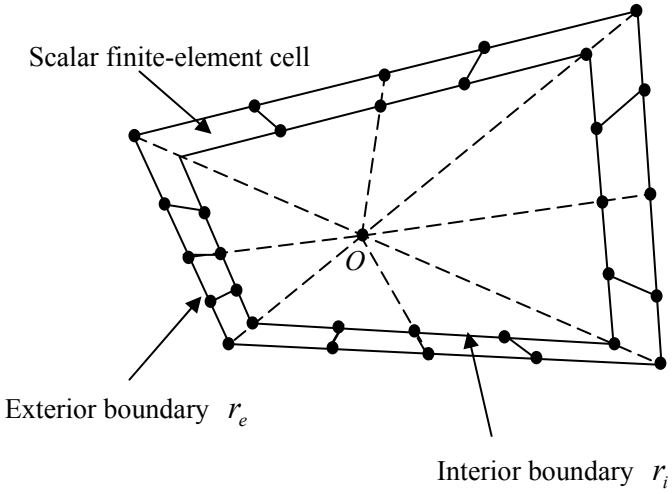

Fig.5.1b A scalar finite-element cell on the boundaries of a bounded medium

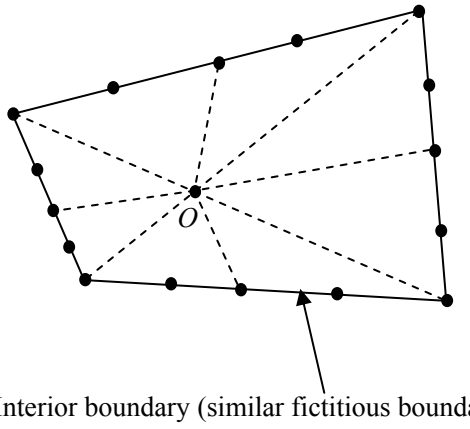

Fig.5.1c Bounded medium with a characteristic length $\mathrm{r_i}$

$$\left(-\mathbf{S}^{\mathrm{b}}(\omega)+\mathbf{E}^{1}\right)\mathbf{E}^{0-1}\left(-\mathbf{S}^{\mathrm{b}}(\omega)+\mathbf{E}^{1\mathrm{T}}\right)+\mathrm{r}\frac{\partial\mathbf{S}^{\mathrm{b}}(\omega)}{\partial\mathrm{r}}-\mathbf{E}^{2}+\omega^{2}\mathbf{M}^{0}=\mathrm{O}(\mathrm{w}) \tag{5.3}$$

Since $\mathbf{S}^{\mathrm{b}}(\mathrm{r},\omega)$ and $\mathbf{S}^{\infty}(\mathrm{r},\omega)$ have the same dimension, the following equation

must be satisfied. The equation is of the same form as that of (2.61), i.e.

$$\mathrm{r}\frac{\partial \mathbf{S}^{\mathrm{b}}(\mathrm{r},\omega)}{\partial \mathrm{r}} = (\mathrm{s}-2)\mathbf{S}^{\mathrm{b}}(\mathrm{r},\omega) + \omega\frac{\partial \mathbf{S}^{\mathrm{b}}(\mathrm{r},\omega)}{\partial \omega} \tag{5.4}$$

Substituting Eq.(5.4) into Eq.(5.3) leads to the final SBFEM formulation in frequency domain for a bounded fluid medium as follows.

$$\begin{aligned}\left(-\mathbf{S}^{\mathrm{b}}(\mathrm{r},\omega)+\mathbf{E}^{1}\right)\mathbf{E}^{0^{-1}}\left(-\mathbf{S}^{\mathrm{b}}(\mathrm{r},\omega)+\mathbf{E}^{1^{\mathrm{T}}}\right)+(\mathrm{s}-2)\mathbf{S}^{\mathrm{b}}(\mathrm{r},\omega)& \\ +\omega\frac{\partial \mathbf{S}^{\mathrm{b}}(\mathrm{r},\omega)}{\partial \omega}-\mathbf{E}^{2}+\omega^{2}\mathbf{M}^{0}=0&\end{aligned} \tag{5.5}$$

All coefficient matrices and the symbol s are the same as those in Eq.(2.62). Usually, Eq.(5.5) is difficult to solve. In order to solve Eq.(5.5), the high-frequency responses are neglected and only the low-frequency responses are retained so that the dynamic-stiffness matrix $\mathbf{S}^{\mathrm{b}}(\omega)$ (for simplicity, $\mathbf{S}^{\mathrm{b}}(\omega)$ stands for $\mathbf{S}^{\mathrm{b}}(\mathrm{r},\omega)$) of the bounded medium with a characteristic length r can be postulated as

$$\mathbf{S}^{\mathrm{b}}(\omega) = \mathbf{K}^{\mathrm{b}} - \omega^{2}\mathbf{M}^{\mathrm{b}} \tag{5.6}$$

where $\mathbf{K}^{\mathrm{b}}$, $\mathbf{M}^{\mathrm{b}}$ are the static-stiffness and static-mass matrices of the bounded medium with a characteristic length r, respectively. Note that this assumption is reasonable because the response of a bounded medium is dominated by its low-frequency modes. Similar to the corresponding matrices of FEM, $\mathbf{K}^{\mathrm{b}}$ and $\mathbf{M}^{\mathrm{b}}$ are independent of the frequency ω and depend only on the geometry of boundaries with the characteristic length r of the bounded medium. The followings show how determines $\mathbf{K}^{\mathrm{b}}$ and $\mathbf{M}^{\mathrm{b}}$.

5.2 STATIC-STIFFNESS MATRIX

By setting $\omega = 0$, Eq.(5.6) is re-formulated as

$$\mathbf{S}^{\mathrm{b}}(\omega) = \mathbf{K}^{\mathrm{b}} \tag{5.7}$$

and then substituting Eq.(5.7) into Eq.(5.5) yields

$$\left(-\mathbf{K}^{b}+\mathbf{E}^{1}\right)\mathbf{E}^{0^{-1}}\left(-\mathbf{K}^{b}+\mathbf{E}^{1^{T}}\right)+(s-2)\mathbf{K}^{b}-\mathbf{E}^{2}=0 \tag{5.8}$$

By re-writing Eq.(5.8) in the form of an algebraic Riccati equation, Eq.(5.8) becomes

$$\mathbf{K}^{b}\mathbf{E}^{0^{-1}}\mathbf{K}^{b}-\left(\mathbf{E}^{1}\mathbf{E}^{0^{-1}}-\frac{s-2}{2}\mathbf{I}\right)\mathbf{K}^{b}-\mathbf{K}^{b}\left(\mathbf{E}^{0^{-1}}\mathbf{E}^{1^{T}}-\frac{s-2}{2}\mathbf{I}\right)-\mathbf{E}^{2}+\mathbf{E}^{1}\mathbf{E}^{0^{-1}}\mathbf{E}^{1^{T}}=0 \tag{5.9}$$

which can be solved by Schur decomposition and produces a symmetric solution. Therefore $\mathbf{K}^{b}$ is symmetric. Note that $\mathbf{K}^{b}$ is singular like an element stiffness matrix $\mathbf{K}^{e}$ in FEM and is semi-positive definite. In order to ensure the positive solution of Eq.(5.9) (the positive definite matrix $\mathbf{K}^{b}$), a term $\varepsilon\mathbf{I}$ having a very small constant ε with the dimension of $\beta\, r_{e}^{s-2}$ (β denotes the bulk modulus of the bounded fluid) is added to $\mathbf{E}^{2}$. Physically, this artificial operation may be interpreted as a flexible support having a very small spring stiffness to each of the boundary node. When the constant ε is very small, the $\mathbf{K}^{b}$ value is hardly changed but becomes positive definite. $\mathbf{K}^{b}$ represents the static-stiffness matrix of the bounded medium.

5.3 MASS MATRIX

To determine the mass matrix $\mathbf{M}^{b}$ of a bounded medium, only the low-frequency behavior of Eq.(5.5) is considered. Substituting Eq.(5.6) into Eq.(5.5) leads to an express on that contains a constant term which is independent of $(j\omega)$, a term of $(j\omega)^{2}$ and higher-order terms of $(j\omega)$. The 3rd and higher-order terms of $(j\omega)$ are ignored because of the low value of the frequency. The constant term which is equal to the left-hand side of Eq.(5.9) vanishes. The coefficient matrix of the remaining term of $(j\omega)^{2}$ is expressed as

$$\left(\left(-\mathbf{K}^{b}+\mathbf{E}^{1}\right)\mathbf{E}^{0^{-1}}-\frac{s}{2}\mathbf{I}\right)\mathbf{M}^{b}+\mathbf{M}^{b}\left(\mathbf{E}^{0^{-1}}\left(-\mathbf{K}^{b}+\mathbf{E}^{1^{T}}\right)-\frac{s}{2}\mathbf{I}\right)+\mathbf{M}^{0}=0 \qquad (5.10)$$

This is the Lyapunov equation, which can be used to obtain the solution of $\mathbf{M}^{b}$ after getting $\mathbf{K}^{b}$ from Eq.(5.9). Note that $\mathbf{M}^{b}$ is symmetric, which can be proven by subtracting the transpose of Eq.(5.10) from Eq.(5.10).

5.4 DYNAMIC SOLUTIONS BY NEWMARK SCHEME

Once the static-mass matrix $\mathbf{M}^{b}$ and the static-stiffness matrix $\mathbf{K}^{b}$ of a bounded medium are determined, the dynamic response of the bounded medium can be solved, the conventional FEM procedures can be followed and thus solutions can be obtained through a Newmark iteration scheme. However, the solutions of the bounded medium were found sensitive to the dissipation coefficient used in the Newmark scheme. In the present SBFEM formulation, no damping ($\mathbf{C}^{b}=0$) is considered. Nevertheless, the general basic equation is

$$\mathbf{M}^{b}\ddot{\Phi}_{n+1}+\mathbf{C}^{b}\dot{\Phi}_{n+1}+\mathbf{K}^{b}\Phi_{n+1}=\mathbf{R}_{n+1} \qquad (5.11)$$

where $\ddot{\Phi}_{n+1}$, $\dot{\Phi}_{n+1}$, Φ_{n+1} and $\mathbf{R}_{n+1}$ denote the second derivative of velocity potential Φ with respect to time, the first derivative of velocity potential Φ with respect to time, velocity potential and an integral of the normal velocity along boundaries of a bounded medium at the time step n+1, respectively. Adopting the Newmark iteration scheme, one can get

$$\ddot{\Phi}_{n+1}=\left(1-\frac{1}{2\beta}\right)\ddot{\Phi}_{n}-\left(\frac{1}{\Delta t\beta}\right)\dot{\Phi}_{n}+\left(\frac{1}{\Delta t^{2}\beta}\right)\Delta\Phi=\ddot{\Phi}_{n}^{*}+\left(\frac{1}{\Delta t^{2}\beta}\right)\Delta\Phi \qquad (5.12a)$$

$$\dot{\Phi}_{n+1}=\left(1-\frac{\gamma}{\beta}\right)\dot{\Phi}_{n}+\left(1-\frac{\gamma}{2\beta}\right)\Delta t\ddot{\Phi}_{n}+\left(\frac{\gamma}{\Delta t\beta}\right)\Delta\Phi=\dot{\Phi}_{n}^{*}+\left(\frac{\gamma}{\Delta t\beta}\right)\Delta\Phi \qquad (5.12b)$$

which is expressed in terms of the $\ddot{\Phi}_{n}$ and $\dot{\Phi}_{n}$ at its previous time step (t_{n+1}- Δt)

and the incremental velocity potential $\Delta\Phi$ $(=\Phi_{n+1}-\Phi_n)$; while $\ddot{\Phi}_n^*$ and $\dot{\Phi}_n^*$ are defined as

$$\ddot{\Phi}_n^* = \left(1-\frac{1}{2\beta}\right)\ddot{\Phi}_n - \left(\frac{1}{\Delta t\beta}\right)\dot{\Phi}_n \tag{5.13a}$$

$$\dot{\Phi}_n^* = \left(1-\frac{\gamma}{\beta}\right)\dot{\Phi}_n + \left(1-\frac{\gamma}{2\beta}\right)\Delta t\ddot{\Phi}_n \tag{5.13b}$$

To ensure second-order accuracy and unconditional stability, the parameters β and γ in Eqs.(5.12) and (5.13) have to be defined through a numerical dissipation coefficient α such that

$$\gamma = 0.5(1-2\alpha) \tag{5.14a}$$

$$\beta = 0.25(1-4\alpha)^2 \tag{5.14b}$$

and the value of α is restricted to the range [-1/3, 0]. Note that $\alpha = 0$ corresponds to the Newmark's constant-average-acceleration scheme. Substituting Eqs.(5.14a) and (5.14b) into Eqs.(5.12) and (5.13) and then into Eq.(5.11) yields

$$\begin{aligned}\left(\frac{\mathbf{M}^b}{(1+\alpha)\Delta t^2\beta}+\frac{\mathbf{C}^b\gamma}{\Delta t\beta}+\mathbf{K}^b\right)\Delta\Phi &= \mathbf{R}_{n+1}\\ -\frac{\alpha}{1+\alpha}\left(\mathbf{R}_n-\mathbf{C}^b\dot{\Phi}_n-\mathbf{K}^b\ddot{\Phi}_n\right)&-\left(\frac{1}{1+\alpha}\mathbf{M}^b\ddot{\Phi}_n^*+\mathbf{C}^b\dot{\Phi}_n^*+\mathbf{K}^b\Phi_n\right)\end{aligned} \tag{5.15}$$

The Newmark scheme implemented together with this numerical dissipation α is capable to yield satisfactory results. It successfully dissipates some spurious high-frequency responses. The details have been discussed in the literature (Broderick et al. (1994)).

5.5 NUMERICAL EXAMPLE

The objective of showing this example is to validate the accuracy of the present SBFEM formulation for a bounded fluid medium, where reflections from the

boundaries are present. A 2-dimensional water column in a rigid container is considered. The bottom and the two vertical boundaries are rigid, while a step pressure p is applied at the top (see Fig.5.2). Along the two vertical rigid boundaries, the movement of the fluid is not restrained in the vertical direction but in the horizontal direction. The properties of material and the time history of the step pressure are shown in Fig.5.2. In the SBFEM procedures, the fluid domain (2D) is discretized into 18 sectors, each represented by an infinitesimal-thin quadratic element lying along the boundaries: one element covered the top surface boundary, one covered the bottom surface boundary and 8 covered each vertical boundary (totalling 1+1+8+8=18). All 18 sectors are radiated outwards from the similar center located at the center of the container as shown in Fig.5.3. In order to keep the matrix $\mathbf{K}^b$ positive definite, a term $\varepsilon\mathbf{I}$ having a very small value ε = 1.0 (10^{-40}) is added to the matrix $\mathbf{E}^2$. The time increment adopts $\Delta t = 1.0$ (10^{-5}) second. This problem was previously analyzed by Bathe and Hahn (1979) and Hamdan (1999), respectively. Bathe and Hahn (1979) used the updated Lagrangian approach to model the fluid column with ten 4-node elements, while Hamdan (1999) modeled it with five 4-node axisymemetric fluid elements. The resulting time-history of pressure at the bottom boundary is investigated. Fig.5.4 shows the results using Newmark's constant average acceleration scheme (i.e. $\alpha = 0$). From Fig.5.4, one can see that though the major wave form has been captured, a lot of noises are exhibited. In order to dissipate those noises, an alternate dissipation factor ($\alpha = -0.3$) is used, and the results are shown in Fig.5.5. One can see that the wave form becomes very clean and tidy and almost identical to the analytical solution. The amplitude is equal to $2P_0$. The resulting time-history of the vertical displacement at the top boundary is also investigated. Fig.5.6 shows the SBFEM results using a Newmark's dissipation factor $\alpha = -0.3$. Results by Bathe and Hahn (1979) and Hamdan (1999) are also included in Fig.5.6. By comparing the results,

one can see that the present SBFEM results are identical to Bathe and Hahn's and Hamdan's but much smoother.

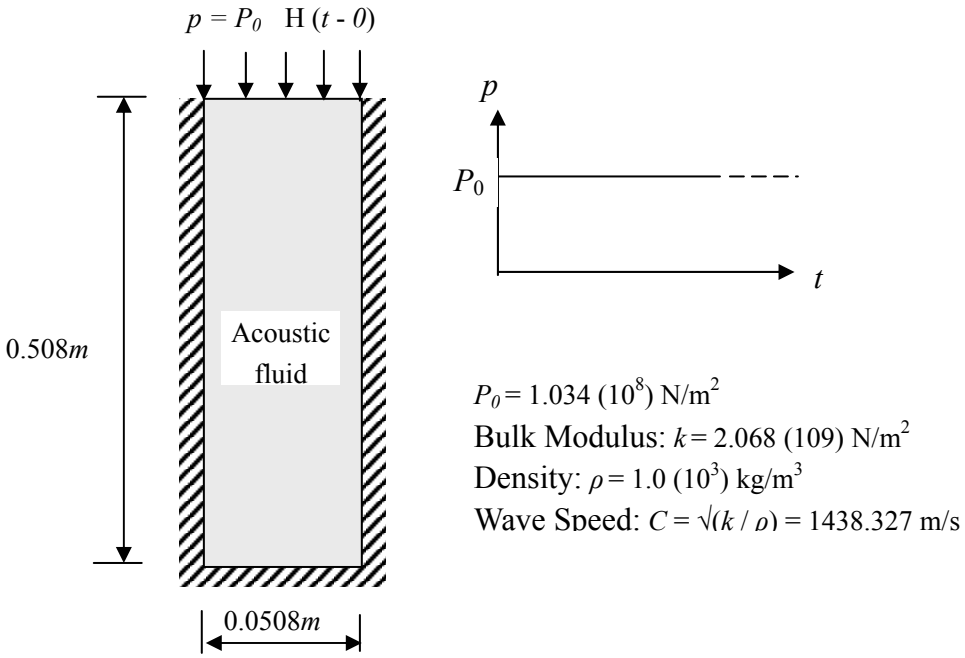

Fig.5.2 Configuration and material properties of a tall water column

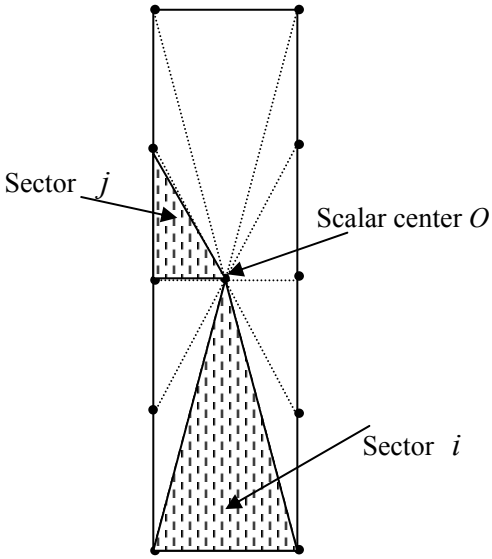

Fig.5.3 SBFEM mesh

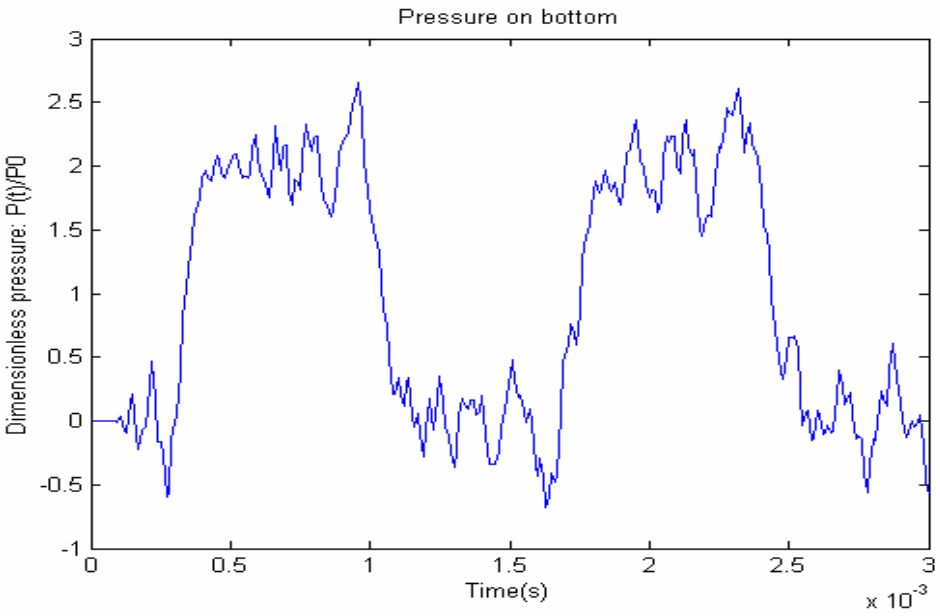

Fig.5.4 Time-history of pressure at bottom boundary using dissipation $\alpha = 0$

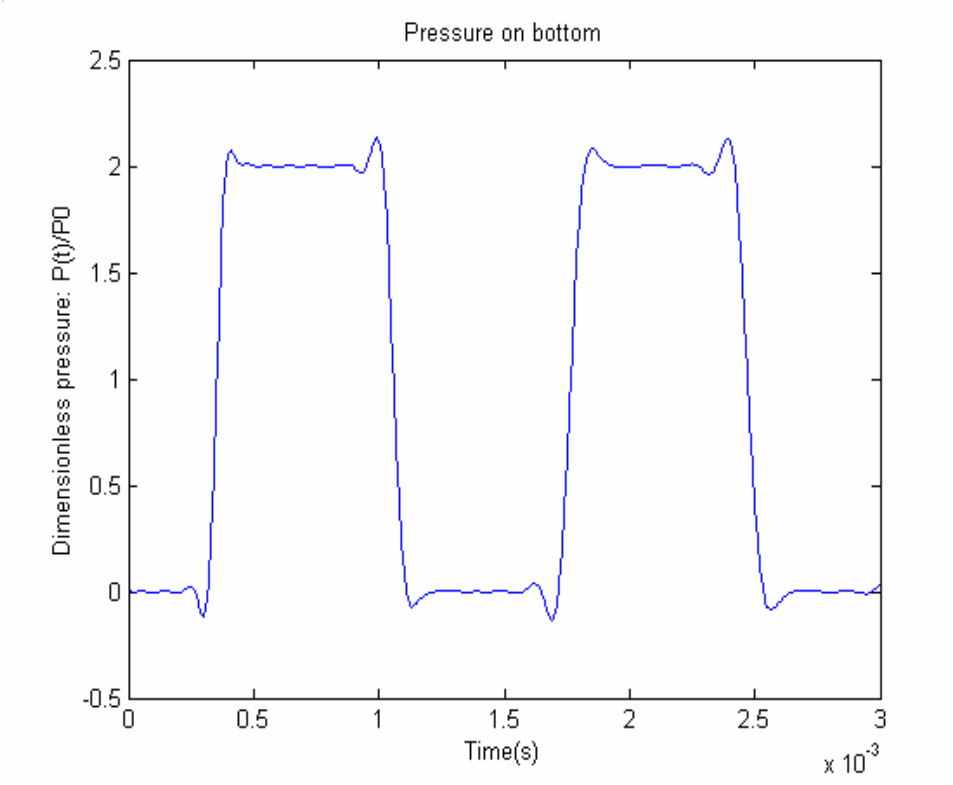

Fig.5.5 Time-history of pressure at bottom boundary using dissipation $\alpha = -0.3$

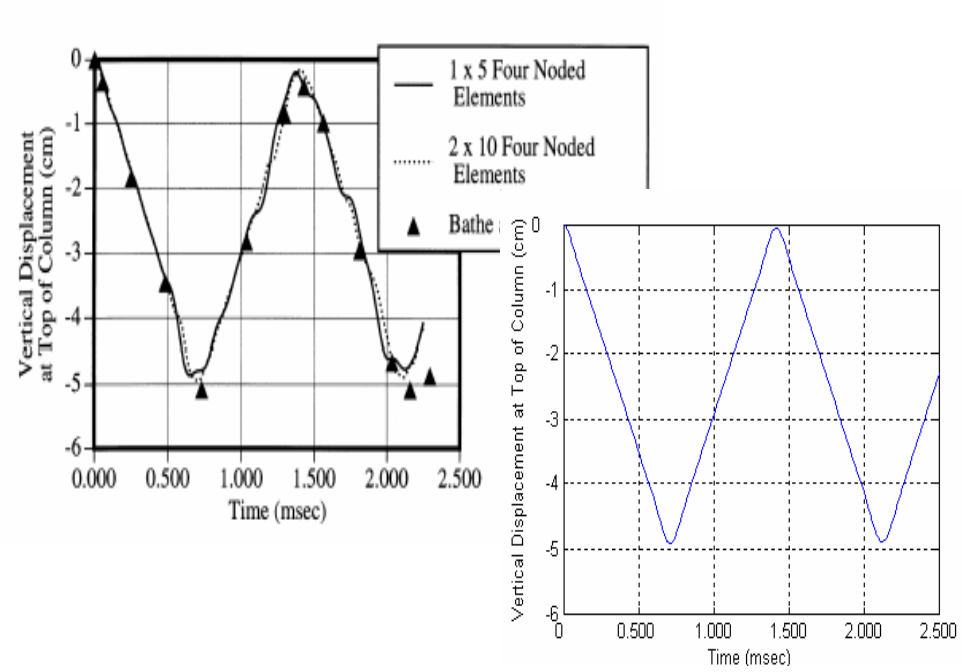

Fig.5.6 Time-history of vertical displacement at top boundary using dissipation $\alpha = -0.3$, ***and comparisons with results by Bathe and Hahn (1979) and Hamdan (1999)***

CHAPTER SIX

DYNAMIC FLUID-STRUCTURE INTERACTION ANALYSIS USING SBFEM/FEM COUPLING METHOD

In this chapter, the scaled boundary finite element method (SBFEM) presented in chapter 2 is applied to dynamic fluid-structure interaction problems. The SBFEM is employed to model the infinite fluid medium, while the structure is modeled by finite element method (FEM). The relationship between the fluid pressure and the fluid velocity corresponding to the scattered waves is derived from the acoustic model. Numerical examples are presented to verify the accuracy and efficiency of the SBFEM-FEM coupling for fluid-structure interaction problems. In comparison with the PWA, VWA and DAA, the present formulation using the SBFEM does not impose any restriction on the structure and the incident wave as well. Hence, it is applicable for both early- and late-time response analyses. In comparison with the FEM-FEM and FEM-BEM coupling procedures, the present formulation has the advantages that no artificial boundaries are needed, no singularity is encountered, no asymmetric matrix appears and no fundamental solution is required.

6.1 SBFEM-FEM COUPLING FORMULATION

In the current study, the SBFEM is used to model the unbounded compressible acoustic fluid medium, while the FEM is used to model the structure.

6.1.1 FEM MODEL FOR THE STRUCTURE

In modeling the structure, the mass matrix $\mathbf{M}$, the damping matrix $\mathbf{C}$ and the stiffness matrix $\mathbf{K}$ can be treated in the standard manner according to the FE discretization procedures. For 2-dimensional thin hollow cylindrical problems, simple two-node beam elements are used.

6.1.2 SBFEM MODEL FOR THE UNBOUNDED ACOUSTIC FLUID MEDIUM

6.1.2.1 Acoustic approximation

When a structure submerged in an unbounded fluid medium is subjected to incident waves, the major concern is the integrity of the structure, in particular its strength adequacy against the dynamic pressure acting on the structural surface (wet surface). To begin, the total fluid pressure and velocity along the wet surface may be considered composing of two components: a free-field component and a scattered component (Fan et al. 2001).

$$\mathbf{p}_{\text{inf}} = \mathbf{p}_{\text{ff}} + \mathbf{p}_{\text{sc}} \tag{6.1}$$

$$\mathbf{v}_{\text{inf}} = \mathbf{v}_{\text{ff}} + \mathbf{v}_{\text{sc}} \tag{6.2}$$

where $\mathbf{p}_{\text{inf}}$ and $\mathbf{v}_{\text{inf}}$ are the total fluid pressure and normal velocity along the wet surface, $\mathbf{p}_{\text{ff}}$ and $\mathbf{v}_{\text{ff}}$ are the corresponding component fluid pressure and normal velocity but are caused by the incident wave in the absence of the structure (usually referred to as the free-field response), and $\mathbf{p}_{\text{sc}}$ and $\mathbf{v}_{\text{sc}}$ are the corresponding component fluid pressure and normal velocity corresponding to the scattered wave, which are the difference between the total and free-field solutions. The relationship between $\mathbf{p}_{\text{sc}}$ and $\mathbf{v}_{\text{sc}}$ is described in the next section. The fluid medium is assumed to have a linear constitutive relationship, which excludes the effect due to cavitation, and thereby the free-field pressure and velocities will be the same as the incident waves; i.e.

$$\mathbf{p}_{\text{ff}} = \mathbf{p}_{\text{inc}} \tag{6.3a}$$

$$\mathbf{v}_{\text{ff}} = \mathbf{v}_{\text{inc}} \tag{6.3b}$$

where $\mathbf{p}_{\text{inc}}$ and $\mathbf{v}_{\text{inc}}$ are the fluid pressure along the wet surface and the corresponding normal velocity caused by the incident wave.

6.1.2.2 Pressure-velocity relationship for the scattered wave

In the PWA approximation, the pressure-velocity relationship corresponding to

scattered waves can be described as

$$\mathbf{p}_{sc} = \rho c \mathbf{v}_{sc} \tag{6.4a}$$

while in the DAA approximation, the relationship can be expressed as

$$\frac{1}{\rho c}\left(\dot{\mathbf{p}}_{inf} - \dot{\mathbf{p}}_{ff}\right) - \mathbf{M}^{-1}\mathbf{A}\left(\mathbf{p}_{inf} - \mathbf{p}_{ff}\right) = \mathbf{a}_{inf} - \mathbf{a}_{ff} \tag{6.4b}$$

where an over-dot denotes differentiation with respect to time, $\mathbf{M}^{-1}$ is the inverse of the fluid-added mass matrix, $\mathbf{A}$ denotes the diagonal matrix which transforms diagonal pressures to forces, and $\mathbf{a}_{inf}$, $\mathbf{a}_{ff}$ denotes the accelerations on the wet surface. ρ and c denote fluid density and wave speed in fluid, respectively. In the current study, another form of the relationship based on the SBFEM and acoustic approximation is developed and described in detail in the next section.

6.1.2.3 SBFEM formulation for the scattered wave

a) Basic description

Basically, the SBFEM describes the dynamic behavior of an unbounded medium through a dynamic stiffness (or mass) matrix in frequency domain relating the displacement (or potential) of the boundary to the corresponding force (or velocity) on it. By discretizing the domain into sectors radiating from a single centre (namely scalar center), the geometry of the sectors can be conveniently described in a transformed coordinate system (in which, one ordinate radiates outward from the scalar center, while others run along the boundary curve/surface). More precisely, the unbounded medium lies in a semi-infinite domain (see Fig.2.1a). Along the radial direction, the near side is bounded while the far side is unbounded. The derivation of the dynamic stiffness/mass matrix is based on a 'cloning' technique, in which the small differential (w) between the two similar semi-bounded sectors (see Fig.6.1) is taken to the analytical limit, zero. Consider the infinitesimal finite-element cell i-j-i'-j' (see Fig.6.1) which lies on the boundary of the semi-infinite fluid domain. Note that the near face i-j is parallel to its cloned surface i'-j', and the two side faces O_i and O_j are both originated from the scalar center O.

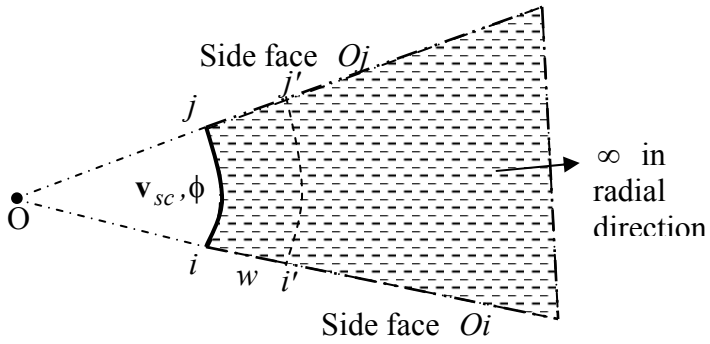

Fig.6.1 A typical SBFEM element with differential width w lying on the boundary of a semi-infinite domain

The governing equation relating the potential and the velocity can be written as

$$\mathbf{V}_{sc}(t) = \int_0^t \mathbf{M}^{\infty}(t-\tau)\ddot{\boldsymbol{\varphi}}(\tau)d\tau \tag{6.5}$$

where $\boldsymbol{\varphi}(t)$ denotes a velocity potential vector composed of nodal velocity potential $\phi(t)$ for scattered waves on the wet surface, $\mathbf{M}^{\infty}(t)$ denotes the mass matrix of the unbounded fluid medium, and $\ddot{\boldsymbol{\varphi}}(t)$ denotes the second derivative of $\boldsymbol{\varphi}(t)$ with respect to time. Note that in Eq (6.5), the scattered velocity $\mathbf{V}_{sc}$ and the velocity potential $\boldsymbol{\varphi}(t)$ along the wet surface are variables. The matrix $\mathbf{M}^{\infty}(t)$ depends only on the geometry of the wet surface and is independent of the dynamic response of the structure and the fluid. Hence, it can be obtained before solving the dynamic response equation. Chapter 2 showed the detail derivation of the dynamic mass matrix and no duplication is given here. In brief, the first step is to establish the integral form of the governing equation in frequency domain, and then by taking the differential width *w* as the analytical limit to zero, it yields a consistent infinitesimal finite-element cell (IFEC) equation in frequency domain. Appling the inverse Fourier transformation to this frequency equation leads to an equivalent IFEC equation in time domain. Subsequently, the mass matrix $\mathbf{M}^{\infty}(t)$ can be obtained by solving the IFEC equation in time domain. (More recently, the same equation was successfully derived using different approaches by Song and Wolf (1997), and Deeks and Wolf (2002), respectively). The scattered wave along the wet surface $\mathbf{V}_{sc}(t)$ in Eq (6.5) can be discretized through conventional finite element technique; i.e.

$$\mathbf{V}_{sc}(t) = \sum_{e} \int_{\Gamma} \mathbf{N}_f v_{sc}(t) d\Gamma \tag{6.6}$$

where v_{sc} denotes the velocity of the scattered wave normal to the wet surface; Γ denotes the wet surface; $\mathbf{N}_f$ is the shape function for the fluid element; and $\sum_{e}$ denotes assemblage of all fluid elements along the wet surface. The details were shown in section 2.1.

b) Formulation for the scattered wave

Now, consider the temporal discretization of Eq (6.5). Within each time step Δt, the mass $\mathbf{M}^{\infty}(t)$ is assumed constant. Hence, Eq (6.5) can be re-written as

$$\mathbf{V}_{sc}(n\Delta t) = \sum_{j=1}^{n} \mathbf{M}^{\infty}((n-j+1)\Delta t) \int_{(j-1)\Delta t}^{j\Delta t} \ddot{\boldsymbol{\varphi}}(t) dt = \sum_{j=1}^{n} \mathbf{M}^{\infty}(n-j+1) \dot{\boldsymbol{\varphi}}\Big|_{(j-1)\Delta t}^{j\Delta t} \tag{6.7a}$$

at the n^{th} time step ($t = n\Delta t$). It can be written in a simpler index form as follows.

$$\mathbf{V}_{sc}^{n} = \sum_{j=1}^{n} \mathbf{M}_{n-j+1}^{\infty} \left(\dot{\boldsymbol{\varphi}}_j - \dot{\boldsymbol{\varphi}}_{j-1} \right) \tag{6.7b}$$

where $\mathbf{V}_{sc}^{n} = \mathbf{V}_{sc}(n\Delta t)$, $\mathbf{M}_{n-j+1}^{\infty} = \mathbf{M}^{\infty}((n-j+1)\Delta t)$ and $\dot{\boldsymbol{\varphi}}_j = \dot{\boldsymbol{\varphi}}\big|_{j\Delta t}$. Re-arranging Eq (6.7b) to make $\mathbf{M}_1^{\infty} \dot{\boldsymbol{\varphi}}_n$ appear on the left hand side, we have

$$\mathbf{M}_1^{\infty} \dot{\boldsymbol{\varphi}}_n = \mathbf{V}_{sc}^{n} - \sum_{j=1}^{n-1} \left(\mathbf{M}_{n-j+1}^{\infty} - \mathbf{M}_{n-j}^{\infty} \right) \dot{\boldsymbol{\varphi}}_j + \mathbf{M}_n^{\infty} \dot{\boldsymbol{\varphi}}_0 \tag{6.7c}$$

Given the following initial conditions,

$$\boldsymbol{\varphi}(0) = \mathbf{0} \tag{6.8a}$$

$$\dot{\boldsymbol{\varphi}}(0) = \mathbf{0} \tag{6.8b}$$

substituting $\mathbf{p}_{sc} = -\rho \dot{\boldsymbol{\varphi}}$ and Eq. (6.8b) into Eq.(6.7c) yields

$$\mathbf{M}_1^{\infty} \mathbf{p}_{sc}^{n} = -\rho \mathbf{V}_{sc}^{n} - \sum_{j=1}^{n-1} \left(\mathbf{M}_{n-j+1}^{\infty} - \mathbf{M}_{n-j}^{\infty} \right) \mathbf{p}_{sc}^{j} \tag{6.9}$$

where $\mathbf{p}_{sc}^{n} = -\rho \dot{\boldsymbol{\varphi}}_n$, $\mathbf{p}_{sc}$ denotes the fluid pressure corresponding to the scattered wave; and $\mathbf{p}_{sc}^{j} = \mathbf{p}_{sc}(j\Delta t)$. Note that Eq (6.9) describes the relationship between the pressure $\mathbf{p}_{sc}$ and the corresponding normal velocity $\mathbf{v}_{sc}$, which is different from Eqs.(6.4a,b).

6.1.3 SBFEM-FEM COUPLING

The FEM formulation for the structure can be written as

$$\mathbf{Ma} + \mathbf{Cv} + \mathbf{Kd} = \mathbf{F}_{\text{ext}} + \mathbf{F}_{\text{inf}} \tag{6.10}$$

where $\mathbf{F}_{\text{ext}}$ is the sum of body and traction forces; $\mathbf{F}_{\text{inf}}$ is the force derived from the unbounded fluid medium; $\mathbf{M}$, $\mathbf{C}$ and $\mathbf{K}$ are the mass, damping and stiffness matrices derived from the structure, respectively; and $\mathbf{a}$, $\mathbf{v}$, and $\mathbf{d}$ denote the structure's acceleration, velocity and displacement vectors, respectively. Derivation of Eq. (6.10) follows the standard FE procedures. What follows will elaborate on the derivation of the last term in Eq. (6.10).

By virtue of the principle of virtual work, the nodal force $\mathbf{F}_{\text{inf}}$ on the wet surface can be expressed in term of the shape function $\mathbf{N}$ for the structure and the total pressure ($= p_{\text{sc}} + p_{\text{ff}}$) as follows.

$$\mathbf{F}_{\text{inf}} = -\int_{\Gamma} \mathbf{N}^{\text{T}} (p_{\text{sc}} + p_{\text{ff}}) d\Gamma = -\int_{\Gamma} \mathbf{N}^{\text{T}} \mathbf{N}_{\text{p}} \mathbf{p}_{\text{sc}} d\Gamma - \int_{\Gamma} \mathbf{N}^{\text{T}} p_{\text{ff}} d\Gamma = -\mathbf{F}_{\text{sc}} - \mathbf{F}_{\text{ff}} \tag{6.11}$$

where Γ denotes the wet surface, $\mathbf{F}_{\text{ff}} = \int_{\Gamma} \mathbf{N}^{\text{T}} p_{\text{ff}} d\Gamma$ and $\mathbf{F}_{\text{sc}} = \int_{\Gamma} \mathbf{N}^{\text{T}} \mathbf{N}_{\text{p}} \mathbf{p}_{\text{sc}} d\Gamma$. Note that $\mathbf{N}$ is the shape function for the structural element, while the shape function for scattered waves can be different, say $\mathbf{N}_{\text{p}}$, i.e.

$$p_{\text{sc}} = \mathbf{N}_{\text{p}} \mathbf{p}_{\text{sc}} \tag{6.12}$$

By substituting Eq. (6.11) into Eq. (6.10), the governing dynamic equation for the structure-infinite fluid system can be obtained, i.e.

$$\mathbf{Ma} + \mathbf{Cv} + \mathbf{Kd} = -\mathbf{F}_{\text{ff}} - \mathbf{F}_{\text{sc}} + \mathbf{F}_{\text{ext}} \tag{6.13}$$

In Eq. (6.13), the first term $\mathbf{F}_{\text{ff}}$ on the right hand side is a function of the incident wave p_{ff}. It can be evaluated easily. What follows are the details for deriving the second term $\mathbf{F}_{\text{sc}}$ on the right hand side.

Consider the conditions along the wet surface. Two conditions should be enforced. Firstly, kinematic continuity across the wet surface requires the normal velocity of the structure to be identical to that of the fluid, i.e.

$$v_{inf} = v_n \tag{6.14a}$$

Secondly, the corresponding dynamic compatibility demands that the compressive traction on the structural surface to be equal to the fluid pressure, i.e.

$$p = -p_{inf} \tag{6.14b}$$

Substituting Eq. (6.14a) into Eq. (6.2), and then the result into Eq. (6.6), and subsequently into Eq. (6.9) leads to

$$\mathbf{M}_l^{\infty}\mathbf{p}_{sc}^{n} = -\rho\sum_e\int_\Gamma \mathbf{N}_f\left(v_n(t) - v_{ff}(t)\right)d\Gamma - \sum_{j=1}^{n-1}\left(\mathbf{M}_{n-j+1}^{\infty} - \mathbf{M}_{n-j}^{\infty}\right)\mathbf{p}_{sc}^{j} \tag{6.15}$$

Note that once $\mathbf{p}_{sc}$ is determined, the second term $\mathbf{F}_{sc}$ on the right hand side of Eq.(6.13) can be obtained.

Now, discretize Eq. (6.13) in the time domain using a Newmark's time-integration scheme. We have

$$\begin{aligned}\left(\mathbf{K} + \frac{1}{\alpha\Delta t^2}\mathbf{M} + \frac{\delta}{\alpha\Delta t}\mathbf{C}\right)\mathbf{d}^{t+\Delta t} = {}& {}^{t+\Delta t}\mathbf{F}_{ext} - {}^{t+\Delta t}\mathbf{F}_{ff} - {}^{t+\Delta t}\mathbf{F}_{sc} \\ & + \mathbf{M}\left[\frac{1}{\alpha\Delta t^2}\mathbf{d}^t + \frac{1}{\alpha\Delta t}\mathbf{v}^t + \left(\frac{1}{2\alpha} - 1\right)\mathbf{a}^t\right] \\ & + \mathbf{C}\left[\frac{\delta}{\alpha\Delta t}\mathbf{d}^t + \left(\frac{\delta}{\alpha} - 1\right)\mathbf{v}^t + \left(\frac{\delta}{2\alpha} - 1\right)\Delta t\mathbf{a}^t\right]\end{aligned} \tag{6.16}$$

where ${}^{t+\Delta t}\mathbf{F}_{sc} = \int_\Gamma \mathbf{N}^T\mathbf{N}_p\mathbf{p}_{sc}^{t+\Delta t}d\Gamma$, $\alpha = 0.25$ and $\delta = 0.5$. Assume $n\Delta t = t + \Delta t$. Hence, Eq. (6.15) can be re-written as

$$\mathbf{M}_l^{\infty}\mathbf{p}_{sc}^{n} = -\rho\sum_e\int_\Gamma \mathbf{N}_f\left(v_n^t(t) - v_{ff}^{t+\Delta t}(t)\right)d\Gamma - \sum_{j=1}^{n-1}\left(\mathbf{M}_{n-j+1}^{\infty} - \mathbf{M}_{n-j}^{\infty}\right)\mathbf{p}_{sc}^{j} \tag{6.17}$$

in which the velocity $v_n^{t+\Delta t}$ of the current time step is approximately set equal to the velocity v_n^t of the previous time step. However in some cases, it is desirable to include that term into the global iteration scheme, i.e.

$$\left(\mathbf{K}+\frac{1}{\alpha\Delta t^2}\mathbf{M}+\frac{\delta}{\alpha\Delta t}\mathbf{C}\right)^{t+\Delta t}\mathbf{d}^{j}={}^{t+\Delta t}\mathbf{F}_{ext}-{}^{t+\Delta t}\mathbf{F}_{ff}-{}^{t+\Delta t}\mathbf{F}_{sc}\left({}^{t+\Delta t}\mathbf{v}_n^{j-1}-{}^{t+\Delta t}\mathbf{v}_{ff}\right)$$
$$+\mathbf{M}\left[\frac{1}{\alpha\Delta t^2}{}^{t}\mathbf{d}+\frac{1}{\alpha\Delta t}{}^{t}\mathbf{v}+\left(\frac{1}{2\alpha}-1\right){}^{t}\mathbf{a}\right] \tag{6.18}$$
$$+\mathbf{C}\left[\frac{\delta}{\alpha\Delta t}{}^{t}\mathbf{d}+\left(\frac{\delta}{\alpha}-1\right){}^{t}\mathbf{v}+\left(\frac{\delta}{2\alpha}-1\right)\Delta t\,{}^{t}\mathbf{a}\right]$$

where j denotes j^{th} iteration within a time step. The term $v_{ff}(t)$ can be obtained via other analytical solutions. For example in shock-wave analysis, Lamb (1932) gives the following explicit expression for the incident fluid pressure along the wet surface (see Fig. 6.8)

$$p_{inc}(x,t)=p_0H\left(t-\frac{R-x}{c}\right)=p_0H\left(t-\frac{R-r\cos\gamma}{c}\right) \tag{6.19}$$

where H is a Heaviside step function, and p_0 is the magnitude of the pressure at the wave front. The parameters r, γ and R are as shown in Fig.6.8. The incident fluid radial velocity is

$$v_{ff}=v_r=-\frac{p_{inc}}{\rho c}\cos\gamma \tag{6.20}$$

6.2 NUMERICAL EXAMPLES

To validate the present SBFEM formulation and the pressure-velocity relationship corresponding to scattered waves based on the SBFEM, several 2-dimensional cases for submerged structures subjected to internal pressures or external shock loadings are considered.

6.2.1 A CYLINDRICAL CAVITY SUBJECTED TO A SUDDENLY APPLIED ACCELERATION

Fig.6.2 shows a cylindrical cavity of radius R in an infinite fluid medium. At $t=0$, a boundary acceleration a is suddenly applied and then kept constant until the end of the analysis. The objective of this analysis is to check the accuracy of the dynamic mass matrix $\mathbf{M}^{\infty}(t)$ for the infinite fluid medium. The surrounding fluid

medium is modeled by the SBFEM using 8 or 32 elements. The dynamic mass matrix $\mathbf{M}^{\infty}(t)$ can be calculated by using the convolution method in section 2.6 or the recurrence method in section 2.7. In this analysis, the time step is chosen as $0.1\frac{R}{c}$. In the recurrence method, the error tolerance "tol" is chosen as 0.002. Using the chosen "tol" yields a "cut-off" time "tc", i.e. $t_c = 0.1\times 104\frac{R}{c}$. If the time "$t_e$" of the analysis is chosen as $0.1\times 400\frac{R}{c}$, the time infinity "t_i" can be approximately chosen as $2.6\times 0.1\times 400\frac{R}{c}$. The results corresponding to 32 elements obtained by using the convolution method and the recurrence method are plotted in Fig.6.3a . The time axis is normalized with respect to R/c, while the pressure axis is normalized with respect to ρaR. From Fig.6.3a, one can see that the results obtained by using the convolution method and the recurrence method are almost the same. But the computational efforts are different. It is obvious that the recurrence method needs less time than the convolution method. The same problem was considered by Mansur et al. (2000) using the FEM-BEM coupling procedures. The FEM-BEM and standard BEM results are plotted in Fig.6.3b and compared with the current result obtained by using the convolution method. From Fig.6.3b, one can see that the 8-element results are close to the 32-element results, and both are almost identical to the FEM-BEM and BEM results, demonstrating the efficiency and accuracy of the present formulation.

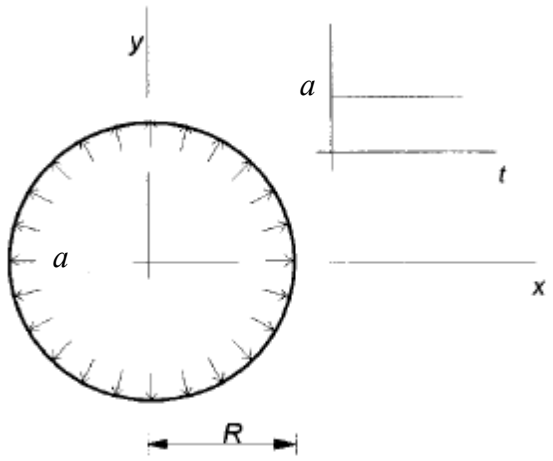

Fig.6.2 A cylindrical cavity subjected to a suddenly applied acceleration

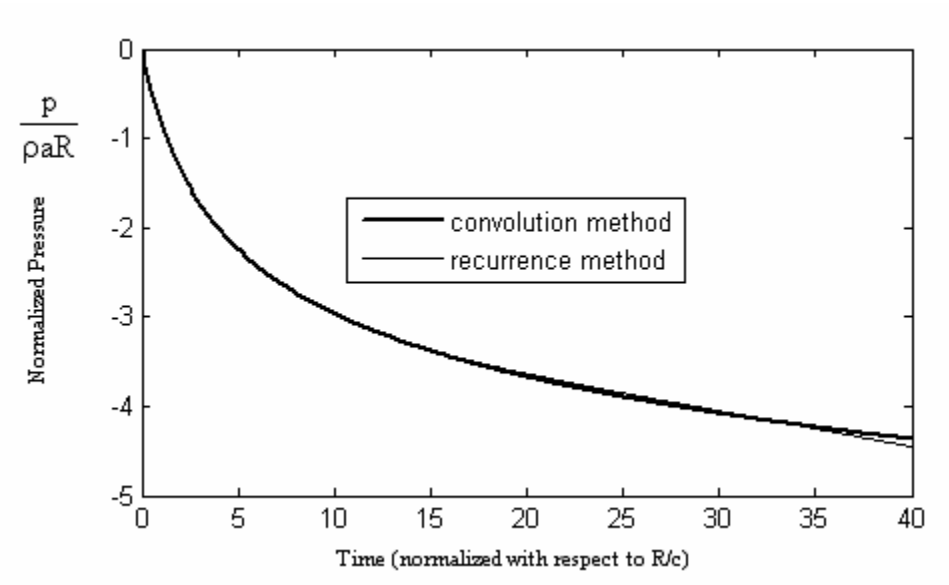

Fig.6.3a Pressure on the cavity boundary

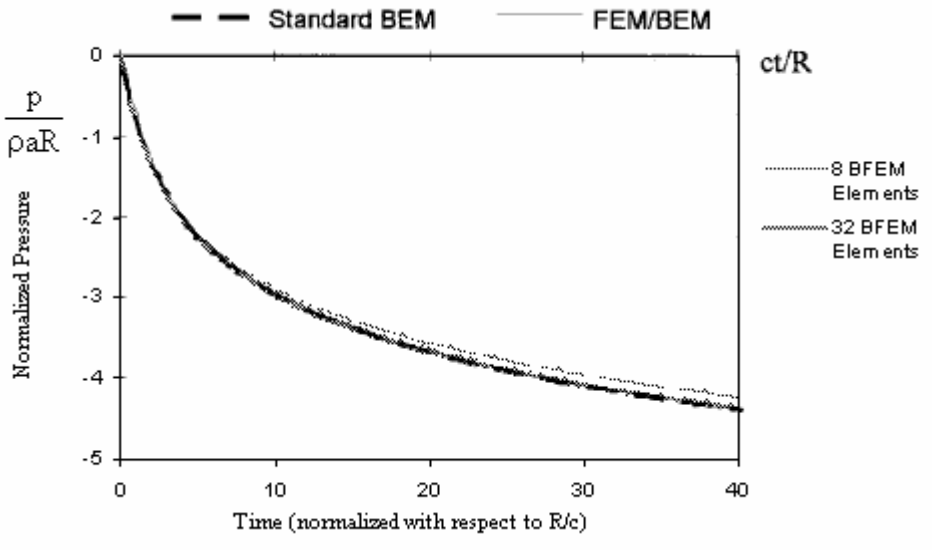

Fig.6.3b Pressure on the cavity boundary

6.2.2 A SUBMERGED INFINITELY LONG CYLINDRICAL SHELL SUBJECTED TO AN INTERNAL PRESSURE

Consider a thin, elastic and infinitely long cylindrical shell, submerged in water. It is subjected to a suddenly applied uniform outward pressure (See Figs. 6.4 and 6.5). A ramp for a very short period (0.5×10^{-4} sec) is put in place in order to avoid numerical difficulties. The mean radius of the cylinder is $R = 0.2$m and the thickness of the wall is $h = 0.006$m. The material properties for the steel cylinder are: Young's modulus $E_s = 210\times10^6\,\text{kN/m}^2$, density $\rho_s = 7.8\times10^3\,\text{kg/m}^3$, and Poisson ratio $\nu = 0.3$. The density of fluid is $\rho = 1.0\times10^3\,\text{kg/m}^3$ and the sound speed in fluid $c = 1500$ m/s.

This problem is a simple 2-dismensional axi-symmetric problem. The steel cylindrical shell is discretized into 16 two-node beam elements. Along the wet surface, the same discretization mesh is applied to the fluid boundary. The 16 SBFEM elements match the 16 structural beam elements side by side (see Fig.6.6). In the analysis, the time increment is set to 0.013333ms. As the time of the analysis is short, the results can be quickly obtained by using the convolution method. Its

corresponding results of the dynamic response are shown in Fig.6.7, which shows the time history of the outward displacement (positive). The displacement is normalized with respect to the corresponding static displacement d_s at the mid-surface $(R = 0.2m)$, i.e.

$$d_s = \frac{R_i^2 P_0}{E_s\left(R_e^2 - R_i^2\right)}\left[\frac{(1+\nu)R_e^2}{R} + (1+\nu)R\right] \tag{6.21}$$

where R_i, R_e are the internal and external radii of the cylindrical shell, respectively. The analytical results based on the plane-wave approximation (PWA) are plotted in Fig.6.7 for comparison. One can see from Fig.6.7 that the present results are in good accord with the PWA results which were obtained by solving a second-order differential equation at early time. Note that the PWA approach can only yield relatively accurate results for early time.

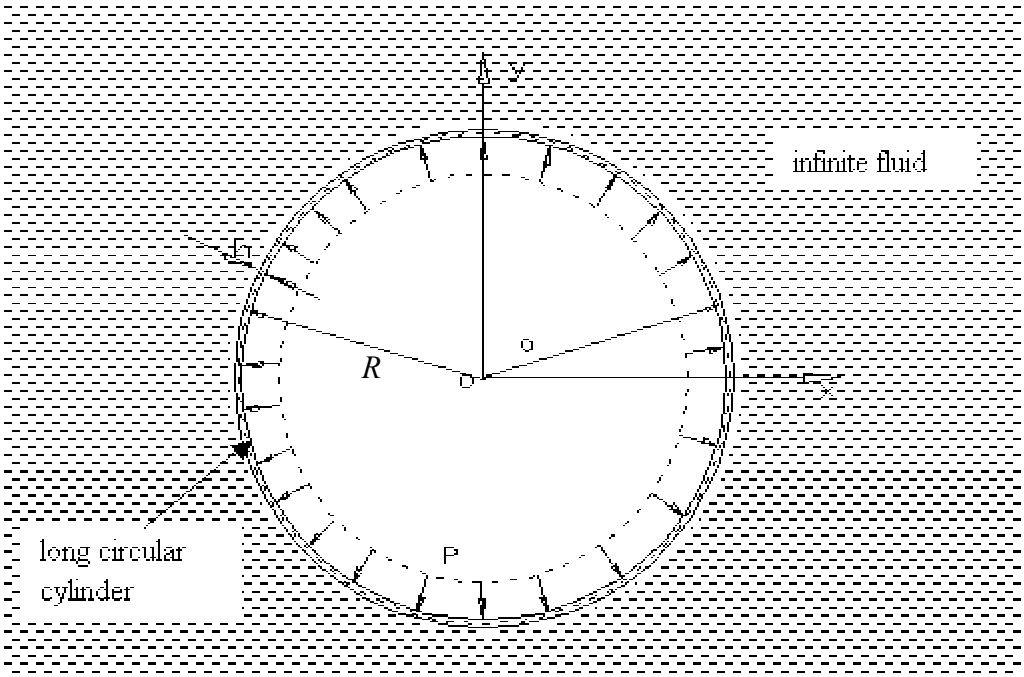

Fig.6.4 Geometry of long cylindrical shell subjected to internal pressure in infinite fluid medium

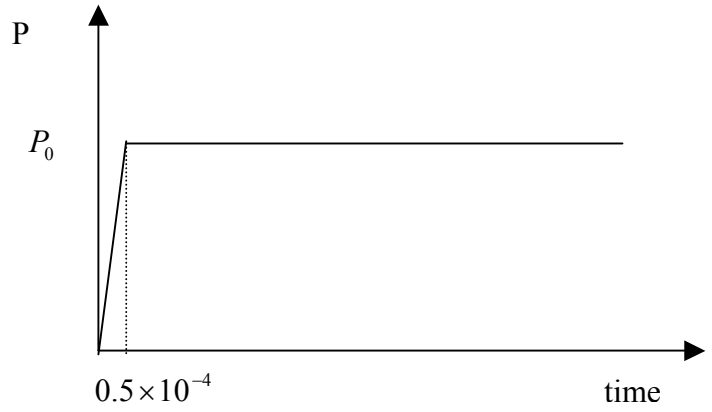

Fig.6.5 Loading conditions for the cylindrical shell

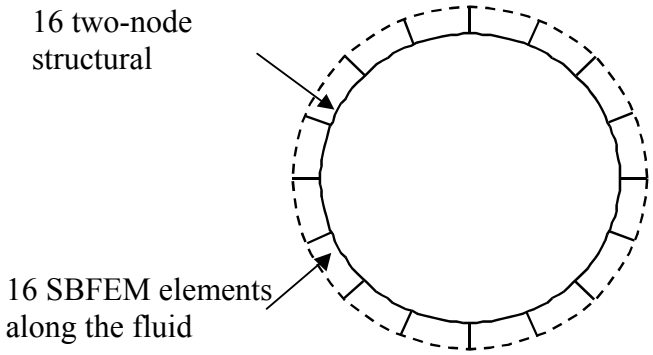

Fig.6.6 Matching discretization meshes for the cylinder and the fluid boundary

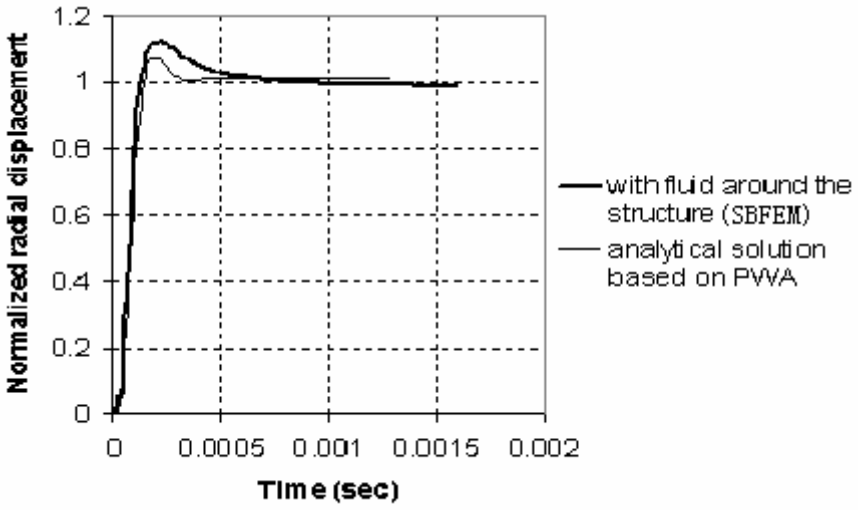

Fig.6.7 Dynamic response of the cylindrical shell

6.2.3 A SUBMERGED INFINITELY LONG CYLINDRICAL SHELL SUBJECTED TO A STEP PLANE WAVE

Consider an elastic infinitely long cylindrical shell subjected to a step plane acoustic wave. The geometry of the cylindrical shell is shown in Fig.6.8. This study is to check the accuracy of the present SBFEM formulation against the benchmark solutions. The geometric and material properties of the cylindrical shell and the surrounding fluid medium are the same as those in section 6.3.2.

The wall of the shell is discrectized into 32 two-node beam elements, while the fluid boundary is matched by 32 SBFEM elements (in a similar manner as that in Fig.6.6). The time increment chosen for the analysis is 0.002667ms. The magnitude of the incident pressure wave impinging on the structure is taken to be equal to ρc^2 at all time. The same problem was investigated by Huang (1970) and reported by Zilliacus (1983), who obtained the velocity history using Fourier series approach ("analytical" solution). The same problem was also analyzed by Fan et al. (2001), who modeled the shell using 2×12 nine-node spline shell elements and modeled the fluid using the plane wave approximation (PWA). Plane-strain conditions were imposed along the axis of the cylinder. Recently, Yu et al. (2002) also analyzed the same problem using a BEM-FEM coupling technique.

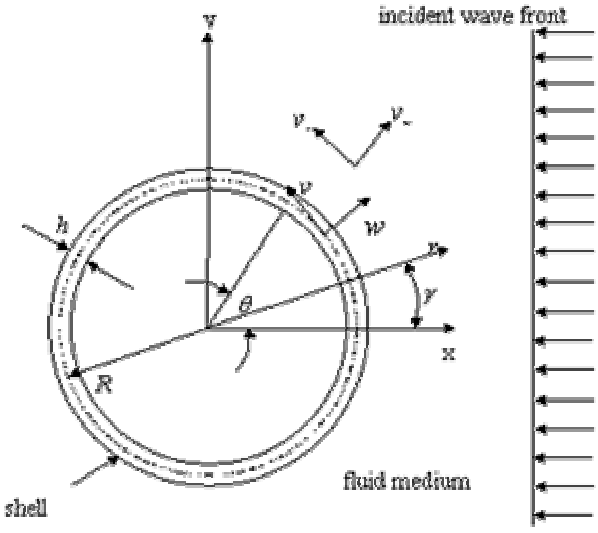

Fig.6.8 Cross-section of the geometry of an infinite cylinder

Results obtained from the present SBFEM formulation are compared with solutions obtained by others. Before determining the response of the cylindrical shell by using the SBFEM/FEM formulation, the dynamic mass matrix $\mathbf{M}^{\infty}(t)$ for the surrounding infinite fluid medium must be solved. Here the $\mathbf{M}^{\infty}(t)$ is solved by using the two types of methods (the convolution method in section 2.6 and the recurrence method in section 2.7), respectively. In the recurrence method, the "cut-off" time "t_c" corresponding to the time step 0.002667ms is chosen as 87×0.002667ms when the error tolerance is chosen as 0.002. The infinity time "t_i" is chosen as $3t_e$ when the time of the analysis "t_e" is chosen as 250×0.002667ms. Figs.6.9a,b shows the dimensionless radial velocity history at different locations ($\theta = 0^0, 90^0, 180^0$). The velocity is normalized with respect to the sound speed in fluid c, while the time is normalized with respect to R/c. The results are obtained by using the convolution method and the recurrence method, respectively, and are plotted in Fig.6.9a together for comparison. From Fig.6.9a, one can see the results obtained by using the two methods are very close to each other. The results obtained by using the convolution method are also plotted in Fig.6.9b together with other methods' results for comparison. From Fig.6.9b, one can see that the present results are in good accord in all time with analytical solutions (Huang (1970)), and also in good agreement in early time with the PWA solutions, which are known to be relatively accurate in early time. On the other hand, the FEM-BEM results are also in fairly good agreement but it exhibits random undulations around the analytical solution, particularly during late time, and the peak value is delayed. It demonstrates that the present SBFEM formulation can yield more accurate results than the PWA and the BEM, in particular at late time. Note that the true velocities at $\theta = 0^0, 180^0$ should approach 1.377 at late time (Huang (1970)). From Fig.6.9, one can see that the SBFEM results approach that true value of 1.377 at late time. Compared to the DAA results obtained by Zilliacus (1983) (not shown in Fig.6.9 for clarity), SBFEM results are closer to the analytical solution and exhibit more subdued oscillations. Of note, the results shown in Fig.6.9 are obtained using the iterative Newmark scheme (Eq.6.18), which includes iterations within each time step. The effects of using a Newmark scheme without iterations are also studied.

The results obtained by using the convolution method shown in Fig.6.10 suggest that a non-iterative Newmark scheme leads to slightly inferior results. In order to study the convergence of the current SBFEM formulation, three different SBFEM meshes (comprising 8, 16 or 32 elements) are used to represent the fluid boundary. The time increment is set to 0.01333ms (dimensionless time step: 0.1) in all analyses. The results obtained by using the convolution method are shown in Fig.6.11. One can see that except the 8-element results, the 16- and 32-element results are nearly the same as the analytical solution. The poorer 8-element results are not unexpected because the velocity variations around the cylinder may not be adequately refined by 8 representative sectors. Nevertheless, the efficiency of the SBFEM formulation has been clearly demonstrated by using a fairly coarse 16-element mesh.

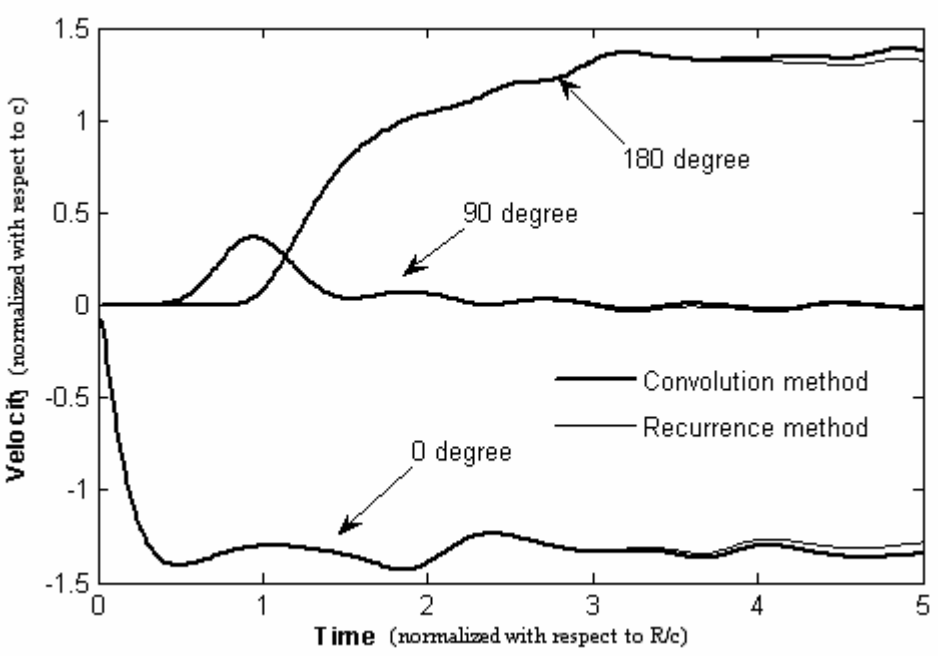

Fig.6.9a Radial velocity of the cylindrical shell

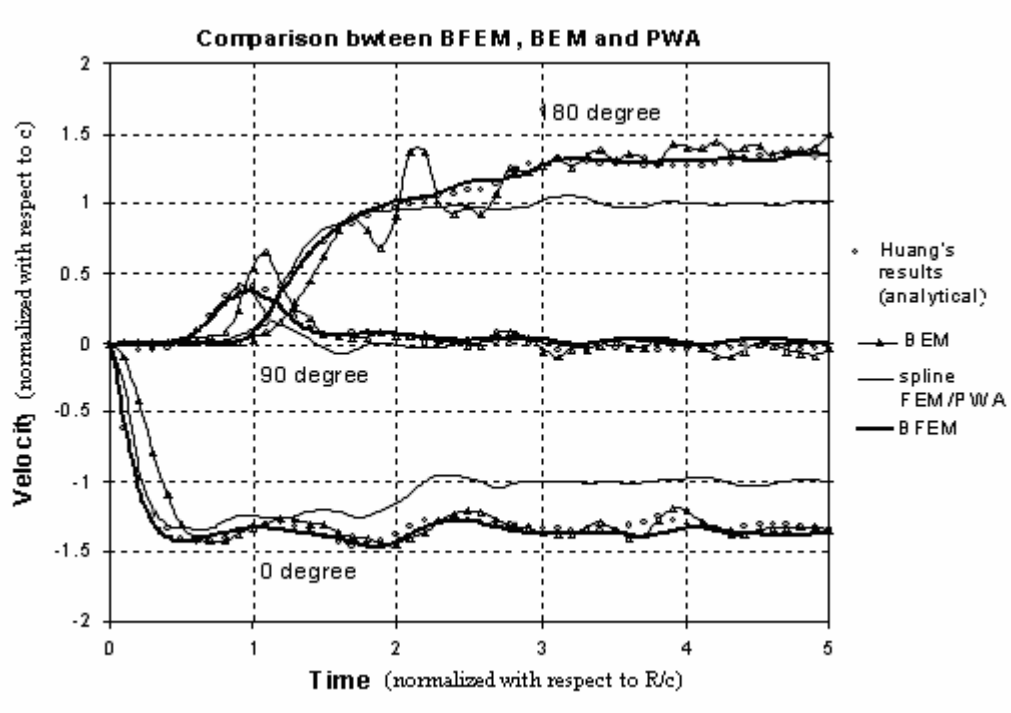

Fig.6.9b Radial velocity of the cylindrical shell

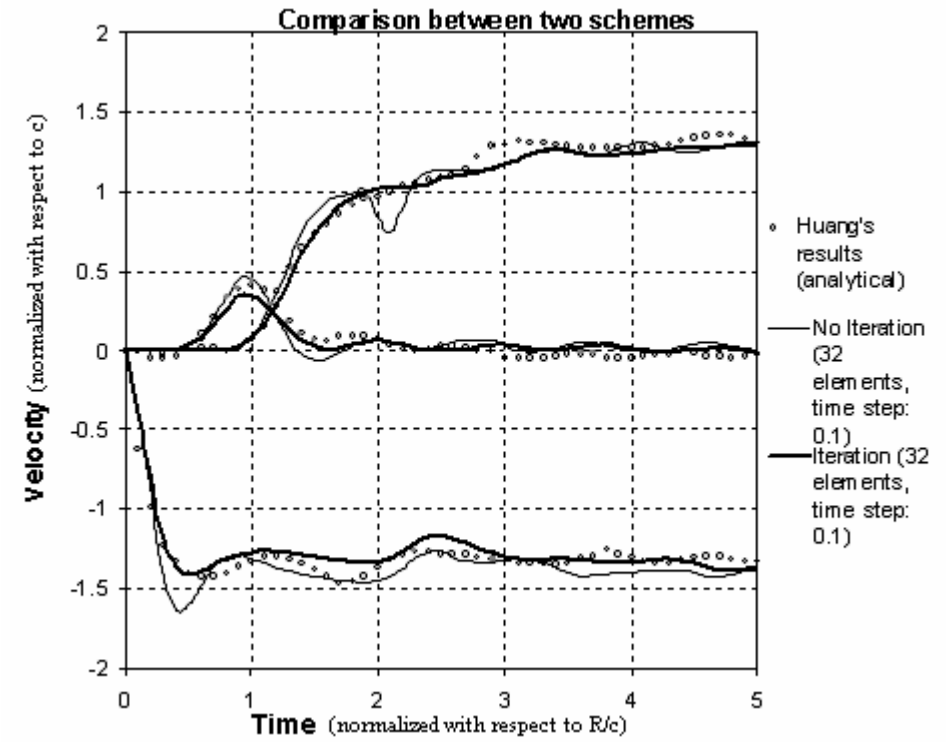

Fig.6.10 Comparison of results obtained from two Newmark schemes

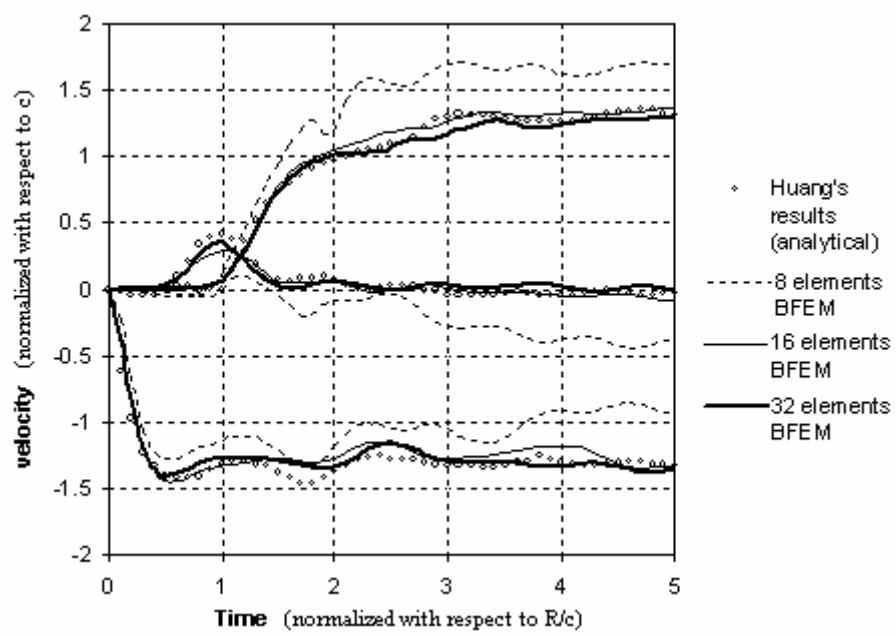

Fig.6.11 Convergence studies using 8-, 16- and 32-elements

6.2.4 A SUBMERGED INFINITELY LONG CYLINDRICAL SHELL SUBJECTED TO AN EXPONENTIAL DECAYING PLANE WAVE

The problem shown in Fig.6.8 is considered again. Here, the incident wave from the far field is considered as an exponential decaying plane wave. Pressure $p_0(t)$ of the wave, which is in a form of exponential function, is expressed as

$$p_0(t) = P_0 e^{-\beta\left(\frac{x}{R}+\frac{ct}{R}-1\right)} \tag{6.22}$$

where β and P_0 are coefficients. In this study, β is set to be 4.8, while P_0 is set equal to ρc^2. After p_{inc} and v_{ff} are determined by Eqs.(6.19-20), the dynamic response can be obtained using Eq.(6.18).

The cylindrical shell is discretized into 36 two-node beam elements, while the fluid boundary is matched by 36 SBFEM elements. The time increment is chosen to be 0.002667ms. The results obtained by using the convolution method at $\theta = 0^0, 180^0$ are plotted in Figs.6.12a and 6.12b, and compared with Huang's "exact" solution (1970). One can see that the present results have almost exactly the same profile as Huang's "exact" solution (1970). Of note, Huang (1970) indicated

that the starting time for an initial motion of the shell at $\theta = 180^0$ should be equal to 0.8457 (normalized with respect to R/c), but Huang's results exhibits some wiggles in Fig.6.12b before the starting time 0.8457, while the SBFEM results show no motion till 0.8457. It illustrates the superiority of the present SBFEM formulation over Huang's Fourier-series approach, particularly at early time. The radial velocities at other locations $\left(\theta = 30^0, 60^0, 90^0, 120^0\right)$ are plotted in Fig.6.13, in which Huang's results coincide with the present results. Once again, the efficiency of the SBFEM is demonstrated.

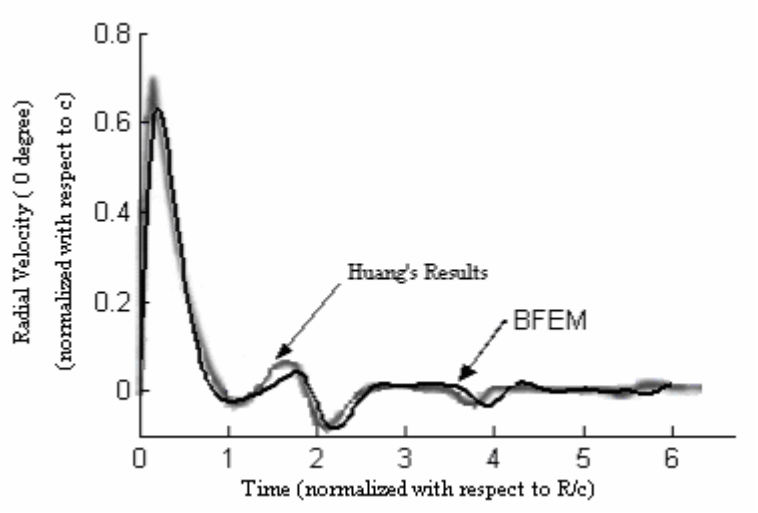

Fig.6.12a Radial velocity $\left(\theta = 0^0\right)$ ***of a cylindrical shell subjected to an exponentially decaying plane wave***

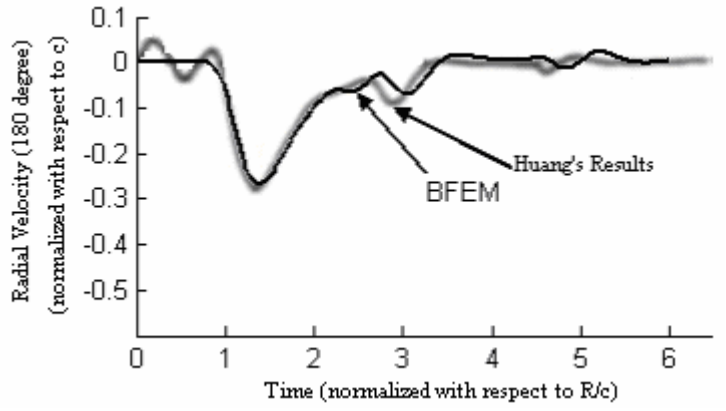

Fig.6.12b Radial velocity $\left(\theta = 180^0\right)$ ***of a cylindrical shell subjected to an exponentially decaying plane wave***

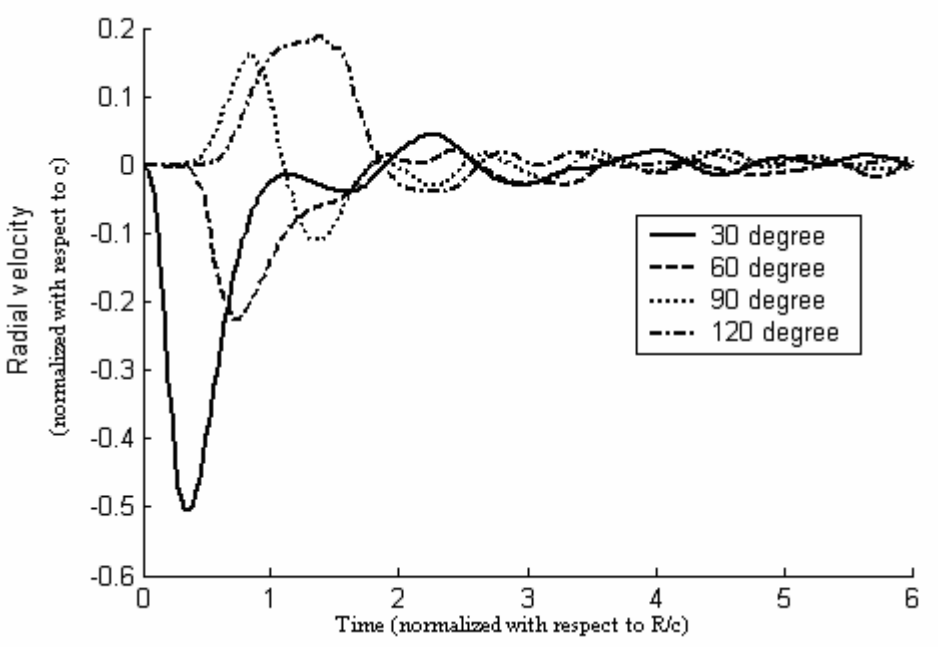

Fig.6.13 Radial velocity at various locations of a cylindrical shell subjected to an exponentially decaying plane wave

6.2.5 PARAMETRIC STUDY FOR A SUBMERGED INFINITELY LONG CYLINDRICAL SHELL SUBJECTED TO A PLANE WAVE

The objective of this parametric study is to gain insights into the effects of the geometric and material parameters of a cylindrical shell on its dynamic response. It is motivated by Huang's comment (1970) that the late-time radial (normal) velocity of a cylindrical shell subjected to a plane wave as defined by Eq.(6.22) should converge to the following value.

$$v = -2M/(M+2) \qquad \text{for } \beta = 0 \tag{6.23a}$$

$$v = 0 \qquad \text{for } \beta > 0 \tag{6.23b}$$

where the dimensionless quantity M is defined as

$$M = \frac{\rho R}{h\rho_s} \tag{6.24}$$

However, Huang (1970) did not mention what dominated the early response of the cylindrical shell. To supplement Huang's comment for the early time, the following parametric study is to gain insights into the early-time response of the cylindrical

shell. The dynamic response can be obtained by Eq.(6.18); the dynamic mass matrix $\mathbf{M}^{\infty}(t)$ for the surrounding infinite fluid medium are obtained by using the convolution method; and the mesh employed for this problem is the same as that in section 6.3.4.

6.2.5.1 Effect of varying the relative thickness $\frac{h}{R}$

With all other parameters held constant, the ratio of the shell thickness (h) to the radius (R) is varied. As seen from Eq.(6.24), the ratio h/R is inversely proportional to the dimensionless parameter M. In this study, M=2.0, 4.41890, 6.41975 and 9.09184 are considered. Material parameters of the fluid and the cylindrical shell are: wave speed in fluid, c=1500m/s; density of fluid, $\rho = 1000\,\text{kg/m3}$; Young's modulus of the shell, $E_s = 210\times10^6\,\text{kN}/\text{m}^2$ and the density of the shell, $\rho_s = 7.8\times10^3\,\text{kg}/\text{m}^3$.

By using Eq.(6.24), one can know that the corresponding h/R ratios for M=2.0, 4.41890, 6.41975, 9.09184 are 2/31, 2/69, 2/100 and 2/142, respectively. For the cases of stepped incident plane waves (i.e. $\beta = 0$), results of varying only R by keeping h constant (h=0.006m) are plotted in Figs.6.14a and 6.14b; while the associated results of varying only h by keeping R constant (R=0.02m) are plotted in Figs.6.14c and 6.14d. From Figs.6.14a-d, one can see that the converged radial velocities at late time all agree with the values calculated using Eq.(6.23a). One can also observe the trend that the larger the M value, the larger is the radial velocity. On the other hand, through comparing Figs.6.14a-b with Figs.6.14c-d, respectively, one can see that the results are almost identical at all time. It can be concluded that the response of the cylindrical shell is dominated by the ratio h/R, not by h or R alone. To further illustrate the validity of the present formulation, results for $\beta = 0$ or 1 and M=2.0 are plotted in Fig.6.15 and compared with Huang's results (1970). They are seen to be agreeable with each other well.

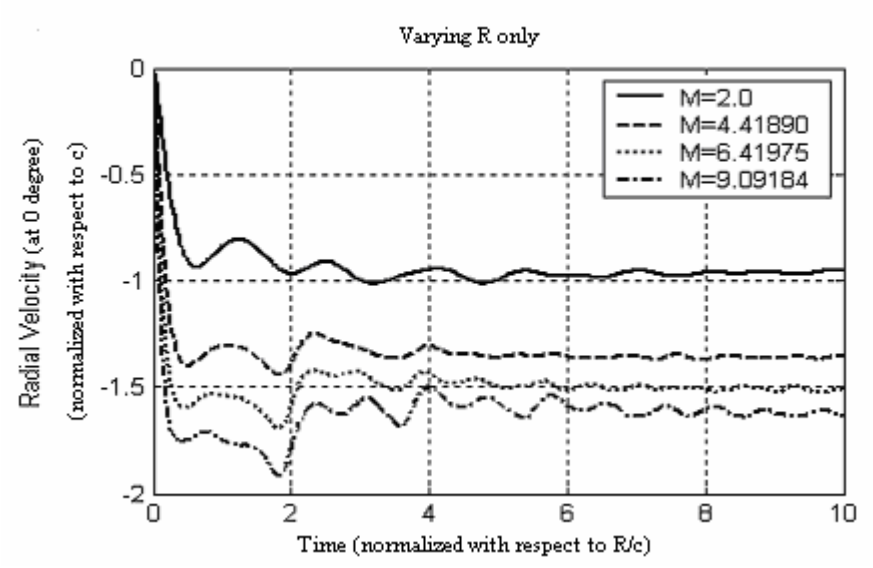

Fig.6.14a Comparison for different M-values due to varying R only $\left(\theta = 0^0\right)$

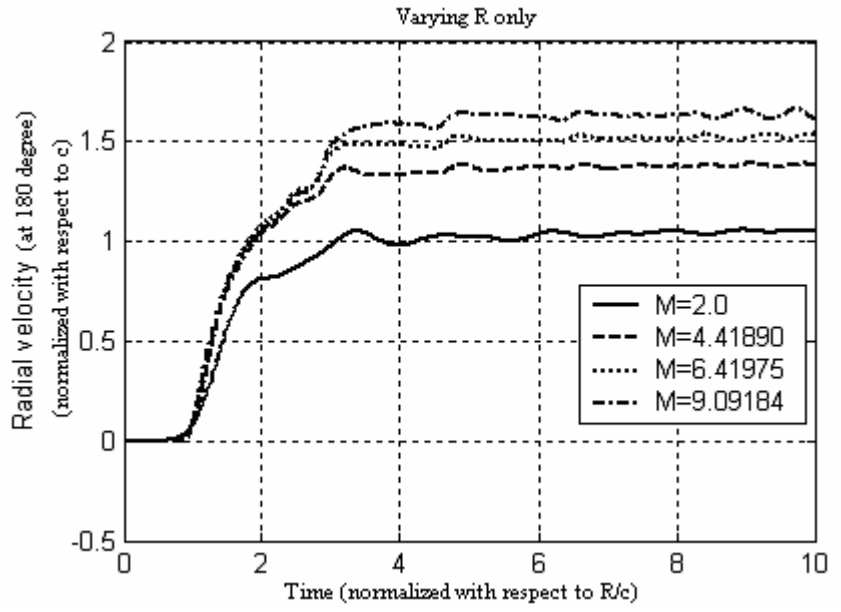

Fig.6.14b Comparison for different M-values due to varying R only $\left(\theta = 180^0\right)$

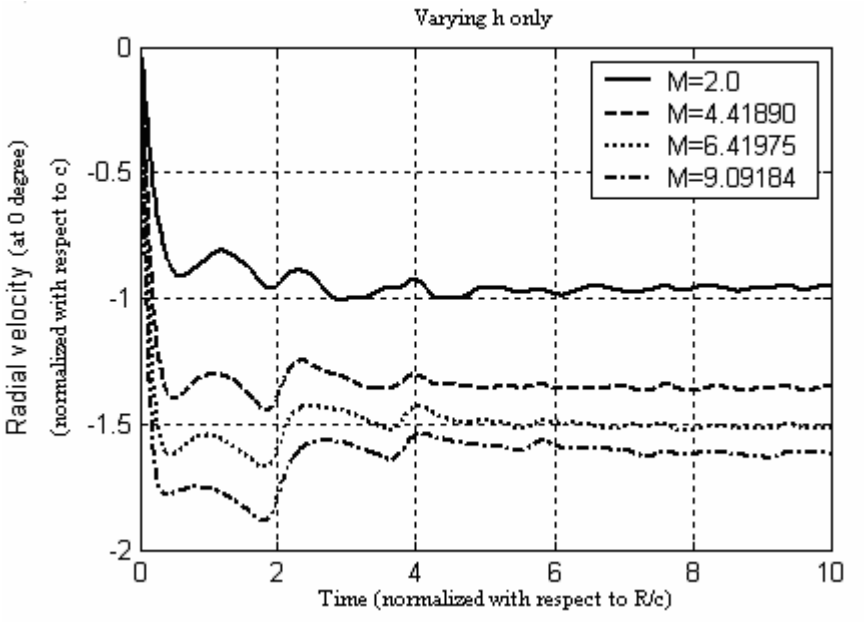

Fig.6.14c Comparison for different M-values due to varying h only $\left(\theta = 0^0\right)$

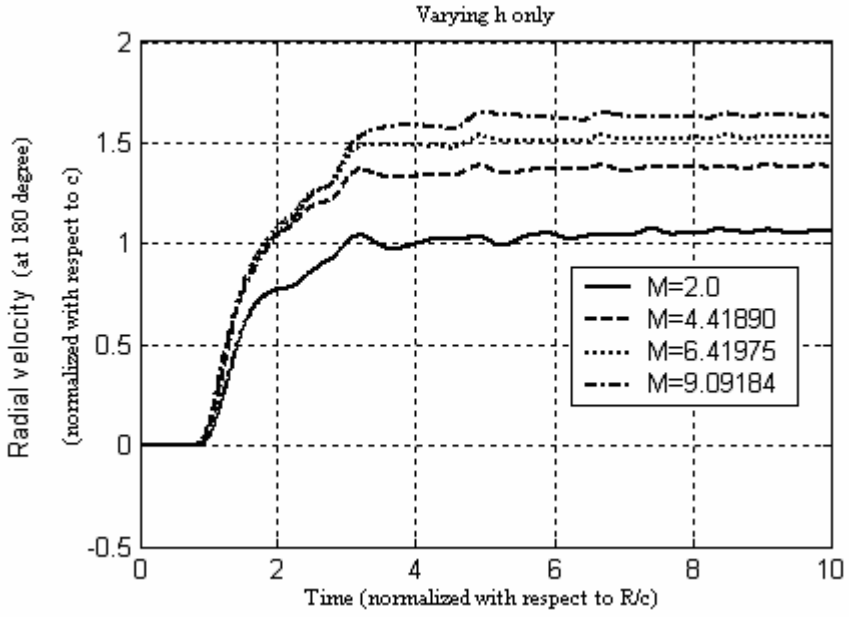

Fig.6.14d Comparison for different M-values due to varying h only $\left(\theta = 180^0\right)$

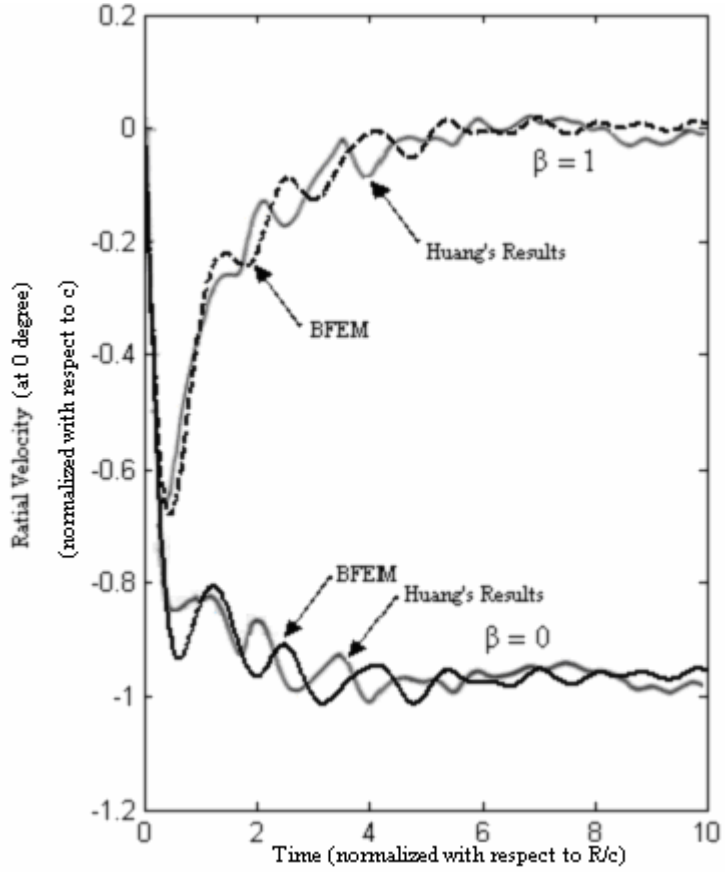

Fig.6.15 Radial velocity of shell due to a stepped $(\beta = 0)$ ***and an exponential incident wave*** $(\beta = 1)$***, (M=2.0)***

6.2.5.2 Effect of varying the shell's density ρ_s *only*

Results for various densities of the shell material are plotted in Fig.6.16. In this study, other parameters are kept constant as follows: h/R=2/69, R=0.2m, $\beta = 0$; and the Young's modulus of the shell is $E_s = 210 \times 10^6 \, kN/m^2$. Of note, Eq.(6.24) shows that the M-value is inversely proportional to the density ρ_s. In other words, the lighter the shell, the larger is the M-value. From Fig.6.16, one can observe that the smaller the density (i.e. larger M), the larger is the velocity. By comparing Fig.6.16 with Figs.6.14a and 6.14c, one can see that the larger the density, the larger the velocity at early time for each M-value, although the velocity at late time

remains the same. Therefore, it can be concluded that the shell's density dominates the early-time response for a chosen M-value.

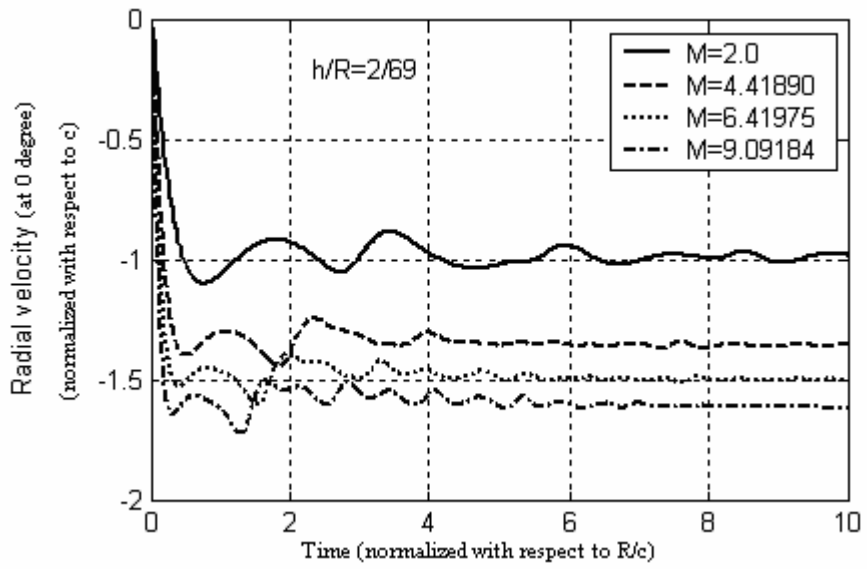

Fig.6.16 Comparison for different M-values due to varying ρ_s ***only*** $\left(\theta = 0^0\right)$

6.2.5.3 Effect of varying the Young's modulus of shell

Results for various Young's modulus of the shell material are plotted in Figs.6.17a-c. In this study, a typical Young's modulus is chosen ($E=210\times10^6\,kN/m^2$) and the effects of varying E (E/2, E or 2E) are investigated, while other parameters are kept unchanged as follows: h/R=2/69, R=0.2m, $\beta = 0$, $\rho_s = 7.8\times10^3\,kg/m^3$. M is kept constant (M=4.41890). From Figs.6.17a-c, one can see that the Young's modulus dominates the early-time responses only.

In conclusion, when a submerged cylindrical shell is subjected to a plane shock wave, the late-time response depends on the dimensionless quantity M only, but its early-time response depends not only on M, but also on the Young's modulus of the shell.

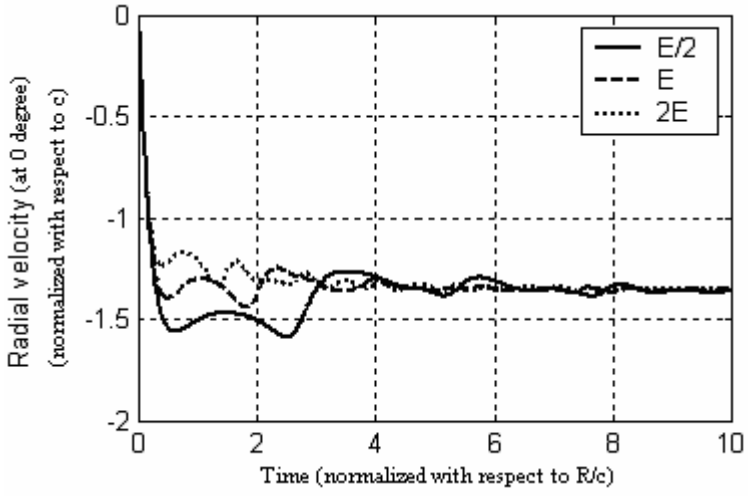

Fig.6.17a Radial velocity for various E $\left(\theta = 0^0\right)$

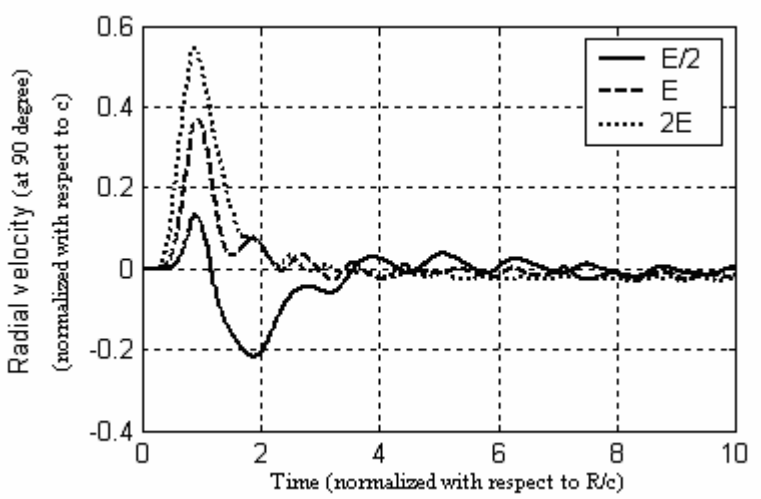

Fig.6.17b Radial velocity for various E $\left(\theta = 90^0\right)$

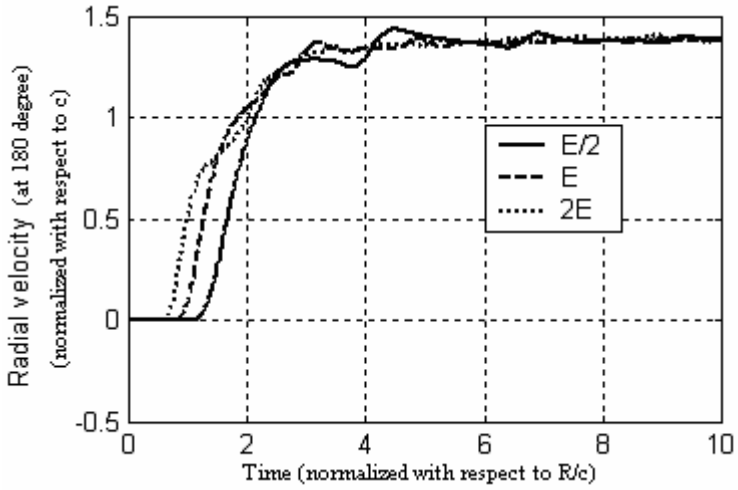

Fig.6.17c Radial velocity for various E $\left(\theta = 180^0\right)$

6.2.6 A SUBMERGED INFINITELY LONG CYLINDRICAL SHELL SUBJECTED TO A NEAR-FIELD SHOCK WAVE

In this study, difficulties have been encountered in finding a benchmark example since most previous studies were carried out by defense organizations. The writer is aware of the free-field pressure p_{inc} (incident pressure) and velocity v_{ff} of a near-field shock wave for a 3-dimensional problem published by Cole (1948) as the early published work. In order to verify the efficiency of the present SBFEM-FEM procedure for a 2-dimensional FSI problem subjected to a near-field shock wave, the p_{inc} and v_{ff} for a 2-dimensional problem are produced using a commercial code LS-DYNA. The results obtained from the FEM analysis by LS-DYNA is treated as a benchmark example. The geometric configuration is shown in Fig.6.18. In it, an explosive is placed at the origin, while a cylindrical shell is sited 1.0 m away from the origin to the right. The cylinder and explosion are surrounded by unbounded fluid medium. The fluid and the shell's properties are as described in section 6.3.2. In order to simplify the simulation of underwater explosion, a pressure surface (the red curve shown in Fig.6.18) is employed to model the underwater explosion. The radius r is 0.1m and the exponentially decaying pressure is taken as $p(t) = e^{-\frac{1}{\theta(\text{at } r=0.1)}t}$ where $\theta(\text{at } r = 0.1)$ is set equal to

3.55×10^{-5}. The FEM mesh used in the LS-DYNA analysis is also shown in Fig.6.18. The radial velocities obtained from LS-DYNA at locations $\theta = 0^0, 90^0, 180^0$ of the cylindrical shell are shown in Fig.6.19. The pressure and velocity obtained from LS-DYNA at locations $\theta = 0^0, 90^0, 180^0$ of the corresponding free field problem are shown in Fig.6.20. Upon determining the p_{inc} and v_{ff} along the fluid-structure interface, the response of the shell can be solved by Eq.(6.18) and results obtained by the present method are then plotted in Fig.6.19 as well. The corresponding FEM and SBFEM mesh and time increment are the same as those in section 6.3.4. As seen from Fig.6.19, the results obtained by the present method are in good accord with those by LS-DYNA. Therefore, it can be concluded that the present SBFEM-FEM procedure is suitable and very efficient for solving FSI problems subjected to near-field shock waves.

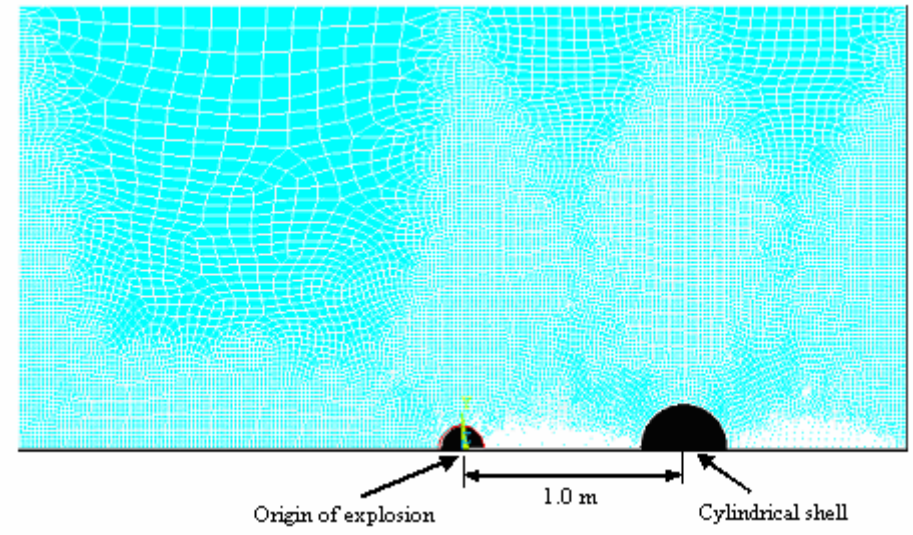

Fig.6.18 FEM mesh for a submerged cylindrical shell subjected to a near-field shock wave

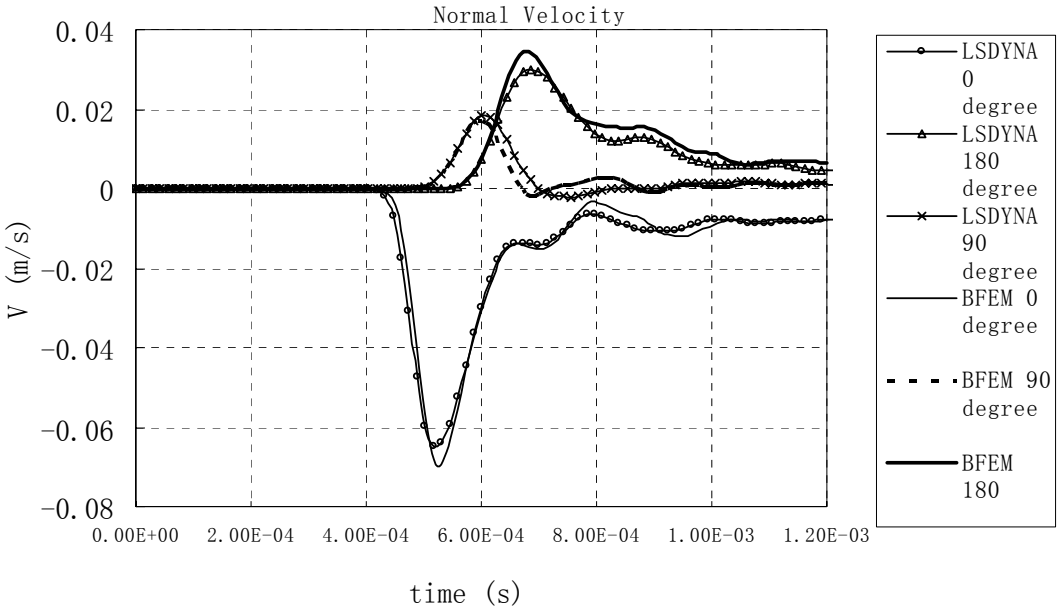

Fig.6.19 Radial velocity of a cylindrical shell subjected to a near-field shock wave

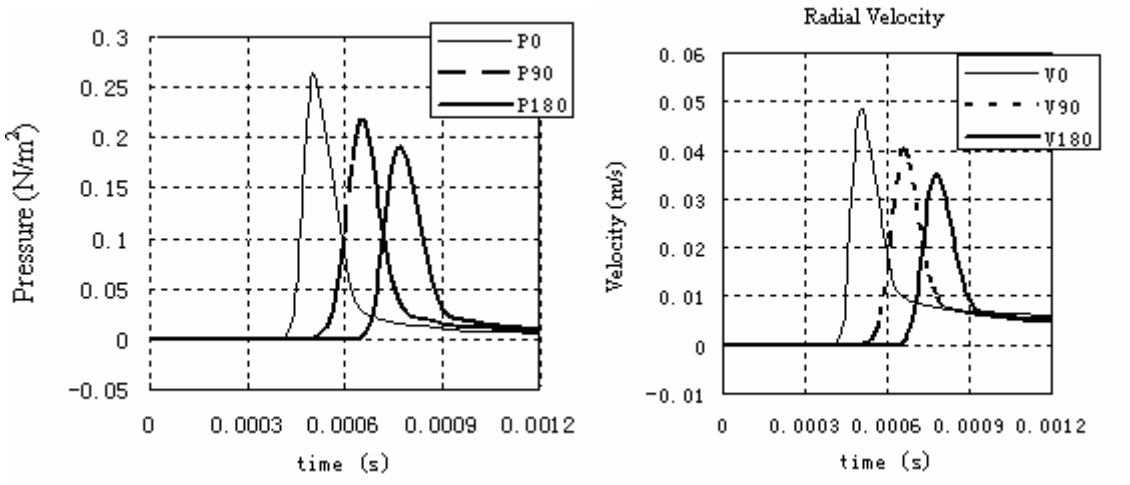

Fig.6.20 Free-field pressure and velocity at $\theta = 0^0, 90^0, 180^0$ ***on the shell surface***

CHAPTER SEVEN

SBFEM/FEM COUPLING METHOD FOR STEADY-STATE ANALYSIS OF DAM-RESERVOIR SYSTEMS

The scaled-boundary-finite-element method (SBFEM) is extended for steady-state analyses of dam-reservoir system problems. In this study, the dam is assumed rigid and subjected to horizontal ground motions, and the liquid in the reservoir is assumed semi-infinite. The vertical ground motion is not considered because the SBFEM needs that the velocity boundary condition at the reservoir's bottom is equal to zero. The semi-infinite reservoir domain is partitioned into two sub-domains: a near-field and a far-field domain. In it, the near-field domain is modeled by finite-element-method (FEM), while the far-field domain is modeled by SBFEM and is treated as a layered semi-infinite fluid domain. A SBFEM/FEM coupling procedure is employed to solve the steady-state response of the reservoir. The coupling procedure is easy to implement and suitable for all frequencies, real or complex. In this chapter, the accuracy and efficiency of the SBFEM formulation described in chapter 3 and the SBFEM/FEM coupling procedure are validated in frequency domain. Numerical results based on the present procedure are in good agreement with analytical and other available numerical solutions.

7.1 PROBLEM STATEMENT

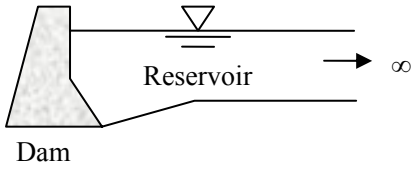

Fig.7.1a A dam-reservoir system

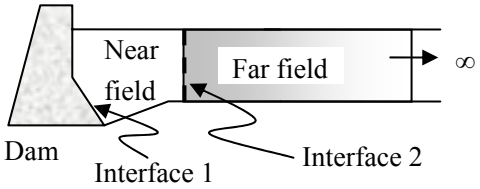

Fig.7.1b Truncation of a reservoir

A dam-reservoir system shown in Fig.7.1a is considered, where the dam is rigid and the fluid in the reservoir is an inviscid isentropic fluid with the fluid particles undergoing small displacements. The analysis is limited to a linear analysis. Not including body force effects, the governing equation of the fluid are as follows.

$$\nabla^2\phi = \frac{1}{c^2}\ddot{\phi} \tag{7.1}$$

where ϕ denotes velocity potential and c denotes the wave speed in the fluid. The pressure p, the velocity vector $\mathbf{v}$ and the velocity potential ϕ have a relationship as follows.

$$\mathbf{v} = \nabla\phi \tag{7.2a}$$

$$p = -\rho\dot{\phi} \tag{7.2b}$$

where ρ denotes the fluid density. Boundary conditions for Eq.(7.1) are as follows.

i) Along the boundary S_v, having a prescribed velocity v_n^S in the direction of the

unit normal vector **n** (pointing outward to the fluid boundary), we have

$$\mathbf{v} \bullet \mathbf{n}\big|_{S_v} = \frac{\partial \phi}{\partial n}\bigg|_{S_v} = v_n^S \tag{7.3a}$$

ii) Along the boundary S_f, having a prescribed pressure p^s, we have

$$p\big|_{S_f} = -\rho\dot{\phi}\big|_{S_f} = p^s \tag{7.3b}$$

Eqs.(7.1) and (7.3) form a boundary value problem. It is difficult to obtain an analytical solution of Eq.(7.1) for the dam-reservoir system as shown in Fig.7.1. To circumvent the difficulties, the fluid in the reservoir is divided into two parts: a near-field and a far-field domain as shown in Fig.7.1b. The interaction between the near-field domain and the far-field domain occurs at Interface 2, while the interaction between the dam and the liquid occurs at Interface 1. Of note, Interface 2 is assumed vertical and the reservoir bottom in the far-field domain is flat (level) and rigid.

7.2 FEM FORMULATION FOR THE NEAR-FIELD DOMAIN

Here, the near-field fluid domain is discretized into an assemblage of finite elements. The corresponding finite-element governing equation of Eq.(7.1) for the near-field domain can be expressed as

$$\mathbf{M}\ddot{\Phi} + \mathbf{K}\Phi = \mathbf{V}_n \tag{7.4}$$

where the global mass **M**, the global stiffness **K** matrices and the global vector $\mathbf{V}_n$ are treated in the standard manner as in the traditional FE procedures as described in section 2.1; and Φ denotes the global vector of nodal velocity potentials ϕ. Its boundary conditions are as follows.

i) At the free surface, by ignoring the effects of surface waves of fluid, the

boundary condition of the free surface is taken as

$$p = -\rho\dot{\phi} = 0 \tag{7.5a}$$

ii) At the dam-reservoir Interface 1, by assuming that the dam's acceleration is a_{n1} in the normal direction, the boundary condition is specified as

$$\frac{\partial p}{\partial n} = -\rho\frac{\partial \dot{\phi}}{\partial n} = -\rho a_{n1} \tag{7.5b}$$

iii) At the bottom of the reservoir, by assuming that the reservoir is rigid, the boundary condition is

$$\frac{\partial p}{\partial n} = -\rho\frac{\partial \dot{\phi}}{\partial n} = 0 \tag{7.5c}$$

iv) At Interface 2, several ways of describing the boundary conditions are available if the far-field is truncated, for example:

- Sommerfeld radiation condition for the truncated surface is given by

$$\frac{\partial p}{\partial n} = -\rho\frac{\partial \dot{\phi}}{\partial n} = 0 \tag{7.6a}$$

- Sharan's boundary condition is

$$\frac{\partial p}{\partial n} = -\frac{p\pi}{2H} \tag{7.6b}$$

where H is the height of the far-field domain.

- A far-boundary condition (Maity and Bhattacharyya (1999)) is expressed as

$$\frac{\partial p}{\partial n} = -\frac{p}{H}Z \tag{7.6c}$$

The expression of Z can be obtained in the literature (Maity and Bhattacharyya (1999)).

Details of the boundary condition as treated by the SBFEM are described in the next

section.

7.3 SBFEM FORMULATION FOR THE FAR-FIELD DOMAIN

What follows shows the SBFEM formulation for the far-field domain. Fig.7.2 shows the SBFEM discretization of the near-field-to-far-field Interface 2. Each element on Interface 2 actually denotes a layered sub-semi-infinite fluid medium. As such, the whole far-field domain is modeled by an assemblage of elements at Interface 2 only and the free surface and the reservoir bottom are not discretized and are prescribed by one node at Interface 2.

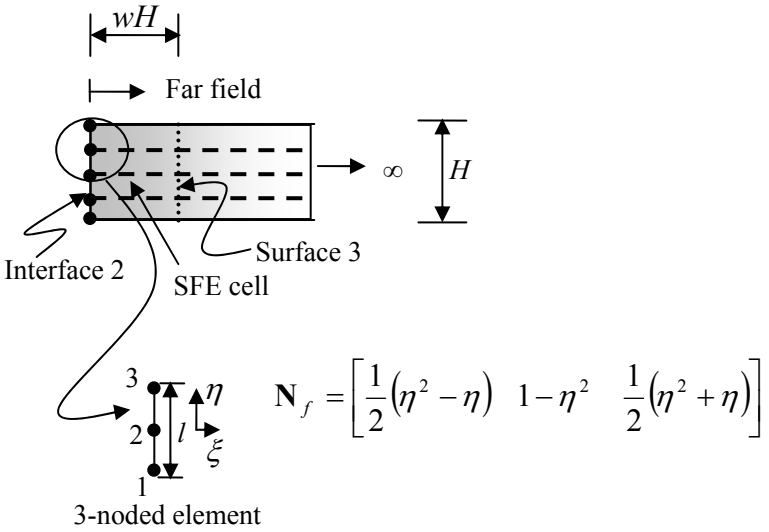

Fig. 7.2 SBFEM mesh for a far-field domain

Along Interface 2, an integral vector of the normal velocity $\mathbf{V}_{n2}$ and a velocity potential vector Φ_2 satisfies the relationship below.

$$\mathbf{V}_{n2}(\omega) = \mathbf{S}^{\infty}(\omega)\Phi_2(\omega) \tag{7.7}$$

where Φ_2 denotes the column vector of nodal velocity potentials ϕ along Interface 2; $\mathbf{S}^{\infty}(\omega)$ is called the "dynamic stiffness" matrix of the whole far-field

domain; and

$$\mathbf{V}_{n2}(\omega)=\sum_{e}\int_{\Gamma_w^e}\mathbf{N}_f^T v_{n2}\,d\Gamma_w^e \tag{7.8}$$

in which v_{n2} denotes the normal velocity; Γ_w denotes Interface 2; $\mathbf{N}_f$ is the shape function for a typical discretized fluid element; and $\sum_e$ denotes an assemblage of all fluid elements on Interface 2. Note that the "dynamic stiffness" matrix $\mathbf{S}^{\infty}(\omega)$ is independent of the response of the far-field domain. It depends on the geometry of Interface 2 only and can be obtained prior to solving Eq.(7.7) . When one of the two variable vectors $\mathbf{V}_{n2}(\omega)$ and $\Phi_2(\omega)$, is known, the other can then be determined. Chapter 3 presents the full details of the derivation of the "dynamic stiffness" matrix $\mathbf{S}^{\infty}(\omega)$ and is not duplicated here. Briefly, the first step is to establish the finite-element governing equation of a scalar-finite-element (SFE) cell between Interface 2 and Surface 3; the second step is to derive the relationship between Interface 2 and Surface 3 using the finite-element governing equation in Eq.(7.4); the last step is to take the SFE cell's characteristic width w as the analytical limit to zero, which yields a consistent infinitesimal finite-element cell (IFEC) equation in frequency domain and the solution of the IFEC equation is the "dynamic stiffness" matrix $\mathbf{S}^{\infty}(\omega)$. The IFEC equation is expressed as

$$\left(\mathbf{S}^{\infty}(\omega)+\mathbf{E}^1\right)\mathbf{E}^{0^{-1}}\left(\mathbf{S}^{\infty}(\omega)+\mathbf{E}^{1^T}\right)-\mathbf{E}^2+\omega^2\mathbf{M}^0=0 \tag{7.9}$$

where the global coefficient matrices $\mathbf{E}^0$, $\mathbf{E}^1$, $\mathbf{E}^2$ and $\mathbf{M}^0$ depend only on the attributes of Interface 2, which can be obtained through assembling all elements' $\mathbf{E}_e^0$, $\mathbf{E}_e^1$, $\mathbf{E}_e^2$ and $\mathbf{M}_e^0$ on Interface 2. The matrices $\mathbf{E}_e^0$, $\mathbf{E}_e^1$, $\mathbf{E}_e^2$ are in the form of $\int_{\Gamma_w^e}\mathbf{B}^T\mathbf{B}\,d\Gamma_w^e$ and $\mathbf{M}_e^0$ is in the form of $\int_{\Gamma_w^e}\frac{1}{c^2}\mathbf{N}_f^T\mathbf{N}_f\,d\Gamma_w^e$, where the matrices $\mathbf{B}$'s are kinds of strain-displacement relationship. Details can be found in chapter 3. For a 2-dimensional 3-node element shown in Fig.7.2, in which the middle node 2

is located mid-way between node 1 and node 3, the element coefficient matrices can be obtained analytically as follows.

$$\mathbf{E}_e^0 = \frac{l}{30\mathrm{H}}\begin{bmatrix} 4 & 2 & -1 \\ 2 & 16 & 2 \\ -1 & 2 & 4 \end{bmatrix} \tag{7.10a}$$

$$\mathbf{E}_e^1 = \begin{bmatrix} 0 & 0 & 0 \\ 0 & 0 & 0 \\ 0 & 0 & 0 \end{bmatrix} \tag{7.10b}$$

$$\mathbf{E}_e^2 = \frac{\mathrm{H}}{3l}\begin{bmatrix} 7 & -8 & 1 \\ -8 & 16 & -8 \\ 1 & -8 & 7 \end{bmatrix} \tag{7.10c}$$

and

$$\mathbf{M}_e^0 = \frac{l\mathrm{H}}{30\mathrm{c}^2}\begin{bmatrix} 4 & 2 & -1 \\ 2 & 16 & 2 \\ -1 & 2 & 4 \end{bmatrix} \tag{7.10d}$$

where H and l denote the heights of the reservoir and a single element, respectively. Upon assembling all of the element coefficient matrices into the corresponding global matrices, it is found that the global matrix $\mathbf{E}^1$ is a zero matrix. Substituting it into Eq.(7.9) yields

$$\mathbf{S}^\infty(\omega)\mathbf{E}^{0^{-1}}\mathbf{S}^\infty(\omega) - \mathbf{E}^2 + \omega^2\mathbf{M}^0 = 0 \tag{7.11}$$

By comparing Eq.(7.11) with Eq.(7.9), one can see that Eq.(7.11) is much easier to solve than Eq.(7.9). The solution of Eq.(7.11) is as follows.

i) Post-multiplying Eq.(7.11) by $\mathbf{E}^{0^{-1}}$ and then rearranging leads to

$$\mathbf{S}^\infty(\omega)\mathbf{E}^{0^{-1}}\mathbf{S}^\infty(\omega)\mathbf{E}^{0^{-1}} = \left(\mathbf{E}^2 - \omega^2\mathbf{M}^0\right)\mathbf{E}^{0^{-1}} \tag{7.12a}$$

ii) Taking square root of Eq.(7.12a) yields

$$\mathbf{S}^\infty(\omega)\mathbf{E}^{0^{-1}} = \sqrt{\left(\mathbf{E}^2 - \omega^2\mathbf{M}^0\right)\mathbf{E}^{0^{-1}}} \tag{7.12b}$$

iii) Post-multiplying Eq.(7.12b) by $\mathbf{E}^0$ leads to

$$\mathbf{S}^{\infty}(\omega)=\sqrt{\left(\mathbf{E}^{2}-\omega^{2}\mathbf{M}^{0}\right)\mathbf{E}^{0^{-1}}}\mathbf{E}^{0} \tag{7.12c}$$

Note that if the exciting frequency ω is given, Eq.(7.12c) can be readily determined, and thus Eq.(7.11) is solved. Usually, Eq.(7.9) is very difficult to solve when the matrix $\mathbf{E}^{1}$ is present even if using the dynamic condensation and substructure deletion methods as proposed by Wolf and Song (1996a). In this regard, whether the matrix $\mathbf{E}^{1}$ vanishes is crucial for obtaining the solutions for the present SBFEM. However, by inspecting Eq.(7.12c), one can see that the values of $\mathbf{S}^{\infty}(\omega)$ may be real or complex for different exciting frequencies ω. It means that there is a cut-off frequency ω_c, such that when the exciting frequency ω is less than ω_c, $\mathbf{S}^{\infty}(\omega)$ is real, or $\mathbf{S}^{\infty}(\omega)$ is complex. Reformulating Eq.(7.12c) yields

$$\mathbf{S}^{\infty}(\omega)=\sqrt{\mathbf{E}^{2}\left(\mathbf{I}-\omega^{2}\mathbf{E}^{2^{-1}}\mathbf{M}^{0}\right)\mathbf{E}^{0^{-1}}}\mathbf{E}^{0} \tag{7.12d}$$

It is obvious that the term $\mathbf{I}-\omega^{2}\mathbf{E}^{2^{-1}}\mathbf{M}^{0}$ can be decomposed into a real power series when the spectral radii of the matrix $\omega^{2}\mathbf{E}^{2^{-1}}\mathbf{M}^{0}$ is less than or equal to 1. Therefore, the cut-off frequency ω_c is determined by $\omega^{2}\mathbf{E}^{2^{-1}}\mathbf{M}^{0}$ and Eq.(7.12d) is a real matrix when $\omega\le\omega_c$.

7.4 FEM-SBFEM COUPLING FORMULATION

Partitioning Eq.(7.4) into sub-matrices corresponding to variables at Interface 1, Interface2 and other interior locations leads to

$$\begin{bmatrix}\mathbf{m}_{11} & \mathbf{m}_{12} & \mathbf{m}_{13}\\ \mathbf{m}_{21} & \mathbf{m}_{22} & \mathbf{m}_{23}\\ \mathbf{m}_{31} & \mathbf{m}_{32} & \mathbf{m}_{33}\end{bmatrix}\begin{Bmatrix}\ddot{\Phi}_1\\ \ddot{\Phi}_2\\ \ddot{\Phi}_3\end{Bmatrix}+\begin{bmatrix}\mathbf{k}_{11} & \mathbf{k}_{12} & \mathbf{k}_{13}\\ \mathbf{k}_{21} & \mathbf{k}_{22} & \mathbf{k}_{23}\\ \mathbf{k}_{31} & \mathbf{k}_{32} & \mathbf{k}_{33}\end{bmatrix}\begin{Bmatrix}\Phi_1\\ \Phi_2\\ \Phi_3\end{Bmatrix}=\begin{Bmatrix}\mathbf{V}_{n1}\\ \mathbf{V}'_{n2}\\ \mathbf{V}_{n3}\end{Bmatrix} \tag{7.13}$$

where the subscripts 1 and 2 refer to nodal variables at Interfaces 1 and 2, respectively; while the subscript 3 refers to other interior nodal variables in the

near-field fluid. At Interface 2, the near-field FEM-domain couples with the far-field SBFEM-domain. The kinematic continuity condition requires that both fields have the same normal velocity at Interface 2. Hence, Eq.(7.7) can be re-written as

$$-\mathbf{V}'_{n2} = \mathbf{V}_{n2} = \mathbf{S}^{\infty}(\omega)\Phi_2 \tag{7.14a}$$

Substituting Eq.(7.12c) into Eq.(7.14a) and re-arranging yields

$$\mathbf{V}'_{n2} = -\sqrt{\left(\mathbf{E}^2 - \omega^2\mathbf{M}^0\right)\mathbf{E}^{0^{-1}}}\,\mathbf{E}^0\Phi_2 \tag{7.14b}$$

Substituting Eq.(7.14b) into Eq.(7.13) leads to

$$\begin{bmatrix} \mathbf{m}_{11} & \mathbf{m}_{12} & \mathbf{m}_{13} \\ \mathbf{m}_{21} & \mathbf{m}_{22} & \mathbf{m}_{23} \\ \mathbf{m}_{31} & \mathbf{m}_{32} & \mathbf{m}_{33} \end{bmatrix} \begin{Bmatrix} \ddot{\Phi}_1 \\ \ddot{\Phi}_2 \\ \ddot{\Phi}_3 \end{Bmatrix} + \begin{bmatrix} \mathbf{k}_{11} & \mathbf{k}_{12} & \mathbf{k}_{13} \\ \mathbf{k}_{21} & \mathbf{k}_{22} + \sqrt{\left(\mathbf{E}^2 - \omega^2\mathbf{M}^0\right)\mathbf{E}^{0^{-1}}}\,\mathbf{E}^0 & \mathbf{k}_{23} \\ \mathbf{k}_{31} & \mathbf{k}_{32} & \mathbf{k}_{33} \end{bmatrix} \begin{Bmatrix} \Phi_1 \\ \Phi_2 \\ \Phi_3 \end{Bmatrix} = \begin{Bmatrix} \mathbf{V}_{n1} \\ \mathbf{0} \\ \mathbf{V}_{n3} \end{Bmatrix} \tag{7.15}$$

For a steady-state response with an exciting frequency ω,

$$\Phi = \overline{\Phi} e^{i\omega t} \tag{7.16}$$

Substituting Eq.(7.16) into Eq.(7.15) leads to

$$\left(-\omega^2 \begin{bmatrix} \mathbf{m}_{11} & \mathbf{m}_{12} & \mathbf{m}_{13} \\ \mathbf{m}_{21} & \mathbf{m}_{22} & \mathbf{m}_{23} \\ \mathbf{m}_{31} & \mathbf{m}_{32} & \mathbf{m}_{33} \end{bmatrix} + \begin{bmatrix} \mathbf{k}_{11} & \mathbf{k}_{12} & \mathbf{k}_{13} \\ \mathbf{k}_{21} & \mathbf{k}_{22} + \sqrt{\left(\mathbf{E}^2 - \omega^2\mathbf{M}^0\right)\mathbf{E}^{0^{-1}}}\,\mathbf{E}^0 & \mathbf{k}_{23} \\ \mathbf{k}_{31} & \mathbf{k}_{32} & \mathbf{k}_{33} \end{bmatrix} \right) \begin{Bmatrix} \overline{\Phi}_1 \\ \overline{\Phi}_2 \\ \overline{\Phi}_3 \end{Bmatrix} e^{i\omega t} = \begin{Bmatrix} \mathbf{V}_{n1} \\ \mathbf{0} \\ \mathbf{V}_{n3} \end{Bmatrix} \tag{7.17}$$

Of note, Eq.(7.17) can be solved for any frequency ω. As the near-field domain is modeled by FEM, Eq.(7.17) is suitable for any arbitrary geometrical shape at the interface between the dam and the near-field domain.

7.5 NUMERICAL EXAMPLES

To validate the present SBFEM/FEM coupling formulation, specific numbers of 2-dimensional cases for dam-reservoir systems subjected to horizontal harmonic ground motions are considered.

7.5.1 NATURAL FREQUENCY ANALYSIS OF A FAR-FIELD DOMAIN

The objective of this analysis is to check the accuracy and efficiency of the "dynamic stiffness" matrix $\mathbf{S}^{\infty}(\omega)$ expressed in Eq.(7.12c). It requires the determinant of Eq.(7.12c) to be set equal to zero to obtain the natural frequency for the far-field domain (shown in Fig.7.2), i.e.

$$\left|\mathbf{S}^{\infty}(\omega)\right| = \left|\sqrt{\left(\mathbf{E}^{2} - \omega^{2}\mathbf{M}^{0}\right)\mathbf{E}^{0^{-1}}}\,\mathbf{E}^{0}\right| = 0 \tag{7.18a}$$

The equivalent equation of Eq.(7.18a) is given by

$$\left|\mathbf{S}^{\infty}(\omega)\right| = \left|\sqrt{\left(\mathbf{E}^{2} - \omega^{2}\mathbf{M}^{0}\right)\mathbf{E}^{0^{-1}}}\right|\left|\mathbf{E}^{0}\right| = \left|\left(\mathbf{E}^{2} - \omega^{2}\mathbf{M}^{0}\right)\right|^{\frac{1}{2}}\left|\mathbf{E}^{0^{-1}}\right|^{\frac{1}{2}}\left|\mathbf{E}^{0}\right| = 0 \tag{7.18b}$$

Therefore, the natural frequency of a far-field domain can be obtained from the equation below.

$$\left|\left(\mathbf{E}^{2} - \omega^{2}\mathbf{M}^{0}\right)\right| = 0 \tag{7.18c}$$

The far-field domain as shown in Fig.7.2 is studied using two discretization meshes. Mesh 1 consists of 10 numbers of 3-node SBFEM elements having the same height $l = \mathrm{H}/10$, while Mesh 2 consists of 20 numbers of similar elements ($l = \mathrm{H}/20$). The dimensions of the global coefficient matrices $\mathbf{E}^{0}$, $\mathbf{E}^{1}$, $\mathbf{E}^{2}$ and $\mathbf{M}^{0}$ are all 21x21 in Mesh 1 and 41x41 in Mesh 2. After dropping the row and column with respect to the free surface, it reduces to 20x20 and 40x40, respectively. Substituting $\mathbf{E}^{2}$ and $\mathbf{M}^{0}$ into Eq.(7.18c) yields the first 20 natural frequencies ω for Mesh 1

and 40 for Mesh 2. The natural frequencies are normalized as $\Omega = \frac{\omega H}{c}$. Results are listed in Table 7.1. In Table 7.1, the analytical solutions $\Omega_a = \omega_k H / c = \frac{2k-1}{2}\pi$ (k=1,2,3,…) (Tsai and Lee 1989) are also given. From Table 7.1, one can see that SBFEM solutions are very close to the analytical solutions, especially at lower frequencies. Also, the convergence of the SBFEM can be observed by comparing results of Mesh 1 and Mesh 2 with analytical solutions. Mesh 2 with increasing mesh density results in better solutions. Nevertheless, as the response of structures is dominated by certain low-order natural frequencies, the coarse Mesh 1 is fine enough to determine the response of a far-field domain accurately.

Table 7.1 Natural frequencies of a far-field domain

Serial no. (ω_k)		1	2	3	4	5	6	7	8	9	10
Analytical $2\Omega_a/\pi$		1	3	5	7	9	11	13	15	17	19
Present $2\Omega/\pi$	Mesh 1	1.00	3.00	5.00	7.01	9.02	11.06	13.13	15.25	17.42	19.55
	Mesh 2	1.00	3.00	5.00	7.00	9.00	11.00	13.01	15.02	17.03	19.06
Serial no. (ω_k)		11	12	13	14	15	16	17	18	19	20
Analytical $2\Omega_a/\pi$		21	23	25	27	29	31	33	35	37	39
Present $2\Omega/\pi$	Mesh 1	22.68	25.13	27.94	31.03	34.36	37.90	41.50	44.87	47.57	49.11
	Mesh 2	21.09	23.15	25.22	27.31	29.43	31.57	33.75	35.94	38.09	39.91

7.5.2 STEADY-STATE ANALYSIS OF A VERTICAL DAM

In this example, a dam having a vertical upstream face and an infinite reservoir subjected to a horizontal harmonic ground acceleration motion ($= ae^{i\omega t}$) in the

upstream direction is examined. The dam and the reservoir floor are assumed rigid. The reservoir floor is assumed flat. The FEM and SBFEM meshes for the reservoir are shown in Fig.7.3. The near-field domain is modeled by 10 numbers of 8-node plane-strain elements, while the far-field domain is modeled by 10 numbers of 3-node SBFEM elements. The width of the near-field is 0.05H where H (=180m) is the height of the reservoir. Figs.7.4a and 7.4b plot the pressure distributions along the y-direction at the interface between the dam and the near-field for different exciting frequencies $\Omega = \omega H / c$. Of note, in the case of vertical dams, the near-field domain is not necessarily put in place and the reservoir can be represented by a far-field domain alone. In this case, the response of the far-field domain can be solved by the SBFEM procedure alone in Eq.(7.7) and results are plotted in Figs.7.4a and 7.4b, too. From these two figures, it can be seen that results of the FEM/SBFEM and those of the SBFEM-alone coincide with each other. The same problem was previously studied by Chopra (1967) and Tsai and Lee (1989). Chopra derived an analytical solution, while Tsai and Lee reported a numerical solution using BEM. The analytical, Tsai and Lee's and SBFEM solutions are all plotted in Figs.7.5a and 7.5b. By comparing these solutions, one can see that the SBFEM solutions coincide with the analytical and Tsai and Lee's solutions. Therefore, it can be concluded that the reservoir with a vertical dam surface can be represented by a far-field-only domain which renders a SBFEM-alone model possible, and yields accurate results, too.

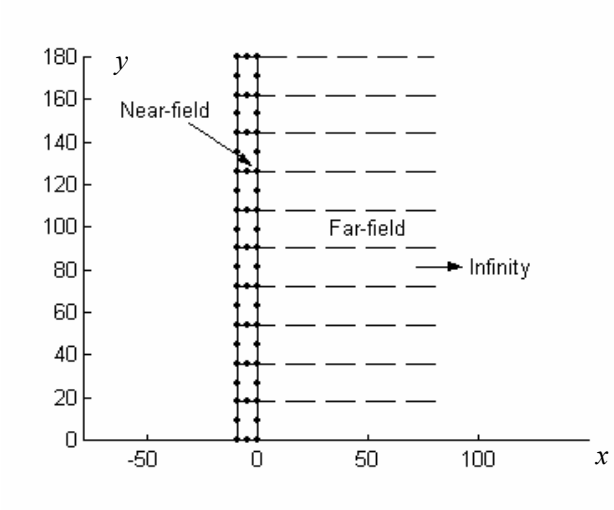

Fig.7.3 FEM and SBFEM meshes of the reservoir

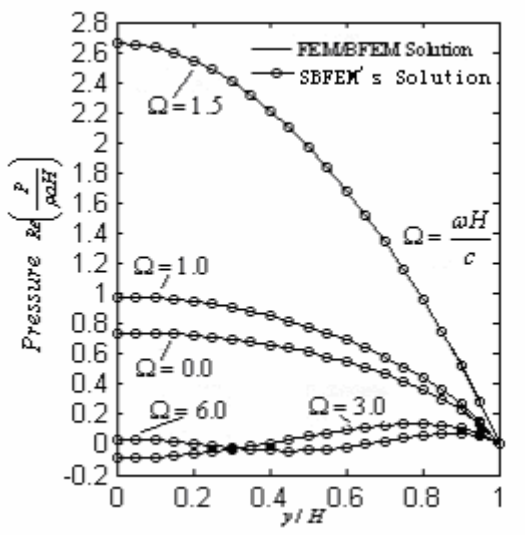

Fig.7.4a Comparison of pressure (real parts) obtained by SBFEM-alone and FEM/SBFEM

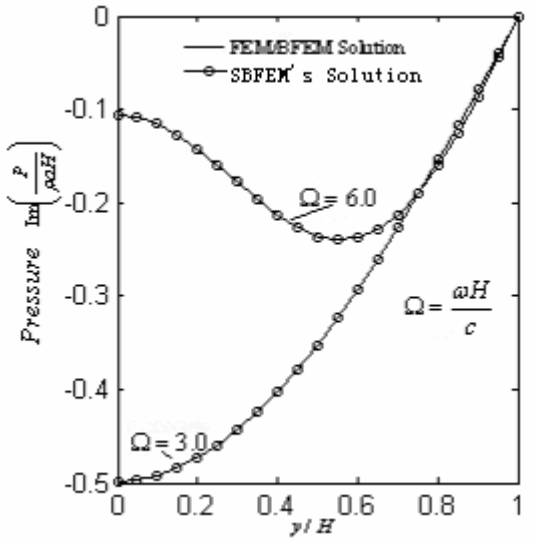

Fig.7.4b Comparison of pressure (Imaginary parts) obtained by SBFEM-alone and FEM/SBFEM

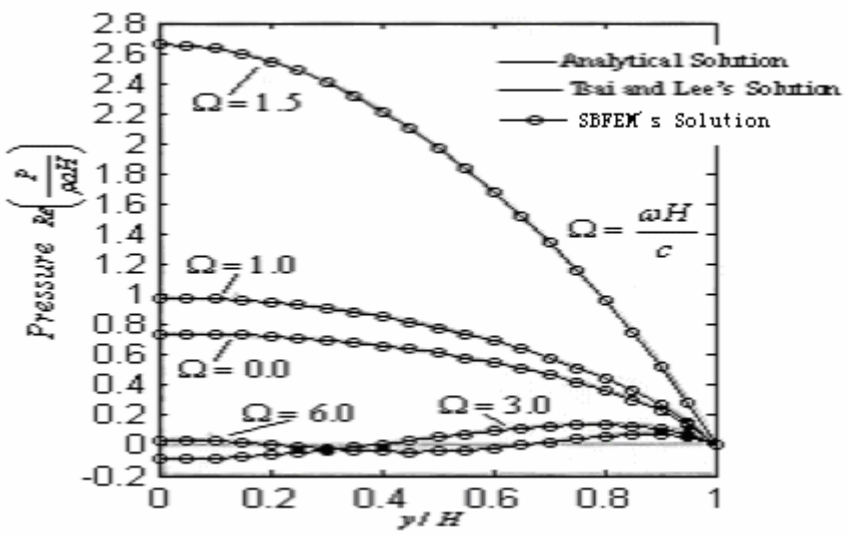

Fig.7.5a Comparison of pressure (real parts) obtained by Tsai and Lee, SBFEM and analytical solution

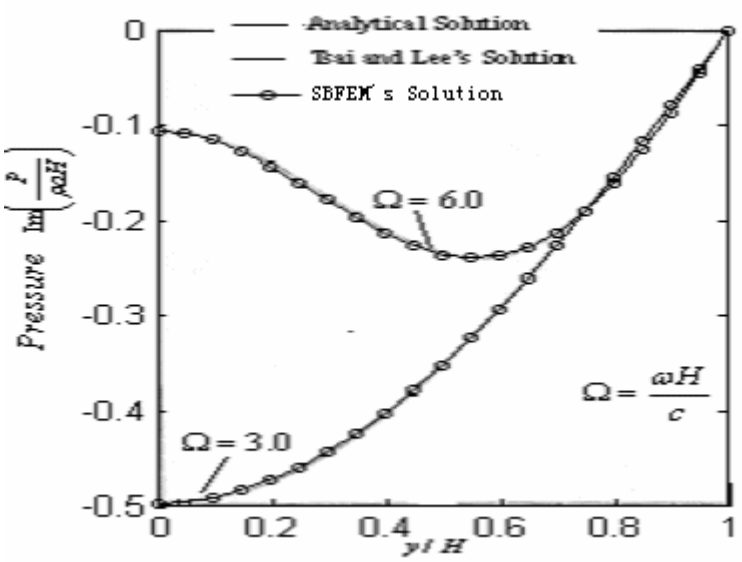

Fig.7.5b Comparison of pressure (Imaginary parts) obtained by Tsai and Lee, SBFEM and analytical solution

7.5.3 STEADY-STATE ANALYSIS OF A SLOPING DAM

A dam having a sloping angle of 20^0 on the upstream face subjected to a horizontal ground acceleration motion ($=ae^{i\omega t}$) is examined in this example. In it, the dam and the reservoir floor are assumed rigid. The reservoir floor is assumed flat. The aim is to validate the accuracy of the present FEM/SBFEM coupling procedure for a sloping dam. The discretized FEM and SBFEM meshes are shown in Fig.7.6. The near-field domain is modeled by 40 numbers of 8-node plane-strain elements, while the far-field domain is modeled by 10 numbers of 3-node SBFEM elements. Pressure distributions along the sloping interface for different exciting frequencies $\Omega = \omega H / c$ are plotted in Figs.7.7a and 7.7b. Tsai and Lee (1989) used FEM and BEM to study the same problem for comparison, respectively. Their results are also plotted in Figs.7.7a and 7.7b. By comparing the present FEM/SBFEM solutions with Tsai and Lee's FEM and BEM solutions, it can be seen that the present real-part solutions fully coincide with Tsai and Lee's solutions while

the present imaginary-part solutions fully coincide with FEM solutions. Of note, Tsai and Lee's BEM and FEM solutions are almost the same, except for a small difference in the imaginary-part results when $\Omega = 6.0$.

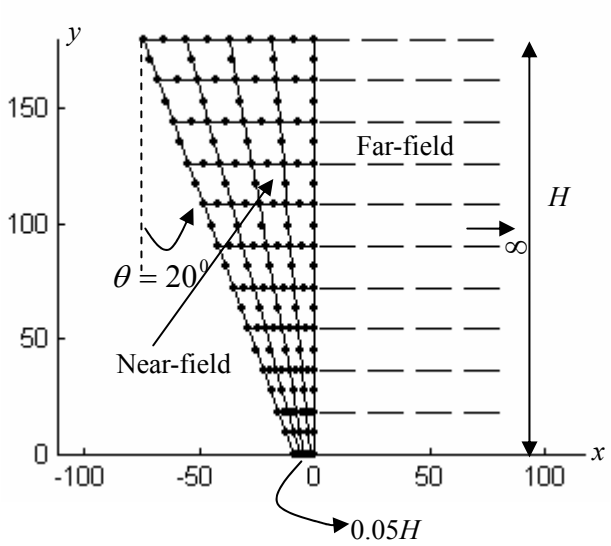

Fig.7.6 Mesh for the reservoir for a dam-reservoir system having a sloping angle $\theta = 20^0$

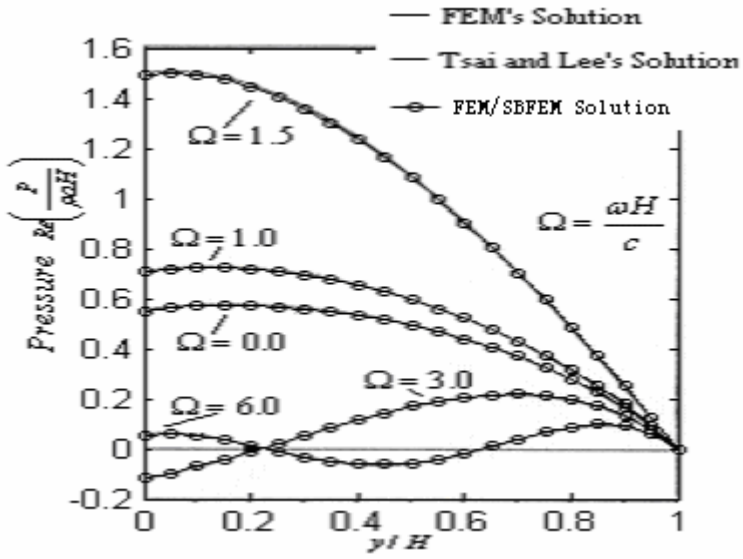

Fig.7.7a Pressure distributions (Real parts) along the dam having a sloping angle $\theta = 20^0$

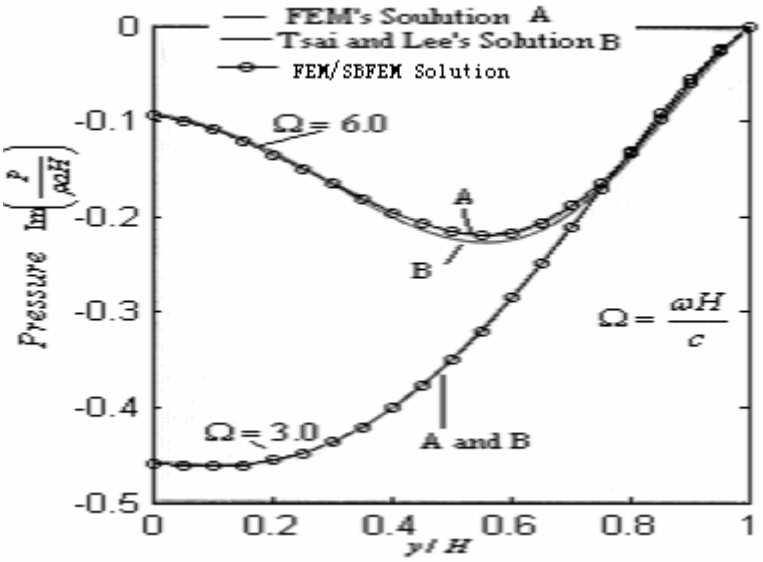

Fig.7.7b Pressure distributions (Imaginary parts) along the dam having a sloping angle

$$\theta = 20^0$$

7.5.4 STEADY-STATE ANALYSIS OF A DAM HAVING MULTI-SLOPES ON THE UPSTREAM FACE

A rigid dam having two slopes on the upstream face as shown in Fig.7.8a is considered. The reservoir floor is assumed rigid and flat. The meshes for the near-field FEM domain and the far-field SBFEM domain of the reservoir are shown in Fig.7.8b. Results of pressure distributions along the dam-reservoir interface for the dam excited by various frequencies horizontal ground acceleration motions ($=ae^{i\omega t}$) are shown in Figs.7.9a and 7.9b. The same problem was previously studied by Tsai (1992) using a semi-analytical method based on the least square method or the Galerkin method. Their results are also plotted in Figs.7.9a and 7.9b for comparison. From Figs.7.9a and 7.9b, it can be seen that FEM-SBFEM results are in very good accord with Tsai's, especially for the vertical part of the dam-reservoir interface. However, the FEM-SBFEM results have higher values than

Tsai's near the heel of dam. In view of Tsai's results being non-analytical, it is not surprising to see greater discrepancy for a large-angle sloping dam. Hence, the present FEM-SBFEM results appear to yield more accurate results.

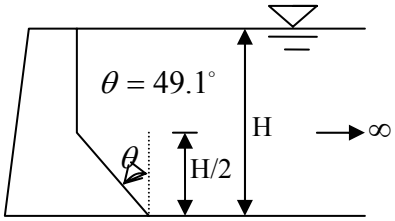

Fig.7.8a Geometry of a dam having two slopes on the upstream face

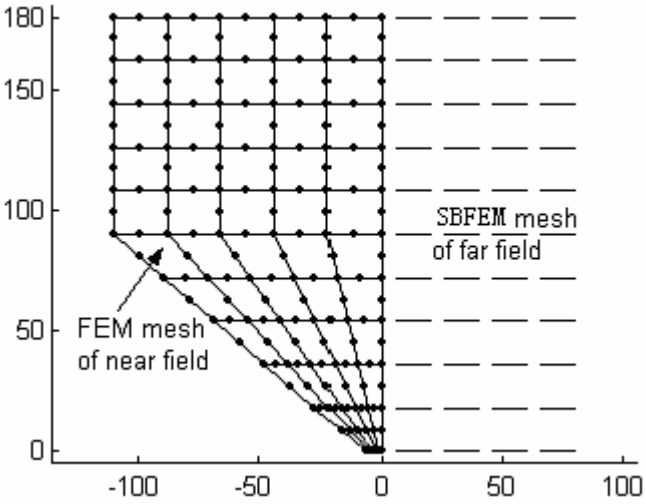

Fig.7.8b FEM and SBFEM meshes of a dam having two slopes on the upstream face

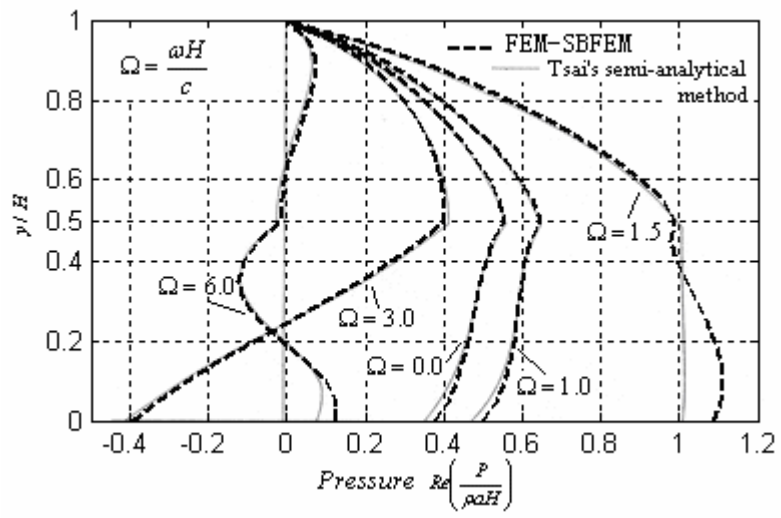

Fig.7.9a Pressure distributions (real parts) along the dam-reservoir interface

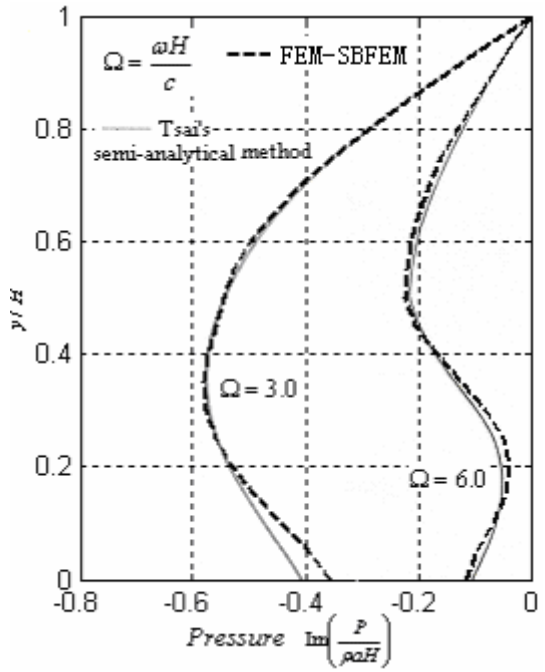

Fig.7.9b Pressure distributions (Imaginary parts) along the dam-reservoir interface

7.5.5 STEADY-STATE ANALYSIS OF SLOPING DAMS AGAINST INCOMPRESSIBLE FLUID

This example is to validate the accuracy of the FEM-SBFEM procedure for the dam-reservoir systems containing incompressible fluid. A rigid dam having a sloping face retains an infinite long fluid domain in the upstream direction. It is subjected to a horizontal ground acceleration motion ($= ae^{i\omega t}$) as shown in Fig.7.10. The reservoir floor is assumed rigid, flat and fluid incompressible. The pressure distributions on the sloping dam for different sloping angles are shown in Fig.7.10 and compared with Chwang's exact solutions (1978) and Tsai's semi-analytical solutions (1992). The FEM mesh for the near-field domain and the SBFEM mesh for the far-field domain are similar to those in Fig.7.6, except that the distance between the dam's heel and the near-to-far-field interface is 0.01H. From Fig.7.10, one can see that the FEM-SBFEM results fully coincide with Chwang's exact solutions and are more accurate than Tsai's solutions (1992). An additional curve for $\theta = 60^0$ obtained by the FEM-SBFEM method is also plotted in Fig.7.10. It exhibits the trend that the greater the sloping angle, the smaller is the pressure.

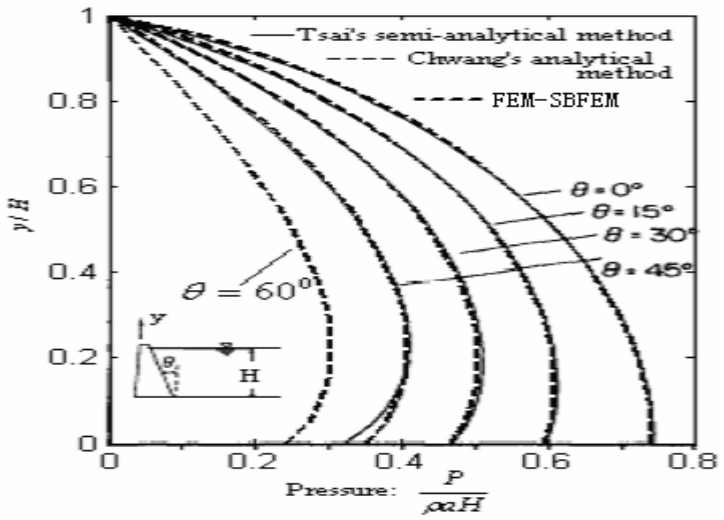

Fig.7.10 Pressure distributions on a sloping dam against incompressible fluid

7.5.6 STEADY-STATE ANALYSIS OF ARCH DAMS AGAINST INCOMPRESSIBLE FLUID

This example is to investigate hydrodynamic pressure distributions along an arch dam against incompressible fluid when subjected to a horizontal ground acceleration motion ($= ae^{i\omega t}$). Here, the upstream face of an arch dam is assumed to take the slope of a partial circular arc. Five different circular arcs are considered. Each arc is defined by 3 points on the curve. The coordinates (x,y) of the points, the associated center and radius are listed in Table 7.2. Note that Arc 5 with an infinite radius is a vertical face. For easy visualization, the circular arcs are plotted in Fig.7.11a, in which the fluid is retained to the right. The near-field FEM mesh and the far-field SBFEM mesh are shown in Fig.7.11b. The results are plotted in Fig.7.12. By comparing the results, one can see that the steeper the arc, the larger is the pressure acting on the arch dam.

Table 7.2 Geometrical configurations (x,y) of different circular arcs

Arc type	Point 1	Point 2	Point 3	Center	Radius
Arc 1	(104,0)	(32,90)	(0,180)	(312.1,240.3)	317.9
Arc 2	(104,0)	(49,90)	(26,180)	(357.7,216.8)	333.7
Arc 3	(104,0)	(65,90)	(52,180)	(409.0,185.6)	357.1
Arc 4	(104,0)	(84,90)	(78,180)	(678.1,174.8)	600.1
Arc 5	(104,0)	(104,90)	(104,180)	without solution	∞

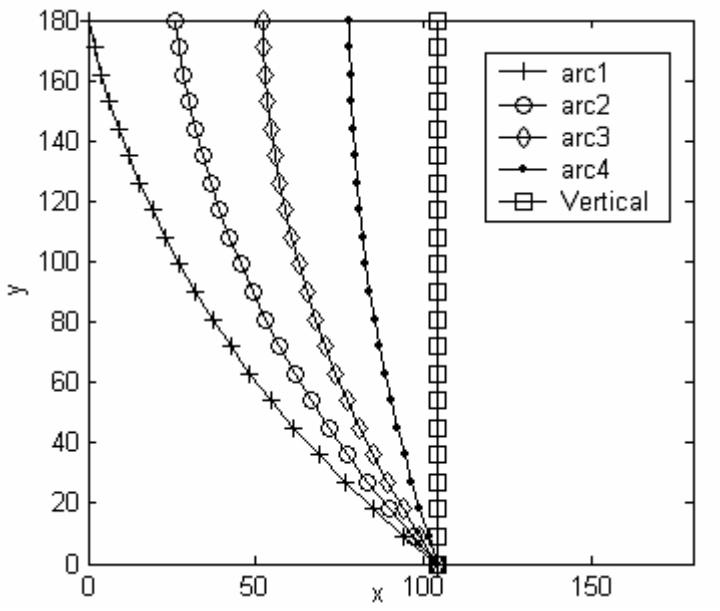

Fig.7.11a Geometry of arcs

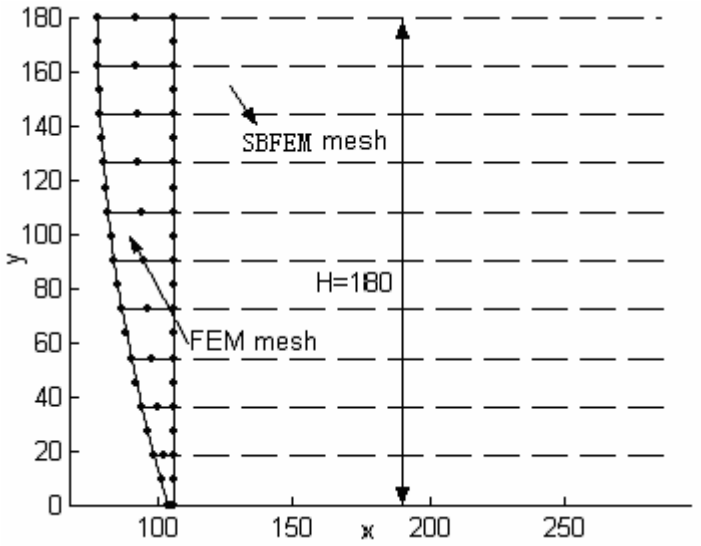

Fig.7.11b FEM and SBFEM meshes

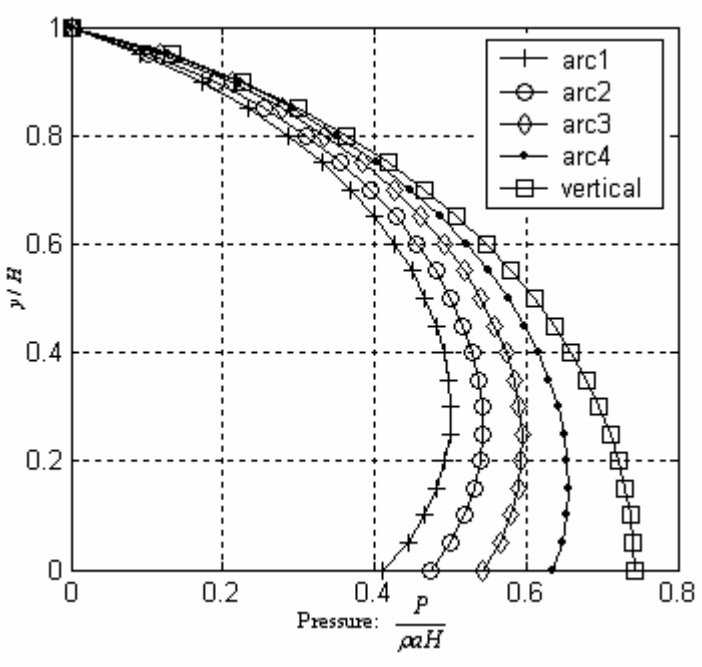

Fig.7.12 Pressure distributions on arch dams against incompressible fluid

7.5.7 STEADY-STATE ANALYSIS OF A RIGID DAM WITH AN ABSORPTIVE RESERVOIR'S BOTTOM

For an absorptive reservoir's bottom, the boundary condition expressed as Eq.(7.5c) must be changed and can be expressed in a simple manner as follows.

$$\frac{\partial \phi}{\partial n} + q\dot{\phi} = 0 \tag{7.19}$$

where the value q is determined by

$$q = \frac{1}{c}\left(\frac{1-\alpha}{1+\alpha}\right) \tag{7.20}$$

in which α denotes the reflection coefficient of pressure striking the bottom of the reservoir. When α equals to 1, Eq.(7.19) becomes Eq.(7.5c). That is to say, the reservoir's bottom is rigid and not absorptive.

For the far-field domain with an absorptive reservoir's bottom, the corresponding

"dynamic stiffness" matrix $\mathbf{S}^{\infty}(\omega)$ does not satisfy Eq.(7.11) any more. By using the same technique presented in Chapter 4, the "dynamic stiffness" matrix $\mathbf{S}^{\infty}(\omega)$ satisfies the following equation.

$$\mathbf{S}^{\infty}(\omega)\mathbf{E}^{0^{-1}}\mathbf{S}^{\infty}(\omega)-\mathbf{E}^{2}-\mathrm{i}\omega\mathbf{C}^{0}+\omega^{2}\mathbf{M}^{0}=0 \tag{7.21}$$

where the global coefficient matrices $\mathbf{E}^{0}$, $\mathbf{E}^{2}$ and $\mathbf{M}^{0}$ are the same as those in Eq.(7.11), and the global coefficient matrices $\mathbf{C}^{0}$ can be obtained through assembling all elements' $\mathbf{C}_{\mathrm{e}}^{0}$. Note that only the $\mathbf{C}_{\mathrm{e}}^{0}$ corresponding to the element adjacent to the reservoir's bottom are not zeros, while those corresponding to other elements are zeros. The non-zero $\mathbf{C}_{\mathrm{e}}^{0}$ is expressed as $\mathrm{qH}\mathbf{N}_{\mathrm{f}}^{\mathrm{T}}\mathbf{N}_{\mathrm{f}}$ with $\eta=-1$, i.e.

$$\mathbf{C}_{\mathrm{e}}^{0}=\mathrm{qH}\begin{bmatrix}1&0&0\\0&0&0\\0&0&0\end{bmatrix} \tag{7.22}$$

Solving Eq.(7.21) leads to

$$\mathbf{S}^{\infty}(\omega)=\sqrt{\left(\mathbf{E}^{2}+\mathrm{i}\omega\mathbf{C}^{0}-\omega^{2}\mathbf{M}^{0}\right)\mathbf{E}^{0^{-1}}}\,\mathbf{E}^{0} \tag{7.23}$$

The FEM-SBFEM coupling formulation for a dam-reservoir system with an absorptive bottom is expressed as follows, which is similar to Eq.(7.17).

$$\left(-\omega^{2}\begin{bmatrix}\mathbf{m}_{11}&\mathbf{m}_{12}&\mathbf{m}_{13}\\\mathbf{m}_{21}&\mathbf{m}_{22}&\mathbf{m}_{23}\\\mathbf{m}_{31}&\mathbf{m}_{32}&\mathbf{m}_{33}\end{bmatrix}+\begin{bmatrix}\mathbf{k}_{11}&\mathbf{k}_{12}&\mathbf{k}_{13}\\\mathbf{k}_{21}&\mathbf{k}_{22}+\sqrt{\left(\mathbf{E}^{2}+\mathrm{i}\omega\mathbf{C}^{0}-\omega^{2}\mathbf{M}^{0}\right)\mathbf{E}^{0^{-1}}}\,\mathbf{E}^{0}&\mathbf{k}_{23}\\\mathbf{k}_{31}&\mathbf{k}_{32}&\mathbf{k}_{33}\end{bmatrix}\right)\begin{Bmatrix}\overline{\Phi}_{1}\\\overline{\Phi}_{2}\\\overline{\Phi}_{3}\end{Bmatrix}\mathrm{e}^{\mathrm{i}\omega t}=\begin{Bmatrix}\mathbf{V}_{\mathrm{n}1}\\\mathbf{0}\\\mathbf{V}_{\mathrm{n}3}\end{Bmatrix} \tag{7.24}$$

The following benchmark examples verified the correctness and efficiency of Eq.(7.23) and Eq.(7.24). Three different geometries of the upstream face of the rigid dam subjected to a horizontal harmonic ground acceleration motion ($=\mathrm{a}\mathrm{e}^{\mathrm{i}\omega t}$) in the upstream direction were considered: (i) vertical dam; (ii) fully inclined dam (a sloping dam as shown in Fig.7.10); (iii) partially inclined dam (dam having

multi-slopes as shown in Fig.7.8a with $\theta = 45^0$). Meshes for the three cases are the same to those used in sections 7.5.2, 7.5.3 and 7.5.4, respectively. For a vertical dam, different exciting frequencies ω and reflection coefficients α were considered. The results were shown in Figs.7.13a-c. The coefficient $C_p = \frac{|P|}{\rho g H}$, while $\omega_1 = \frac{\pi c}{2H}$. From Figs.7.13a-c, one can see that the hydrodynamic pressure $|P|$ decreases when the exciting frequency ω increases.

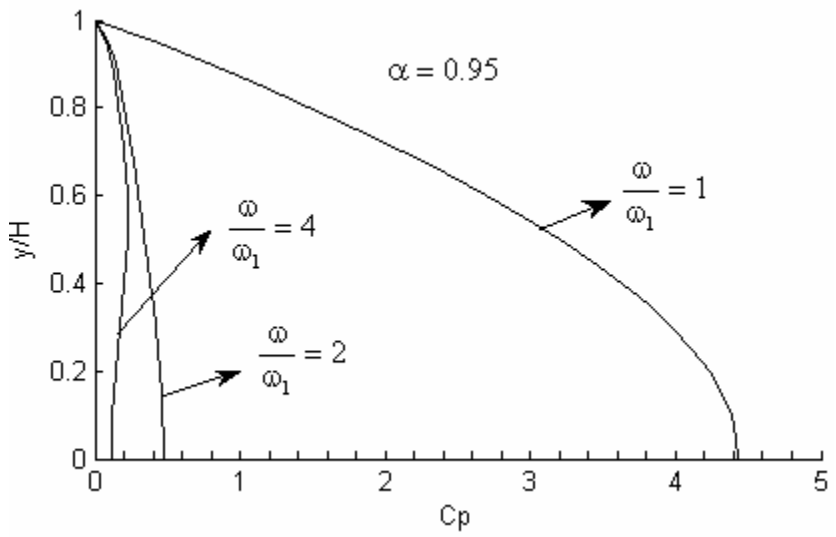

Fig.7.13a Hydrodynamic pressures on vertical dam face, $\alpha = 0.95$

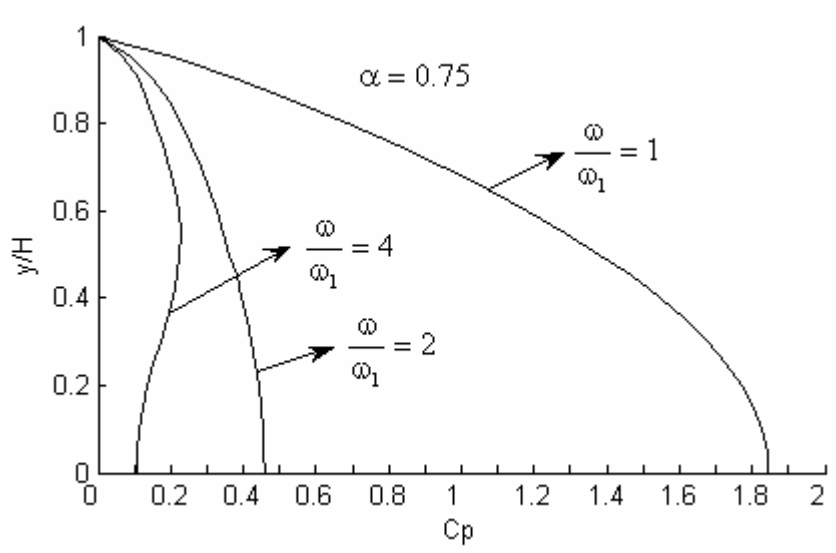

Fig.7.13b Hydrodynamic pressures on vertical dam face, $\alpha = 0.75$

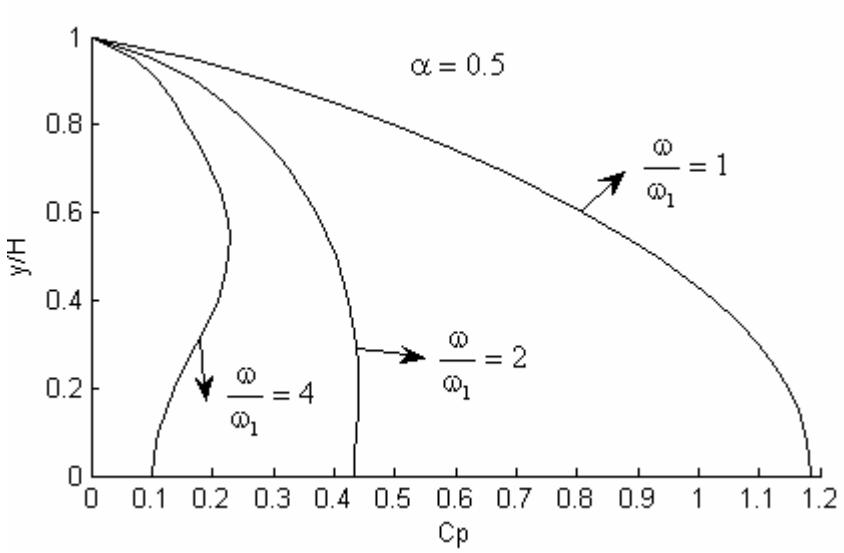

Fig.7.13c Hydrodynamic pressures on vertical dam face, $\alpha = 0.5$

For a sloping dam, two different angles were considered. The first was $\theta = 30^0$. The other was $\theta = 60^0$. The results were plotted in Figs.14a,b.

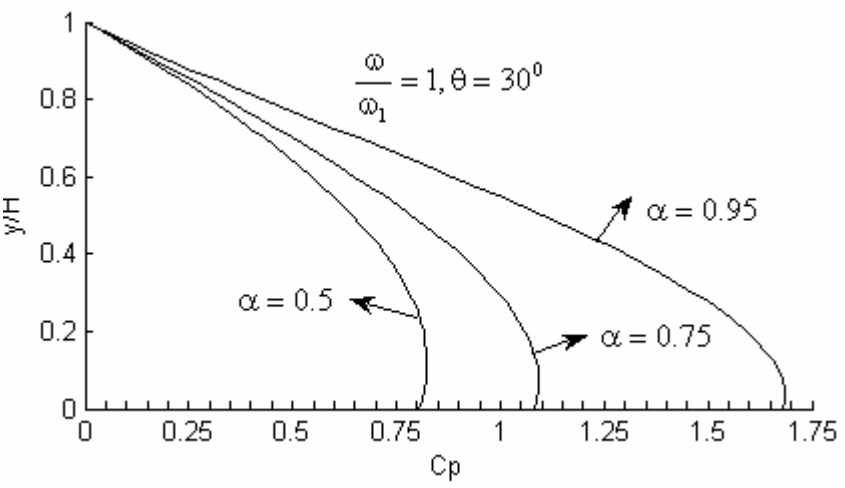

Fig.7.14a Hydrodynamic pressures on sloping dam face, $\frac{\omega}{\omega_1} = 1, \theta = 30^0$

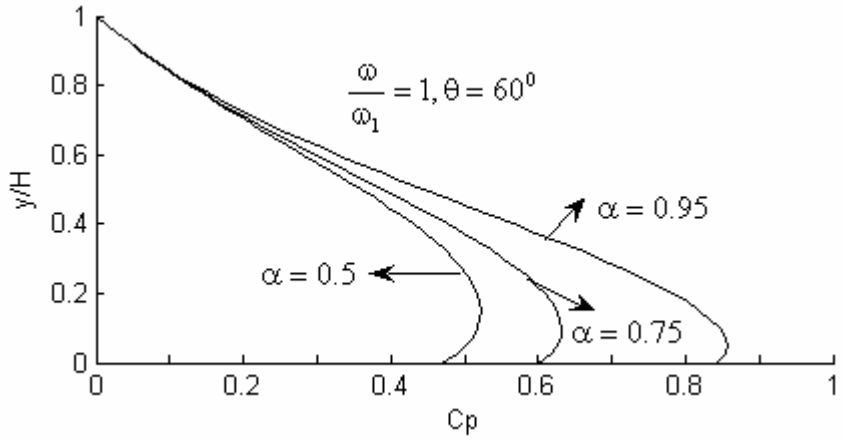

Fig.7.14b Hydrodynamic pressures on sloping dam face, $\frac{\omega}{\omega_1} = 1, \theta = 60^0$

The results for a dam have multi-slopes were plotted in Fig.7.15.

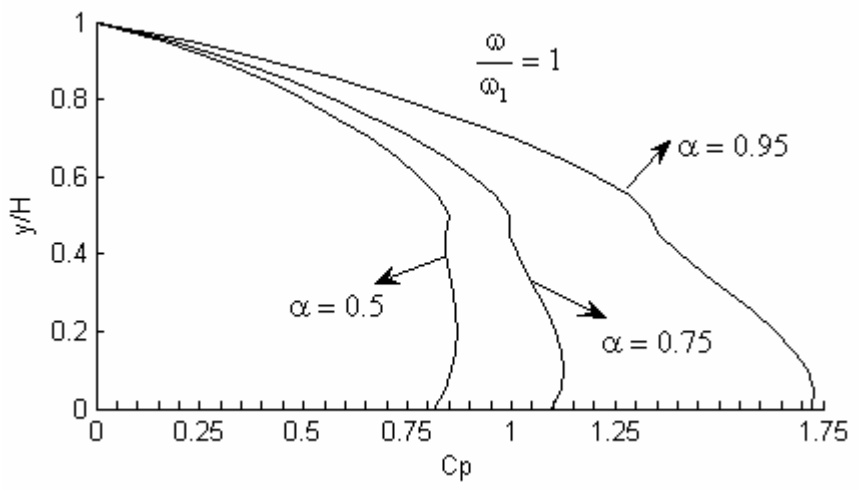

Fig.7.15 Hydrodynamic pressures on a dam face having multi-slopes, $\frac{\omega}{\omega_1}=1$

From Figs.7.13-15, it can be found that the reflection coefficient α affects the hydrodynamic pressure. The pressure increases when α increases. The same problems were considered by Sharan (1992). He used FEM to the near-field domain, while the far-field domain was modeled by using a radiation boundary. The boundary condition on the radiation boundary was expressed as an infinite series. Through comparing the above results with Sharan's results, it can be found that the above results are almost the same to those of Sharan. (Here Sharan's results were not plotted for clarity.) So Eqs.(7.23) and (7.24) are correct. As the all coefficient matrices $\mathbf{E}^0$, $\mathbf{E}^2$, $\mathbf{C}^0$ and $\mathbf{M}^0$ are easy to obtain, Eqs.(7.23) and (7.24) are efficient.

CHAPTER EIGHT

SBFEM/FEM COUPLING METHOD FOR TIME-DOMAIN ANALYSIS OF DAM-RESERVOIR INTERACTION PROBLEMS

In this chapter, the boundary finite element method (SBFEM) is extended to time-domain analyses of dam-reservoir interaction problems. Dams can be rigid or flexible, while the fluid medium in the reservoir is semi-infinite and compressible. The dam-reservoir interaction is analyzed by using a FEM/SBFEM coupling procedure when dams are subjected to horizontal ground motions. Two types of FEM-SBFEM coupling procedures are presented. In the first type, the dam is modeled by FEM, while the fluid medium in the reservoir is modeled by the SBFEM alone. In the second type, the dam is still modeled by FEM but the fluid medium is modeled by a combination of FEM and SBFEM. In the case of a vertical dam-reservoir system, the fluid medium can be modeled by the SBFEM alone. In the case of non-vertical dam-reservoir systems, the fluid medium is divided into a near-field FEM domain and a far-field SBFEM domain. Two benchmark examples are studied. The numerical results obtained by the present procedure are compared with those from analytical or other available numerical solutions. In this chapter, the accuracy and efficiency of the SBFEM formulation described in Chapter 3 for time-domain analyses are validated.

8.1 PROBLEM STATEMENT

A dam-reservoir system shown in Fig.7.1a is considered. In it, the dam can be rigid or flexible, while the fluid in the reservoir is inviscid isentropic with the fluid particles undergoing only small displacements. For dams having arbitrary geometries, analytical solution for the reservoir in time-domain analyses has not been reported in literature. To circumvent the difficulties, the fluid in the reservoir is divided into two parts: a near-field and a far-field domain as shown in Fig.7.1b. The interaction between the near-field domain and the far-field domain occurs at Interface 2, while the interaction between the dam and the liquid occurs at Interface 1. Of note, Interface 2 is assumed vertical and the reservoir bottom in the far-field domain is level and rigid. These assumptions are necessary in SBFEM formulation, because the SBFEM requires no energy to be radiated from the infinity towards the dam.

8.2 FEM-SBFEM MODELING

For the dynamic analysis of a dam-reservoir system subjected to a horizontal ground motion or an external force, both the dam and the near-field domain medium can be modeled by finite-element method, while the far-field domain medium can be represented by a boundary condition at the near-to-far-field interface (i.e. Interface 2).

8.2.1 MOTION EQUATION FOR A DAM

The motion equation for a dam subjected to both ground motions and external forces can be written in the standard finite element form as follows.

$$\mathbf{M}^{\mathrm{d}}\ddot{\mathbf{U}}+\mathbf{C}^{\mathrm{d}}\dot{\mathbf{U}}+\mathbf{K}^{\mathrm{d}}\mathbf{U}=-\mathbf{M}^{\mathrm{d}}\mathbf{R}\ddot{\mathbf{U}}_{\mathrm{g}}+\mathbf{F}_{\mathrm{e}}+\mathbf{F}_{\mathrm{f}} \tag{8.1}$$

where $\mathbf{M}^{\mathrm{d}}$, $\mathbf{C}^{\mathrm{d}}$ and $\mathbf{K}^{\mathrm{d}}$ denote the global mass, damping and stiffness matrices for the solid dam, respectively; $\ddot{\mathbf{U}}$, $\dot{\mathbf{U}}$ and $\mathbf{U}$ are the vectors of the nodal acceleration, velocity and displacement of dams, respectively; $\ddot{\mathbf{U}}_{\mathrm{g}}$, $\mathbf{F}_{\mathrm{e}}$ and $\mathbf{F}_{\mathrm{f}}$ are the ground acceleration vector, the external force vector and the hydrodynamic force vector, respectively; and $\mathbf{R}$ denotes the acceleration transformation matrix. In Eq.(8.1), all matrices and vectors except $\mathbf{U}$ and $\mathbf{F}_{\mathrm{f}}$ can be derived in the standard manner using the traditional finite element procedures. It leads to an expression such that the displacement $\mathbf{U}$ is a function of the hydrodynamic force $\mathbf{F}_{\mathrm{f}}$.

8.2.2 FEM FORMULATION FOR THE NEAR-FIELD FLUID DOMAIN MEDIUM

An efficient approach for the expression of the hydrodynamic force $\mathbf{F}_{\mathrm{f}}$ is to discretize the near-field fluid domain medium using FEM. Not including body force effects, the governing equation of the near-field domain medium is as follows:

$$\nabla^2\phi=\frac{1}{c^2}\ddot{\phi} \tag{8.2}$$

where ϕ and c denote the velocity potential of fluid particle and the sound speed in the fluid, respectively. The fluid pressure and the velocity potential ϕ have a relationship as follows:

$$p=-\rho\dot{\phi} \tag{8.3}$$

where ρ denotes the fluid density. The corresponding finite-element equation of Eq.(8.2) is given by

$$\mathbf{M}^{\mathrm{f}}\ddot{\Phi}+\mathbf{K}^{\mathrm{f}}\Phi=\mathbf{V}_{\mathrm{n}} \tag{8.4}$$

where the matrices $\mathbf{M}^{\mathrm{f}}$ and $\mathbf{K}^{\mathrm{f}}$ denote the global mass matrix and stiffness matrix of the near-field fluid domain, respectively; the vector $\mathbf{V}_{\mathrm{n}}$ denotes the integral vector of the normal velocity along the near-field fluid medium boundaries. Of note, $\mathbf{M}^{\mathrm{f}}$, $\mathbf{K}^{\mathrm{f}}$ and $\mathbf{V}_{\mathrm{n}}$ can be derived in the standard manner using the traditional fluid element procedures. Φ denotes the global column vector of nodal velocity potential ϕ. Its boundary conditions are described as in section 7.3. In the next section, a SBFEM boundary condition at Interface 2 is described.

8.2.3 SBFEM FORMULATION FOR THE FAR-FIELD FLUID DOMAIN MEDIUM

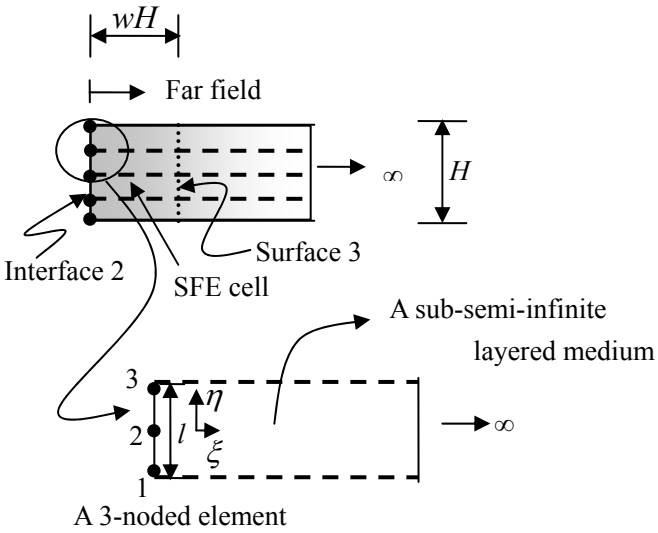

Fig.8.1 Typical SBFEM mesh for a far-field domain

When the SBFEM is employed to model a far-field domain medium, the far-field domain medium is regarded as a semi-infinite layered medium. The typical SBFEM mesh for the far-field domain is shown in Fig.8.1. Only Interface 2 is discretized while the free surface and the reservoir bottom are each represented by a node at Interface 2. Each element at Interface 2 actually represents a sub-semi-infinite layered medium. As such, the whole far-field domain is represented by an

assemblage of elements at Interface 2. The effect of the whole far-field domain can be obtained by incorporating the elements at Interface 2.

The SBFEM formulation for Interface 2 is expressed as follows:

$$\mathbf{V}_{n2}(t) = \int_0^t \mathbf{M}^{\infty}(t-\tau)\ddot{\Phi}_2(\tau)d\tau \tag{8.5}$$

where Φ_2 denotes the column vector of the nodal velocity potential ϕ at Interface 2; $\mathbf{M}^{\infty}(t)$ is called a "dynamic mass" matrix of the whole far-field domain; and

$$\mathbf{V}_{n2}(t) = \sum_e \int_{\Gamma_2^e} \mathbf{N}_f^T v_{n2} d\Gamma_2^e \tag{8.6}$$

in which v_{n2} denotes the normal velocity; Γ_2 denotes Interface 2; $\mathbf{N}_f$ is the shape function for a typical discretized fluid element; and $\sum_e$ denotes an assemblage of all fluid elements at Interface 2. Note that the "dynamic mass" matrix $\mathbf{M}^{\infty}(t)$ is independent of the response of the far-field domain. It depends only on the geometrical attributes at Interface 2 and can be obtained prior to solving Eq.(8.5). Therefore, if one of the two variable vectors $\mathbf{V}_{n2}(t)$ and $\Phi_2(t)$ is known, the other can then be determined. Chapter 3 presents the full details of the derivation of the "dynamic mass" matrix $\mathbf{M}^{\infty}(t)$ and the details are not duplicated here. In brief, the first step is to establish the finite-element governing equation of a scalar-finite-element (SFE) cell between Interface 2 and the Surface 3 and to derive the relationship between Interface 2 and the Surface 3 using the finite-element governing equation in Eq.(8.4); the second step is to take the SFE cell's characteristic width w as the analytical limit to zero, which yields a consistent infinitesimal finite-element cell (IFEC) equation in frequency domain; the last step is to apply the inverse Fourier transformation to the IFEC equation, so that it is converted to an equivalent IFEC equation in time domain. Subsequently, the

"dynamic mass" matrix $\mathbf{M}^{\infty}(t)$ can be obtained by solving the IFEC equation in time domain.

Upon discretization of Eq.(8.5) with respect to time and assuming all initial conditions equal to zero, one can get the following equation.

$$\mathbf{V}_{n2}^{n} = \mathbf{M}_{1}^{\infty}\dot{\Phi}_{2}^{n} + \sum_{j=1}^{n-1}\left(\mathbf{M}_{n-j+1}^{\infty} - \mathbf{M}_{n-j}^{\infty}\right)\dot{\Phi}_{2}^{j} \tag{8.7}$$

in which $\mathbf{M}_{n-j+1}^{\infty} = \mathbf{M}^{\infty}\left((n-j+1)\Delta t\right)$, $\Phi_{2}^{j} = \Phi_{2}(j\Delta t)$ and $\mathbf{V}_{n2}^{n} = \mathbf{V}_{n2}(n\Delta t)$ where Δt denotes an increment in time step. Of note, Eq.(8.5) or Eq.(8.7) describes the relationship between the normal velocity and the velocity potential at Interface 2. The relationship can be regarded as the boundary condition at Interface 2 for the near-field domain.

8.2.4 FEM-SBFEM COUPLING FORMULATION

For a dam-reservoir system, the force term $\mathbf{F}_{f}$ on the right hand side of Eq.(8.1) is the force derived from the reservoir. It can be expressed as

$$\mathbf{F}_{f} = \sum_{e}\int_{\Gamma_1^e}\mathbf{N}^{T}\mathbf{N}_{f}\mathbf{p}_{1}d\Gamma_{1}^{e} \tag{8.8}$$

where $\mathbf{N}$ and $\mathbf{N}_{f}$ denote the shape functions of a typical solid element for a dam and of a typical element for the near-field fluid medium, respectively; Γ_1 denotes Interface 1; the pressure $\mathbf{p}_1$ is a nodal pressure column vector, which is obtained from the near-field fluid domain. Note that $\mathbf{N}$ is not the same as $\mathbf{N}_{f}$.

Partitioning Eq.(8.4) into sub-matrices corresponding to variables at Interface 1, Interface 2 and other interior locations leads to

$$\begin{bmatrix} \mathbf{m}_{11}^{f} & \mathbf{m}_{12}^{f} & \mathbf{m}_{13}^{f} \\ \mathbf{m}_{21}^{f} & \mathbf{m}_{22}^{f} & \mathbf{m}_{23}^{f} \\ \mathbf{m}_{31}^{f} & \mathbf{m}_{32}^{f} & \mathbf{m}_{33}^{f} \end{bmatrix} \begin{Bmatrix} \ddot{\Phi}_1 \\ \ddot{\Phi}_2 \\ \ddot{\Phi}_3 \end{Bmatrix} + \begin{bmatrix} \mathbf{k}_{11}^{f} & \mathbf{k}_{12}^{f} & \mathbf{k}_{13}^{f} \\ \mathbf{k}_{21}^{f} & \mathbf{k}_{22}^{f} & \mathbf{k}_{23}^{f} \\ \mathbf{k}_{31}^{f} & \mathbf{k}_{32}^{f} & \mathbf{k}_{33}^{f} \end{bmatrix} \begin{Bmatrix} \Phi_1 \\ \Phi_2 \\ \Phi_3 \end{Bmatrix} = \begin{Bmatrix} \mathbf{V}_{n1} \\ \mathbf{V}'_{n2} \\ \mathbf{V}_{n3} \end{Bmatrix} \tag{8.9}$$

where the subscripts 1 and 2 refer to nodal variables at Interfaces 1 and 2, respectively; while the subscript 3 refers to other interior nodal variables in the near-field fluid domain. At Interface 2, the near-field FEM-domain couples with the far-field SBFEM-domain. To satisfy the kinematic continuity at Interface 2, Eq.(8.7) is re-written as:

$$-\mathbf{V}'^{n}_{n2} = \mathbf{V}^{n}_{n2} = \mathbf{M}_1^{\infty}\dot{\Phi}_2^{n} + \sum_{j=1}^{n-1}\left(\mathbf{M}^{\infty}_{n-j+1} - \mathbf{M}^{\infty}_{n-j}\right)\dot{\Phi}_2^{j} \tag{8.10}$$

Substituting Eq.(8.10) into Eq.(8.9) and re-arranging leads to

$$\begin{bmatrix} \mathbf{m}_{11}^{f} & \mathbf{m}_{12}^{f} & \mathbf{m}_{13}^{f} \\ \mathbf{m}_{21}^{f} & \mathbf{m}_{22}^{f} & \mathbf{m}_{23}^{f} \\ \mathbf{m}_{31}^{f} & \mathbf{m}_{32}^{f} & \mathbf{m}_{33}^{f} \end{bmatrix} \begin{Bmatrix} \ddot{\Phi}_1^{n} \\ \ddot{\Phi}_2^{n} \\ \ddot{\Phi}_3^{n} \end{Bmatrix} + \begin{bmatrix} \mathbf{0} & \mathbf{0} & \mathbf{0} \\ \mathbf{0} & \mathbf{M}_1^{\infty} & \mathbf{0} \\ \mathbf{0} & \mathbf{0} & \mathbf{0} \end{bmatrix} \begin{Bmatrix} \dot{\Phi}_1^{n} \\ \dot{\Phi}_2^{n} \\ \dot{\Phi}_3^{n} \end{Bmatrix}$$
$$+ \begin{bmatrix} \mathbf{k}_{11}^{f} & \mathbf{k}_{12}^{f} & \mathbf{k}_{13}^{f} \\ \mathbf{k}_{21}^{f} & \mathbf{k}_{22}^{f} & \mathbf{k}_{23}^{f} \\ \mathbf{k}_{31}^{f} & \mathbf{k}_{32}^{f} & \mathbf{k}_{33}^{f} \end{bmatrix} \begin{Bmatrix} \Phi_1^{n} \\ \Phi_2^{n} \\ \Phi_3^{n} \end{Bmatrix} = \begin{Bmatrix} \mathbf{V}_{n1}^{n} \\ -\sum_{j=1}^{n-1}\left(\mathbf{M}^{\infty}_{n-j+1} - \mathbf{M}^{\infty}_{n-j}\right)\dot{\Phi}_2^{j} \\ \mathbf{V}_{n3}^{n} \end{Bmatrix} \tag{8.11}$$

where the superscript n denotes the instant at time $t = n\Delta t$. Note that a damping matrix appears on the left hand side of Eq.(8.11). It can be regarded as the damping effect derived from the far-field medium and imposed on the dam-reservoir system. Upon determining the velocity potential Φ through Eq.(8.11), the fluid pressure $\mathbf{p}_1$ can be evaluated by using Eq.(8.3) as follows.

$$\mathbf{p}_1 = -\rho\dot{\Phi}_1 \tag{8.12}$$

Note that $\mathbf{p}_1$ depends on the normal velocity v_{n1} at Interface 1, while the solution of Eq.(8.1) including v_{n1} also depends on $\mathbf{p}_1$. Therefore, Eq.(8.1) and Eq.(8.11) form a coupling system. Following the numerical procedure with a Newmark scheme, one can solve the coupling system by assuming

$$\mathbf{p}_1(t) = f\left(v_{n1}^{t}\right) \approx f\left(v_{n1}^{t-\Delta t}\right) \tag{8.13}$$

where f denotes a function. If the time increment Δt is small, accurate results can be obtained. However, if Δt is relatively large, an iteration scheme should be used in each time step, i.e., a term ${}^{t}v_{n1}^{j-1}$ is used instead of $v_{n1}^{t-\Delta t}$ in the global iteration scheme, where j denotes the j^{th} iteration within a time step.

8.3 NUMERICAL EXAMPLES

Two numerical examples are studied to validate the FEM-SBFEM coupling procedure.

8.3.1 DYNAMIC RESPONSE OF A VERTICAL DAM-RESERVOIR SYSTEM

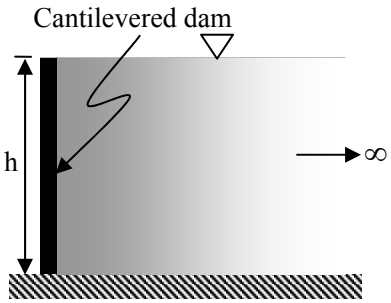

Fig.8.2 A vertical dam

Fig.8.2 shows a vertical dam-reservoir system having a rigid reservoir bottom. The dynamic response of the system subjected to a horizontal ground motion is studied. The aim is to verify the efficiency and accuracy of the FEM-SBFEM coupling formulation for a vertical dam-reservoir system. In the case of a vertical dam, no reflecting waves from the free surface or the rigid reservoir bottom are radiated back to the dam, so that a near-field fluid domain is not necessary and the whole reservoir can be modeled by a far-field domain alone. The dynamic response of this system is solved through coupling Eqs.(8.1) and (8.7). Sound speed in the fluid is

taken as 1438.656m/s and the fluid density ρ is 1000kg/m^3. The weight per unit length of the cantilevered dam is 36000kg/m. The height of the cantilevered dam h is equal to 180m. The dam is modeled by 20 numbers of simple 2-node beam elements with rigidity EI (=9.8437x10^{13} Nm^2), while the whole fluid domain is modeled by 10 numbers of SBFEM 3-node elements, whose nodes match side by side with the nodes of the solid dam. Time step increment is 0.005 sec. Two types of horizontal ground motions are considered. The first is a ramp acceleration, while the other is the *El Centro* earthquake acceleration, as shown in Figs.8.3a and 8.3b. Results for the pressure at the heel of dam for case 1 (ramp-acceleration) are obtained by using a "no-iteration" scheme using in Eq.(8.13) and also by using an iteration scheme. Both results are plotted in Fig.8.4. From Fig.8.4, it can be seen that the results obtained from no-iteration scheme yield noises at late time; whereas the results obtained by both schemes are the same at early time. As such, the iteration scheme is adopted in the following studies. The pressures at the heel of a flexible or rigid dam are plotted in Fig.8.5. Not surprisingly, Fig.8.5 shows that the pressure on a flexible dam is greater than that on a rigid dam. Of note, results for the rigid dam are solved by the SBFEM in Eq.(8.7) only. The displacement at the top of a flexible dam with a full reservoir is plotted in Fig.8.6. The same problem was previously studied by Lee and Tsai (1991) and they offered an analytical solution. Their corresponding analytical solutions are also plotted in Figs.8.5 and 8.6 for comparison. From Figs.8.5 and 8.6, it can be seen that both the FEM-SBFEM and SBFEM-alone solutions are very close to the analytical solutions, especially at early time. The dynamic responses of the dam with a full reservoir subjected to the *El Centro* horizontal ground acceleration are plotted in Figs.8.7 and 8.8. The corresponding analytical solutions (Lee and Tsai 1991) are also plotted in Figs.8.7 and 8.8. From Figs.8.7 and 8.8, it can be seen that the FEM-SBFEM solutions are very close to analytical solutions. In addition, Figs. 8.6 and 8.7 show that the fluid effect dominates.

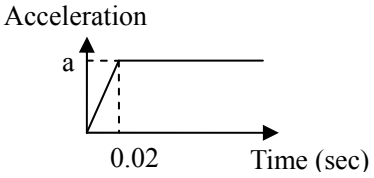

Fig.8.3a Ramp acceleration

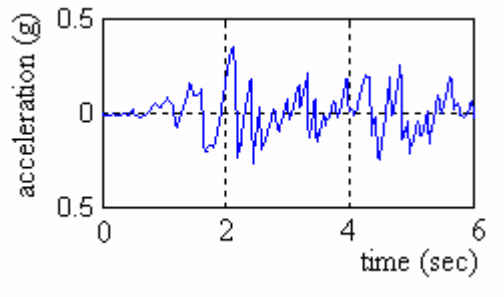

Fig.8.3b El Centro N-S ground excitation

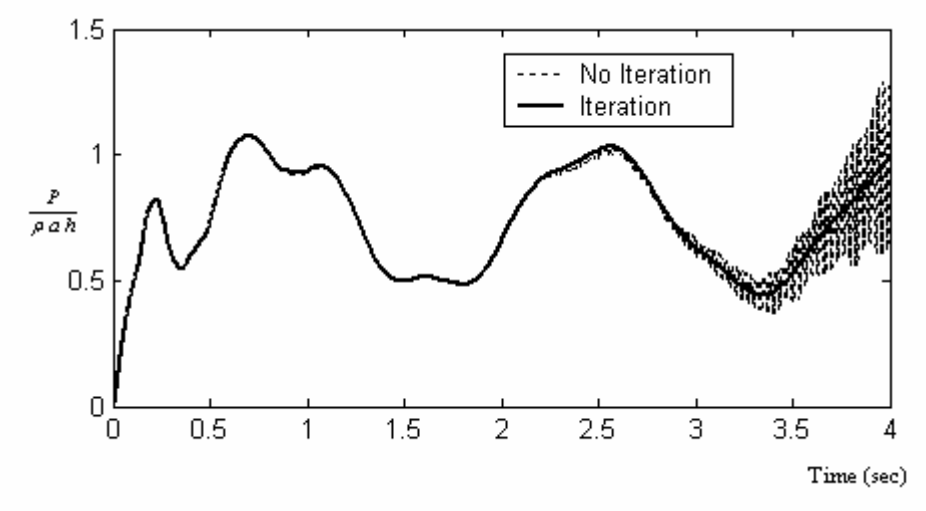

Fig.8.4 Pressures at the heel of a flexible dam subjected to ramp acceleration

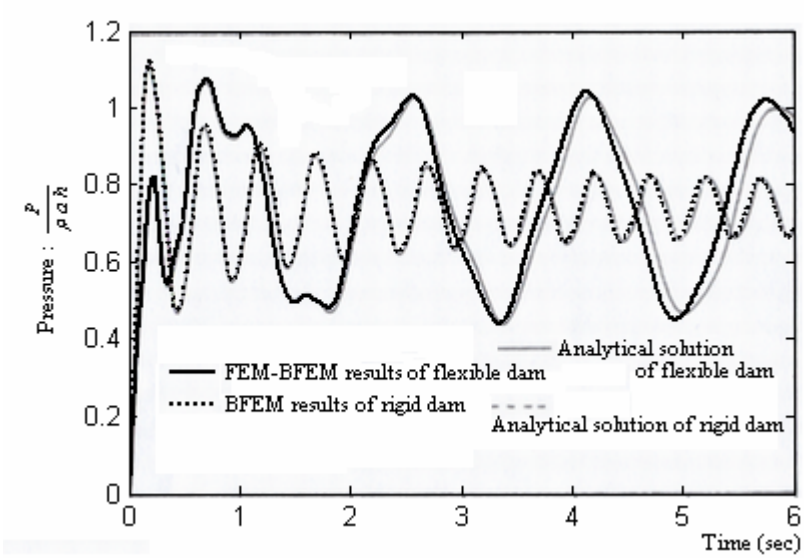

Fig.8.5 Pressure at the heel of a flexible or rigid dam subjected to ramp acceleration

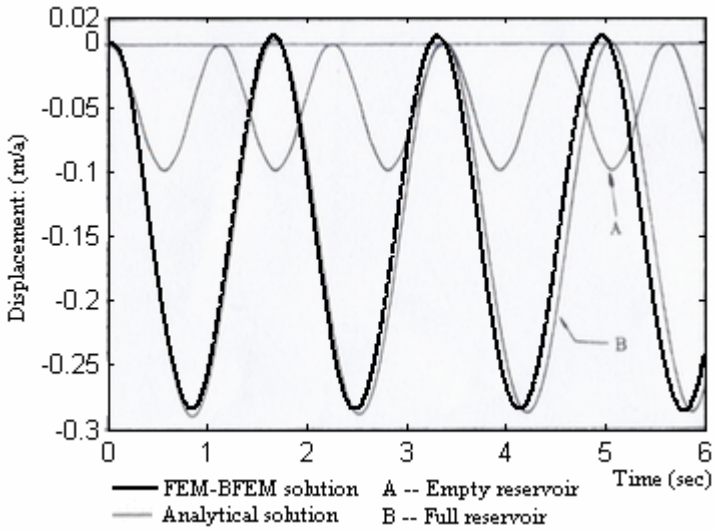

Fig.8.6 Displacement at the top of a flexible dam subjected to ramp acceleration

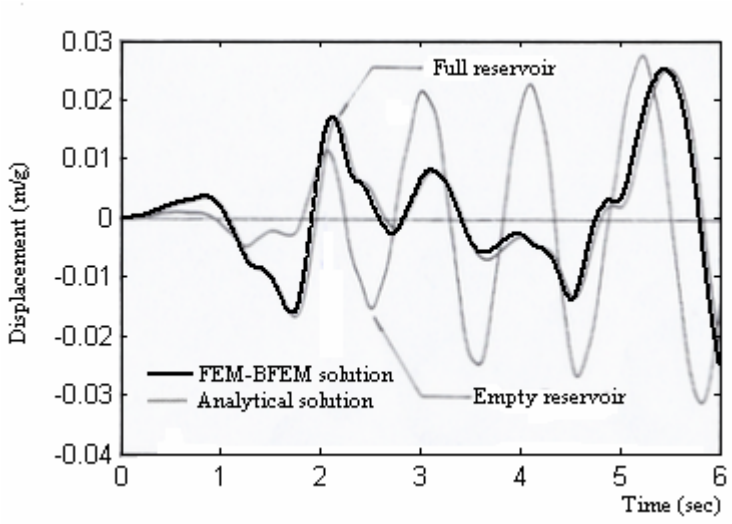

Fig.8.7 Displacement at the top of a flexible dam subjected to El Centro N-S earthquake acceleration

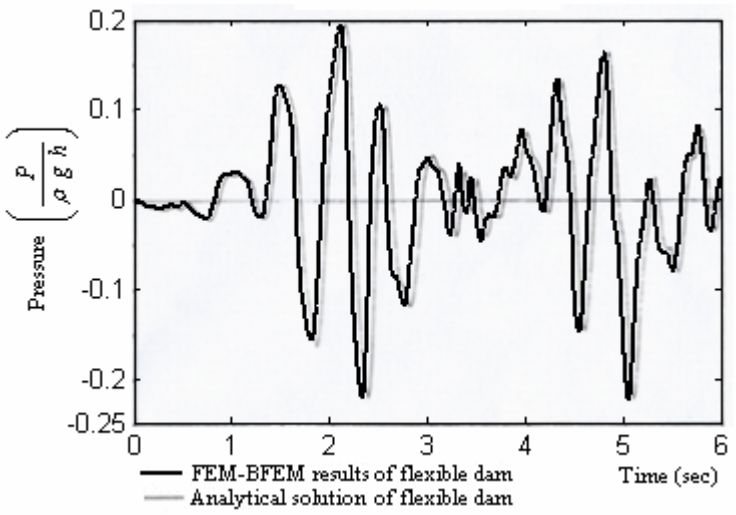

Fig.8.8 Pressure at the heel of a flexible dam with full reservoir subjected to El Centro earthquake acceleration

8.3.2 DYNAMIC RESPONSE OF A GRAVITY DAM

This example is to verify the accuracy and efficiency of the FEM-SBFEM coupling formulation for a gravity-dam-reservoir system having arbitrary slopes at the dam-reservoir interface. A typical gravity-dam-reservoir system is shown in Fig.8.9. The density, Poisson's ratio and Young's modulus of the dam are 2400 kg/m^3, 0.2 and 2.5x10^{10} N/m^2, respectively. The fluid density ρ is 1000 kg/m^3, and wave speed in the fluid is 1438.656m/s. The height of the dam H is 120m. The gravity-dam-reservoir system is subjected to the same ground acceleration as shown in Figs.8.3a and 8.3b. The FEM and SBFEM meshes are shown in Fig.8.10. Both the solid dam and the near-field fluid are modeled by using FEM while the far-field fluid is modeled by using the SBFEM. The distance between the heel of the dam and the near-far-field interface is 6 m (=0.05H). For the FEM mesh, 8-node plane-strain elements are used, while 3-node SBFEM elements are used to match the 8-node elements node-by-node along the interface. In the FEM zone, 40

numbers and 20 numbers of 8-node elements are used to model the dam and the near-field fluid domain, respectively; whereas in the SBFEM zone, 10 numbers of 3-node SBFEM elements are employed to model the whole far-field fluid domain. Note that the size of the near-field fluid domain can be small compared to those used in other methods.

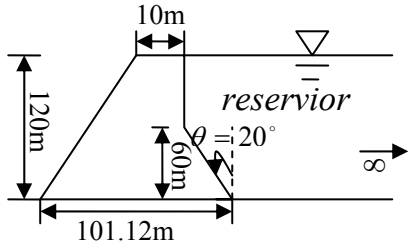

Fig.8.9 Geometry of a typical gravity dam

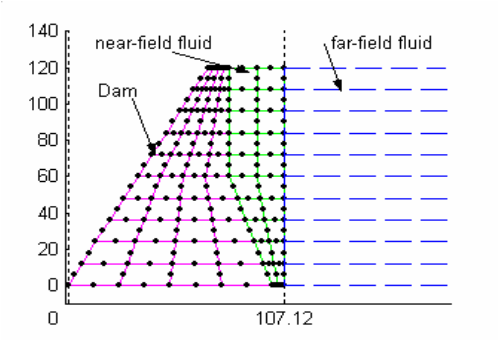

Fig.8.10 FEM and SBFEM meshes for the gravity dam-reservoir system

The displacement and pressure caused by the ramp acceleration are plotted in Figs.8.11 and 8.12. The time increment is 0.003sec. The results obtained by sub-structures method (Tsai and Lee 1991) are also plotted in Figs.8.11 and 8.12, respectively, for comparison. From Fig.8.11, it can be observed that the amplitudes of displacement at the top of dam agree well in general but differ slightly and systematically, especially at late time. From Fig.8.12, similar trends are observed for the pressure distributions. The displacement and pressure caused by the *El Centro* ground motion are plotted in Figs.8.13 and 8.14, respectively. The time increment is 0.002sec. Results obtained by the sub-structures method (Tsai and Lee

1991) are also plotted in Figs.8.13 and 8.14. From Figs.8.13 and 8.14, it can be seen that both the displacements and the pressures obtained by the present method agrees well with Tsai and Lee's results, especially at early time. Fig.8.15 shows the results for displacement at the top of a dam (either full or empty reservoir). From Fig.8.15, one can see that the damping effect of the full reservoir dominates. Fig.8.16 shows the results for pressure on a flexible or rigid dam with a full reservoir. From Fig.8.16, one can see that the resulting pressure on a flexible dam is much greater than that on a rigid dam at late time.

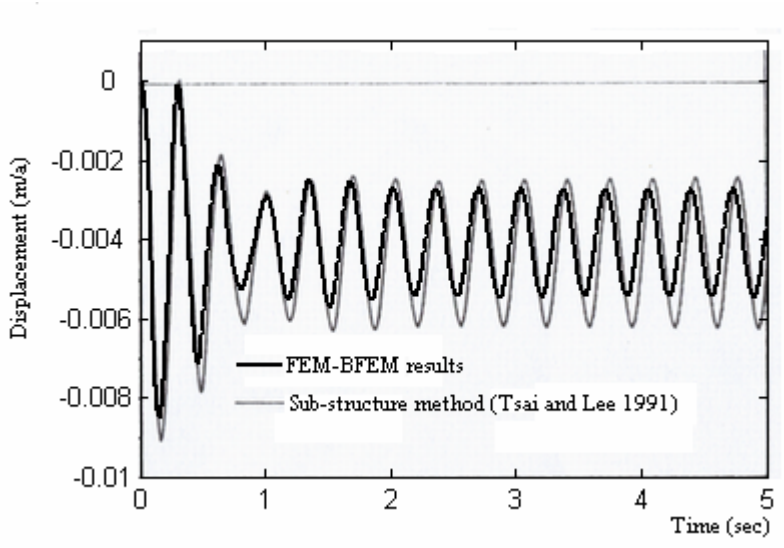

Fig.8.11 Displacement at the top of gravity dam subjected to ramp acceleration

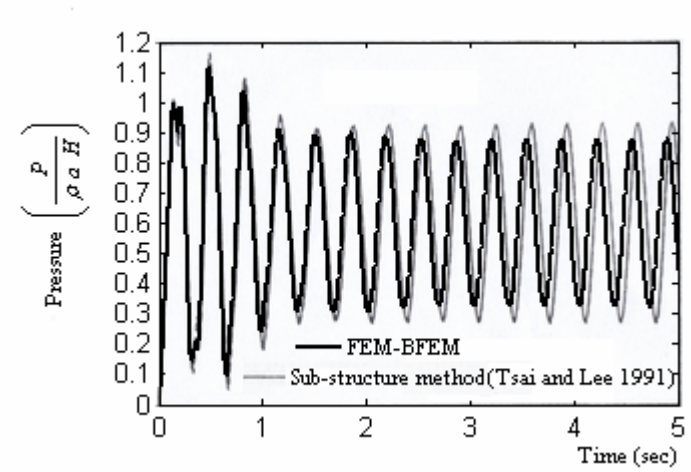

Fig.8.12 Pressure at the heel of gravity dam subjected to ramp acceleration

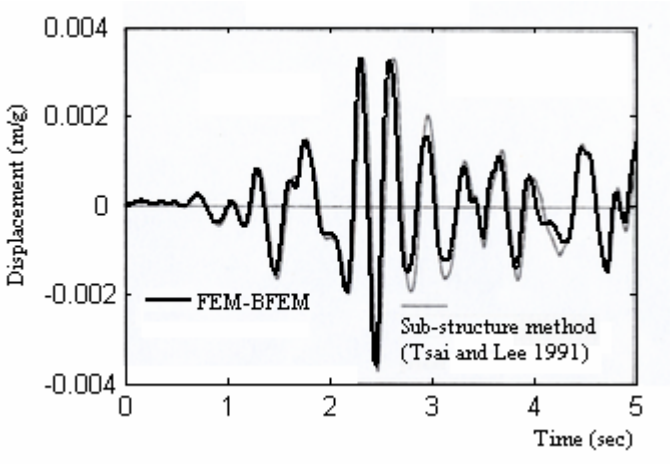

Fig.8.13 Displacement at the top of gravity dam subjected to El Centro ground excitation

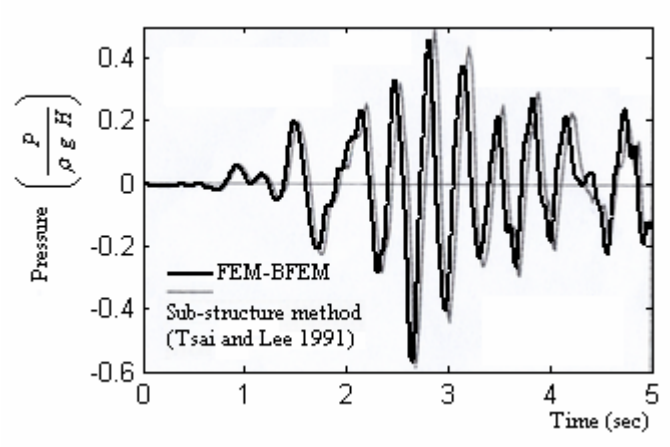

Fig.8.14 Pressure at the heel of gravity dam subjected to El Centro ground excitation

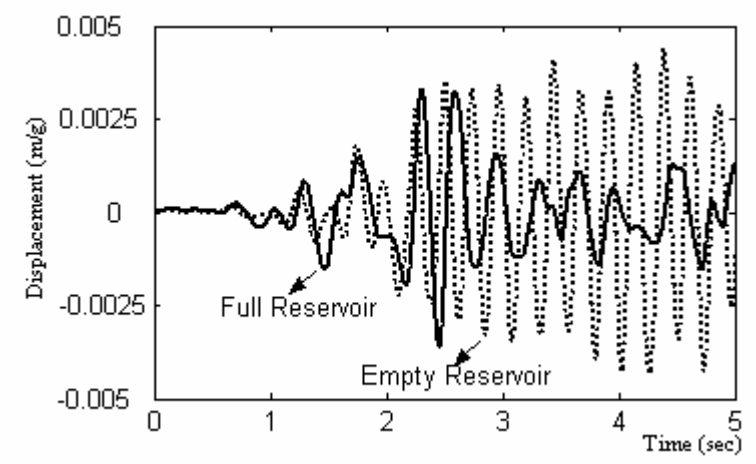

Fig.8.15 Displacement at the top of flexible gravity dam subjected to El Centro earthquake acceleration

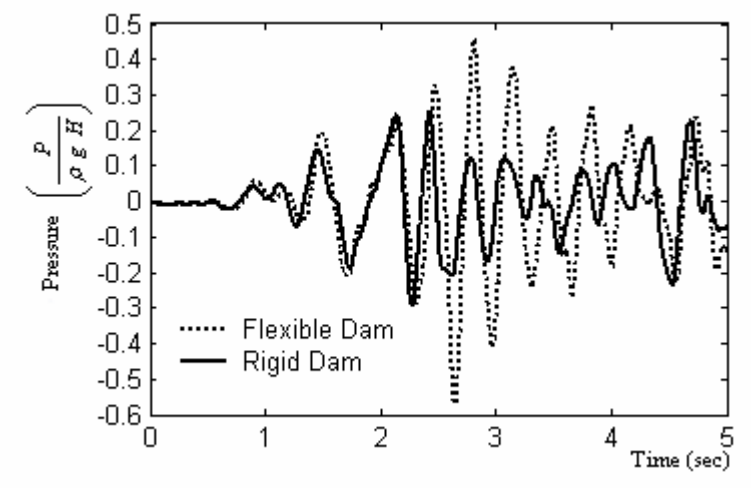

Fig.8.16 Pressure at the heel of a flexible or rigid gravity dam with full reservoir subjected to El Centro earthquake acceleration

8.3.3 DYNAMIC ANALYSIS OF 2-DIMENSIONAL ARCH DAMS

The objective of this study is to gain an insight into the effect of the geometry of a dam on the dynamic response of a dam-reservoir system. Four arch geometries are considered and are shown in Fig.8.17. Amongst the 4 arch dams, Dam 'A' has the greatest curvature away from the reservoir. With gradual reducing curvature from Dam 'A', to Dam 'B' and then Dam 'C', the Dam 'D' has zero curvature and stands upright against the reservoir. The heights of all dams are set at 180m, while the widths at bottom and the top are set at 30m and 6m, respectively. The material parameters for the dam and the fluid are kept to the same as those described in section 8.3.2. The fluid medium is on the right hand side of the dam. The curve on either side of the dam assumes different partial circular arc. Each arc is defined by 3 points on the curve. The coordinates of points for the four dams are listed in Table 8.1. Note that the two curves for the Dam 'D' actually are straight lines. In the analysis, both the dam and the near-field fluid are modeled by using FEM, while the far-field fluid is modeled by using the SBFEM. Their corresponding meshes are similar to those depicted in Fig.8.10. The dynamic responses of the four dams when

subjected to a horizontal ramp ground acceleration (see Fig.8.3a) are shown in Figs.8.18 and 8.19. The displacements shown in Fig.8.18 are normalized by the ramp ground acceleration "*a*", while the pressures shown in Fig.8.19 are normalized by the quantity ρaH with H=180m. From Figs.8.18, one can see that the undulation profiles of displacements at the top and mid-height of the dam are similar to each other. From Fig.8.19, the same responses for pressure are observed. With regard to the amplitudes of the undulations, Dams 'B' and 'C' always exhibit moderate values between the two extreme cases in Dams 'A' and 'D'. Of note, Dam 'A' experiences the lowest fluid pressure, but the largest displacement. On the other hand, Dam 'D' experiences the highest fluid pressure, but the smallest displacement. All these observations are to be expected. The more flexible Dam 'A' allows more deflection and hence provides more relief to the fluid pressure.

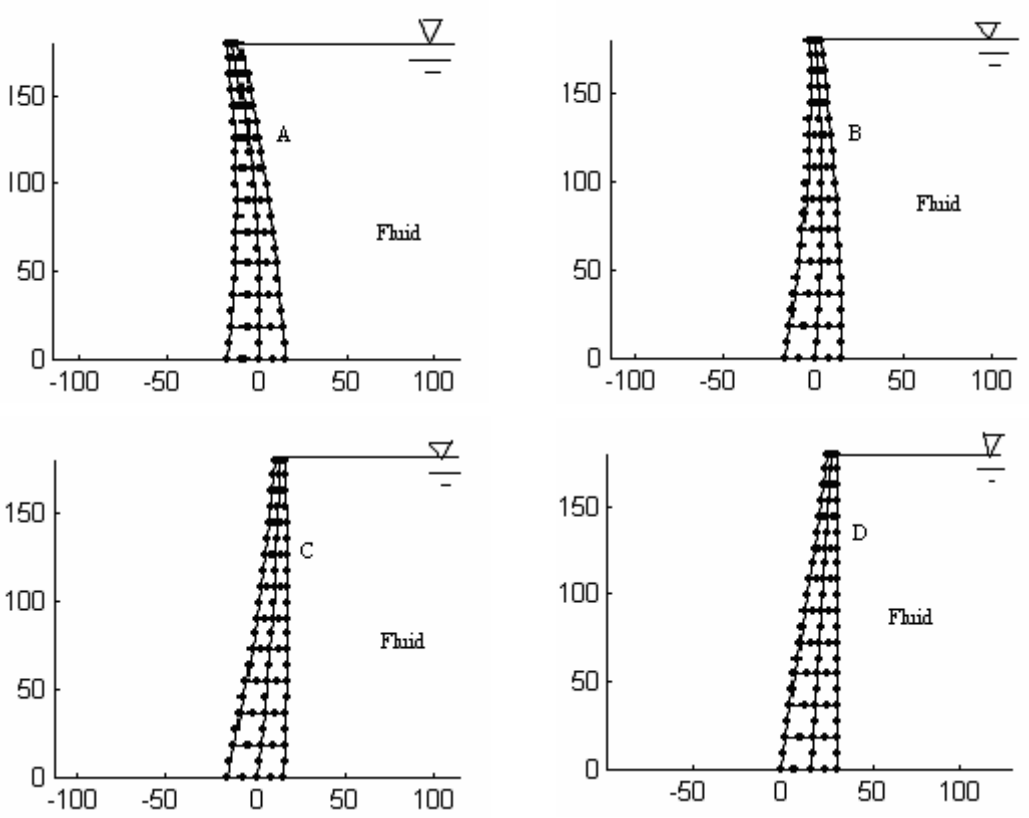

Fig.8.17 Geometries of arch dams and theirs FEM meshes

Table 8.1 Geometrical configuration (x,y) of arch dams

Dam type		Point 1	Point 2	Point 3
Dam 'A'	Left side	(-15, 0)	(-10, 90)	(-15.59, 180)
	Right side	(15, 0)	(5, 90)	(-9.59, 180)
Dam 'B'	Left side	(-15, 0)	(-5, 90)	(-3, 180)
	Right side	(15, 0)	(12, 90)	(3, 180)
Dam 'C'	Left side	(-15, 0)	(0, 90)	(9.59, 180)
	Right side	(15, 0)	(17, 90)	(15.59, 180)
Dam 'D'	Left side	(0, 0)	(12, 90)	(24, 180)
	Right side	(30, 0)	(30, 90)	(30, 180)

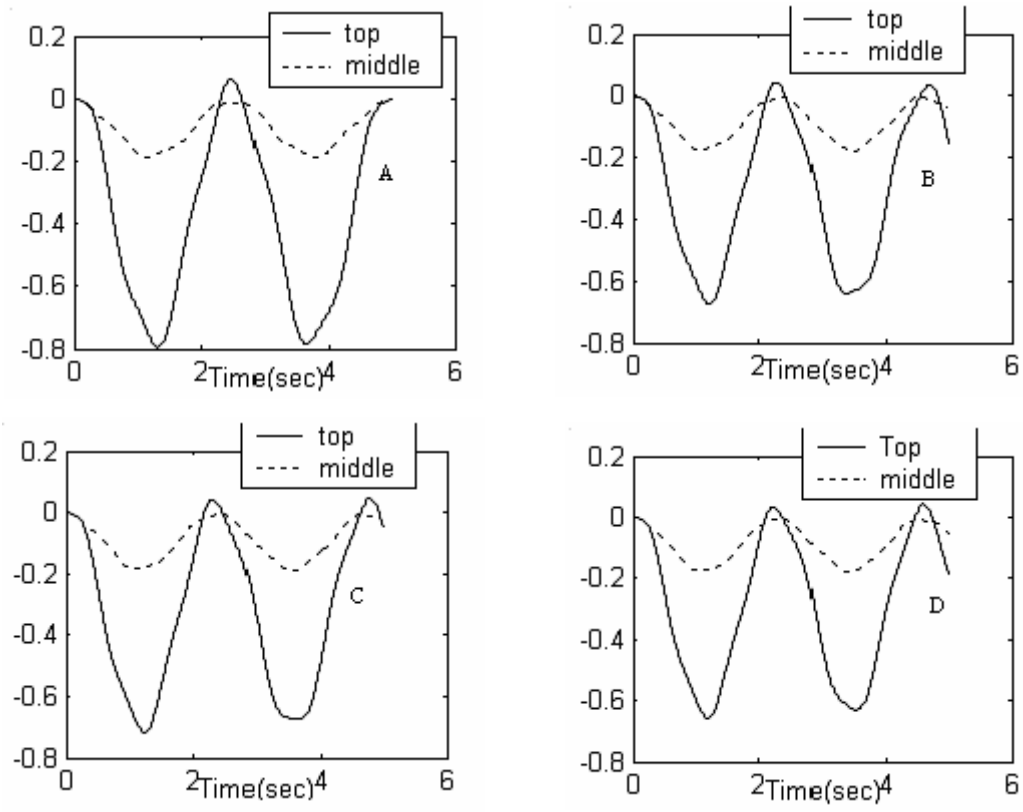

Fig.8.18 Displacements at mid-height and the top of the arch dam at the dam-fluid interface

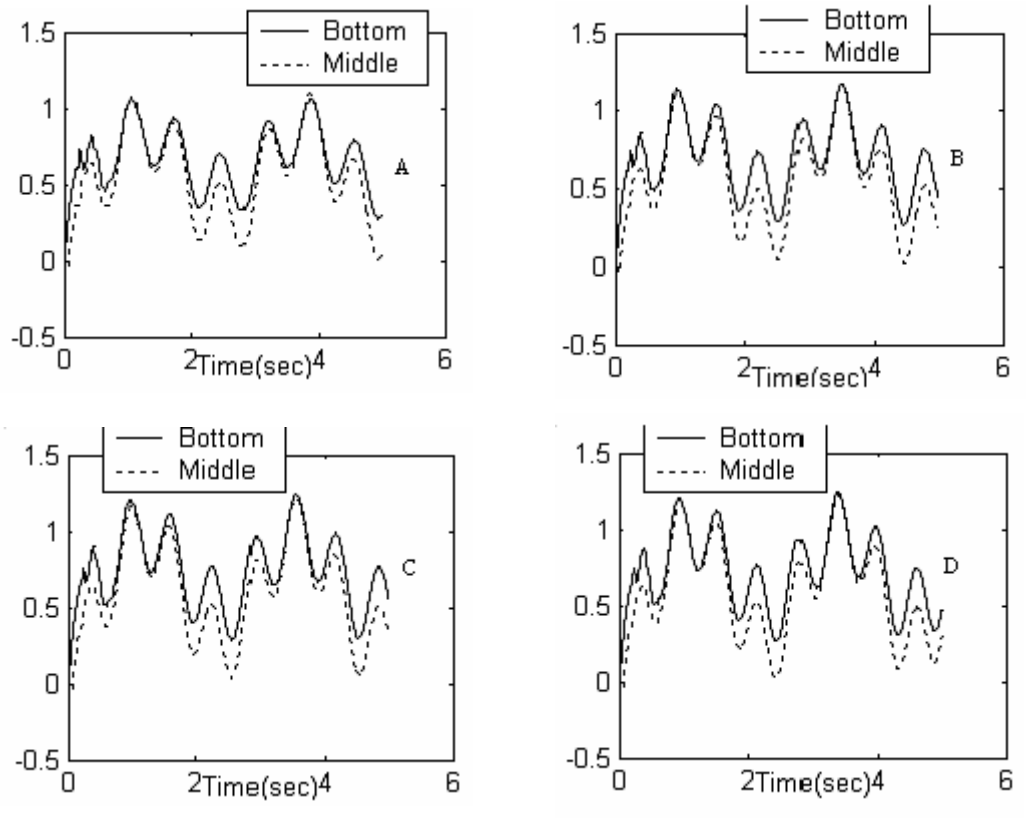

Fig.8.19 Pressures at mid-height and bottom of the arch dam at the dam-fluid interface

CHAPTER NINE

CONCLUSIONS AND RECOMMENDATIONS

9.1 CONCLUSIONS

This thesis presented the Scaled Boundary Finite Element Method (SBFEM) formulation for modeling unbounded and bounded fluid medium. For the bounded fluid medium, the solutions of SBFEM were found to be sensitive to the dissipation coefficient when the numerical Newmark time-integration scheme was used. For the unbounded fluid medium, FEM-SBFEM coupling procedures were developed for solving problems of acoustic fluid-structure interaction (FSI), such as submerged structures subjected to shock waves, and dam-reservoir interaction system subjected to horizontal ground acceleration motions. In the course of tackling the problems of submerged structures subjected to shock waves, the author developed the velocity-to-pressure relationship for scattered waves based on the SBFEM formulation. In the course of tackling the dam-reservoir interaction problems, the author discovered a zero matrix which leads to the development of an efficient SBFEM formulation in the frequency-domain. In the time-domain analyses, an efficient FEM-SBFEM procedure was presented for dam-reservoir interaction systems. All these developments enhanced the successful extensions of the SBFEM for FSI problems. These developments were also verified by checking against benchmark solutions which are either analytical or/and available numerical solutions. The results show that the present formulations are able to yield accurate solutions, and typically lead to more accurate solutions than other prevailing numerical results (such as BEM, FEM solutions). In addition, the SBFEM had been extended to solve problems related to infinite beams on visco-elastic-typed fluid foundations. A modified SBFEM formulation was developed and validated by checking against benchmark results. The development also provided an insight into the SBFEM formulations. Using a same concept in the development derived a new SBFEM formulation for a dam-reservoir system with an absorptive reservoir's

bottom. The new SBFEM formulation was verified by studying a benchmark example. In conclusion, the present extended SBFEM formulation has been shown to be useful and efficient in solving unbounded fluid-structure interaction problems. The methodology is able to model accurately the unbounded fluid medium.

To have a clear understanding about the SBFEM's application range, here a summary is given below.

(i) For submerged structures subjected to external loading cases where the acoustic fluid medium surrounding submerged structures is infinite and does not include free surface and seabed, the proposed SBFEM coupling acoustic approximations can generate excellent results and are more efficient that BEM, PWA, DAA and Infinite-element method. It is because the SBFEM is a semi-analytical solution. Structural geometries can be arbitrary. In a linear analysis, the surrounding infinite fluid medium can be modeled by the SBFEM only, while in a non-linear analysis, the domain having non-linear behavior can be modeled by FEM and then the remaining fluid domain can be modeled by the SBFEM.

(ii) For dam-reservoir interaction systems where dams are bounded and the reservoirs are infinite and horizontal, the reservoir's boundary includes the free surface, dam-reservoir interface and the reservoir bed. Such that, it satisfies the SBFEM requirements that the boundary conditions should be zero along the free surface and reservoir bed in the far field of the reservoir. However, in the special case of an absorptive reservoir bed, the proposed SBFEM can be applied too. Of note, the proposed SBFEM can only be applied to the dam-reservoir system which is subjected to horizontal loadings. When using the proposed SBFEM to solve the dam-reservoir interaction problems, the domain of the near field of reservoir can be very small. Furthermore in frequency-domain analysis, the SBFEM formulation for the far field of reservoir has a very simple form, which is easy to solve.

9.2 RECOMMENDATIONS FOR FUTURE WORKS

The SBFEM can be further extended for solving other fluid-structure interaction problems. The following aspects are recommended.

(i) 3-Dimensional problems. In this thesis, the studies were limited to 2-dimensional problems. The present extended SBFEM formulations are also suitable for 3-dimensional problems. In this regard, further developments for 3-dimensional problems are recommended.

(ii) FSI problems involving reflective waves. This category of problems includes floating structures and structures submerged in shallow fluid domain or near a seabed subjected to shock waves. In those problems, the free surface or the seabed produces reflective waves when the shock waves or the scattered waves reach there. When it occurs, the reflective waves will then travel back into the fluid medium and thus influence the structural responses. However, the reflected waves are difficult to be formulated and the present SBFEM is unable to handle it accurately. In this regard, a further development is required.

(iii) Cavitation problems. The present SBFEM formulation does not have the facility to cater for cavitaion in the fluid medium. In reality, cavitation does occur in the fluid medium. Where contains it is significant, the problems need to be addressed, and a new SBFEM formulation needs to be developed accordingly.

(iv) Non-linear problems. When high-energy shock waves are involved, high pressure is generated and may lead to large deflections on the structures. In such cases, the structure may behave in a non-linear manner, or collapse. To address this category of problems, development of a non-linear FEM-SBFEM procedure is recommended.

(v) Convolution integral problems. The kernel of the present SBFEM formulation in the time-domain is a convolution integral. The solution of the convolution integral requires a large storage volume to store all previous relative quantities before the current time step. It affects the SBFEM efficiency and may be heavy on the resources. In this regard, it is recommended to develop an efficient method to handle the convolution integral and reduce the required storage volume.

REFERENCES

Achenbach, J.D. (1973), Wave Propagation in Elastic Solids, North-Holland, London

Achenbach, J.D. and Sun, C.T. (1965), "Moving load on a flexibly supported Timoshenko beam", International Journal of Solids and Structures, Vol. 1, pp. 353-370.

Atkatsh, R.S., Bieniek, M.P. and Baron, M.L. (1983), "Dynamic elasto-plastic response of shells in an acoustic medium-EPSA code", International Journal for Numerical Methods in Engineering, Vol. 19, pp. 811-824.

Bathe, K.J. (1996), Finite Element Procedures, Prentice Hall, Upper Saddle River, New Jersey.

Bathe, K.J. and Hahn, W.F. (1979), "On transient analysis of fluid-structure systems", Computers and Structures, Vol. 10, pp. 383-391.

Bathe, K. J., Nitikitpaiboon, C. and Wang, X. (1995), "A mixed displacement-based finite element formulation for acoustic fluid-structure interaction", Computers and Structures, Vol. 56, pp. 225-237.

Bedrosian, B. and Dimaggio, F.L. (1972a), "Acoustic approximations in fluid-shell interactions", Journal of Engineering Mechanics, ASCE, Vol. 98, pp. 731-742.

Bedrosian, B. and Dimaggio, F.L. (1972b), "Transient response of submerged spheroidal shells", International Journal of Solids and Structures, Vol. 8, pp.

111-129.

Belytschko, T. (1977), "Methods and programs for analysis of fluid-structure systems", Nuclear Engineering and Design, Vol. 42, pp. 41-52.

Belytschko, T. (1980), "Fluid-structure interaction", Computers and Structures, Vol. 12, pp. 459-469.

Berot, F. and Peseux, B. (1998), "Vibro-acoustic behavior of submerged cylindrical shells: analytical formulation and numerical model", Journal of Fluids and Structures, Vol. 12, pp. 959-1003.

Bettess, P. (1977), "Infinite elements", International Journal for Numerical Methods in Engineering, Vol. 11, pp. 53-64.

Bettess, P. and Bettess, J. (1991), "Infinite elements for dynamic problems: Part 2", Engineering Computations, Vol. 8, pp. 125-151.

Bettess, P. and Zienkiewicz, O.C. (1977), "Diffraction and Refraction of Surface Waves Using Finite and Infinite Elements", International Journal for Numerical Methods in Engineering, Vol. 11, pp. 1271-1290.

Billger, D.V.J. and Folkow, P.D. (1998), "The imbedding equations for the Timoshenko beam", Journal of Sound and Vibration, Vol. 209, pp. 609 – 634.

Biswal, K.C., Bhattacharyya, S.K. and Sinha, P.K. (2003), "Free-vibration analysis of liquid-filled tank with baffles", Journal of Sound and Vibration, Vol. 259, pp. 177-192.

Bleich, H.H. and Sandler, I.S. (1970), "Interaction between structures and bilinear fluids", International Journal of Solids and Structures, Vol. 6, pp. 617-639.

Broderick, B.M., Elnashai, A.S. and Izzuddin, B.A. (1994), "Observations on the effect of numerical dissipation on the nonlinear dynamic response of structural systems", Engineering Structures, Vol. 16, pp. 51-62.

Buragohain, D.N. and Agrawal, B.L. (1981), "Hydrodynamic forces on large offshore structures under ground excitation", Numerical Methods for Coupled Problems, E. Hinton et al., eds., Pineridge Press, Swansea, UK

Cetin, M. and Mengi, Y. (2003), "Transmitting boundary conditions suitable for analysis of dam-reservoir interaction and wave load problems", Applied Mathematical Modelling, Vol. 27, pp. 451-470.

Chelghoum, A.E.K. (1986), Dynamics of Structures Including Fluid Interaction, Ph.D. Thesis, Univ. of London.

Chen, P.-T., Ju, S.-H. and Cha, K.-C. (2000), "A symmetric formulation of coupled BEM/FEM in solving responses of submerged elastic structures for large degrees of freedom", Journal of Sound and Vibration, Vol. 233, pp. 407-422.

Chen, Y.H., Hung, Y.H. and Shih, C.T. (2001), "Response of an infinite Timoshenko beam on a viscoelastic foundation to a harmonic moving load", Journal of Sound and Vibration, Vol. 241, pp. 809 – 824.

Chertok, G. (1970), "Transient flexural vibrations of ship-like sructures exposed to underwater explosions", The Journal of the Acoustical Society of America, Vol. 48,

pp. 170-180.

Chopra, A.K. (1967), "Hydrodynamic pressures on dams during earthquakes", Journal of the Engineering Mechanics Division, ASCE, Vol.93, pp. 205-223.

Chwang, A.T. (1978), "Hydrodynamic pressures on sloping dams during earthquakes. Part 2. Exact theory", Journal of Fluid Mechanics, Vol.87, pp. 343-348.

Chwang, A.T., and Housner, G.W. (1978), "Hydrodynamic pressures on sloping dams during earthquakes. Part 1. Momentum method", Journal of Fluid Mechanics, Vol.87, pp. 335-341.

Cole, H. (1948), Underwater explosion, Princeton; New Jersey.

Czyan, O. and Von Estorff, O. (2002), "Fluid-structure interaction by coupling BEM and nonlinear FEM", Engineering Analysis with Boundary Elements, Vol. 26, pp. 773-779.

Deeks, J.A. and Wolf, J.P. (2002a), "A virtual work derivation of the scaled boundary finite-element method for elastostatics", Computational Mechanics, Vol. 28, pp. 489-504.

Deeks, A. J. and Wolf, J. P. (2002b), "An h-hierarchical adaptive procedure for the scaled boundary finite-element method", International Journal for Numerical Methods in Engineering, Vol. 54, pp. 585-605.

Deeks, A. J. and Wolf, J. P. (2002c), "Stress recovery and error estimation for the scaled boundary finite-element method", International Journal for Numerical

Methods in Engineering, Vol. 54, pp. 557-583.

Deeks, A.J. and Wolf, J.P. (2003), "Semi-analytical solution of Laplace's equation in non-equilibrating unbounded problems", Computers and Structures, Vol. 81, pp. 1525-1537.

DeRuntz, J.A. and Geers, T.L. (1978), "Added mass computation by the boundary integral method", International Journal for Numerical Methods in Engineering, Vol. 12, pp. 531-549.

DiMaggio, F.L., Sandler, I.S., and Rubin, D. (1981), "Uncoupling approximations in fluid-structure interaction problems with cavitation", Journal of Applied Mechanics, Vol. 48, pp. 753-756.

Doherty, J. P. and Deeks, A. J. (2003a), "Scaled boundary finite-element analysis of a non-homogeneous axisymmetric domain subjected to general loading", Int. J. Num. Anal. Meth. Geomech., Vol. 27, pp. 813-835.

Doherty, J. P. and Deeks, A. J. (2003b), "Elastic response of circular footings embedded in a non-homogeneous half-space", Geotechnique, Vol. 53, pp. 703-714.

Donea, J., Giuliani, S. and Halleux, J.P. (1982), "An arbitrary Lagrangian-Eulerian finite element method for transient dynamic fluid-structure interactions", Computer Methods in Applied Mechanics and Engineering, Vol. 33, pp. 689-723.

Ekevid, T. and Wiberg, N.E. (2002), "Wave propagation related to high-speed train: A scaled boundary FE-approach for unbounded domains", Computer. Methods in Applied Mechanics and Engineering, Vol. 191, pp. 3947-3964.

Ergin A. (1996), "The response behavior of a submerged cylindrical shell using the doubly asymptotic approximation method (DAA)", Computers and Structures, Vol. 62, pp. 1025-1034.

Estorff, O.V. and Antes, H. (1991), "On FEM-BEM coupling for fluid-structure interaction analyses in the time domain", International Journal for Numerical Methods in Engineering, Vol. 31, pp. 1151-1168.

Everstine, G.C.A. (1976), "A nastran implementation of the doubly asymptotic approximation for underwater shock response", Proceedings of the fifth NASTRAN Conference, N77-20497, pp. 207-228.

Fan, S.C., Wang, K, Yu, G.Y. and Lie, S.T. (2001), "Spline shell element and plane-wave approximation for dynamic response of submerged structures", Computers and Structures, Vol. 79, pp. 1635-1644.

Fan, S.C., Li, S.M. and Yu, G.Y. (2002), "Dynamic fluid-structure interaction analysis using boundary finite element method / finite element method", Journal of Applied Mechanics, (to appear).

Felippa, C.A. (1977), "Top-down derivation of doubly asymptotic approximations for structure-fluid interaction analysis", Innovative Num. Anal. for the Applied Eng. Sciences, Eds. Shaw et al., pp. 79-88.

Felippa, C.A. (1980), "Family of early time approximation for fluid-structure interaction", Journal of Applied Mechanics, ASME, Vol. 47, pp. 703-708.

Felippa, C.A. (1981), "Interfacing finite element and boundary discretisations", Applied Mathematical Modelling, Vol. 5, pp. 383-386.

Felippa, C.A. and DeRuntz, J.A. (1984), "Finite element analysis of shock-induced hull cavitation", Computer Methods in Applied Mechanics and Engineering, Vol. 44, pp. 297-337.

Felippa, C.A. and DeRuntz, J.A. (1991), "Acoustic fluid volume modeling by the displacement potential formulation, with emphasis on the wedge element", Computers and Structures, Vol. 41, pp. 669-686.

Felszeghy, S.F. (1996a), "The Timoshenko beam on an elastic foundation and subjected to a moving step load. Part 1: steady-state response", Journal of Vibration Acoustics, ASME, Vol. 118, pp. 277-284.

Felszeghy, S.F. (1996b), "The Timoshenko beam on an elastic foundation and subjected to a moving step load. Part 2: transient-state response", Journal of Vibration Acoustics, ASME, Vol. 118, pp. 285 – 291.

Feng, Z.H. and Cook, R.D. (1983), "Beam elements on two-parameter elastic foundation", Journal of Engineering Mechanics, Vol. 109, pp. 1390-1402.

Fenves, G. and Chopra, A.K. (1985), "Earthquake analysis of concrete gravity dam including reservoir bottom absorption and dam-water-foundation rock interaction", Earthquake Engineering & Structural Dynamics, Vol. 13, pp. 13-31.

Fenves, G. and Vargas-Loli, L.M. (1988), "Nonlinear dynamic analysis of

fluid-structure systems", Journal of Engineering Mechanics, Vol. 114, pp. 219-240.

Folkow, P.D., Kristensson, G. and Olsson, P. (1998), "Time domain Green functions for the homogeneous Timoshenko beam", Quarterly Journal of Mechanics and Applied Mathematics, Vol. 51, pp. 125-141.

Fok, K.-L. and Chopra, A.K. (1986), "Earthquake analysis of arch dams including dam-water interaction, reservoir boundary absorption and foundation flexibility", Earthquake Engineering & Structural Dynamics, Vol. 14, pp. 155-184.

Geers T.L. and Lewis B.A. (1997), "Doubly asymptotic approximations for transient elasto-dynamics", International Journal of Solids and Structures, Vol. 34, pp. 1293-1305.

Geers T.L. and Zhang P. (1994a), "Doubly asymptotic approximations for submerged structures with internal fluid volumes: formulation", Journal of Applied Mechanics, ASME, Vol. 61, pp. 893-899.

Geers T.L. and Zhang P. (1994b), "Doubly asymptotic approximations for submerged structures with internal fluid volumes: validation", Journal of Applied Mechanics, ASME, Vol. 61, pp. 900-906.

Geers, T.L. (1970), "Response of an elastic cylindrical shell to a transverse acoustic shock wave in a light fluid medium", The Journal of the Acoustical Society of America, Vol. 48, pp. 692-701.

Geers, T.L. (1978), "Doubly asymptotic approximations for transient motions of submerged structures", The Journal of the Acoustical Society of America, Vol. 64,

pp. 1500-1508.

Geers, T.L. (1969), "Excitation of an elastic cylindrical shell by a transient acoustic wave", Journal of Applied Mechanics, Vol. 36, pp. 459-469.

Genes, M.C., and Kocak, S. (2002), "A combined finite element based soil-structure interaction model for large-scale systems and applications on parallel platforms", Engineering Structures, Vol. 24, pp. 1119-1131.

Givoli, D. (1991), "Non-reflecting boundary conditions: a review", Journal of Computational Physics, Vol. 94, pp. 1-29.

Givoli, D. (1992), Numerical methods for problems in infinite domains, Elsevier.

Givoli, D. (1999), "Exact representations on artificial interfaces and applications in mechanics", Applied Mechanics Review, Vol. 52, pp. 333-349.

Gong, S.W. and Lam, K.Y. (1999), "Transient response of floating composite ship section subjected to underwater shock", Composite Structures, Vol. 46, pp. 65-71.

Gong, S.W. and Lam, K.Y. (1998), "Transient response of stiffened composite submersible hull subjected to underwater explosive shock", Composite Structures, Vol. 41, pp. 27-37.

Gong, S.W., Lam, K.Y. and Lu, C. (2000), "Structural analysis of a submarine pipeline subjected to underwater shock", International Journal of Pressure Vessels and Piping, Vol. 77, pp. 417-423.

Hamdan, F.H. (1993), Finite element solutions for transient fluid-structure interaction, Ph.D. thesis, Department of Civil Engineering, Imperial College of Science Technology and Medicine, University of London.

Hamdan, F.H. and Dowling, P.J. (1995), "Far-field fluid-structure interaction", Computers and Structures, Vol. 56, pp. 949-958.

Hamdan, F.H. (1999), "Near-field fluid-structure interaction using Lagrangian fluid finite elements", Computers and Structures, Vol. 71, pp. 123-141.

Hamdi, M.A., Ousset, Y. and Verchery, G. (1978), "A displacement method for the analysis of vibrations of coupled fluid-structure systems", International Journal for Numerical Methods in Engineering, Vol. 13, pp. 139-150.

Hanna, Y.G. and Humar, J.L. (1982), "Boundary element analysis of fluid domain", Journal of Engineering Mechanics Division, ASCE, Vol. 108, pp. 436-450.

Hu, H.C. (1984), Variational principles of theory of elasticity with applications, Science Press, Beijing, China.

Huang, H. (1969), "Transient interaction of plane acoustic waves with a spherical elastic shell", The Journal of the Acoustical Society of America, Vol. 45, pp. 661-670.

Huang, H. (1970), "An exact analysis of the transient interaction of acoustic plane waves with a cylindrical elastic shell", Journal of Applied Mechanics, Vol. 37, pp. 1091-1099.

Huang, H. (1986), "Numerical analysis of the linear interaction pressure pulses with submerged structures", Proceeding of the international conference on advances in marine structures, admiralty research establishment, dunfermline, 20-23 May, Smith, C. S. and Clarke, J. D. (eds.), Elsevier Applied Science Publishers, London.

Junger, M.C. (1996), "Acoustic fluid-elastic structure interactions: basic concepts", Computers and Structures, Vol. 65, pp. 287-293.

Kausel, E., Tassoulas, J.L. and Waas, G. (1975), "Dynamic analysis of footings on layered media", Journal of Engineering Mechanics, Vol. 101, pp. 679-941.

Kenney, Jr., J.T. (1954), "Steady state vibrations of beam on elastic foundation for moving load", Journal of Applied Mechanics, Vol. 21, pp. 359-364.

Kucukarslan, S. (2005), "An exact truncation boundary condition for incompressible-unbounded infinite fluid domains", Applied Mathematics and Computation, Vol. 163, pp. 61-69.

Kulak, R.F. (1985), "Three dimensional fluid-structure coupling in transient analysis", Computers and Structures, Vol. 21, pp. 529-542.

Lam, K.Y., Zhang, Z.J., Gong, E.S. and Chan E.S. (1998), "The transient response of submerged orthotropic cylindrical shells exposed to underwater shock" Composite Structures, Vol. 43, pp. 179-193.

Lam, K.Y., Zhang, Z.J., Gong, E.S. and Chan E.S. (1998), "The transient response of a two-layered elastic cylindrical shell impinged by an underwater shock wave", Composites Part B, Vol. 29B, pp. 673-685.

Lamb, H. (1932), Hydrodynamics, 6th ed., New York, Dover, pp. 476-477.

Lee, G.C. and Tsai, C.S. (1991), "Time-domain analyses of dam-reservoir system, I: exact solution", Journal of Engineering Mechanics, Vol. 117, pp. 1990-2006.

Liu, P.L.-F. and Cheng, A.H.-D. (1984), "Boundary solutions for fluid structure interaction", Journal of Hydraulic Engineering, Vol. 110, pp. 51-64.

Liu, T. and Li, Q. (2003), "Transient elastic wave propagation in an infinite Timoshenko beam on viscoelastic foundation", International Journal of Solids and Structures, Vol. 40, pp. 3211-3228.

Liu, T. and Xu, Q. (2002), "Discrete artificial boundary conditions for transient scalar wave propagation in a 2D unbounded layered media", Computer Methods in Applied Mechanics and Engineering, Vol. 191, pp. 3055-3071.

Liu, W.K. and Chang, H.G. (1985), "A method of computation for fluid structure interaction", Computers and Structures, Vol. 20, pp. 311-320.

Liu, W.K. and Ma, D.C. (1982), "Coupling effects between liquid sloshing and flexible fluid-filled systems", Nuclear Engineering and Designs, Vol. 72, pp. 345-357.

Lotfi, V., Roesset, J.M. and Tassoulas, J.L. (1987), "A technique for the analysis of the response of dams to earthquakes", Earthquake Engineering and Structural Dynamics, Vol. 15, pp. 463-490.

Maity, S.K. and Bhattacharyya S.K. (1999), "Time-domain analysis of infinite reservoir by finite element method using a novel far-boundary condition", FiniteElements in Analysis and Design, Vol. 32, pp. 85-96.

Makinen, K. (1998), "Cavitation models for structures excited by a plane shock wave", Journal of Fluids and Structures, Vol. 12, pp. 85-101.

Manoj, K.G. and Bhattacharyya, S.K. (2000), "Transient acoustic radiation from impulsively accelerated bodies by the finite element method", The Journal of the Acoustical Society of America, Vol. 107, pp. 1179-1188.

Mansur, W.J., Yu, G.Y, Carrer, J.A.M., Lie, S.T. and Siqueira, E.F.N. (2000), "The θ scheme for time-domain BEM/FEM coupling applied to the 2-D scalar wave equation", Communications in Numerical Methods in Engineering, Vol. 16, pp. 439-448.

Mathews, I.C. and Geers, T.L. (1987), "A doubly asymptotic, nonreflecting boundary for ground shock analysis", Journal of Applied Mechanics, Vol. 54, pp. 489-497.

McCoy, R.W. and Sun, C.T. (1997), "Fluid-structure interaction analysis of a thick-section composite cylinder subjected to underwater blast loading", Composite Structures, Vol. 37, pp. 45-55.

McGhie, R.D. (1990), "Flexural wave motion in infinite beam", Journal of Engineering Mechanics, Vol. 116, pp. 531-548.

Mellado, M. and Rodriguez, R. (2001), "Efficient solution of fluid-structure vibration problems", Applied Numerical Mathematics, Vol. 36, pp. 389-400.

Mindlin, R.D., and Bleich, H.H. (1953), "Response of an elastic cylindrical shell to a transverse step shock wave", Journal of Applied Mechanics, Vol. 20, pp. 189-195.

Morand, H. and Ohayon, R. (1979), "Substructure variational analysis of the vibrations of coupled fluid-structure systems. Finite element results", International Journal for Numerical Methods in Engineering, Vol. 14, pp. 741-755.

Nachbin, A. and Wrobel, L.C. (1984), "An efficient infinite element for fluid-structure interaction", Numerical Methods for Transient and Coupled Problems, R.W. Lewis et al., eds., Pineridge Press, Swansea, UK, pp. 454-464.

Nicolas-Vullierme B. (1991), "A contribution to Doubly asymptotic approximations: an operator top-down derivation", Journal of Vibration, Acoustics, Stress, and Reliability in Design, Vol. 113, pp. 409-415.

Nicolas-Vullierme, B. and Blumstein, D. (1984), "Study of harmonic vibrations of fluid-structure coupled systems of revolution by means of the Bettes-Zienkiewicz mapped infinite element", Numerical Methods for Transient and Coupled Problems, R.W. Lewis et al., eds., Pineridge Press, Swansea, UK, pp. 439-446.

Nitikitpaiboon, C. and Bathe, K.J. (1993), "An arbitrary lagrangian-eulerian velocity potential formulation for fluid-structure interaction", Computers and Structures, Vol. 47, pp. 871-891.

O'Reagan, S.D. and DiMaggio, F.L. (1990), "Dynamic response of submerged shells with appendages", Engineering Mechanics, Vol. 116, pp. 2275-2292.

Olson, L.G. and Bathe, K.J. (1985), "An infinite element for analysis of transient fluid-structure interactions", Engineering Computations, Vol. 2, 319-329.

Olson, L.G. and Bathe, K.J. (1985), "Analysis of fluid-structure interactions. A direct symmetric coupled formulation based on the fluid velocity potential", Computers and Structures, Vol. 21, pp. 21-32.

Pal, N.C., Bhattacharyya, S.K. and Sinha, P.K. (2003), "Non-linear coupled slosh dynamics of liquid-filled laminated composite containers: a two dimensional finite element approach", Journal of Sound and Vibration, Vol. 261, pp. 729-749.

Ponthot, J.P. and Belytschoko, T. (1998), "Arbitrary Lagrangian-Eulerian formulation for element-free Galerkin method", Computer Methods in Applied Mechanics and Engineering, Vol. 152, pp. 19-46.

Pracht, W. E. (1975), "Calculating three dimensional fluid flows at all speeds with an Eulerian-Lagrangian computing mesh", Journal of Computational Physics, Vol. 17, pp. 132-159.

Rajakumar, C. and Ali, A. (1996), "Boundary element-finite element coupled eigenanalysis of fluid-structure systems", International Journal for Numerical Methods in Engineering, Vol. 39, pp. 1625-1634.

Ranlet, D., DiMaggio, F.L., Bleich, H.H., and Baran M.L. (1977), "Elastic response of submerged shells with internally attached structures to shock wave loading", Computers and Structures, Vol. 7, pp. 355-364.

Rao, S.S. (1989), The finite element method in engineering, Second Edition,

Pergamon Press, Oxford.

Rehak, M.A., DiMaggio, F.L. and Sandler, I.S. (1985), "Interactive approximations for a cavitating fluid around a floating structure", Computers and Structures, Vol. 21, pp. 1159-1175.

Saini, S.S., Bettess, P. and Zienkiewicz, O.C. (1978), "Coupled hydrodynamic response of concrete gravity dams using finite and infinite elements", Earthquake Engineering & Structural Dynamics, Vol. 6, pp. 363-374.

Shantram, D., Owen, D.R. and Zienkiewicz, O.C. (1976), "Dynamic transient behavior of two and three dimensional structures including plasticity, large deformation effects and fluid interaction", Earthquake Engineering & Structural Dynamics, Vol. 4, pp. 561-578.

Sharan, S.K. (1985), "Finite element analysis of unbounded and incompressible fluid domains", International Journal for Numerical Methods in Engineering, Vol. 21, pp. 1659-1669.

Sharan, S.K. (1992), "Efficient finite element analysis of hydrodynamic pressure on dams", Computers and Structures, Vol. 42, pp. 713-723.

Sheby, A. and Severn, R. T. (1972), "An experimental assessment of the added mass of some plates vibrating in water", Earthquake Engineering & Structural Dynamics, Vol. 1, pp. 189-200.

Shin, Y.S. (2004), "Ship shock modeling and simulation for far-field underwater explosion", Computers and Structures, Vol. 82, pp. 2211 – 2219.

Shin, Y.S. and Hooker, D.T. (1996), "Damage response of submerged imperfect cylindrical structures to underwater explosion", Computers and Structures, Vol. 60, pp. 683-693.

Singh, K.R., Kant, T. and Kadokar, A. (1990), "Efficient partitioning schemes for fluid-structure interaction problems", Engineering Computations, Vol. 7, pp. 101-115.

Singh, K.R., Kant, T. and Kadokar, A. (1991), "Three dimensional transient analysis of a single submerged cylindrical shell", Engineering Computations, Vol. 8, pp. 195-213.

Singh, K.R., Kant, T. and Kadokar, A. (1992), "Three dimensional transient analysis of two coupled submerged cylindrical shell", Engineering Computations, Vol. 9, pp. 39-48.

Sobolev, S.L. (1964), Partial Differential Equations of Mathematical Physics, Permagon Press, Oxford.

Soliman, M. and DiMaggio, F.L. (1983), "Doubly asymptotic approximations as non-reflecting boundaries in fluid-structure interaction problems", Computers and Structures, Vol. 17, pp. 193-204.

Sommerfeld, A. (1949), Partial differential Equations in physics, Academic Press, New York.

Song, C. and Wolf, J.P. (1997), "The scaled boundary finite-element method – alias consistent infinitesimal finite-element cell method – for elastodynamics",

Computer Methods in Applied Mechanics and Engineering, Vol. 147, pp. 329-355.

Song, C. and Wolf, J.P. (1996), "Consistent infinitesimal finite-element cell method: three-dimensional vector wave equation", International Journal for Numerical Methods in Engineering, Vol. 39, pp. 2189-2208.

Song, C. and Wolf, J.P. (1998), "The scaled boundary finite-element method: analytical solution in frequency domain", Computer Methods in Applied Mechanics and Engineering, Vol. 159, pp. 249-264.

Song, C. and Wolf, J.P. (1999), "Body loads in scaled boundary finite-element method", Computer Methods in Applied Mechanics and Engineering, Vol. 180, pp. 117-135.

Song, C. and Wolf, J.P. (2000), "Scaled boundary finite-element method - a primer: solution procedures", Computers and Structures, Vol. 78, pp. 211-225.

Song, C. and Wolf, J.P. (2002), "Semi-analytical representation of stress singularities as occurring in cracks in anisotropic multi-materials with the scaled boundary finite-element method", Computers and Structures, Vol. 80, pp. 183-197.

Stadler, W. and Shreeves, R.W. (1970), "The transient and steady-state response of the finte Bernoulli-Euler beam with damping and an elastic foundation", Quarterly Journal of Mechanics and Applied Mathematics, Vol. 23, pp. 197-208.

Sun, L. (2001), "A closed-form solution of a Bernoulli-Euler beam on a viscoelastic foundation under harmonic line loads", Journal of Sound and Vibration, Vol. 242, pp. 619-627.

Sundqvist, J. (1983), "An application to the solution of fluid-structure interaction problems", Computers and Structures, Vol. 17, pp. 793-807.

Timoshenko, S.P. and Goodier, J.N. (1970), Theory of Elasticity, McGraw-Hill, London.

Tsai C.S. (1992), "Semi-analytical solution for hydrodynamic pressures on dams with arbitrary upstream face considering water compressibility", Computers and Structures, Vol. 42, pp. 497-502.

Tsai, C.S. and Lee G.C. (1987), "Arch dam-fluid interactions: by FEM-BEM and substructure concept", International Journal for Numerical Methods in Engineering, Vol. 24, pp. 2367-2388.

Tsai, C.S. and Lee, G.C. (1989), "Hydrodynamic pressure on gravity dams subjected to ground motions", Journal of Engineering Mechanics, ASCE, Vol. 115, pp. 598-617.

Tsai, C.S. and Lee, G.C. (1991), "Time-domain analyses of dam-reservoir system. II: substructure method", Journal of Engineering Mechanics, Vol. 117, pp. 2007-2026.

Tsai, C.S., Lee, G.C. and Ketter, R.L. (1990), "A semi-analytical method for time-domain analyses of dam-reservoir interactions", International Journal for Numerical Methods in Engineering, Vol. 29, pp. 913-933.

Tsynkov, S. (1998), "Numerical solution of problems on unbounded domains, a review", Applied Numerical Mathematics, Vol. 27, pp. 465-532.

Valliappan, S. and Zhao, C. (1992), "Dynamic response of concrete gravity dams including dam-water-foundation interaction", International Journal for Numerical and Analytical Methods in Geomechanics, Vol. 16, pp.79-99.

Wang, K. (2001), "Fluid-structure interaction using spline finite element method", Master Thesis, Nanyang Technological University, Singapore.

Wang, M.C., Badie, A. and Davids, N. (1984), "Traveling waves in beam on elastic foundation", Journal of Mechanics Engineering, Vol. 110, pp 879-893.

Wang, T.M. and Gagnon, L.W. (1978), "Vibration of continuous Timoshenko beam on Wenkler-Pasternak foundation", Journal of Sound and Vibration, Vol. 59, pp. 211-220.

Westergaard, H.M. (1933), "Water pressures on dams during earthquakes", Transactions, ASCE, Vol. 98, pp. 418-433.

Wilson, E.L. (1975), Finite elements for foundations, joints and fluids, Chapter Ten, Finite Elements for Geomechanics, Ed. Gudehus. G., Wiley, London, pp. 319-350.

Wilson, E.L. and Khalvati, M. (1983), "Finite elements for the dynamic analysis of fluid-solid systems", International Journal for Numerical Methods in Engineering, Vol. 19, pp. 1657-1668.

Wolf J.P. and Song C. (1996a), Finite-Element Modeling of Unbounded Media, Wiley, Chichester.

Wolf, J.P. and Song, C. (1996b), "Consistent infinitesimal finite element cell

method: three-dimensional scalar wave equation", Journal of Applied Mechanics, Vol. 63, pp. 650-654.

Wolf, J.P. and Song, C. (1998), "Unit-impulse response of unbounded medium by scaled boundary finite-element method", Computer Methods in Applied Mechanics and Engineering, Vol. 159, pp. 355-367.

Wolf, J.P. and Song, C. (2000), "Scaled boundary finite-element method - a primer: derivations", Computers and Structures, Vol. 78, pp. 191-210.

Wolf, J.P. and Song, C. (2001), "The scaled boundary finite-element method- a fundamental solution-less boundary-element method", Computer Methods in Applied Mechanics and Engineering, Vol. 190, pp. 5551-5568.

Wright, J.P., Misovec, A. and Baron, M.L. (1981), "Pressures in a submerged fluid filled cylindrical shell subjected to a step wave", Computers and Structures, Vol. 14, pp. 495-500.

Yang R., Tsai C.S., Lee G.C. (1993), "Explicit time-domain transmitting boundary for dam-reservoir interaction analysis", International Journal for Numerical Methods in Engineering, Vol. 36, pp. 1789-1804.

Yu G.Y., Lie S.T. Fan S.C. (2002), "Stable boundary element method/finite element method procedure for dynamic fluid-structure interactions," Journal of Engineering Mechanics, Vol. 128, pp. 909-915.

Zienkiewicz, O.C. and Bettess, P. (1978), "Fluid-structure dynamic interaction and wave forces. An introduction to numerical treatment", International Journal for

Numerical Methods in Engineering, Vol. 13, pp. 1-16.

Zienkiewicz, O.C. and Taylor, R.L. (1989), The Finite Element Method, Fourth Edition. Vol 1, Mcgraw-Hill Book Company.

Zienkiewicz, O.C., Bettess, P., Chiam, T.C. and Emson, E. (1981), "Numerical methods for unbounded field problems and a new infinite element formulation", Computational Methods for Infinite Domain Media Structure Interaction, A.J. Kalinowski, Ed. ASME, New York, 1981.

Zienkiewicz, O.C., Paul, K.D. and Hinton, E. (1983), "Cavitation in fluid-structure response (with particular reference to dams under earthquake loading)", Earthquake Engineering & Structural Dynamics, Vol. 11, pp. 463-481.

Zilliacus, S. (1983), "Fluid-structure interaction and ADINA", Computers and Structures, Vol. 17, pp. 763-773.

Zilliacus, S., Toridis, T. and Giacofci, T. (1979), "Analysis of wave excited submerged structures", Proceedings of ADINA conference held at MIT, pp. 425-445.

ADDENDUM

- ORIGINALITY OF THIS THESIS

The originality of this thesis includes the following aspects:

1. When using the Scaled Boundary Finite Element Method (SBFEM) for unbounded fluid domain, one of the major task is to derive the dynamic mass matrix $\mathbf{M}^{\infty}(t)$. This thesis presented a new formulation to derive the $\mathbf{M}^{\infty}(t)$, particularly for solving shock waves problems. The new formulation is efficient and recursive in nature.
2. When using the SBFEM to solve the fluid-structure interaction (FSI) problems, a pressure-velocity (*p*-*v*) relationship needs to be established. The rigorous SBFEM-based *p*-*v* relationship could be very complicated and difficult to implement. In this thesis, a new SBFEM-based *p*-*v* relationship is derived by adopting an acoustic approximation. It is easy to implement, and thus extends the applicability of SBFEM, in particular for submerged FSI problems.
3. In the SBFEM formulation, it results in a few coefficient matrices, which usually do not have physical meaning. This thesis unveils the mystery of one of the coefficient matrix $\mathbf{E}^{1}$, which becomes zero for a particular geometry of semi-infinite fluid domain, that is bounded by two parallel radial lines. In enables the present SBFEM formulation easily to yield solutions for dam-reservoir FSI problems, though its applications are limited to flat-bottom reservoirs. In addition, this thesis presented a new SBFEM formulation for reservoir with absorptive flat bottom, in particular for steady-state analysis in the frequency domain.
4. This thesis extended the SBFEM to solve dam-reservoir system in the time domain. Its solutions are verified and appear to be superior to other available solutions, which are obtained by other prevailing methods and for isolated cases only.